FTIR-ATR studies on polymer/polymer and polymer/liquid interfaces.

Pereira, Marcia Rodrigues

FTIR-ATR Studies on Polymer/Polymer and Polymer/Liquid Interfaces.

by

Márcia Rodrigues Pereira

(Diploma in Chemical Engineering - Universidade do Estado do Rio de Janeiro

M.Sc. in Polymer Science and Technology - Universidade Federal do Rio de Janeiro)

A thesis submitted in partial fulfilment of the requirements for the degree of Doctor of Philosophy of the University of Durham

Department of Chemistry

University of Durham

June-1994

ABSTRACT

Fourier Transform Infrared Attenuated Total Reflection Spectroscopy (FTIR-ATR) has been employed to study polymer laminates composed of poly (methylmethacrylate) (PMMA) and poly(vinyl alcohol) (PVOH) using different base layer thicknesses and different angles of incidence on a ZnSe substrate.

By varying the "barrier" layer of PMMA it has been confirmed that different effective penetration depths into the PVOH are achieved, in very good agreement with the calculated electric field as a function of distance away from the substrate surface. These results show that the two-layered model system can be successfully employed to provide a semi-quantitative depth profile of the laminate.

Following the FTIR-ATR study on polymer/polymer interface we have demonstrated how the evanescent field absorption from a IR beam can also be used to monitor *in situ* the molecular interaction at polymer/liquid interfaces. The chosen system was a series of sulphonated polyethersulphones (SPES) and water. The $\nu_s(SO_3^-)$ and $\nu_a(SO_3^-)$ vibrational modes were monitored as the degree of hydration was varied. It has been found that the $\nu_s(SO_3^-)$ mode increases with hydration suggesting that, with hydration the sulphonic acid groups of SPES are dissociated into SO_3^- ions. It has been found that changes also occur in the benzene ring vibrational band that are dependent on the degree of hydration. Spectral subtraction has been employed to highlight changes in the $\nu_a(SO_3^-)$ mode which were not readily observed in the raw spectra due to overlapping bands.

The particular behaviour of $\nu(OH)$ vibrational mode of water molecules has also been analysed. The main conclusion in this case was that the average hydrogen bond strength of the sorbed water is considerable lower than that in pure water. This would favour an efficient flux of water through the membrane.

A method based on monitoring the time dependent change in the $\nu(OH)$ mode of water has been developed to calculate the diffusion of water on SPES membranes. After reaching a steady state, the normalised absorbance plot versus time has been used for

numerical evaluation. Two models have been developed, one for Fickian diffusion and another for the dual sorption mode. The experimental results show a much better agreement for the second model.

The diffusion coefficient values have been calculated for different samples and interesting variations of the diffusion coefficient as a function of sulphonation level, solvent and film thickness have been analysed in detail.

To Mariana

ACKNOWLEDGEMENTS

The work described in this thesis was carried out under the supervision of Prof. J. Yarwood and I wish to record my appreciation of his help throughout.

I also would like to thank Prof. R.Harris for taking on responsibility for the completion of my studies in Durham.

Thanks are also due to Dr. Peter Cardew for very helpful suggestions and discussions.

Very special thanks go to my brilliant husband for his help with the numerical methods and Pascal programs and also for his encouragement and support during the course of this work.

Finally I would like to thank the Brazilian agency, Conselho Nacional de Desenvolvimento Científico e tecnológico (CNPq) for financial support.

MEMORANDUM

The research presented in this thesis has been carried out in the Department of Chemistry, University of Durham, between January 1991 and May 1994. It is original work of the author unless stated otherwise. None of this work has been submitted for any other degree.

CONTENTS

Chapter 1

Fourier Transform Infrared Spectroscopy in Polymer Science

Chapter 2

Depth-Profiling of Polymer Laminates Using FTIR-ATR Spectroscopy.

Chapter 3

Water Absorption Studies on Polymeric Membranes Using FTIR-ATR Spectroscopy

Chapter 4

FTIR- ATR Spectroscopic Determination of Diffusion Coefficient of Water in Polymeric Membranes.

Part I

Chapter 5

Models, Simulation and the Monte Carlo Method

Chapter 6

FTIR-ATR Spectroscopic Determination of Diffusion Coefficient of Water in Polymeric Membranes.

Part II

Chapter 1

Fourier Transform Infrared Spectroscopy in Polymer Science

CONTENTS

1.1 - INTRODUCTION

Vibrational spectroscopy has been applied to the identification of polymeric materials for both qualitative and quantitative determination of chemical composition. Many parameters can be investigated[1-3], including polymer end groups, chain branching, configuration and conformation, as well as steric and geometric isomerism. Infrared spectroscopy has also been used to identify and determine the concentration of impurities, antioxidants, emulsifiers, plasticizers, fillers and residual monomers in polymeric materials. Many reaction mechanisms of polymers are relatively slow so that processes such as vulcanisation, polymerisation, and degradation can be followed using rapid-scanning spectrometers. The effects of external conditions on polymers have been studied as well.

Originally, IR spectra of polymers were measured using a dispersive instrument equipped with an optical element of a prism or grating to disperse the infrared radiation. Using a scanning mechanism, the dispersed radiation is passed over a slit system that isolates the frequency range falling on the detector. In this manner, the spectrum; that is, the energy transmitted through a sample as a function of frequency is obtained. This dispersive IR method is severely limited in sensitivity because most of the available energy is thrown away, i.e., it does not fall on the open slits aperture and hence does not reach the detector. To improve the sensitivity of an infrared instrument, a multiplex optical device was sought which allows the continuous detection of all the transmitted energy simultaneously. The Michelson interferometer (which will be described in more detail in the next section) is such an optical device and the IR instrumentation which resulted is termed a Fourier Transform Infrared (FT-IR) Spectrometer[4-5]. The Fourier transform process was well known to Michelson, but the computational difficulty of making the transformation prevented the application of this powerful technique to spectroscopy. An important advance was made with the discovery of the Fast Fourier Transform (FFT) algorithm by Cooley and Tukey[4] which breathed new life into the field of spectroscopy using interferometers by allowing the calculation of the Fourier

transform to be carried out rapidly. As computers have improved, the time required for a Fourier transform has been reduced to such an extent that the spectra can be calculated during the time needed for the moving mirror to return to its starting position.

With the advent of Fourier transform infrared (FTIR) spectroscopy, numerous problems in the field of polymer characterisation became readily accessible as a result of an increase in the signal-to-noise ratio, higher energy throughput, data processing capability and rapid scanning. The possibility of obtaining a reasonably high quality spectrum in a matter of a few seconds opens up whole new areas of investigation of physical and chemical structures which would not be possible without the aid of an interferometer system.

The following sections describe briefly the theory involved in Fourier transform infrared spectroscopy, and some of the recent advances made in polymer spectroscopy due to Fourier transform infrared instrumentation. No attempt will be made to give a complete coverage of the rapidly growing FTIR spectroscopy literature and only a limited treatment of the Fourier transform theory will be presented. More detailed discussion of these subjects can be found in references[1-9].

1.2 - *INSTRUMENT BACKGROUND*

1.2.1 - The Michelson Interferometer

The design of most interferometers being used for infrared spectroscopy today is based on that of the first interferometer originally designed by Michelson in 1880[5]. Many other two-beam interferometers have been designed subsequently which may sometimes be more useful for certain specific applications than the Michelson interferometer. However, the theory of interferometry is more readily understood by first acquiring an understanding of the way in which a basic Michelson interferometer can be used for the measurement of infrared spectra.

The Michelson interferometer is an optical device that can divide a beam of radiation into two paths and then recombine them so that the intensity variations of the exit beam can be measured by a detector as a function of path difference[3]. The simplest form of the interferometer is shown in Fig. 1.1. It consists of two mutually perpendicular plane mirrors, one of which can move along the axis shown. The movable mirror is either moved at a constant velocity or is held at equidistant points for short, fixed periods of time and rapidly stepped between these points. Between the fixed mirror and the movable mirror is a beamsplitter, where a beam of radiation from an external source can be partially reflected to the fixed mirror (at point F) and partially transmitted to the movable mirror (at point M). After each beam has been reflected back to the beamsplitter, they are again partially reflected and partially transmitted. Thus, 50 % of the beams that have travelled in the path to both the fixed and movable mirrors reach the detector, while the remaining 50 % of each beam also travel back toward the source.

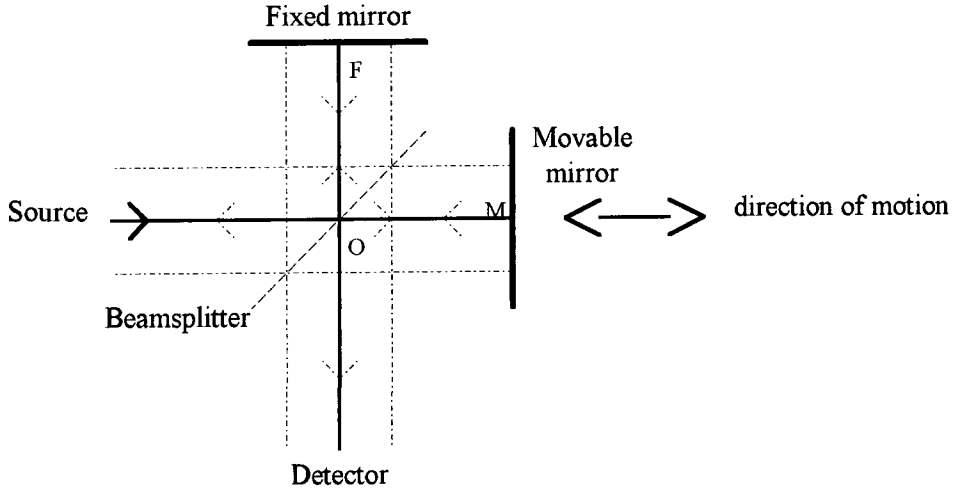

Fig. 1.1 - Schematic diagram of a Michelson interferometer.

The beam that returns to the source is only occasionally of interest for spectroscopy and only the output beam passing in the direction perpendicular to that of the input beam is usually measured. However, it is important to remember that both of the output beams contain equivalent information. The main reason for measuring only

one of the output beams is the difficulty of separating the second output beam from the input beam if the beamsplitter is at 45° to each mirror.

1.2.2 - Light Sources

To understand the process occurring in a Michelson interferometer better, let us first consider an idealised situation where a source of monochromatic radiation produces an infinitely narrow, perfectly collimated beam. If the fixed and movable mirrors are equidistant from the beamsplitter, no path difference exists between the two beams. They interfere constructively for path differences equal to any integral number of the wavelength $n\lambda$. In the case of path differences equal to $(n + 1/2)\lambda$, the two beams interfere destructively and for a monochromatic source of intensity $I(\nu)$, the intensity of the transmitted beam through the interferometer as a function of optical path difference, or retardation, x (cm) is given by[7]:

$$I(x) = 0.5I(\bar{\nu})(1+\cos 2\pi\bar{\nu}x) \qquad \text{(eq.1.1)}$$

In a scanning Michelson interferometer, the optical path difference x is varied by moving one mirror at a constant velocity v. It can be seen that $I(x)$ is composed of a constant (dc) component equal to $0.5I(\nu)$ and a modulated (ac) component equal to $0.5I(\nu)\cos 2\pi\nu x$. Only the ac component is important in spectrometric measurements, and it is this modulated component that is generally refereed to as the *interferogram*, I(x). In the case of a polychromatic source, the interferogram is the sum of the individual interferograms due to each wavenumber, i.e.:

$$I'(x) = 0.5\sum_{i=1}^{n} I(\bar{\nu}_i)\cos 2\pi\bar{\nu}_i x \qquad \text{(eq. 1.2)}$$

And if we consider a continuous source, the interferogram is the integral of the contributions from all wavenumbers in the spectrum:

$$I'(x) = 0.5\int_{-\infty}^{+\infty} I(\bar{\nu})\cos 2\pi\bar{\nu}x d\bar{\nu} \qquad \text{(eq.1.3)}$$

In practice, the amplitude of the interferogram as observed after detection and amplification is proportional not only to the intensity of the source but also to instrument characteristics (detector response, beamsplitter efficiency, etc.). These factors remain constant for a given configuration and eq. 1.3 can be expressed as:

$$I'(x) = \int_{-\infty}^{+\infty} B(\bar{\nu})\cos 2\pi\bar{\nu}x d\bar{\nu} \qquad \text{(eq. 1.4)}$$

Where B(ν) represents the intensity of the source at a frequency ν cm^{-1} taking into account the instrumental characteristics. It can be seen from eq. 1.4 that I'(x) is the cosine Fourier transform of the spectrum B(ν) which can be recovered by taking the Fourier transform of I'(x)[7]:

$$B(\bar{\nu}) = \int_{-\infty}^{+\infty} I'(x)\cos 2\pi\bar{\nu}x dx \qquad \text{(eq. 1.5)}$$

In practice, data acquisition involves signal-averaging of interferograms and requires that the signals are added coherently. For this purpose the interferogram of a monochromatic source (He-Ne laser) is measured along with the main interferogram. The different interferograms can be digitised at exactly the same position during each scan by sampling at each zero value of the sinusoidal reference interferogram arising from the He-Ne laser. It is however necessary for the first data point to be sampled at an identical retardation for every scan. This is achieved using a third interferogram arising from a white light source[7]. The very sharp interferogram produced by this source gives a reproducible marker at the same retardation, and whenever this interferogram exceeds a certain threshold voltage, data collection begins at the next zero crossing of the laser

reference interferogram. A detailed treatment of theory and instrumentation has been published by Griffiths[3].

1.3 - *ADVANTAGES OF FTIR SPECTROSCOPY*

In contrast to usual dispersive infrared spectrometers for which the radiation is divided into individual frequency elements, all the information is included in the interferogram obtained from a single scan of the movable mirror of the interferometer. The interferometer contains no slits and the amount of the energy falling onto the detector is greatly enhanced compared to dispersive systems (Jacquinot's advantage). In theory, Jacquinot's advantage, which depends on the resolution, may be as much as 80 to 200 times greater than that of a dispersive instrument[3-5]. This advantage is particularly valuable for the study of optical dense materials such as carbon-black filled, highly coloured or absorbing polymers.

The multiplex or Fellgett's advantage arises from the fact that all spectral frequencies are measured at the same time in one scan of the interferometer. This results in an important increase of signal-to-noise ratio as compared with a dispersive instrument for identical measurement times.

In addition to these advantages, the availability of computers is certainly the main reason for the tremendous development of FTIR spectroscopy in the polymer field. Because of the direct interfacing of the computer to the spectrometer, spectra can be arithmetically manipulated in such way that, for example, interfering absorbances can be eliminated by subtracting out from composite spectra. In addition, the rapid scanning capability of the interferometer has allowed the recent development of analysis of chemical and physical structural changes in polymers as a function of time over the entire mid infrared frequency range[4].

1.4 - *INFRARED SPECTROSCOPIC TECHNIQUES*

A short discussion of the various infrared techniques will be given here as an introduction. Special emphasis will be placed on the ATR technique because it was the technique used in this work. Apart from ATR, it is not the purpose of this chapter to discuss the individual techniques in detail, since their adaptation and development have been the subject of several excellent reviews[3,5].

1.4.1 - Transmission Spectroscopy

About transmission, Chalmers and Mackenzie[6] have written: Transmission is the oldest known method for obtaining infrared spectra. The infrared examination of solids was usually undertaken on samples prepared as alkali halide disks, mineral oil mulls or thin films. For polymers the preferred method is to prepare free-standing thin films either by solvent casting or melt pressing. In general these procedures yield good quality spectra from which qualitative and quantitative information may be derived. Consequently, transmission will probably remain the preferred technique of examining solids whenever possible since the effects of sample form on spectral details are well understood and reasonably predictable. However, on some occasions the preparation method can alter the crystallinity of a semicrystalline polymer, and either induce or destroy molecular orientation. On other occasions the polymers are too tough to grind easily even at liquid nitrogen temperatures. Furthermore, *in situ* information is increasingly being sought on materials forming integral parts of composite structures. Sampling techniques that allow solids to be examined without extensive sample preparation are, therefore, of considerable value to the infrared spectroscopist[6].

1.4.2 - External Reflectance Spectroscopy

External reflectance spectroscopy was originally applied to study thin films on metal surfaces at near grazing angles of incidence[11]. For this application the term reflection-absorption is often used. Only at near grazing incidence is the presence of a thin (⟨10nm) organic layer on metallic substrate detectable by reflectance methods[10]. Furthermore only the radiation polarised parallel to the plane of incidence is sensitive to surface layers[1]. These phenomena have been explained in terms of classical electromagnetic theory. Basically, the incident and reflected radiation coherently interfere with each other and form a standing wave at the interface. For parallel polarisation at high angles of incidence this standing wave can interact with any organic layer which is present. For perpendicular polarisation or low incident angles the standing wave has a node at the interface, and hence there is no electric field to interact with the organic layer. This condition begins to break down when the film thickness reaches around 200 nanometers. According to ref. 6, the spectrum recorded frequently has the appearance of the first derivative of the absorption spectrum and for substance of low refractive index tends to be weak. For this reason, external reflection spectroscopy, has not been used widely as a method of examining polymer surfaces; however, it has proved more valuable for studying inorganic solids. For example, information has been obtained on the average crystal orientation of plasma-sprayed metal oxide deposits, which can be correlated with measurements of both hardness and coefficient of friction[6].

1.4.3 - Diffuse Reflectance Spectroscopy

Diffuse reflectance spectroscopy has recently become a powerful technique for the analysis of powders and coarse solids in the infrared. Because of the high energy through-put and signal-to-noise ratio of FTIR, it is now possible to obtain infrared diffuse reflectance spectra of microgram quantities of sample. A significant advantage of

diffuse reflectance infrared Fourier transform spectroscopy (DRIFTS) over other techniques is the non-destructive capability of the sample preparation. For polymer systems that can be difficult to grind it may be sufficient to simply roughen the surface to be studied. For many coarse systems spectra can be obtained of the neat sample without grinding or other treatment[1].

The theories for diffuse reflectance have been broadly classified into either continuum or statistical models[1,6]. Continuum theory involves the use of phenomenological constants, while statistical theories utilise fundamental quantities such as absorptivity, refractive index and particle size[10]. Most of these theories attempt to model a system of particulate absorbing particles dispersed in a particulate non-absorbing medium[10]. For particulate samples, most of the incident radiation is diffusely reflected, while for non-particulate samples a large portion of the radiation may be specularly reflected. For such sample systems the reflected radiation has both diffuse and specular components. For a detailed account of the process involved in diffuse reflectance it is suggested the reader refers to reference 10.

1.4.4 - Photoacoustic Spectroscopy

Photoacoustic spectroscopy (PAS) is another technique that has held promise for polymer samples, since the sample preparation is negligible. PAS has the additional advantage that the sample form (pellet, powder, film) does not affect the relative intensity of most bands in the spectrum. The principle of Photoacoustic spectroscopy is that modulated IR radiation striking the surface of a sample will cause the surface to alternately heat and cool[1]. This cyclic heating and cooling of the sample surface is conducted to a coupling gas in the Photoacoustic cell. A standing wave develops which is detected by a microphone. If a particular frequency is not absorbed then the sample surface will not heat up and no sound wave will develop. Hence, in Photoacoustic spectroscopy, sound waves are used to detect infrared absorption frequencies[1]. The

Photoacoustic signal has a variable penetration depth which allows it in principle to be used for depth profiling experiments[6]. Nevertheless, the depth of penetration of the incident radiation is highly dependent on the modulation frequency, so that the velocity of the moving mirror must never be altered once the desired value has been determined. PAS is also very susceptible to environmental interferences, such as noise in the laboratory. Considerable effort is being directed to the solution of these problems, and it is anticipated that PAS will start to manifest its true potential in the near future[1].

1.4.5 - Ellipsometry Spectroscopy

Ellipsometry has long been used in the UV-visible region of the spectrum for probing the thickness and optical properties of surface layers and films. Sensitivities on the order of angstrons are achieved with visible light laser Ellipsometry[1]. Ellipsometry is concerned with the change in polarisation which a sample induces in a wave. The polarisation of the input is known and controlled and the output polarisation is measured. From the difference between the input and output polarisation states the differential phase change, delta, and the differential amplitude, psi, can be calculated[3]. Photometry, conversely, deals with the change in intensity which a sample induces in a wave.

There are several reasons for doing infrared Ellipsometry[1,3]. Firstly, to measure the thickness of thin films on surfaces in the range of 10-1000nm. Secondly, to measure the optical constants n (refractive index) and k (absorption index) of the surface film. Thirdly, in a reflection experiment only the reflected intensity can be measured by normal photometry. With Ellipsometry one can also measure delta, the differential phase change, and thus obtain phase as well as intensity information. The infrared region itself contains more chemical functional group information than is available in the UV-visible region. In the last decade interest in infrared Ellipsometry has increased. Although to date there have been few studies of polymer systems, the application of infrared Ellipsometry to thin polymer layers on a variety of substrates seems certain to increase.

1.4.6 - Attenuated Total Reflectance Spectroscopy

When light passes through two media having different refractive indices (n_1, n_2, n1>n2) which are in contact with each other, its path is refracted. The magnitude of this distortion depends on the angle of incidence (Θ) at which the light enters the medium and the optical densities of both media. Figure 1.2 depicts the physical process that affects light passing through two materials in optical contact with different refractive indices[11]. Light is reflected and transmitted at a 90° angle of incidence, reflected and refracted at angle $\Theta<\Theta_c$, or totally reflected at $\Theta>\Theta_c$.This is the bases of internal reflectance spectroscopy. The angle of incidence, Θ, is measured from the normal. The critical angle is defined by:

$$\Theta_c = \sin^{-1} n_{21} \qquad \text{(eq. 1.6)}$$

Where $n_{21} = n_2/n_1$.

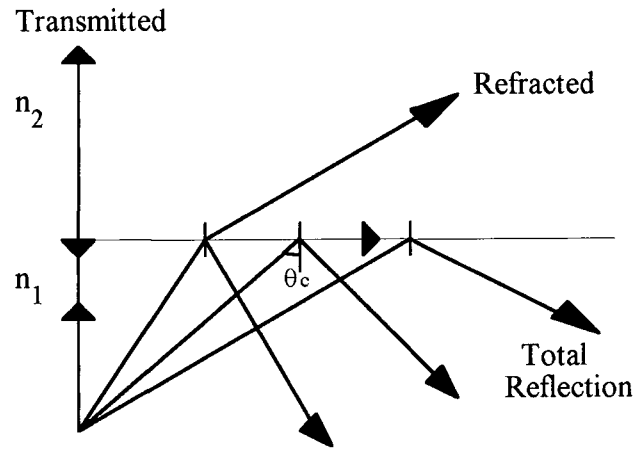

Fig. 1.2 - Effect of refractive index on the light path as a function of the angle of incidence.

Internal reflectance or attenuated total reflectance (ATR) spectroscopy is probably the second most commonly used infrared technique after transmission. Its history began nearly two centuries ago with the observation by Newton of an evanescent field in a lower index of refraction medium in contact with a higher index of refraction medium in which a propagating wave of radiation undergoes total internal reflection (TIR). However, the exploitation of this phenomenon for the production of absorption spectra did not begin until the pioneering development work of Fahrenfort[12] and Harrick[13]. After the disclosure of the technique in the literature in 1960, a flurry of publications exploiting it for a wide variety of applications ensued. By 1967 a large body of literature existed which was sufficient to justify a monograph by Harrick[14] and a review by Wilks and Hirschfeld[15].

The theoretical treatment of ATR is not easy. To simplify it, medium 2 is assumed to have a very low absorption coefficient[14]. In this approximation, the time averaged energy flux is zero in medium 2.

The radiation propagating in the optically more dense medium 1, with refractive index n_1, undergoes total internal reflection at the interface with the optically more rare medium 2, with refractive index n_2, when the angle of incidence, Θ, exceeds the critical angle Θ_c.

For internal reflectance just as was the case for external reflection, the incident and reflected light beams coherently interfere at the interface and form a standing wave. This standing wave does not extend into the rarer medium, instead a non-propagating evanescent wave is present in the rarer medium (fig. 1.3). The physical explanation for this evanescent wave is that the normal component of the electric field must be continuous across the interface, but at the same time there can be no net transfer of energy into the rarer medium for internal reflection. The electric field of the evanescent wave decays exponentially with distance from the interface. If the rarer medium is absorbing, then the evanescent wave will interact with the rarer medium and energy will be lost upon total reflection, hence attenuated total reflection[13].

The amplitude of the evanescent field in medium 2 under these conditions can be conveniently expressed as an exponential function of distance along the z-axis in medium 2. The decay of the electric field amplitude at the surface of medium 2, E_0, to some value E at a distance Z from the surface, can be written as[16]:

$$E = E_0 \exp -\frac{2\pi}{\lambda_1}\left(\sin^2\Theta - n_{21}\right)^{1/2} Z \qquad \text{(eq. 1.7)}$$

Where $\lambda_1 = \lambda/n_1$ is the wavelength of the radiation in medium 1, λ is the wavelength in free space and Z is the distance from the surface[14]. The exponential constant in eq. 1.7

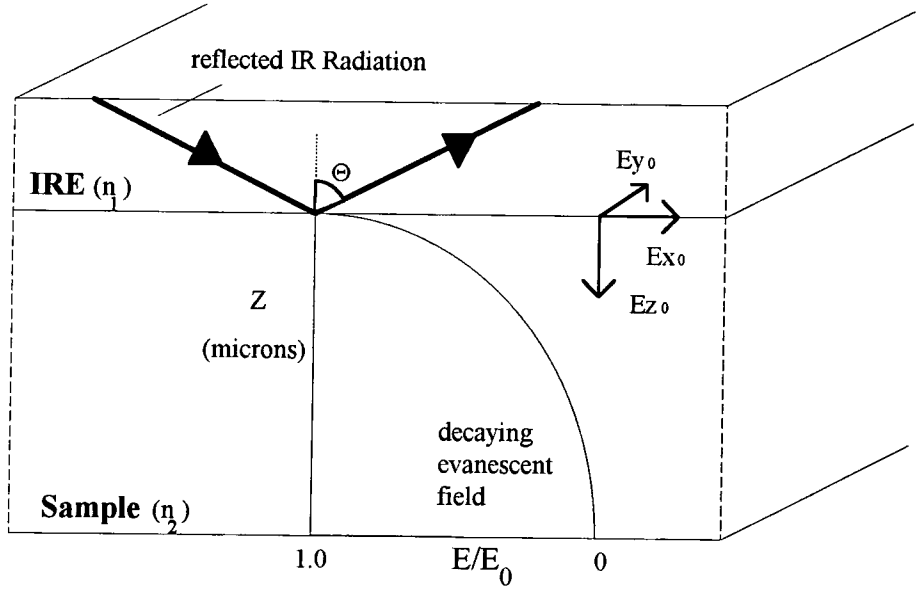

Fig. 1.3 - Representation of the base ATR experiment. The IR radiation propagates through the IRE, and the evanescent field penetrates the rarer sample medium and decays exponentially with distance from the IRE/sample interface. The evanescent field is a nontransverse wave having components in all spatial orientations. Reproduced from ref. 16.

can be replaced by γ , the electric field amplitude decay coefficient and eq. 1.7 can be rewritten as:

$$E = E_0 \exp[-\gamma Z] \qquad \text{(eq. 1.8)}$$

An important feature of the evanescent wave is that it is not a transverse wave and, therefore, has vector components in all spatial orientations and can interact with dipoles in all orientations.

The reflectance of the attenuated wave can be written as[16]:

$$R = \frac{I}{I_0} = \exp(-\alpha d_e) \qquad \text{(eq.1.9)}$$

$$R = 1 - \alpha d_e = 1 - a \qquad \text{(eq.1.10)}$$

Where d_e is the effective thickness, α is the absorptivity and a the absorption parameter. The effective thickness represents the thickness that is necessary in transmittance measurements to obtain the same absorbance as a single reflection at the phase boundary of medium 1. The absorption parameter, a, is equal to αd_e for a single reflection.

In order to increase the sensitivity, multiple reflections are used. With N fold reflections, the total reflectance is expressed as:

$$R^N = (1 - \alpha d_e)^N \qquad \text{(eq.1.11)}$$

Treatments of the theory of attenuated total reflection spectroscopy (ATR) centre on the properties of the evanescent field, since by virtue of its existence the phenomenon of internal reflection spectroscopy is possible. The properties of the evanescent field are illustrated in fig. 1.4. As shown in this figure, there are two polarizations, one parallel to the plane of incidence called transverse magnetic, TM, parallel, or P waves, and the other perpendicular, TE, senkrecht, or S waves. The plane

of incidence is perpendicular to the plane formed by the surfaces of the denser and rarer plane formed by the surfaces of the denser and rarer media. There are three electric field amplitudes that can be defined at the surface of the rarer medium. The TE wave has one electric field amplitude associated with it, E_{y0} perpendicular to the plane of incidence and parallel to the plane of surface. The TM wave becomes elliptically polarized at the surface due to the oblique angle of incidence with the rarer medium, giving rise two electric field amplitudes associated with it, one is parallel to the plane of incidence, E_z and perpendicular to the plane of surface, and the other is parallel to the plane of incidence, E_{x0}, and parallel to the plane of surface. The mutually parpendicular electric field are shown in fig. 1.4.

The electric field intensity of standing wave at the reflecting interface (E_0) is one of the factors that controls the strenght of the coupling. The electric field will be considered separately for bulk materials and thin films.

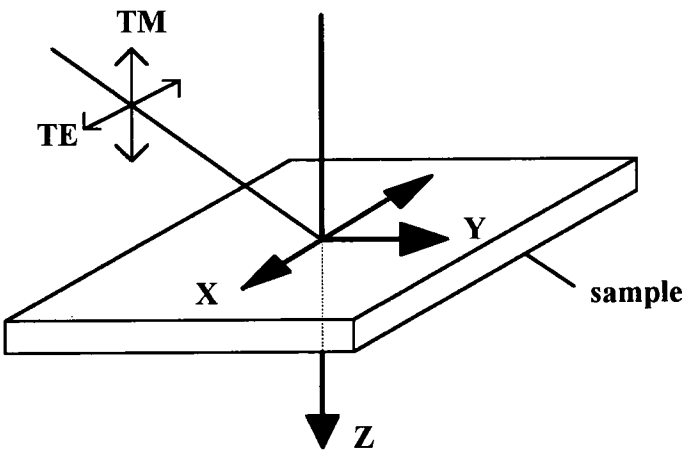

Fig. 1.4 - Definition of the axis and two TE and TM polarizations for FTIR-ATR studies. Reproduced from ref. 16.

Bulk Materials

For bulk materials, where the electric field amplitude falls to a very low value within the thickness t, that is, t»1/γ its amplitude is given by[14,16]:

TE Wave

$$E_{\perp} = E_{y_0} = \frac{2\cos\Theta}{\left(1-n_{21}^2\right)^{1/2}} \qquad \text{(eq. 1.12)}$$

TM Wave

$$E_{x_0} = \frac{2\left(\sin^2\Theta - n_{21}^2\right)^{1/2}\cos\Theta}{\left(1-n_{21}^2\right)^{1/2}\left[\left(1+n_{21}^2\right)\sin^2\Theta - n_{21}^2\right]^{1/2}} \qquad \text{(eq. 1.13)}$$

$$E_{z_0} = \frac{2\sin\Theta\cos\Theta}{\left(1-n_{21}\right)^{1/2}\left[\left(1+n_{21}^2\right)\sin^2\Theta - n_{21}^2\right]^{1/2}} \qquad \text{(eq. 1.14)}$$

The electric field amplitude is greater for //-polarisation than it is for ⊥-polarisation. The calculated decrease of E_0 with Θ is shown in fig. 1.5 for a non absorbing interface. E_0 is assumed to be unchanged for a very weakly absorbing interface.

The E values all increase slowly from the vicinity of Θ = 90° (grazing incidence). The values of E_{y0} and E_{Z0} reach a maxima at the critical angle while E_{x0} decreases abruptly near Θc and falls to zero near the critical angle due to the boundary conditions at the interface of the dense and rare media.

Returning to the absorption parameter, a, for the bulk case, it is given by:

$$a = \frac{n_{21}\alpha E_0^2}{2\gamma\cos\Theta} \qquad \text{(eq.1.15)}$$

Since $a = \alpha d_e$, eq. 1.15 can be rearranged to give the effective thickness. The values of d_e become:

TE Wave

$$d_{e\perp} = \frac{n_{21}\lambda_1 \cos\Theta}{\pi\left(1-n_{21}^2\right)\left(\sin^2\Theta - n_{21}\right)^{1/2}} \qquad \text{(eq.1.16)}$$

$$d_{e//} = \frac{n_{21}\lambda_1\left(2\sin^2\Theta - n_{21}^2\right)\cos\Theta}{\pi\left(1-n_{21}^2\right)\left[\left(1+n_{21}^2\right)\sin^2\Theta - n_{21}^2\right]\left(\sin^2\Theta - n_{21}^2\right)^{1/2}} \qquad \text{(eq.1.17)}$$

Thin Films

Another case of interest that can be treated in a straighforward manner is that of very thin films. In this case, where medium 2 is so thin as to have no controlling effect on the evanescent field, clearly, medium 3, behind medium 2 would control the decay of the field. Thus, for the thin film case, n_{21} must be replaced by $n_{31} = n_3/n_1$ or $n_{32} = n_3/n_2$ and the amplitudes of the electric fields at the surface of the rarer medium are given by[14,16]:

$$E_\perp = \frac{2\cos\Theta}{\left(1-n_{31}^2\right)^2} \qquad \text{(eq. 1.18)}$$

$$E_{//} = \frac{2\cos\Theta\left[\left(1+n_{32}^4\right)\sin^2\Theta - n_{31}^2\right]^{1/2}}{\left(1-n_{31}^2\right)^{1/2}\left[\left(1+n_{31}^2\right)\sin^2\Theta - n_{31}^2\right]^{1/2}} \qquad \text{(eq. 1.19)}$$

The absorption parameter will be given by:

$$a = \frac{n_{21}\alpha E_0^2 d}{\cos\Theta} \qquad \text{(eq. 1.20)}$$

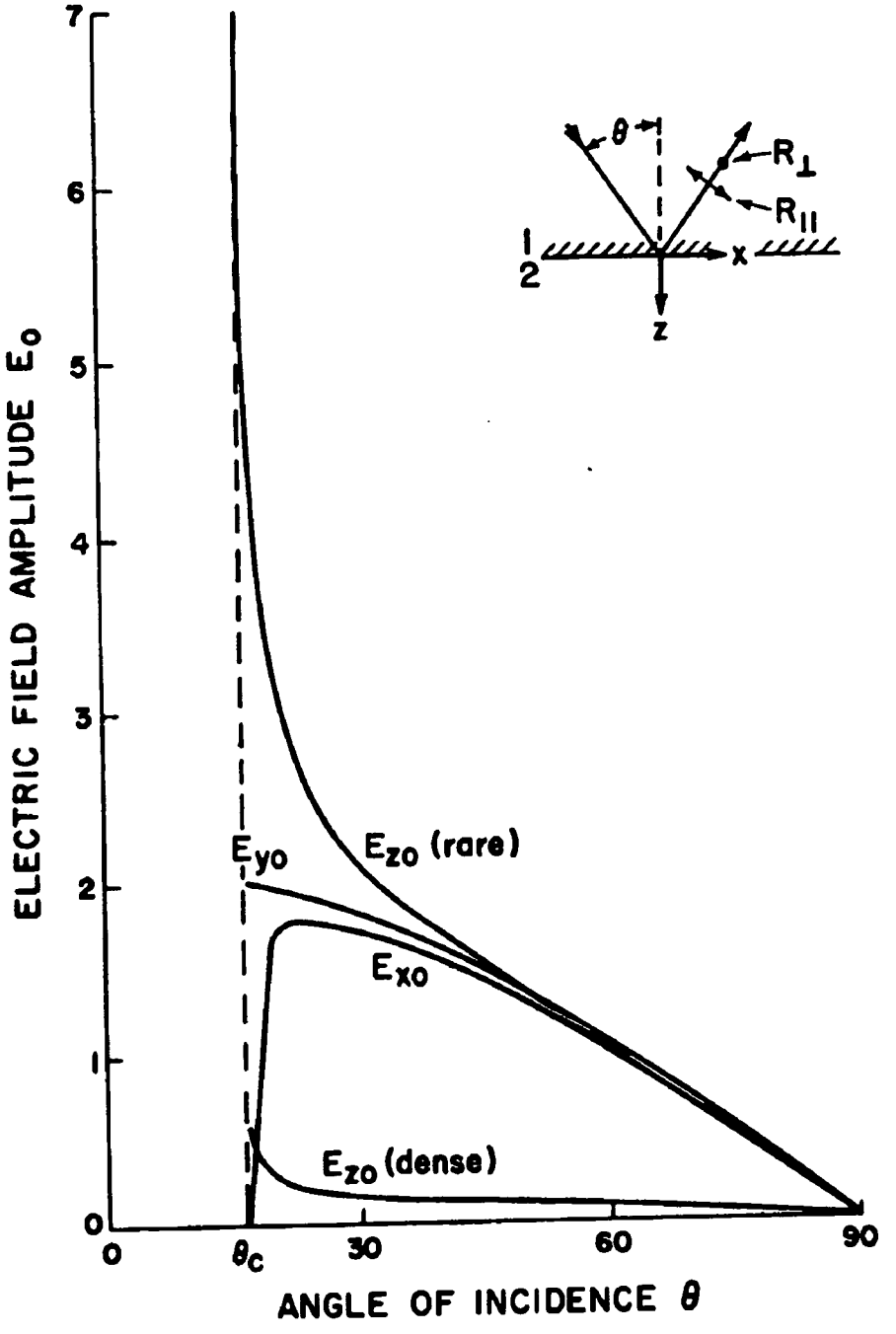

Fig. 1.5 - Electric field amplitudes for polarized radiation as a function of angle of incidence, Θ. Two values of E_{z0}, differing by n_{12}^2, are shown; the larger refers to the rarer medium 2. E_y is the field for ⊥-polarisation whereas E_x and E_z are the components of the field for //-polarisation. Reproduced from ref.14

Where d is the film thickness. Inserting the values of E in eq. (1.20), the effective thickness for perpendicular and parallel polarisations are, respectively:

$$d_{e_\perp} = \frac{4n_{21}d\cos\Theta}{\left(1-n_{31}^2\right)} \qquad \text{(eq. 1.21)}$$

$$d_{e_{//}} = \frac{4n_{21}d\cos\Theta\left[\left(1+n_{32}^4\right)\sin^2\Theta - n_{31}^2\right]}{\left(1-n_{31}^2\right)\left[\left(1+n_{31}^2\right)\sin^2\Theta - n_{31}^2\right]} \qquad \text{(eq. 1.22)}$$

It should be noted that in both cases (bulk material and thin film) the effective thickness for unpolarised radiation d_{e_u}, is given by:

$$d_{e_u} = \frac{d_{e_{//}} + d_{e_\perp}}{2} \qquad \text{(eq. 1.23)}$$

Harrick defined a parameter called depth of penetration[14]. The depth of penetration is defined as the distance required for the electric field strength of the evanescent field reach 1/e of its initial value at the interface as shown in fig. 1.6.

$$d_p = \frac{\lambda_1}{2\pi\left(\sin^2\Theta - n_{21}^2\right)^{1/2}} \qquad \text{(eq. 1.24)}$$

Where λ_1 is the wavelength of the radiation in the denser medium. The arbitrary nature of this parameter is emphasised by noting that the depth of penetration was defined as the depth at which the electric field amplitude falls to one-half its value at the surface ($Z = 0.693/\gamma$). However, since the electric field amplitude is 37% of its value at the surface, it appears that the depth that is actually sampled is greater than d_p. This was tested for polypropylene and polystyrene on KRS-5, and it was found that the actual depth sampled (d_s) was about three times d_p[17].

One of the first applications of FTIR-ATR was for the study of the surface and bulk properties of semiconductors. For this application, the internal reflection element

(IRE) was the material itself. However, for the study of most solids and liquids, an IRE made of a suitable dielectric is brought into contact or close proximity with the material to be studied. Typically, materials like Ge, ZnSe, KRS-5 (an alloy of TiBr and TiI) and sapphire are used because their transparency over a wide range in the mid-infrared radiation region.

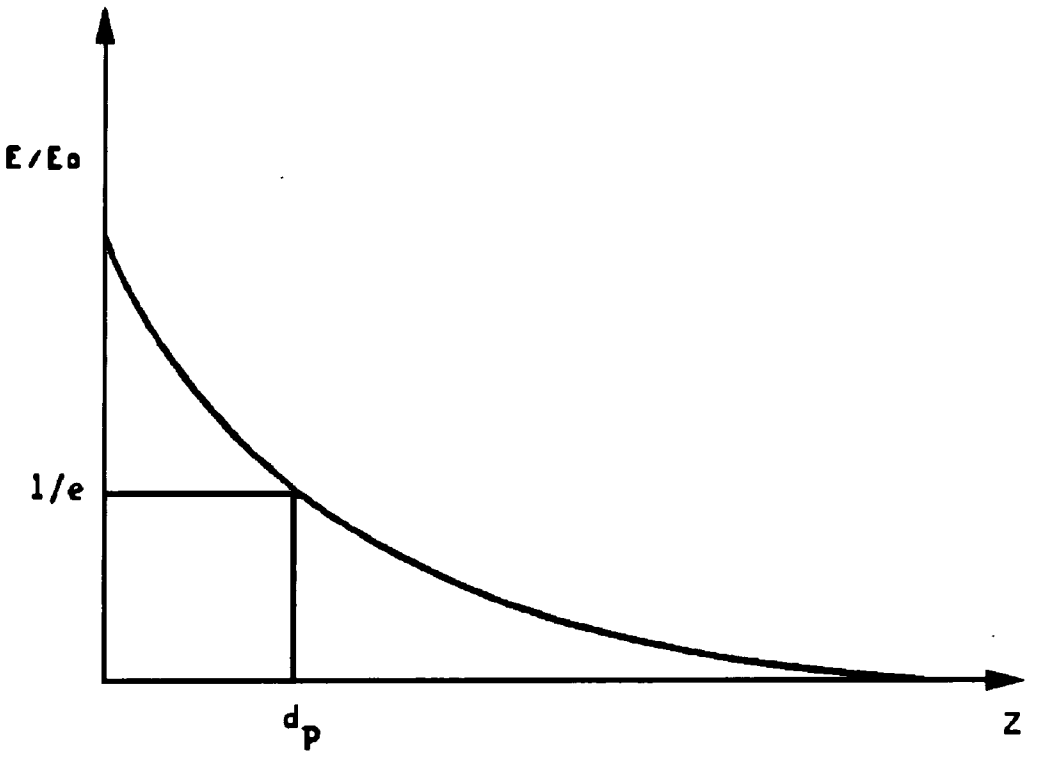

Fig 1.16 - Evanescent Field decay as a function of the depth from surface. Reproduced from ref. 11.

The optical contact between the sample and the dielectric element is the critical factor in obtaining a good spectrum. For hard or brittle polymers, it can be very difficult to reproduce the optical contact. Furthermore, it is also much more difficult to reproduce the optical contact for comparative quantitative measurements. However, for soft or

pliable polymers or solutions, ATR is an extremely versatile technique. Unlike transmission, the spectrum obtained is independent of sample thickness for all but the thinnest films. Thus one need not worry about having samples which are too thick. For liquids this thickness independence is even more of an advantage, since liquid transmission cells are often too thick for strongly absorbing liquids, and the liquid must often be diluted.

The application of FTIR-ATR in polymer science has been well documented[1-2,6-7,9]. Uses of FTIR-ATR in surface studies (including identification, modification and adsorption) and in biological systems have been very successful[16,18-21]. A very comprehensive review on theory and applications of FTIR-ATR was published by F.M.Mirabella[16]. In the next chapter we will demonstrate the use of FTIR-ATR for depth profiling study on polymer laminates. In this work surface and second layer spectra were obtained using an ATR device and digital subtraction.

1.5 - DATA ANALYSIS

Polymer systems are often complex. For example, crystalline and amorphous regions coexist in semi-crystalline polymers. In addition different conformational structures may be observed in these regions. Any physical or chemical treatment of a polymer will induce structural changes. The knowledge of which is essential for a better understanding of polymer properties[22].

Using a variety of data processing techniques developed basically by Koenig and co-workers[2,4,22,23] it is possible to analyse quantitatively such complex systems as well as eliminate spectral distortions caused by scattering and reflection and isolate spectral features.

Such techniques include factor analysis, ratio method, spectral subtraction and Fourier self-deconvolution. Many of these data processing algorithms rely on the

intensities of spectral bands being linearly proportional to the concentration of each component in the sample.

1.5.1 - Integrated Intensities

The absolute intensity of an infrared absorption band relates the spectrum to the number of molecules being observed. If infrared radiation of intensity I_0 is incident on a cell of pathlength l/cm then the transmitted radiation I is given by:

$$I = I_0 \exp(-\varepsilon.l.c) \qquad \text{(eq. 1.25)}$$

Where c is the concentration (moles.dm^{-3}) and ε is the extinction coefficient. The extinction coefficient is the reciprocal value of the pathlength through which the light must pass to be reduced to the 1/eth part. Eq. 1.24 is the well know Bouguer-Beer-Lambert law, which is simply abbreviate as Beer's law[3], and applies to monochromatic radiation.

As the radiation reaching the detector is not monochromatic, this means that Beer's law can never be exactly obeyed. Beer's law may also not be obeyed when solutions are highly concentrated or when there are strong intermolecular interactions. In these cases, molecular aggregates may be formed thus effectively reducing the number of solute species and hence the absorption.

Generally is useful to discuss the total integrated absorption of the band. Quoting only the peak height gives no information on width or shape, whereas the integrated absorption intensity, if obtainable, includes this information by definition.

If it is assumed that an isolated absorption band is being described, then ε starts from zero, goes through a maximum and returns to zero. A band may be described by the Lorentzian function[3]:

$$\varepsilon = \frac{a}{b^2 + (\nu - \nu_0)^2} \qquad \text{(eq. 1.26)}$$

Where 2b = half-width , a/b^2 = maximum intensity and ν and ν_0 are the frequencies.

This function only reaches zero at ± infinity, so the limits of integration must be chosen such that the error in the wings is small. Were the exact form of the band shape truly Lorentzian then the integrated intensity (A) would be found easily:

$$A = \frac{1}{c.l}\int \log(\frac{I}{I_0})d\nu \qquad \text{(eq. 1.27)}$$

1.5.2 - Spectral Subtraction

Spectral subtraction has become a most important tool in the arsenal of the IR spectroscopist and its utility is widespread. Spectral subtraction allows one to study solid samples with high precision since we can correct for differences in sample thickness. One can remove interfering absorbances, purify the spectrum by removing artefacts, solvents, or others impurities[4].

There are many problems using spectral subtraction, i.e. when the components interact with each other to produce frequency shifts and changes in intensities. Problems in subtraction also arise when the samples are too thick or imperfect so that the absorbances are not linear. Finally, spectral subtraction is only applicable to spectra obtained in the absorbance mode, that is, spectra plotted in the %T mode are not linear but exponential and should never be digitally subtracted. Optical subtraction (solution minus solvent) is possible if one has a truly double beam instrument and perfectly matched cells.

One example of use of spectral subtraction is on separation of a heterophase system that exhibits a composite spectrum. Specifically, it is possible to obtain spectra of pure crystalline or pure amorphous phase materials when a pure sample of either does not exist[3]. Because the crystalline phase often has a different, and more ordered,

orientation than amorphous phase, these differences can lead to different spectral characteristics. If samples can be obtained in which the relative concentration of crystalline and amorphous phase changes, then spectra of the pure components can be obtained. Of course, this technique is not limited to heterophase crystalline/amorphous polymers samples, but it can be applied to a wide variety of similar problems[24-27]. Another characteristic of polymers that can often be detected by absorbance subtraction is compatible and incompatible blends. In an incompatible mixture, two or more polymers are mixed but they do not interact. Therefore, the spectrum of the blend is equivalent to the sum of the spectra of the pure polymers in the appropriate concentrations. On the other hand, a compatible blend has an interaction between chains such that significant changes in the chain conformations occur and there is a chemical interaction that affects the hydrogen or dipolar bonding sufficiently to perturb the normal vibrations of one or both polymer chains. Either change in a compatible blend can alter the spectra of the pure components so that the spectrum of the blend is not a linear combination of the pure component spectra. After the subtraction, a residual spectrum remains that corresponds to the interaction of the compatible components. A great deal of study of compatible and incompatible polymer blends has been completed by M.M. Coleman[28]. Spectral subtraction will be discussed in more details in next chapter.

Chapter 2

Depth-Profiling of Polymer Laminates Using FTIR-ATR Spectroscopy.

CONTENTS

2.1 - *INTRODUCTION*

Polymeric materials have become increasingly important in technology, as have multilayered structures, composite material (polymeric matrixes reinforced with fillers to improve mechanical properties) and blends (polymer mixtures). Applications of polymer films are now vital in various fields like the design and construction of biocompatible surfaces [29-30], gas and liquid separation membranes[31-32] and in the coating and adhesives industry[33-34]. As a consequence, adequate knowledge of the chemical composition and distribution near to a polymer surface or across a polymer-polymer interface is extremely important, since a significant proportion of the properties of these materials depend on these surface and/or interface properties.

The ability to characterise the chemical and morphological structure of surface and/or interface is important for the evaluation of performance.

The surface and interface properties of polymers depend on both the processing conditions used and the composition of the polymer. The surface properties can change in an unpredictable manner due to contamination, weathering and migrations of additives or groups. Alternatively, the surface layer can be deliberately changed by chemical reactions, an electric discharge, plasma and ion beams and chemical or physical etching[35].

Studying surface and interfaces is difficult for two main reasons. The first is the necessity of observing a layer of limited thickness, so that surface properties can be distinguished from bulk properties; the second is sensitivity because very often the species of interest are present in rather small amounts.

Infrared reflection spectroscopy has been used for many years as a means of obtaining spectral information that is more representative of the surface of a material than the bulk[6,36-38]. For example, spectroscopists in the plastic industry have used reflection technique extensively, not only to qualitatively characterise polymer surfaces but also to provide quantitative measurements relating to a wide range of physical and chemical properties[6]. These have included the degree of molecular orientation at the

surface of films and fibres[39-41] and the effect of photodegradation and thermal curing as a function of time and depth[42]. The definition of what constitutes a surface or surface layer has become rather vague, particularly with the widespread introduction of techniques such as X-ray photoelectron spectroscopy (XPS) and secondary ion mass spectrometry (SIMS)[6]. These techniques yield elemental and structural information from a depth of ≈5 to 50 Å from the sample boundary, and in many cases can justifiably claim to provide spectroscopic data from a depth more relevant to the effect of interest. However, they also present some disadvantages as, for example, the requirement for a high vacuum and the need for specific surface preparation. The development of FT-IR leading to increasing sensitivity and selectivity made the FTIR one of the most versatile, fast, inexpensive and conclusive methods for surface characterisation with the advantages that: 1) the measurements are done under ambient atmosphere, 2) it is a non-destructive technique, and 3) it has the capability to give detailed structural information. The disadvantage is the relatively poor surface sensitivity; although it has reached a level of 0.01μm for wide range of samples[1].

2.1.1 - FTIR-ATR for Surface and Interface Studies

The ability of ATR infrared spectroscopy to detect and quantify a thin surface or interface layer, arises from the nature of the evanescent wave produced in attenuated total reflection, already discussed in chapter 1.

In internal reflection spectroscopy, an optical attachment to the spectrometer is used to direct the sample beam through a transparent internal reflection element (IRE) against which the sample is placed. An angle of incidence is selected which permits the radiation to traverse the crystal and be reflected from the crystal-sample interface a selected number of times, and then ultimately be redirected into the spectrometer. Some of the energy of radiation penetrates the sample at the point of reflection, with the absorption of energy occurring in the same way as in transmission spectroscopy[16].

The geometry of the internal reflection optics and the relative refractive indices of the sample and IRE determine the number of interface reflections and the depth of penetration of the sample (Eq.I.24) and, therefore, the absorption intensity of a given sample.

The depth of penetration of the wave is also a function of the wavelength of the radiation. A greater depth of sample is penetrated at longer wavelengths than at shorter wavelengths.

Practical application of FTIR-ATR involves the control of these variables. The spectra obtained may be quite similar in appearance to transmission spectra or differ considerably in band shape, intensity and, to a lesser extension, position.

For versatile applications to surface analysis, internal reflection attachments, which permit a selection of angle of incidence and a choice of IRE, are needed. The choice of these two major, controllable operating parameters has been considered in detail elsewhere[17]. Some of the primary considerations are as follows[16-17]. The effective thickness and the penetration depth increase as the critical angle is approached, so that one can sample various depths by adjusting the angle of incidence. However, the number of reflections will decrease, as well as a decrease in the penetration depth, as Θ approaches grazing incidence. Further, the area sampled varies with the angle of incidence, increasing with Θ as a function of $1/\cos\Theta$. For non normal incidence on the IRE aperture, one must correct for the effects of refraction of the beam. The effective thickness and penetration depth increase as n_2/n_1 increases toward 1. Usually, only n_1 is controllable, so that by choosing an IRE with higher refractive index, one can sample a thinner surface layer. However, as n_2/n_1 decreases, the penetration depth decreases. These points are emphasised because it is often desired to observe thinner surface layers by varying these parameters, but this involves the disadvantage of weaker signal intensities.

2.1.2 - Practical Considerations

Some considerations necessary to obtain a high quality spectrum and quantitative data in ATR are considered in this section. The primary problem in obtaining high quality spectra or to perform quantitative ATR work is the difficulty in obtaining good and reproducible contact of the sample with the IRE. In this work this problem was solved by depositing the film directed on the ZnSe prism.

Alignment of the ATR accessory inside the instrument is a practical problem that can lead to poor results if not done properly, or can be more time consuming than desired. The use of an oscilloscope can substantially aid the experimentalist in aligning the system. By monitoring the detector output signal with an oscilloscope, the system can be aligned for maximum energy throughput with the free-standing IRE. Then, when the sample is in place, the reduction of the detector output signal is a direct measure of the absorption of the sample, neglecting other possible losses which are typically small.

Cleaning of the IRE varies according to the requirements of the measurements to be made, but in any case an appropriately cleaned IRE surface is necessary. Simply looking at the background spectrum of the cleaned IRE will reveal if it is sufficiently free of contaminants in most cases. Cleaning procedures can be as simple as dipping in an appropriate solvent followed by gentle wiping with a non-abrasive optical lens tissue. More rigorous cleaning involves washing in a series of solvent baths, rinsing thoroughly, followed by drying in a vapour dryer[7]. Ultimate cleaning methods involve glow discharge and vacuum baking. In our case the first procedure was applied.

2.13 - Depth Profiling in FTIR-ATR

The first statement that can be made concerning depth profiling in FTIR-ATR is that there is presently no accepted and tested theoretical treatment for ATR data that can yield an absolute, quantitative concentration depth profile of an absorbing species at a

surface. The reason that concentration depth profiling is not straightforward in ATR is that even in the absence of absorption, the evanescent wave decays exponentially in the sample surface, and is, therefore not characterised by one constant field intensity throughout the depth observed. The problem of defining an unknown concentration depth profile with an exponentially decaying probing field is formidable. A simplification used in the majority of depth profiling studies was to assume that the depth sampled was d_p[43-46]. Although this approach should at least give a semi quantitative description of the concentration depth profile, d_p is not the actual depth sampled as discussed in chapter 1. Furthermore, no simple relationship between the depth profile, based on d_p, and the true depth profile can be expected, as pointed out in one such study[44]. In other studies[47-48] the effective thickness, d_e, was used as the parameter defining the depth sampled. However, this is not a legitimate use of d_e since it is a total interaction parameter as discussed in chapter 1, and can not be correlated to d_p except when very close to the critical angle. Several attempts have been made to treat the depth profiling problem in a more rigorous way. Tompkins[49] presented arguments to demonstrate that some profiles could not be distinguished from one another, but if a step distribution was assumed, information about depth and concentration could be obtained by making measurements at several angles of incidence. A method was proposed and demonstrated to obtain the concentration depth profile of an assumed step profile. Little use of these methods was made in subsequent publications of depth profiling studies.

Clearly d_p depends on several parameters simultaneously, but equally obviously it may be varied systematically for a given polymer system on a given IRE by varying the incident angle. Fig. 2.1 shows how the infrared absorbance proportional to $(E/E_0)^2$,[14], is predicted to vary as a function of incident angle for varying d_p values calculated from Eq. 1.7 for a single absorbing system.

However, the penetration of the infrared radiation can be reduced below the

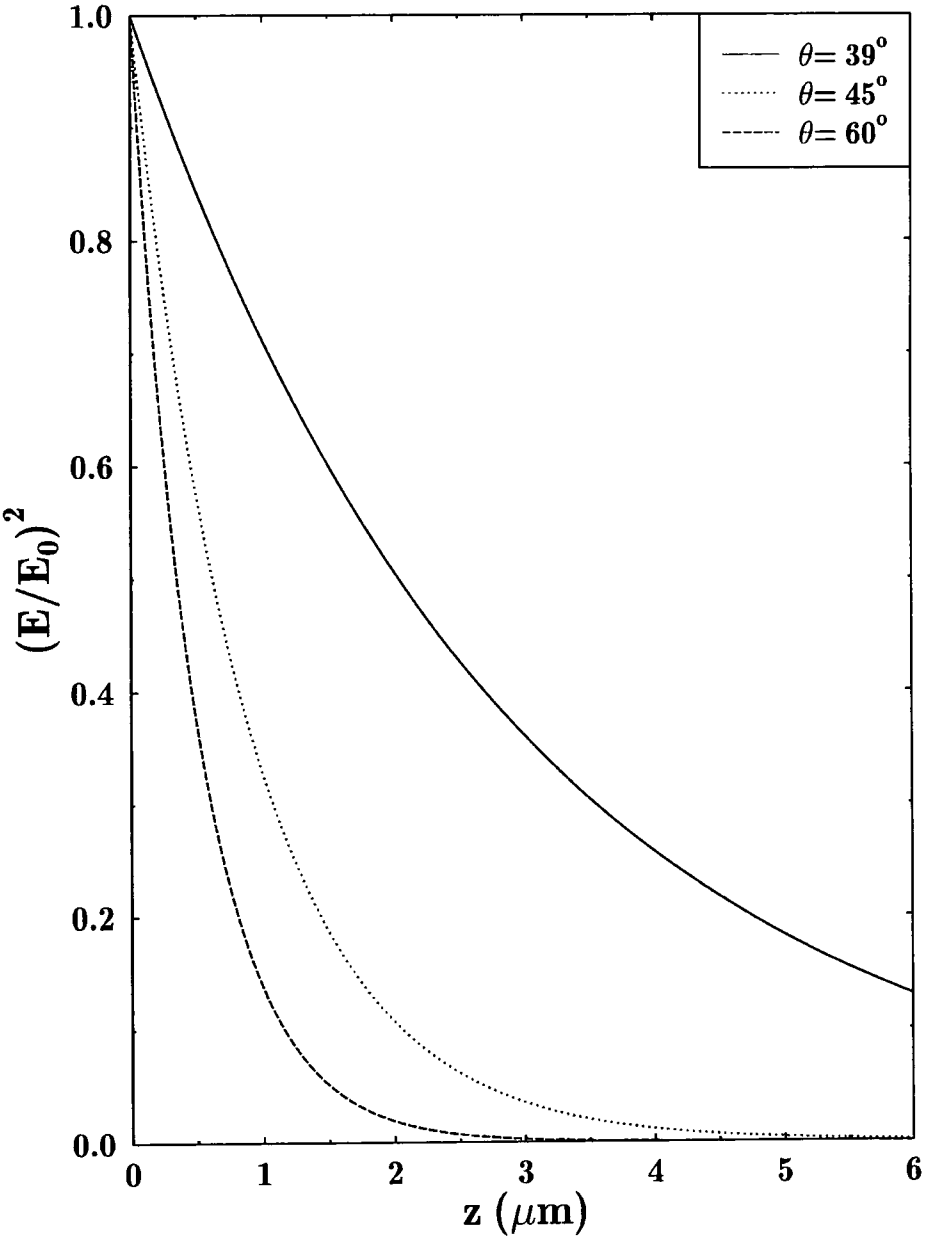

Fig. 2.1 - Electric field distribution for a ZnSe ATR crystal as a function of the incidence angle.

limits allowed by variation in angle of incidence and refractive index of IRE, by depositing on the examined surface a film of controlled and uniform thickness. This experimental approach is called "the barrier film method". Of course, this reduces not only the thickness of the observed layer but also the sensitivity. If the thickness of the barrier layer can be determined, the penetration of the fraction of the evanescent field beyond the barrier layer can be estimated. Typically, the thickness of the barrier layers is determined by monitoring a "thickness" band in the transmission IR spectrum. The measured variable can then be plotted against the depth beyond the barrier layer penetrated by the evanescent wave. This yields an approximation to a depth concentration profile. Most often the variable used to determine the depth sampled was d_p. The use of these methods for ATR has been well documented[50-54].

In this chapter we will describe some experiments carried out using the barrier film technique. As part of a programme aimed at the study of molecular interactions and diffusion at a polymer/solution and polymer/polymer interface, we have carried out a detailed assessment of the reliability of the commonly used equations for the distribution of the electric field intensity for laminates constituted of poly(methylmethacrylate) (PMMA) and poly(vinyl alcohol) PVOH at different base layer thicknesses and different angles of incidence on a ZnSe substrate. By varying the "barrier" layer of PMMA we will demonstrate that different effective penetration depths into the PVOH are achieved, in very good agreement with the calculated electric field as a function of distance away from the substrate surface. Such work forms the basis for depth profiling measurements in order to detect interfacial interactions between the polymer molecules.

2.1 - Deposition Techniques

Generally, for qualitative studies, sample preparation does not require significant effort, and IR spectra of polymers can be readily obtained. Polymer mixed with potassium bromide and then pressed into pellets, or films prepared from melt or cast

from solution, can be easily studied. However, for quantitative studies, where the thickness control must be rigorous, the sample preparation requires much more attention.

The next paragraph will briefly describe the main techniques available to obtain thin films[7].

a) **Dry-casting** - This involves evaporation of the solvent from a solution of the polymer spread on a horizontal surface. The substrate must be thoroughly cleaned and wiped with soft tissue. Better uniformity of thickness can be obtained when drying is carried out slowly, e.g. by covering the substrate with polymer solution with a small inverted beaker. The traces of solvent can be removed by heating the film in a vacuum oven. With this technique, knowing the volume and concentration of the polymer solution, the polymer density and the substrate area, the film thickness can be estimated.

b) **Wet-casting** - Involves precipitation of the polymer film from a solution onto a substrate. The substrate is immersed in a solvent in which the polymer is insoluble but it is miscible with the solvent used to form the polymer solution.

c) **Melt-casting** - This technique involves melting the polymer between two flat polished metal plates separated by spacing pins under high pressure at the required temperature. Quick cooling may give a sample with little or no crystallinity.

d) **Dip-coating** - This involves the covering of a surface with a film by withdrawal of the substrate from solution at a constant speed. The film thickness will increase with increasing viscosity and withdrawal speed, and will decrease with increasing surface tension. The angle of withdrawal and the shape of the substrate also have an influence[55]. This technique will produce films with some preferential orientation of the molecules, especially if the polymer used has a high molecular weight. One way of minimising this effect is to anneal the film for several hours at a temperature above the glass transition temperature.

e) **Adsorption from solution** - The material which is intended to act as the adsorbed (adsorbant) is subject to a static or flowing stream environment of the adsorbate. The system can be examined after a period of equilibrium or *in situ.*

f) **Spin-coating** - Involves the covering of a surface by dropping a polymer solution into a substrate. In this case, the substrate is placed on a rotating platform, where it is possible to control the rotation speed. The film thickness will increase with decreasing rotation speed.

2.2 - *EXPERIMENTAL*

2.2.1 - Polymer Film Preparation

The two layered model sample consisted of a surface layer of poly(vinyl alcohol) (PVOH) of constant thickness and a base layer of poly(methylmethacrylate) (PMMA) varying in thickness as showed on Fig 2.2. Both polymers are commercial samples purchased from Aldrich. The characterisation data available are: PMMA of very high molecular weight and PVOH (99.8 % of hydrolysis).

This experimental system was chosen for two reasons. The most important reason was the fact that it was possible to find a solvent that dissolves the PVOH but not the PMMA. Therefore the PVOH could be placed in direct contact within the PMMA film, establishing optical contact. The second reason was that it is not unreasonable to expect interfacial interactions (by hydrogen bonding) between these two polymers.

The PMMA base layer was prepared directly onto the IRE by dip coating procedures[55]. The dipping equipment used is showed on Fig 2.3 and 2.4. The equipment allows speed variations on a range from 2 to 60 mm/min. By varying the withdrawal speed and/or the solution concentration it was possible to obtain PMMA films in a

thickness range from 0.1 to 10μm.

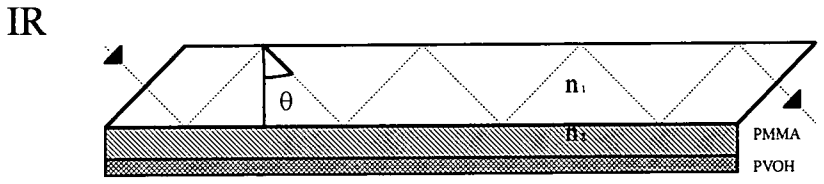

Fig. 2.2 - The internal reflection element (IRE) and associated polymer laminate of PMMA and PVOH.

Dichloromethane(DCM) of spectroscopic grade, purchased from Aldrich, was used as solvent for dipping the PMMA films. The manipulation of this and all the others solvents described in this work was carried out in a fumehood using safety glasses and suitable gloves. Solutions of different concentrations were used to produce the desired thickness. After the dipping, the crystal and film were transferred to a vacuum desiccator. The film was placed in an oven to remove residual solvent for 12 hours at 60° C. At the end of this time, the film was removed from the oven and allowed to cool to room temperature inside a desiccator.

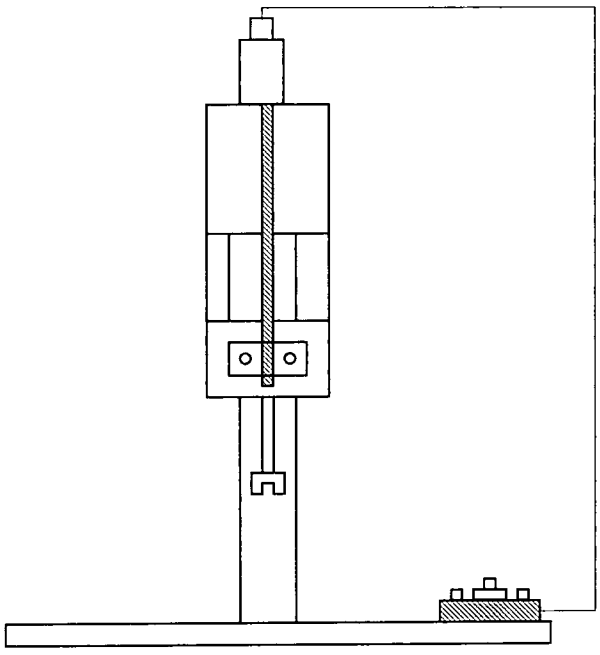

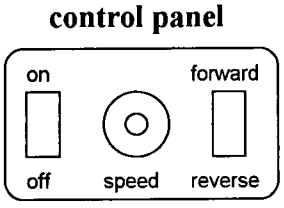

Fig. 2.3 - Dipping equipment - front view

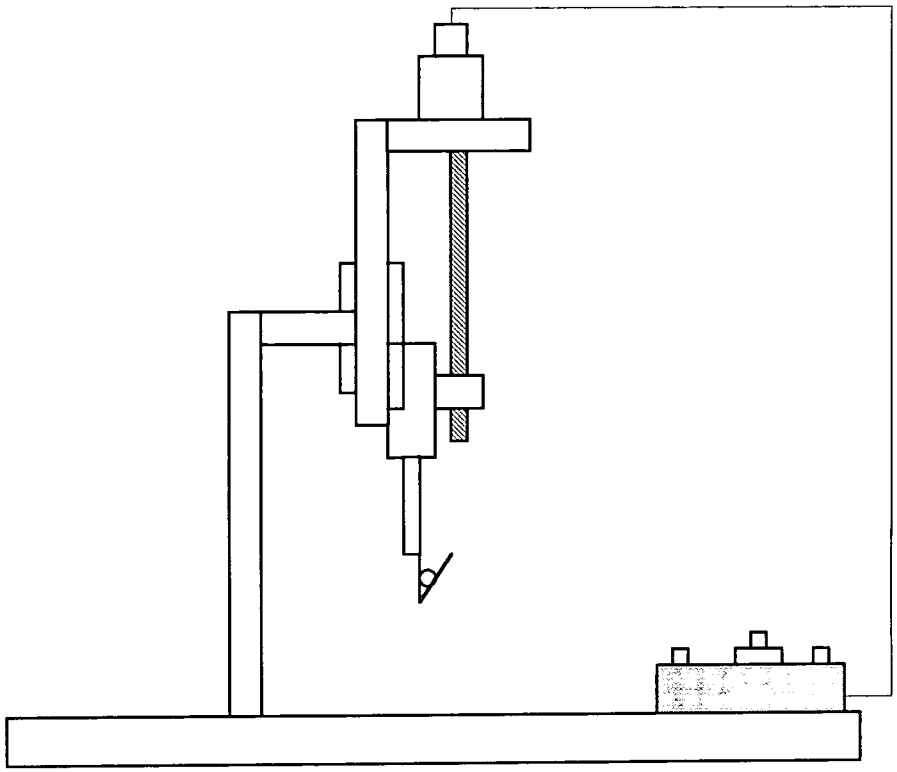

Fig. 2.4 - Dipping equipment - Side view

The PVOH was deposited over the PMMA film by the same technique using water as a solvent. The PVOH thickness was kept constant at 0.1μm. After the deposition, the same drying procedure was used.

The thickness of the two-layered system was determined mechanically using a α-step 200 trademark of Tencor Instruments Ltd. This equipment allows thickness measurements in a range of 100Å to 160μm. For this measurement a sharp knife edge was used to chip out a portion of the film to leave a bare substrate surface and the step height then was measured at several locations. The results presented represent an average of 10 measurements done at 5 different points of the crystal.

The PMMA thickness was obtained from calibration curve constructed using IR transmission measurements on the ester ν(C=O) band.

2.3.2 - FTIR-ATR Procedures

Measurements of the infrared spectra were made using a Mattson Sirius 100 spectrometer fitted with a broad band MCT detector. Data were collected over 250 scans with a resolution of 4 cm^{-1}. The ATR measurements were made on a ZnSe IRE at nominal incident angles varying from 39° to 60° using a variable-angle ATR unit purchased from Graseby Specac Ltd. Optical alignment of the unit was made to achieve maximum throughput of the infrared beam energy to the detector. Once an optimal alignment at a given angle of incidence was attained from an individual cell, insertion or removal of the cell from the holder did not affect the alignment. However, it was necessary to readjust the optics every time the incident angle was changed.

For each of the different thicknesses of PMMA, FTIR-ATR and transmission spectra were first measured for the dried and cooled base layer alone. The transmission spectra were used to determine the film thickness using a calibration curve previously prepared. The surface layer was then deposited and FTIR-ATR spectra were obtained for the two-layered samples at different incident angles. The ATR "absorbance" spectra were calculated by ratioing the sample spectrum against the appropriate reference spectrum, which had been previously collected without the sample.

2.3 - *RESULTS AND DISCUSSION*

2.3.1 - Solution Deposition - Control of Thickness

The main objective of this part of the work was to obtain thin polymer films with a uniform thickness in a controllable and reproducible way. The technique used, as already stated, was the dip-coating. We will show, with the aid of some typical results, that this is an effective technique.

The first experiment was performed with a 1% solution of PMMA in dichloromethane and using different dipping speeds. The results are shown on table 2.1:

Table 2.1 - Thickness values as a function of dipping speed for a 1% solution

Speed	Day			
	1	2	3	4
4mm/mim	(0.20±0.04)μm	(0.17±0.03)μm	(0.18±0.02)μm	(0.18±0.03)μm
60mm/min	(0.21±0.02)μm	(0.22±0.01)μm	(0.22±0.02)μm	(0.22±0.02)μm

The second experiment was done using a more dilute solution (0.5%). The results are shown on table 2.2:

Table 2.2 - Thickness values as a function of dipping speed for a 0.5% solution

Speed	Day			
	1	2	3	4
4mm/min	(0.09±0.01)μm	(0.10±0.04)μm	(0.06±0.03)μm	(0.10±0.01)μm
60mm/min	(0.20±0.08)μm	(0.17±0.02)μm	(0.17±0.06)μm	(0.19±0.07)μm

These kind of experiments allowed us to draw two important conclusions. Firstly, that the thickness variation is much more sensitive to concentration variations than speed variations and secondly, that for the system in question (PMMA/dichloromethane) more concentrated solutions produce more uniform films.

Several other experiments were done using different concentrations and speeds and films were obtained in a thickness range of 0.1μm to 10μm. Using these different values, it was possible to construct a calibration curve, shown on fig. 2.5. This

calibration curve was used to estimate the film thickness of the PMMA layer in the laminate.

Another technique used to demonstrate the film uniformity was to obtain the transmission spectra at different points of the crystal and compare the values obtained for a band area. In our case, the ν(C=O) band was chosen. Table 2.3 shows some of the results.

Only films where the differences between the area at different points do not exceed 15% were used.

Table 2.3 - Values of absorbance for the ν(C=O) band at different points of the IRE

Position	ν(C=O) (cm^{-1})			
	exp.1	exp.2	exp.3	exp.4
1	0.90	0.32	0.56	0.48
2	0.62	0.31	0.54	0.47
3	0.56	0.28	0.48	0.45

2.3.2 - Results of Spectral Investigation

Before starting to analyse the results obtained for the laminates we will first discuss the results obtained with each one of the polymers (PMMA and PVOH) separately.

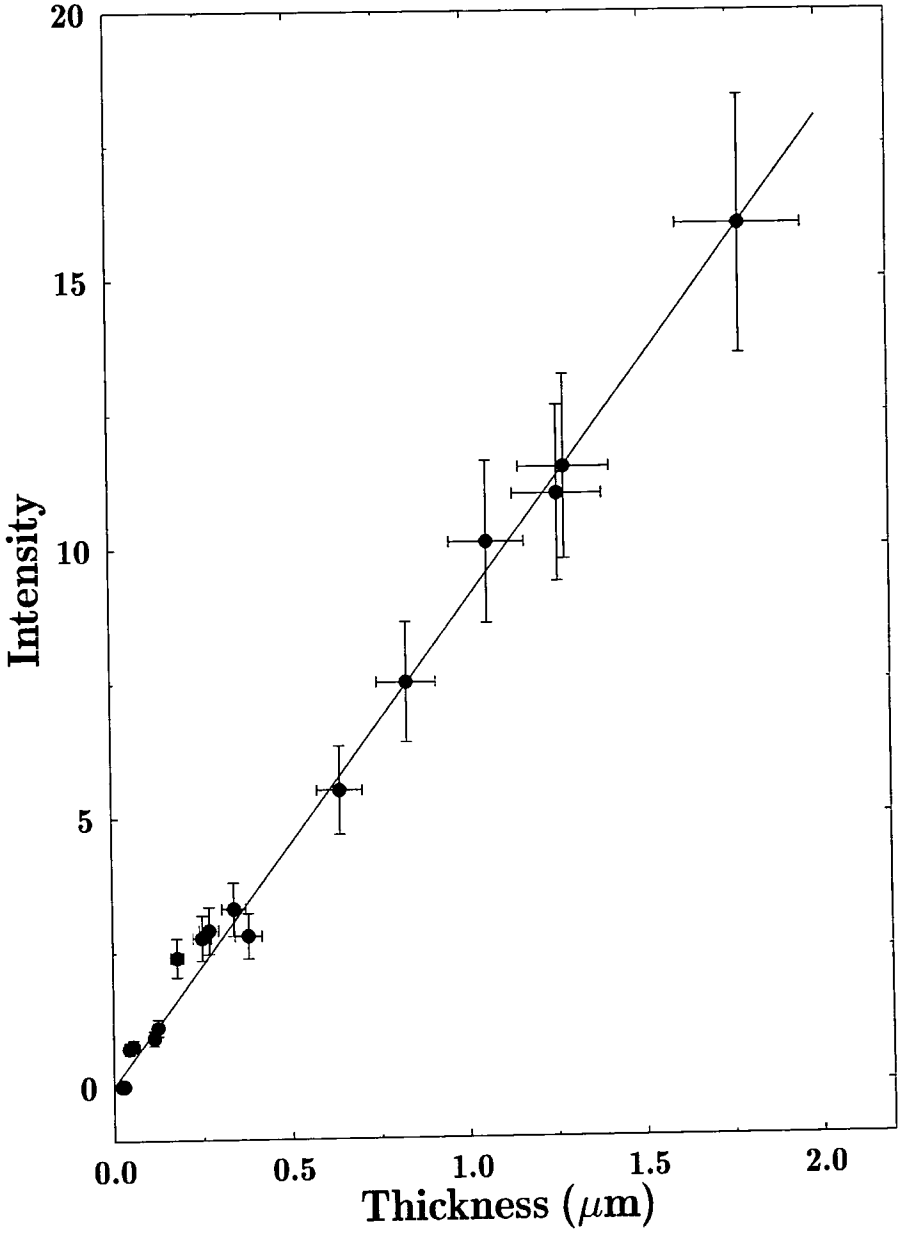

Fig. 2.5 - Calibration curve for the system PMMA/DCM.

2.3.2.1 - Poly(methylmethacrylate)

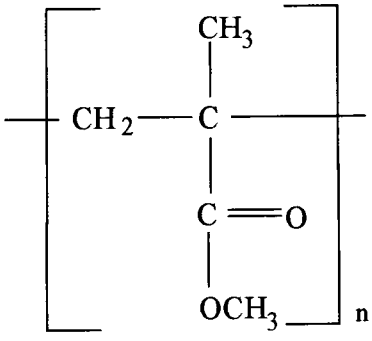

PMMA is a glass forming polymer and is the main component of well-known plastics (e.g. "Plexiglas") with excellent optical properties. The commercial polymer, which is produced by radical polymerisation, was formerly regarded as "atatic". Pure syndiotatic and pure isotatic PMMA can be prepared using ionic initiators.

The spectral investigation on the system PMMA/DCM started by checking the band assignments with the values found in literature[56-57]. The results are in very good agreement and can be seen below. The IR spectrum of PMMA is shown in fig.2.6 and assignments are given in table 2.4.

The spectrum consists basically of four groups of bands:

1) The range of C-H stretching vibrations is dominated by the methyl groups $I(CH_3)/I(CH_2)= 2$, see formula of basic unit.

2) The C=O stretching range shows a strong homogeneous ester carbonyl band at 1725cm^{-1}. According to Schouten[56] the band at 1729 cm^{-1} is split in the spectrum of the crystalline form, into a doublet at 1738 and 1725 cm^{-1}. Analogous splitting of the C=O stretching mode has been observed previously in the spectra of ordered structures of syndiotatic PMMA.

Differences in the IR spectra between amorphous and partially crystalline samples have been discussed previously[56-58]. Band characteristics of the amorphous phase were found at 1047 and 938 cm^{-1}, while characteristic bands of the crystalline phase were found at 1338, 1298 and 882 cm^{-1}.

3) CH deformation range showing 4 peaks in the region 1483 to 1388 cm^{-1}.

4) The C-O stretching of the ester band is a typical "regularity band" as can be seen from the behaviour of band splitting[56].

Splitting vanishes in copolymers with low MMA-content and decreases with increasing bulkiness of the alkyl group.

Although PMMA is a X-ray amorphous, some short-range order seems to be preserved in the amorphous solid, most probably helixes. The 1060 cm^{-1} peak is only found in syndiotatic PMMA.

Following the study of each polymer separately, the next step was to get transmission spectra of PMMA, using polarised light to investigate if there is some preferential molecular orientation caused by the dipping process, bearing in mind that no special precautions were taken to reduce this effect.

Here, we will refer to the parallel polarisation to the dipping direction as 0° and perpendicular to this direction as 90°. Fig. 2.7 shows the ν(C=O) mode for both polarisation as well as the result of subtraction. As we can see, the spectrum obtained with 0° polarisation it is not identical to the spectrum obtained with 90° polarisation. The spectrum obtained by subtracting the 90° and 0° spectra illustrates the dichroic effects observed.

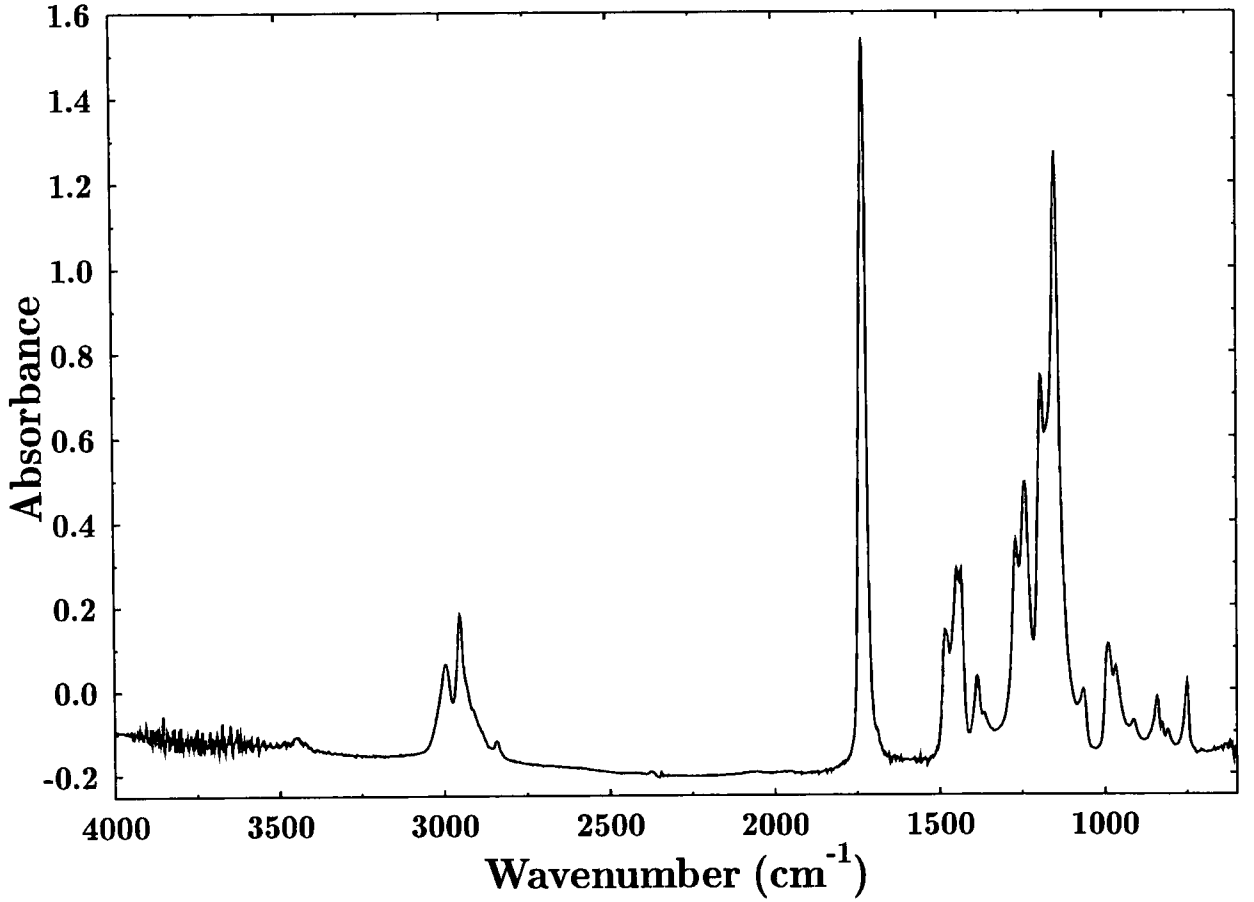

Fig. 2.6 - PMMA spectrum obtained by ATR. Film thickness = 0.34 μm.

Table 2.4 - Assignments of IR bands of PMMA

Wavenumber (cm^{-1})	Assignments
2995	α-CH_3 antisymmetric stretching, OCH_3 antisymmetric stretching
2958	α-CH_3 symmetric stretching, OCH_3 symmetric stretching, CH2 symmetric stretching
2930	CH_2 antisymmetric stretching
1726	C=O symmetric stretching
1483	α-CH_3 symmetric bending, CH_2 bending
1465	OCH_3 antisymmetric stretching
1448	CH_2 scissor bend
1455	OCH_3 symmetric stretching
1388	α-CH_3 symmetric bend
1296	delocalised, containing mostly backbone and methylene vibrations, characteristic of crystalline i-PMMA
1265	out-of-phase antisymmetric C-C-O stretching coupled with CH_2
1255	in phase antisymmetric C-C-O stretching coupled with CH_2
1190	no clear assignment, possibly C-O-C stretching
1150	combination of delocalised modes of various ester vibrations and CH_2 rocking modes
996	OCH_3 rocking
951	α-CH_3 rocking
842	not clear, probably CH_2 rocking

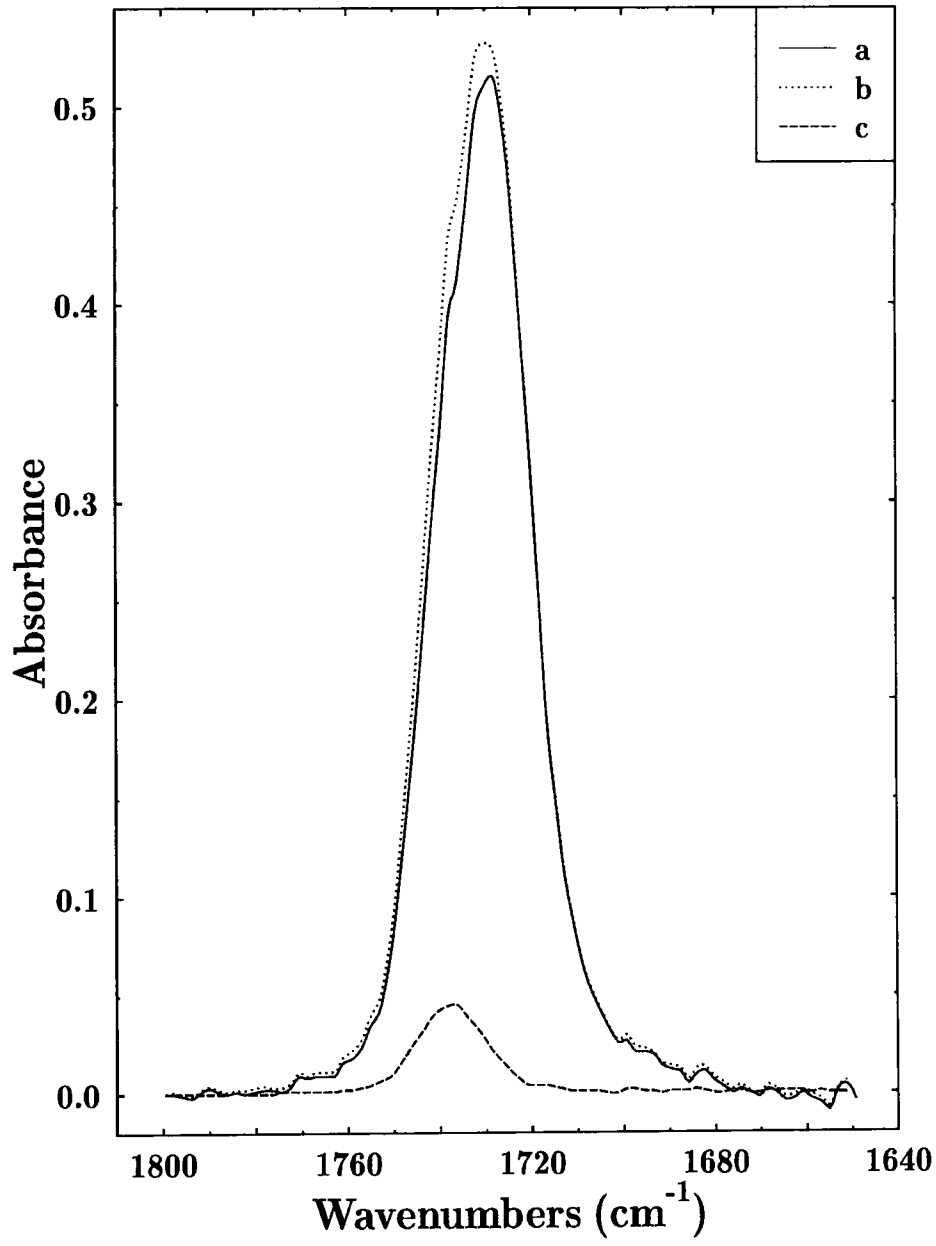

Fig. 2.7 - Polarisation effects on a PMMA film. a) 0^{o} polarisation, b) 90^{o} polarisation, and c) difference spectrum.

Fig. 2.7 also shows that the 1725 cm^{-1} absorption band is not a single band but that it is split into 1728 and 1736 cm^{-1}. As described before the splitting is characteristic of a crystalline form or a ordered structure of syndiotatic PMMA. Since the bands characteristic of crystalline phase were not found we can conclude that the material is not crystalline but do contain some ordered structure. Therefore, configurational regularity (tacticity) facilitates conformational order, the latter can induce crystallinity, but is not bound to do so (as in this case).

In order to try to quantify this orientation effect, Schouten[56] introduced an orientation parameter (OP) defined as:

$$OP_x = \frac{I_{90^\circ} - I_{0^\circ}}{I_{90^\circ} + I_{0^\circ}} \qquad \text{(eq.2.1)}$$

in which I_{90° and I_{0° represent the absorption intensities of band x using light polarised perpendicular and parallel to the dipping direction, respectively. For the case that all the helixes are oriented parallel to the substrate, it can be easily shown that depending on the orientation in the xy plane this value can vary in theory between 1 and -1. For the C=O stretching vibration, positive values for this parameter indicate a preferential orientation of the helical structures parallel to the dipping direction.

Using two experiments with different thickness, the OP values obtained were:

a) thickness(d) = 0.06μm

I_{90° = 0 533 cm^{-1}

I_{0° = 0 515 cm^{-1}

OP = 0.017

b) thickness(d) = 1.30μm

I_{90° = 1.881 cm^{-1}

I_{0° = 1.940 cm^{-1}

OP = 0.015

If we compare these values with the one found in literature for PMMA, (from 0.07 to 0.09) we can see that they are much smaller and, this fact was already expected since the above values were calculated for PMMA films obtained by LB technique which is designed to produce films with very distinct orientation al order. So in our case we can

conclude that for PMMA the dip coating introduces very little preferential orientation.

2.3.2.2 - Poly(vinyl alcohol)

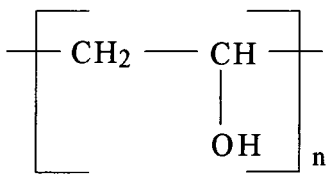

PVOH is produced by the hydrolysis of poly(vinyl acetate) (PVAc) yielding either a completely hydrolysed product (PVOH) or polymers containing residual acetate groups that can be considered as copolymers of vinyl alcohol and vinyl acetate. According to the supplier, the polymer studied is 99.8 % hydrolysed.

The major uses of PVOH fall into two categories. In one type of application, use is made of the water solubility of the polymer. It serves as a thickening agent for various emulsion and suspension, and as packing film where water solubility is desired. A major outlet is wet-strength adhesives. In the second type of use, the final form of the polymer is insoluble in water as a result of chemical treatment. The use of PVOH as a textile fibre is the major example.

The IR spectrum of PVOH is shown on fig. 2.8 and it is similar to that of its monomeric model substance 2-propanol[58]. The broad intense band with maximum of absorption at 3340 cm^{-1} is due to ν(OH) band shifted from its position at 3600 cm^{-1} to longer wavelengths and broadened by hydrogen bonding. The formation of hydrogen bonds (O-H...O) evidently weakens the O-H bond; within a series of similar compounds the spectral shift Δν is roughly proportional to the strength of the hydrogen bond[58].

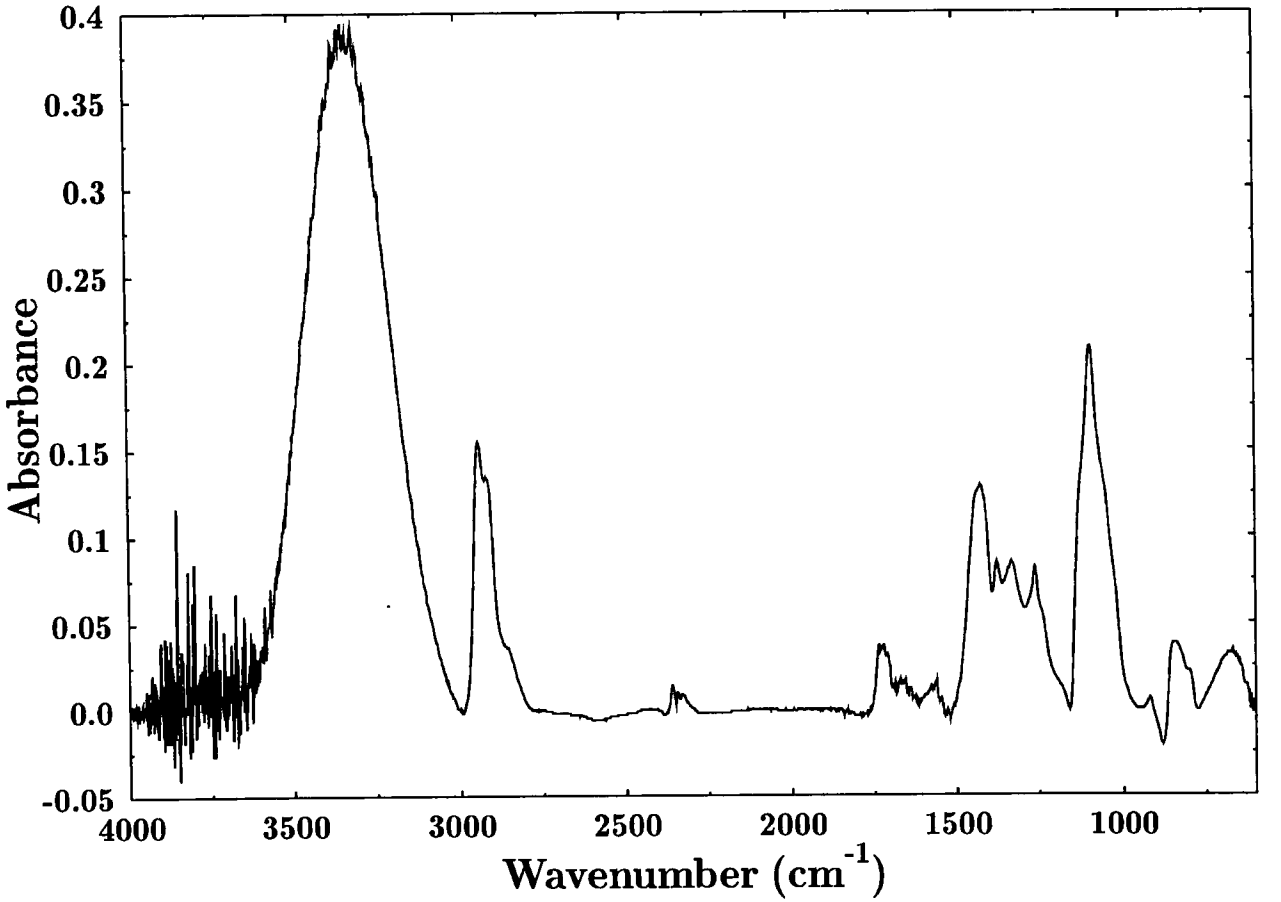

Fig. 2.8 - PVOH spectrum obtained by ATR. Film thickness = 0.1 μm.

The complete absence of any peak at 3600 cm^{-1} indicates the absence of any appreciable fraction of free OH groups in solid PVOH. This spectral range can only be evaluated for careful dried polymer samples, since water absorbs strongly in the same region and may act both as hydrogen donor and hydrogen acceptor in polymers showing no hydrogen bonds in pure state.

The stretching C-H vibrations in PVOH (fig.2.8) are found at 2920 cm^{-1} and 2950 cm^{-1}. The absence of any stretching C=O absorption near 1740 cm^{-1} as found in PVAc indicates complete hydrolysis of the starting material.

A second hydroxyl band in PVOH is the at ν(C-O) band of secondary OH groups at 1090 cm^{-1} near a "crystallinity band" at 1150 cm^{-1}.This peak increases by annealing and extensive dehydration over P_2O_5; IR measurements using polarised radiation and oriented samples also indicate the crystalline origin of these bands[57,59].

An extensive discussion of PVOH spectrum has been published by Krimm[59-60] and Tadokoro[61]. According to these authors, the 922 cm^{-1} band is characteristic of syndiotatic sequences.

As for PMMA, band in the 1400 cm^{-1} range are due to C-H deformation vibrations.

2.3.2.3 - LAMINATES

Before starting to analyse the results we will discuss the applicability of the spectral subtraction on FTIR-ATR spectroscopy. There are two fundamental assumptions in the use of absorbance subtraction[2,4]. First, it is assumed that the absorbance and shape of a band does not change with the optical thickness (defined by refractive index x thickness). Generally, one must prepare the absorbance values to be below 1 in order to meet the requirements of this assumption. The assumption is tested with every subtraction and, if the residual absorbance after a subtraction has a different shape from that of the original absorbance bands, then this assumption is violated and the

procedure or samples should be re-examined for the basis of the non-linear effects (i.e. holes, non uniformity, orientation, etc.).

The second assumption is that the absorbance of a laminate is the linear sum of the absorbances of the components, that is, that the components do not interact with each other differently at different relative concentrations. Such concentration-dependent interactions will lead to frequency shifts and band shape changes[4].

Care must be exercised since the technique is also sensitive to optical spectroscopic errors as well. As one example we show below (table 2.5) some results obtained when comparing the ν(C=O) band intensity obtained for the pure PMMA with the same region in the laminate spectra. Since The PVOH does not have any absorption on this region, we should expect to obtain exactly the same value. The results on table 2.5 show some variation in intensity that will cause problems when trying to obtain the subtracted spectra. The difference between the values is possible due to optical alignment changes that occur when we change even slightly the prism position in the cell. The results are plotted on fig. 2.9 which also shows another interesting point related with the variation on the incident angle.

As we can see from fig. 2.9, the intensities change considerably according to the angle of incidence. Starting with an incident angle of 39° that is very close to the critical angle ($\Theta_c = 38.4°$) for the system, the intensity increases, reaches a maximum at 45° and then starts to decrease again. To explain that behaviour we will refer to fig. 2.2 where we can see that the IRE crystal is parallelepipeds cut to a given angle (45° in our case). Thus, although the nominal angle of incidence is variable, the radiation is only incident at 90° to the crystal surface for an angle of incidence of 45°. If the angle of incidence is different of 45° the radiation will not be normal to the crystal surface anymore and therefore losses by refraction will occur. This explains the maximum value for intensity at 45° compared which the other angle of incidence used.

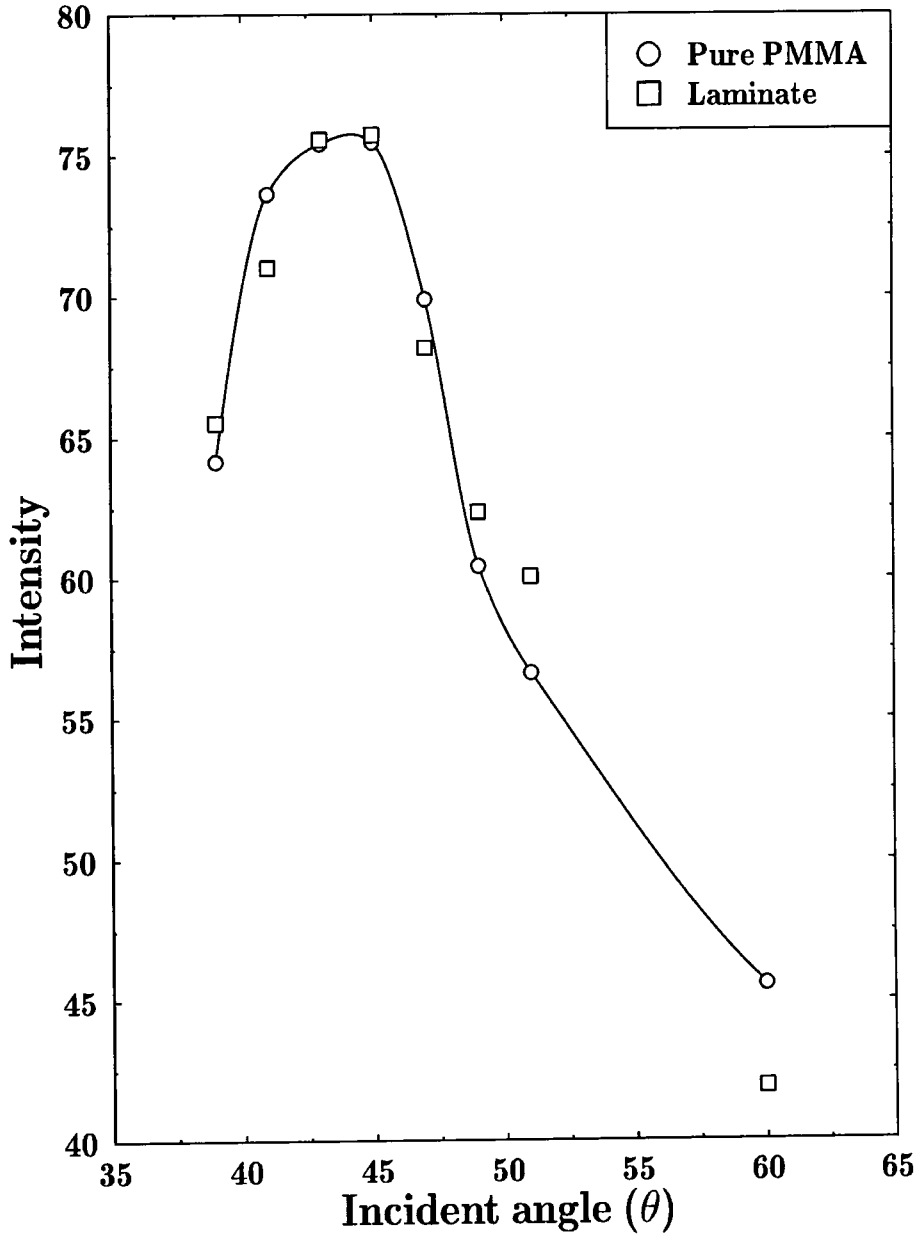

Fig. 2.9 - ν(C=O) intensities for PMMA pure and on laminate.

Table 2.5 - ν(C=O) intensities for the PMMA pure and on the laminate

Angle of incidence (Θ)	ν(C=O))	
	PMMA pure	Laminate
39	64.17	65.54
41	73.65	71.04
43	75.43	75.58
45	75.48	75.75
47	69.90	68.18
49	60.43	62.35
51	56.61	60.06
60	45.56	41.90

Fig. 2.10b shows the FTIR-ATR spectrum of the two layered film samples. In this case the base layer is 0.396μm thick, the surface layer is 0.1μm thick and the incident angle is 45°. Fig 2.9c shows the spectra of pure PVOH and, if we compare the spectra (2.10b and 2.10c) we can see that the bands due to the minor component (PVOH) can not be observed on the two-layered sample spectrum because the PVOH adsorptions are hidden by the absorptions of the major component (PMMA). However, by subtraction, it is possible to isolate the component spectrum of the surface layer by subtracting an absorption spectrum of the pure sample of the base layer. Fig 2.10a shows the result of subtraction and as we can see, the PVOH bands are now easily observed. Hence, the subtraction brings about a clear appearance of the surface layer spectrum. It should be noted that the scale of the ordinate in fig. 2.10a is expanded by several times with no distortion of the absorption bands resulting from subtraction for this case. The above example clearly demonstrates the capability of the FTIR-ATR spectra subtraction for analyses of a very thin surface layer.

The same kind of experiment was repeated using different thicknesses for the

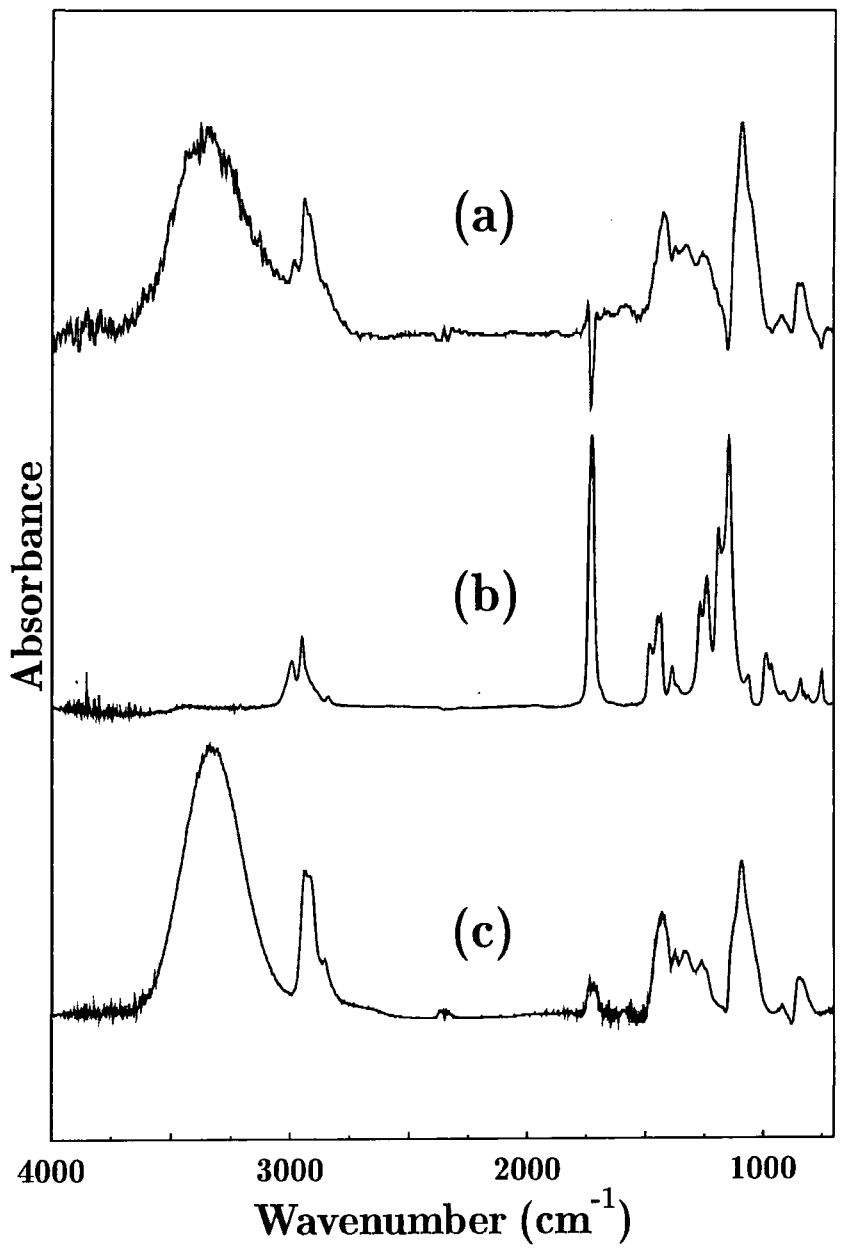

Fig. 2.10 - FTIR-ATR spectra of the system studied, (b) the laminate spectrum, (c) the pure PVOH spectrum, (a) the difference spectrum (b) - (c) showing the PVOH spectrum in the laminate.

PMMA base layer and keeping the PVOH surface layer constant. The results of the subtraction have been evaluated using the PVOH band at 1093 cm^{-1}. Fig. 2.11 shows the results for an incident angle of 39° and we notice that as the thickness (t) of the PMMA base layer is increased from 0.4 to 2.0 μm the 1093 cm^{-1} band decreases in intensity. The decrease in intensity is a consequence of the decreasing of the electric field strength at the interface.

The same experiment was performed using now 45° and 60° as the incident angle. The same behaviour was observed, that is, the PVOH band intensity decreased as the PMMA base layer thickness increased but, in these cases all the PVOH intensities were smaller than the intensities obtained at 39°. As shown in fig.2.1 the depth probed by the IR beam on the polymer surface is a strong function of the incident angle (Θ). Generally, this depth drops sharply at a higher incident angle. Consequently, for incident angles of 45° and 60° the increase on the incident angle leads to a smaller "effective penetration" into the PVOH surface layer and therefore the PVOH band intensities are smaller compared with the same experiment at 39°. This result reflects the importance of the decrease in the electric field strength with the incident angle.

With the results obtained at different angles and different thicknesses for the base layer we plotted the 1093 cm^{-1} band areas of PVOH as a function of the electric field decay $(E/E_0)^2$ in order to yield an approximation to the depth-concentration profile. The range of incident angles used correspond to a depth range of about 1 to 6μm.

Before discussing these results we will return to the problem caused by a non-normal incidence on the IRE surface.

The incident angle is a function of two variable angles: the IRE end face angle, β (in our case 45°) and the optical angle (ψ), which is determined by the optical alignment of the internal reflection cell. If the two variable angles are identical, then the particular angle is the incident angle (Θ=β=ψ) and the electromagnetic waves entering the IRE are normal to the end face of the crystal. The incident angle is then the angle between the z-axis and the incident electromagnetic waves striking the interface between the IRE and

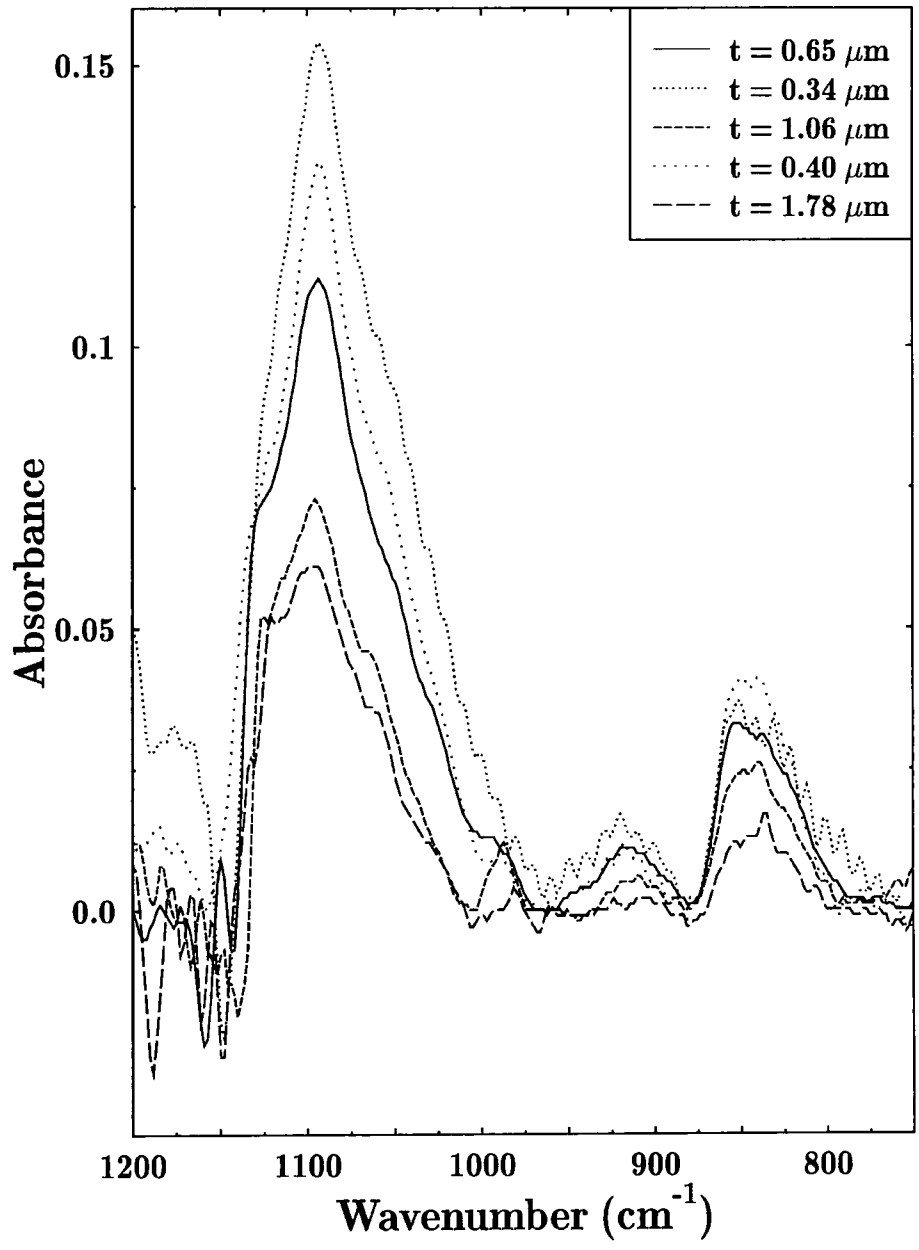

Fig 2.11 -The PVOH spectra obtained by subtraction on different PMMA base layers thicknesses, t.

the polymer sample. However, if the optical angle is different to that of the end face crystal the electromagnetic waves are no longer normal to the end face of the IRE. In this case, the effective incident angle is a function of two variable angles (end face and optical) and the index of refraction of the IRE. Fig. 2.12 illustrates the effect of an unequal variable angle of incidence at the interface between the IRE and the polymer. The effective angle can be calculated using Snell's law and appropriate trigonometric identities as shown below:

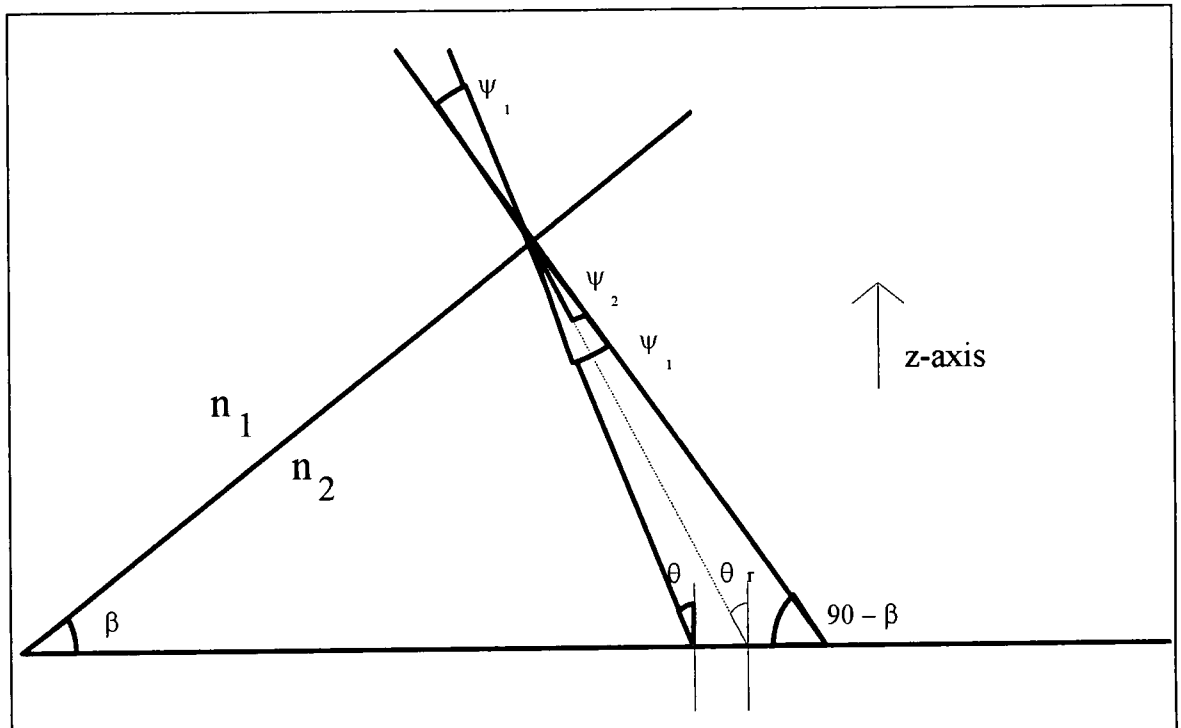

Fig. 2.12 - Geometrical construction required to make a correction for Θ_{inc} at angles other than the IRE angle of 45°.

From the Snell's law:

$$n_1 \sin \Psi_1 = n_2 \sin \Psi_2 \qquad \text{(eq. 2.2)}$$

From trigonometric relationships:

$$\Psi_2 + 90 - \beta + \Theta_r + 90 = 180 \;\; \therefore \;\; \Theta_r = \beta - \Psi_2 \qquad \text{(eq. 2.3)}$$

$$\Psi_1 + 90 - \beta + \Theta + 90 = 180 \quad \therefore \quad \Theta = \beta - \Psi_1 \qquad \text{(eq. 2.4)}$$

From (eq. 2.2):

$$\Psi_2 = \sin^{-1}\left[(n_1 / n_2)\sin\Psi_1\right] \qquad \text{(eq. 2.5)}$$

Substituting 2.3 and 2.4 into 2.5:

$$\Theta_r = \beta - \sin^{-1}\left[(n_1 / n_2)\sin(\beta - \Theta)\right] \qquad \text{(eq. 2.6)}$$

For a crystal with an end face angle β of 45°:

$$\Theta_r = 45 - \sin^{-1}\left[(n_1 / n_2)\sin(45 - \Theta)\right] \qquad \text{(eq. 2.7)}$$

Fig. 2.13, 2.14 and 2.15 show the results for 39°, 45° and 60° respectively. The areas were normalised to the area at t=0 for the pure PVOH 0.1μm film. For the plots we used the normal incident angle and the effective one. As may be observed from fig. 2.13, the experimental data agree much better with the effective incident angle (42.5° instead of 39°) than with the nominal ones. This result illustrates the importance of corrections to the nominal incident angle. From the results we can conclude that the correction is very important when we are working close to the critical angle. The agreement between the experimental data and the effective angles are extremely good considering the experimental errors in t (±10%) and in the area (±10%). These results show that the two-layered model system may be successfully employed to control the effective penetration depth into the PVOH layer, thus providing a semi quantitative depth profile of the surface layer.

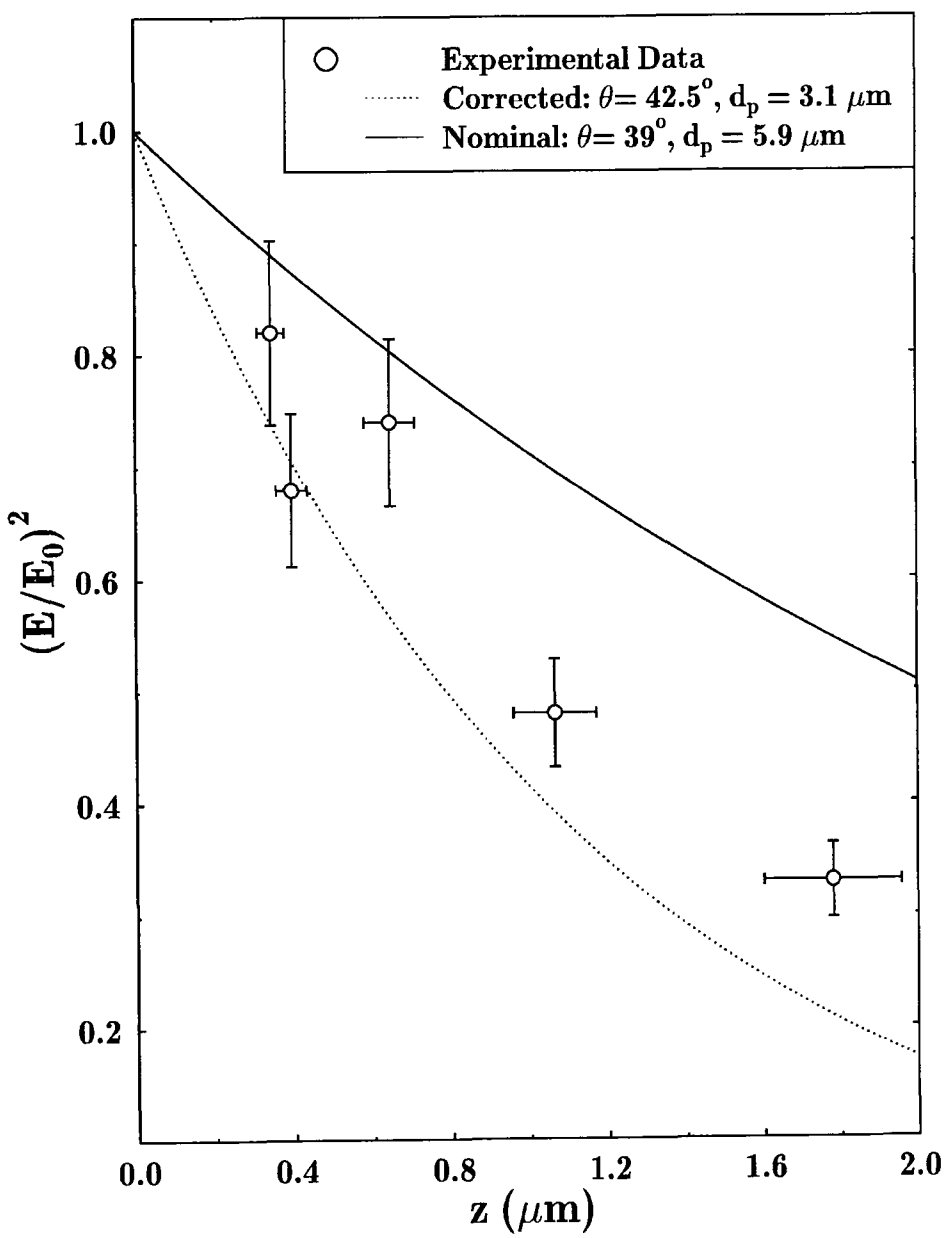

Fig. 2.13 - Comparison of observed PVOH band intensities and the calculated electric field distribution as a function of the base layer thickness, t. Nominal incident angle of 39°.

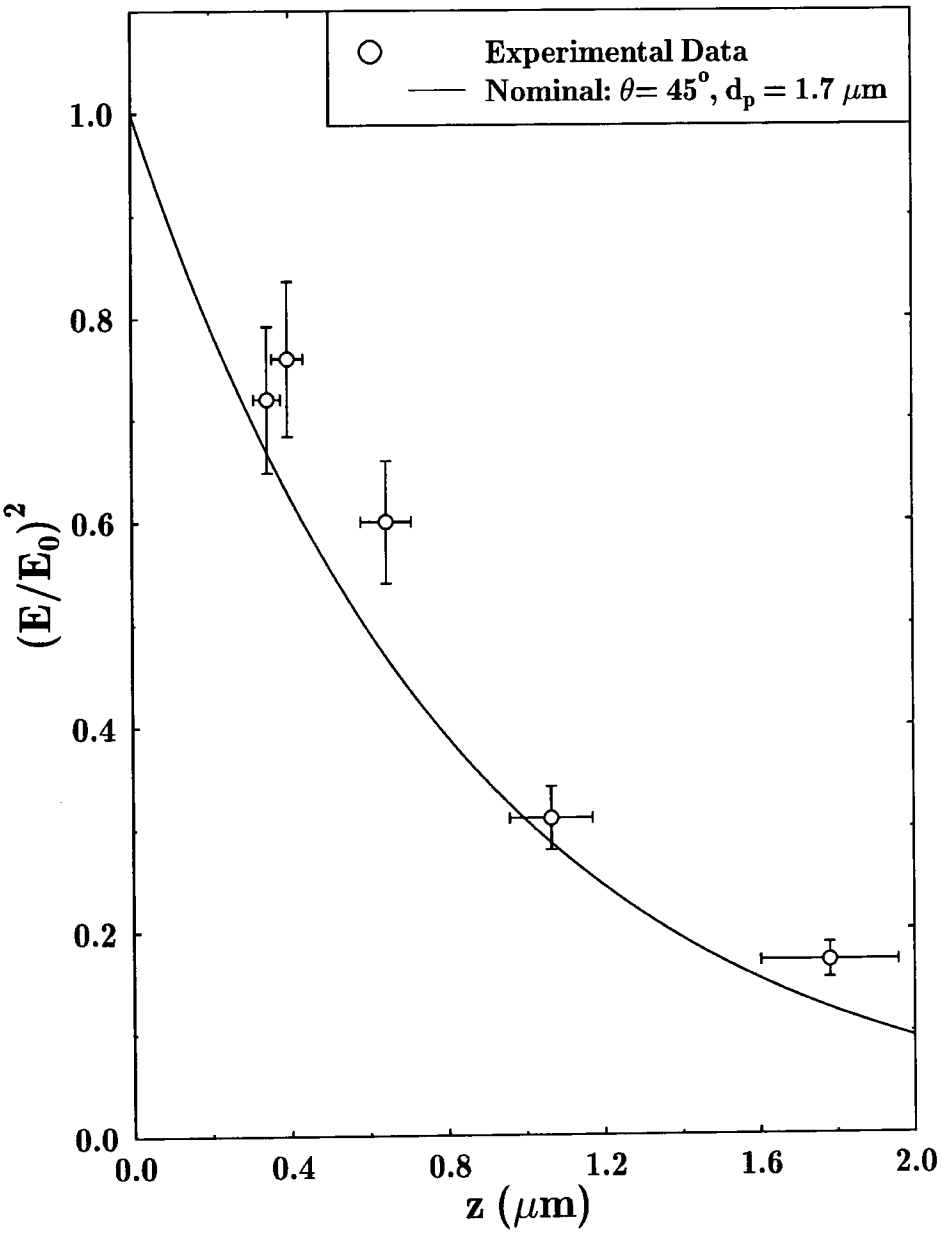

Fig. 2.14 - Comparison of observed PVOH band intensities and the calculated electric field distribution as a function of the base layer thickness, t. Nominal incident angle of 45°.

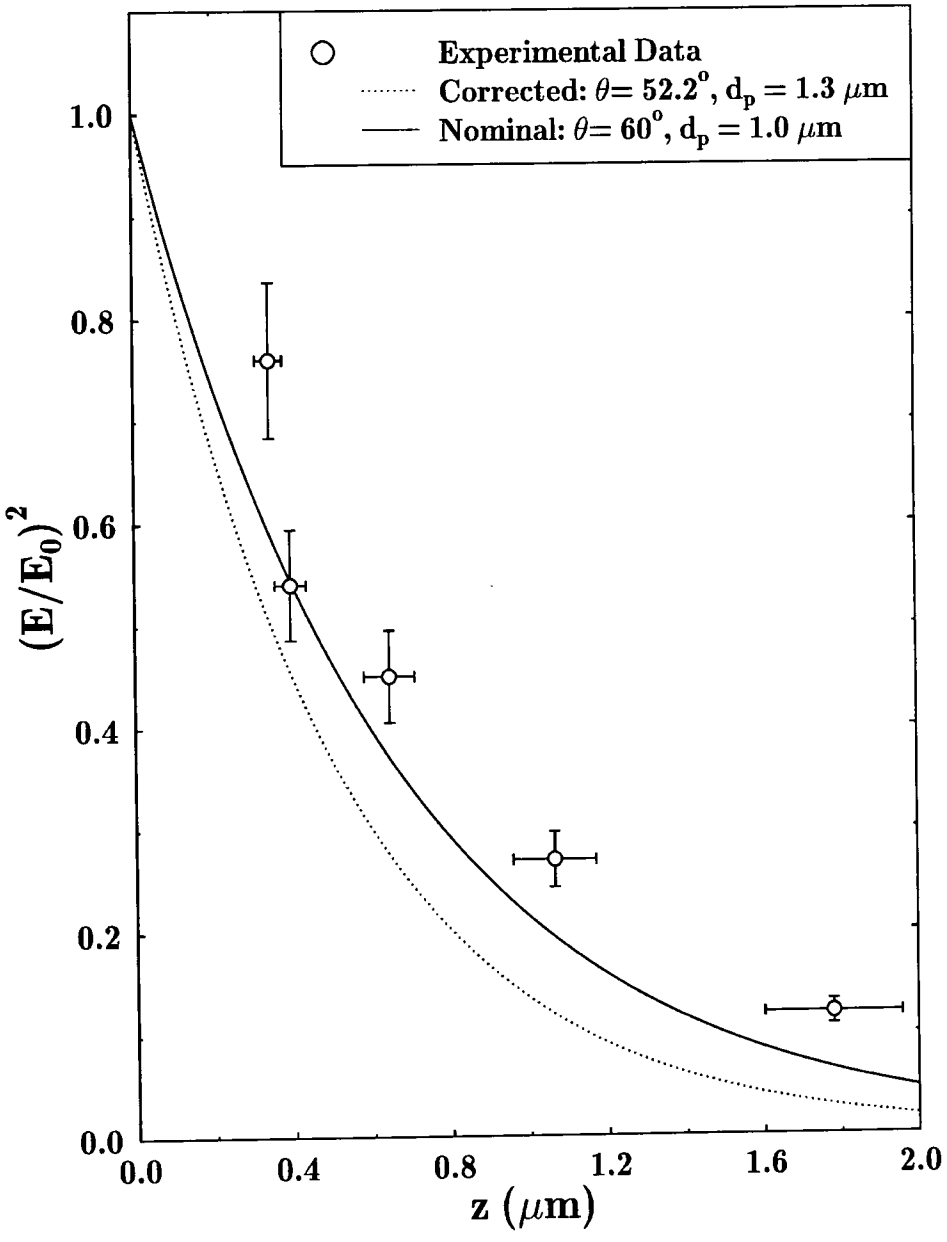

Fig. 2.15 - Comparison of observed PVOH band intensities and the calculated electric field distribution as a function of the base layer thickness, t. Nominal incident angle of 60°.

Chapter 3

Water Absorption Studies on Polymeric Membranes Using FTIR-ATR Spectroscopy

CONTENTS

3.1 - *INTRODUCTION*

This chapter describes how the evanescent field absorption from an IR beam can be used to monitor *in situ* the molecular interaction at polymer/solution interface. The system chosen was sulphonated polyethersulphones(SPES) and water.

Sulphonated polyethersulphones have been successfully used in reverse osmosis for a number of years[62-65]. The mechanism of selectivity is still controversial. Clearly the state of water in SPES is crucial to the understanding of their transport properties. Furthermore, an improved understanding of the structural and dynamic properties of water in these synthetic membranes is likely to advance our knowledge in much more complex biological membranes[66].

Results are presented to demonstrate that the FTIR-ATR technique can provide information regarding the molecular state of the penetrant and polymer film at various times (this chapter) as well as information on water sorption kinetic (following chapters).

3.1.1 - Membrane Separation Process

To think about membranes is generally to think of separations. Indeed, 60% of synthetic polymeric membranes are today employed as semipermeable barrier layers that permit certain components of solutions or suspensions to permeate more rapidly than others. The absolute rate at which permeant traverses a membrane is known as *permeability*, and the rate at which two different species permeate relative to one another is *selectivity*. Permeability and selectivity are the primary, but by no means the sole, determinants of the practicality of any membrane separation[67,68]. A membrane separation process can be generally represented as in fig. 3.1.

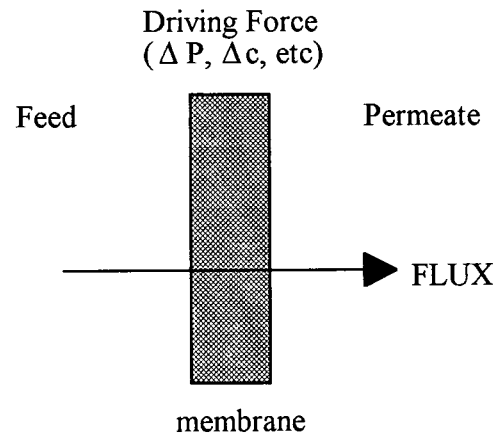

Fig. 3.1 - Schematic representation of a membrane process.

The membrane separation processes are driven by only three forces: gradients of concentration, electricity and pressure. The steric qualities of both membrane and solute are always involved, which in turns implies that sieving plays a significant role in every such separation. However, as the sizes of both solute and membrane pores decrease, other factors such as diffusion and solution come into play.

3.1.1.1 - Concentration-driven Process

Diffusion refers to the migration of a substance across a concentration gradient[67]. It is perhaps most easily understood in case of gaseous diffusion, when concentration can be replaced with pressure. Bringing together two gases at opposite sides of a permeable interface will cause the gases to cross this interface even if pressure is initially equal. This is so because the partial pressure of a gas in a mixture is independent of any other gases that may be present. For similar reasons diffusion occurs in condensed states as well. The diffusion process will be described in more detail in the next chapter.

3.1.1.2 - Pressure-driven Process

Pressure-driven membrane separations are a continuum process designed to separate suspended or dissolved particles of different sizes by utilisation of membranes containing appropriately sized pores. In order of decreasing particle and pore size these are microfiltration (MF), ultrafiltration (UF) and hyperfiltration (HF). The last named is also known as reverse osmosis (RO)[67]. Each of these processes employs a porous membrane that inhibits the passage of dissolved or suspended particles based primarily (MF and UF), or partially (HF), on the size and shape of the permeant species and the membrane pores.

a) **Microfiltration** - Microfiltration, the oldest of the pressure-driven process, covers the pore-diameter range among 0.1 and 10μm. Industrially, it is utilised to sterilise, that is, to remove viable microorganisms such as bacteria and yeast cells from aqueous solutions. It is also utilised to remove inanimate particular matter from both aqueous and non aqueous suspensions. Because MF membranes have relatively large pores, there is relatively little resistance to flow and low (≅30 psi) pressures suffice as a driving force. The high porosity of MF membranes is still another reason why low pressures are utilised, since such membranes are subject to destruction under pressure.

b) **Ultrafiltration** - In ultrafiltration the dispersed phase (solute in its most general sense) passes through the membrane less readily than the "solvent" for one of several reasons.

1 - It is adsorbed in the surface of the filter and its pores (primary adsorption)

2 - It is either retained within the pores or excluded therefrom (blocking)

3 - It is mechanically retained on top of the filter.

UF occupies that portion of the spectrum that separates MF from HF[69,70]. UF begins at the point where the size of the solute particle is approximately 10 times greater than the size of solvent molecules[70]. Perhaps the most significant difference between HF

and UF is that the former treats solutions of low Mw and high concentrations where osmotic pressure is appreciable, whereas the latter treats solutions of high Mw and low concentration so that osmotic pressure is negligible[71].

c) **Hyperfiltration** - HF or reverse osmosis lies at the tight end of pressure-driven membrane separation process spectrum. As a result, membrane pore size is smaller, porosity lower, and pore density higher than for UF and MF membranes. These properties enable HF membranes to retain microsolutes (including ions) whose size is less than 10 Å. The small size and formula weight of these particles in turn means that their concentrations, even if modest when expressed as percent by weight, tend to be appreciable in molar terms.

The osmotic pressure of sea water (~ 3.5% NaCl) is approximately 350 psi at 25°C. Therefore, if a semipermeable membrane separates sea water from a fresh water reservoir, the concentration gradient will cause water to permeate to dilute the sea water. This migration of solvent across a semipermeable barrier from a less concentrated to a more concentrated solution is known as *osmosis*[67]. If pressure is applied to the concentrated solution, the passage of water will be diminished. If the applied pressure equals the osmotic pressure, no net flow of water will take place. Finally, if the applied pressure exceeds the osmotic pressure, the osmotic flow will be reversed and a net flow of water from the more concentrated to the less concentrated solution will occur. This is the process known as *reverse osmosis* or hyperfiltration[67]. Any pressure in excess of the osmotic is known as the effective pressure and constitutes the driving force for solvent (water) transport.

The tremendous impetus given to desalination with the invention of the integrally skinned cellulose acetate membrane by Loeb and Sourirajan[72], moved hyperfiltration to the forefront of interest in membrane separation process during the last two decades. It is not surprising, therefore, that a considerable amount of emphasis has been placed upon functional descriptions of this process. Details about the models which have been

proposed are beyond the scope of this chapter and the interested reader can refer to references 73 and 74.

Variations in permeability and selectivity can be accommodated on the basis of the existence of pores of various sizes. In fact, it is now held that two size distributions of pores exist: numerous small pores (≤10 Å) which are thought to exist in perfect or ideal membranes and occasional large (≥100 Å) pores which are attributable to the inevitable existence of defects in the skin layer or integrally-skinned membranes.

Koros[75] explained the selectivity of membrane ions diffusion on the basis of the energy of interaction between water and membrane sites and between water and dissolved ions. In this case the efficiency of hyperfiltration varies with the nature of the ionic solute. Ions that have a high charge density (small radius and/or high charge) tend to be more strongly hydrated than those with a low charge density. Moreover, as the crystal radii increase, a point is reached beyond which hydration no longer takes place. This accounts for the fact that selectivity increases in the series $K^+ < Na^+ < Li^+$, whereas $Cs^+ > Rb^+ > K^+$.

3.1.2 - Membrane Polymers - Essential Characteristics

The large average size of macromolecules, their size distribution, their architecture, the specific nature of their chemical groups, the arrangement of these groups in the chain, and the state of aggregation of macromolecules, are the fundamental polymer properties which in turn are responsible for all their characteristics. Depending upon such factors several possible states of molecular aggregation are possible: liquid, amorphous (glassy or rubbery) and semicrystalline[67].

3.1.2.1 - Neutral Polymers

Polysulphone (PS) is the polymeric product of the reaction between the di-sodium salt of bisphenol-A and di-p-dichlorodiphenyl sulphone:

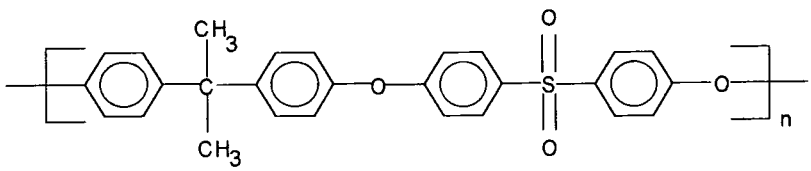

Fig. 3.2 - Molecular Structure of Polysulphone.

Among the properties which qualify PS as an outstanding membrane polymer are the T_g of 195°C, an amorphous glassy state, thermal and oxidative stability, excellent strength and flexibility, resistance to extremes of pH and low creep even at elevated temperature[67]. The closely related polyethersulphone (PES) shown on fig. 3.3, is totally devoid of aliphatic hydrocarbon groups therefore it exhibits even higher thermal stability. It has a T_g of 230°C and other properties similar to those of PS.

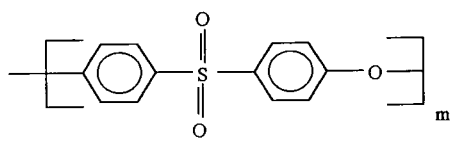

Fig.3.3 - Molecular Structure of Polyethersulphone.

Neither of these polymers is particularly solvent resistant. Both PS and PES are Lewis bases (sulphone, aromatic and ether groups) and are soluble in acidic solvents and

chlorinated hydrocarbons. They are also soluble in polar solvents that are employed in wet-process casting solutions that are utilised in membrane preparation[76-77].

The combination of phenyl rings attached to sulphone groups results in a high degree of resonance stabilisation. The sulphone group acts as a sink for the electrons in the aromatic groups and confers both thermal and oxidative resistance. Two additional stabilising effects of resonance are increased bond strength and a planar configuration which contributes to rigidity even at elevated temperatures. The ether groups in the backbone provide some flexibility which results in inherent toughness. Because of their aromatic moieties, membranes from both polymers are resistant to high energy irradiation. Another desirable property of the aromatic groups is that they may be sulphonated, thereby providing an excellent means of introducing both strong cation-exchange groups and potential cross-linking sites. Membranes from unmodified PS and PES are utilised in both flat-sheet and hollow-fibre forms in hyperfiltration (HF), ultrafiltration (HF) and gas-separation membranes, both by themselves (UF and MF) and in series with other membranes (HF and gas separation). They are widely utilised as porous support in thin film composite membranes for HF.

Sulphonation of the aromatic rings in PS and PES leads to materials which have been widely investigated as the barrier layer in both integrally-skinned (asymmetric) and thin film composite ultrafiltration membranes[78-79]. Because of the low reactivity of the aromatic rings in PS and PES, the polymer must be modified to allow the sulphonation. The modified form of PES used in this work is shown in the experimental part of this chapter. Sulphonated PS with a capacity of sulphonic acid moieties sufficient to render it water soluble is currently used as an HF barrier layer (after cross-linking) in series with microporous supports of unmodified PS[80]. The advantage of this combination is that both support and barrier layers are chlorine resistant, the only quality lacking in all other HF membranes today.

3.1.2.2 - Ion Exchange Polymers and Ionomers

The term *ion exchange* and *ionomer* are both used to qualify membrane polymers which bear fixed acidic and/or basic groups or their salts. Although they are sometimes used interchangeably, there is a difference in degree, with ion exchange used to refer to those polymers with higher capacities, whose strong tendency to hydrate and swell is held in check by a high density of covalent cross-links[67,80]. The latter are usually introduced in the form of polyfunctional monomers, such as divinyl benzene (DVB) during polymerisation. Ionomers, on the other hand, usually contain between 2 and 15% mol of monomers with ionic groups present in the side chains. Owing to their lower capacities, they often do not require cross-linking to inhibit swelling. Another difference between traditional ion exchange membranes and the ionomeric types is the generally superior film forming characteristics of the latter. The presence of ionic groups in ionomers, particularly of the SO_3^- M^+ variety, changes some of its properties dramatically. Ionic polymers have been very much studied, in particular by Eisenberg and his co-workers[81-85]. Increases in the elastic modulus and the viscosity of several orders of magnitude have been observed, and changes in the glass transition of hundreds of degrees are possible. Chain stiffness is inversely proportional and polymer solubility is directly proportional to the size of the M^+ counterion. Of course, as the ion exchange capacity (IEC) of an ion is increased, so will its tendency to hydrate and swell with the result that its utility as a stable water-insoluble film former diminishes. Ultimately, this may result in the formation of water soluble polymers known as *polyelectrolytes*.

The characteristic that distinguishes ion-exchange and ionomer membranes from other types is the presence of charges or ionic groups in their component polymer molecules. Mobile ions containing a charge opposite to that borne by the fixed ions are known as counterions; those containing the same charge are co-ions. Polymers containing positively charged groups are polycations. Because of the electroneutrality requirement they will have a stoichiometric amount of exchangeable anions in association with their fixed cations. Since such anions are mobile and can be exchanged

for others in an external solution, polycations are known as anion exchangers. For similar reasons polyanions are termed cation exchangers.

Whereas the ion-exchange resins and water soluble polyelectrolytes are situated in the high capacity range of ion-containing polymers, the ionomers tend to occupy the low capacity range. The first representatives of this class were addition copolymers in which the minority component was ionic. Today, however, the term encompasses condensation polymers as well[81].

Ionomers can either be utilised as the sole membrane polymer or they can be utilised in blends or block copolymers with other, usually nonionogenic polymers. There are advantages to utilising blends or copolymers of ionomers and neutral polymers compared to utilising an ionomer by itself. One advantage is lower polymer cost since a blend or copolymer of expensive ionomers with inexpensive neutral polymer costs less than an equal amount of expensive ionomer. A second advantage is increased reproducibility. It is easier to vary blend or copolymer ratios to obtain a final membrane with a given capacity than to synthesise an ionomer with a capacity defined within narrow limits[67].

Because of the low dielectric constant of most organic polymers, the ionic groups tend to aggregate, forming ionic domains, which contain the anionic groups and the cations associated with them. The characteristics of these domains have been fully investigated[86-95]. Their size and structure varies with the nature of the polymer, the properties of the cation, the overall stoichiometry of the ionomer, the degree of solvation of the system, and the preparative and thermal history of the ionomer. They can be as small as ion pairs or small multiplet, but in some cases they are reported to be in the 20-100Å diameter range[85].

A multiplet can be defined as an aggregate consisting of several ion pairs and containing only ionic material. The factors that govern the formation of multiplets have been reviewed recently[85,96]. According to the authors, the most important ionic parameter that affects multiplet formation is the strength of the electrostatic interactions between ion pairs. This is determined by the sizes of the ions and the partial covalent

character of the ionic bond. Although none of these parameters can be varied independently of the others, they are important factors in multiplet formation. If the electrostatic interactions between ion pairs are too weak to overcome the elastic forces of the chains to which they are attached, no multiplet will form.

The ion content of the ionomer is also a crucial factor in influencing multiplet formation. The proximity of the ion pairs to one another is determined by the ion content of the system. If the ion pairs are very dilute, they are too far apart to experience significant electrostatic attraction and hence do not tend to aggregate.

The characteristics of the host polymer are also important in determining the extent of multiplet formation in a random ionomer. A low dielectric constant and low T_g of the host polymer tend to favour ionic aggregation, while a high dielectric constant and/or high T_g tends to inhibit multiplet formation.

As the ion content is increased, the average distance between multiplets decreases. Eventually a point is reached where some overlap is encountered among the regions of restricted mobility surrounding each multiplet. It should be stressed, however that only the regions of restricted mobility overlap, the multiplet themselves remain intact. As this overlap becomes more frequent, relatively large contiguous regions of restricted mobility must form. When such a region is large enough to have its own T_g it constitutes a cluster and exhibits behaviour characteristic of a phase separated region.

According to Eisenberg[85] it is not necessary to invoke electrostatic interactions between the multiplets within a cluster. Although weak electrostatic intermultiplet forces may exit, they are considered to be less important than the factors mentioned above. The multiplets thus do not "condense" to form the cluster but are close together by virtue of the proximity of the ion pairs on the polymer chain.

3.1.3 - Water Structure and Membrane-Water Interaction

Because of the importance of membrane separation in aqueous systems, the properties of water and water-soluble interactions will be used to present the general case of solvent-solvent and solvent-solute.

Although the unique properties of water and aqueous solutions have been the object of intensive research, there are widely differing opinions of what the structure of water really is. According to the flickering-cluster model of Frank and Wen[97], the formation of hydrogen bonds in liquid water is a cooperative phenomenon in which a number of hydrogen bonds are formed and broken simultaneously between a group of water molecules (Fig.3.3). The slight covalence of the hydrogen bonding leads to a certain amount of charge separation and therefore formation of new bonds by molecules that are already bonded. The water molecules will group together so that the number of hydrogen bonding in the cluster is a maximum (about 100 molecules per cluster at 25°C), resulting in spheres in which stabilisation per hydrogen bond for molecules in the interior is greater than those at the surface. The formation and dissolution of these clusters is governed by local high energy fluctuations. Their lifetime, although short, is nevertheless two or three orders of magnitude greater than the period of molecular vibration.

On the model mentioned above[97] water is considered to be an open structure and full of cavities similar to those present in ice. The cavities are believed to contain a dense liquid composed of non-hydrogen-bonding molecules. Clustered and non-hydrogen-bonding water molecules are in equilibrium with one another. The sensitive order-disorder equilibrium within liquid water is responsible for its unusual properties, such as its ability to increase in order both by interaction with active species such as cations of high charge density and by its reaction in the presence of inert solutes with which it has no direct or specific interaction.

When solutes are added to water, the water structure will be enhanced or reduced depending upon the nature of the interactions. In structure enhancement (or

structure making) the presence of solute shifts the water structure to large or more ordered clusters at the expense of the dense monomeric species. In structure breaking, on the other hand, the presence of solute shifts the structure equilibrium toward smaller and/or less ordered clusters and increasing concentrations of dense monomeric water.

The behaviour of water within membranes and at their surface has being the subject of broad speculation[98-102]. There is a dichotomy of opinion, with some authors[98-99] appearing reluctant to accept the idea of any form of long-range ordering near aqueous interfaces and others[101] tending to credit the existence of considerable amounts of bound water.

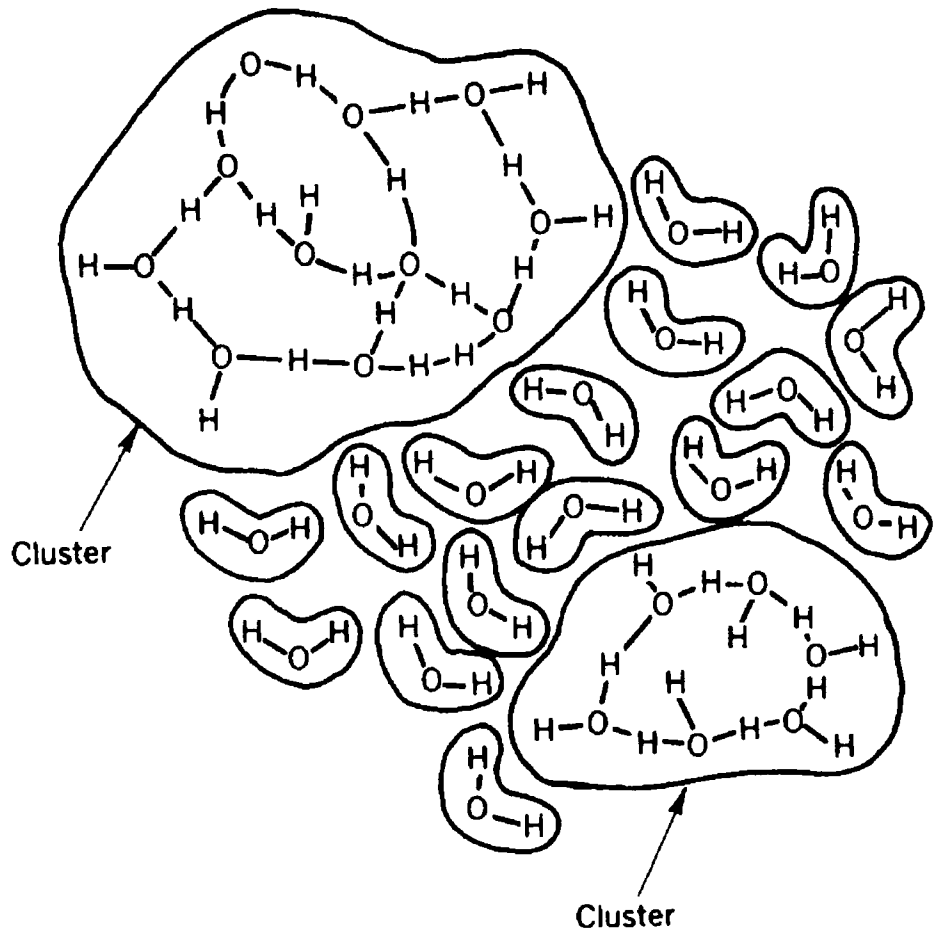

Fig 3.3 - Schematic representation of liquid water, showing hydrogen bonding clusters and unbounded molecules. Reproduced from ref. 67

Bound water relaxes at frequencies between those characteristic of ice and those characteristic for normal water. Therefore, from a structural point of view, bound water stands between normal water and ice. A broader spectrum of time constant is involved in the relaxation of bound water than in that of normal water, which is indicative of variation in the characteristics of the former associated with different activation energy. In other words, not only can water be bound, but it can also be bound to various extents. Very probably a continuum exists, with the more highly (primarily) bound water molecule in the inner hydration shell and less highly (secondarily) bound water molecules in successive hydration shells.

By analogy to the known effects of solutes on the structure of water, Berendson and Migchelsen[103] predicted the following polymer-water effects:

1 - polar side chains should hydrate individually but have a structure-breaking influence beyond the first layer.

2 - non polar side chains should induce order of the cage type similar to the effects of non polar solutes.

3 - backbone structures able to form hydrogen-bonds to water will have structure breaking or structure promoting effects, depending on the geometry of the hydrogen-bonding sites. If the geometry is such that the sites to which water may be bound from an array fitting into the ice I structure, a structure promoting influence is to be expected. With hydrophobic backbones, similar effects might occur if short polar side chains repeat in a pattern fitting into a regular water lattice. The effects will be stronger for rigid backbones or side chains.

Bound water is believed to be of importance in many separations of aqueous solutions. It is one of the reasons for the selectivity of ion-exchange membranes, and its presence is believed to constitute the basis for their salt-retention capacity.

3.2 - *EXPERIMENTAL*

3.2.1 - Preparation of Polymer Film

The sulphonated polyethersulphones used in these experiments are random copolymers commercially available and kindly supplied by ICI. The structure of each block can be seen below:

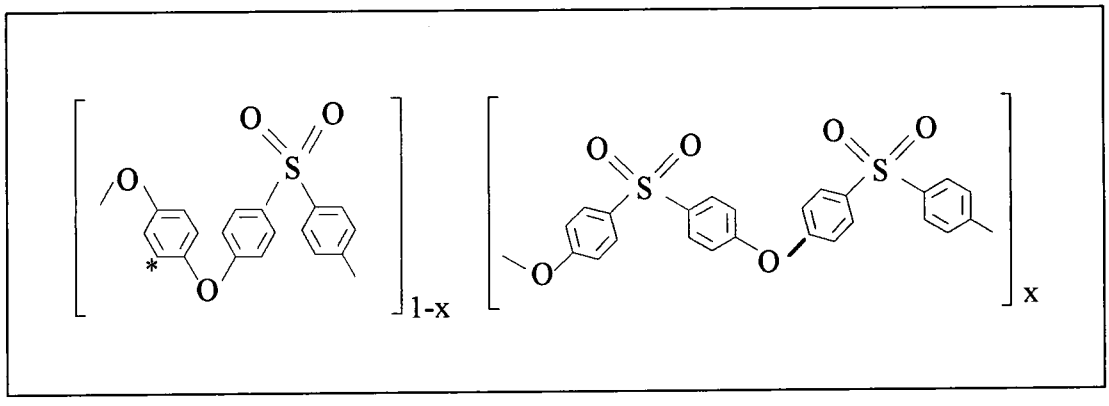

According to the literature[104] the range value of x is from 0.05 to 0.80. The sulphonation occurs only at the hydroquinone residue* so that ion exchange capacity of sulphonated polymer is pre-determinate by copolymer composition.

The difference between the two samples used relies on the degree of sulphonation. The degree of sulphonation (called S-number) is defined as:

S = N° of non-sulphonatable rings / N° of sulphonatable rings

Hence, higher S values denote a lower degree of sulphonation. The following designation will be used here to describe the samples in study:

SPES(S5)

SPES(S20)

The characteristics of the above samples are given on table 3.1.

Table 3.1 - Characterisation of the Polymeric Membranes

Polymer	Exchange Capacity (eq./Kg)	Water uptake (%)
SPES(S5)	1.297	12.7
SPES(S20)	0.398	5.5

The refractive index of the polymer is 1.65 as reported by the supplier. Films were prepared by solution from formic acid, dimethylformamide (DMF) and n-methyl-pyrrolidone(NMP) of technical grade, in a range from 0.10 to 15μm. The solvent evaporation was performed using temperatures of 60°C and 80°C for 24 and 42 hours respectively. Different times and temperatures were used in order to investigate the influence of the drying conditions on the membrane structure. At the end of the drying process the films were removed from the oven and allowed to cool inside the desiccator to room temperature. Although residual water may remain in the films, the spectra of these samples will be defined as the dry spectra. Thin films were obtained by dipping while the thicker one were prepared by casting. IR analysis of the dry films shows no structural differences between thin and thick films due to different processes used.

3.2.2 - FTIR-ATR Measurements

All FTIR-ATR measurements were performed on a Mattson Sirius "100" spectrometer equipped with a liquid nitrogen cooled wide band MCT detector. Liquid and dry cell accessories and a 45° ZnSe ATR crystal were used. All spectra were collected at 4 cm^{-1} resolution. According to the cell used different procedures were adopted as described below:

a) **Dry Cell** - the film covered ATR element was mounted in the dry cell and the spectrum of the dry membrane was obtained. The sample was then removed from the

accessory, immersed in distilled water, removed at the appropriate time, blotted dry with filter paper, remounted on the accessory and the spectrum was obtained.

b) **Liquid Cell** - the film covered ATR element was mounted in a flow through ATR cell (Graseby Specac), as shown in fig. 3.4 and the spectrum of the dry membrane was collected. After that, without removing the sample from the ATR accessory, or the accessory from the spectrometer, distilled water was injected into the cell while starting the data acquisition. After the filling the inlet and outlet ports were sealed to prevent water evaporation. The data collection time for 30 scans was 31 seconds while the elapsed time was 43 seconds. Every 43 seconds a spectrum was taken during the first 10 minutes, then the time interval increased to 10 minutes and, after the first hour, increased to 1 hour. The final spectrum, taken after 8 hours, served as a reference for the $A\infty$ values of the absorption bands.

The diffusion of water in the polyethersulphones was measured by observing the OH stretching band. The peak was integrated from 2780 to 3780 cm^{-1} to obtain the integrated intensity at each time. Computer subtraction using a factor of 1 and quantification of the peak height of the ν(OH) band were automatically performed with Mattson software.

In both cases, upon completion of the spectral sampling, the variable angle holder and the cell were dismounted from the spectrometer. The crystal was removed from the liquid cell and examined visually for defects or delamination. The crystal was allowed to dry in a desiccator, and then the film thickness was measured mechanically as already described in previous chapter.

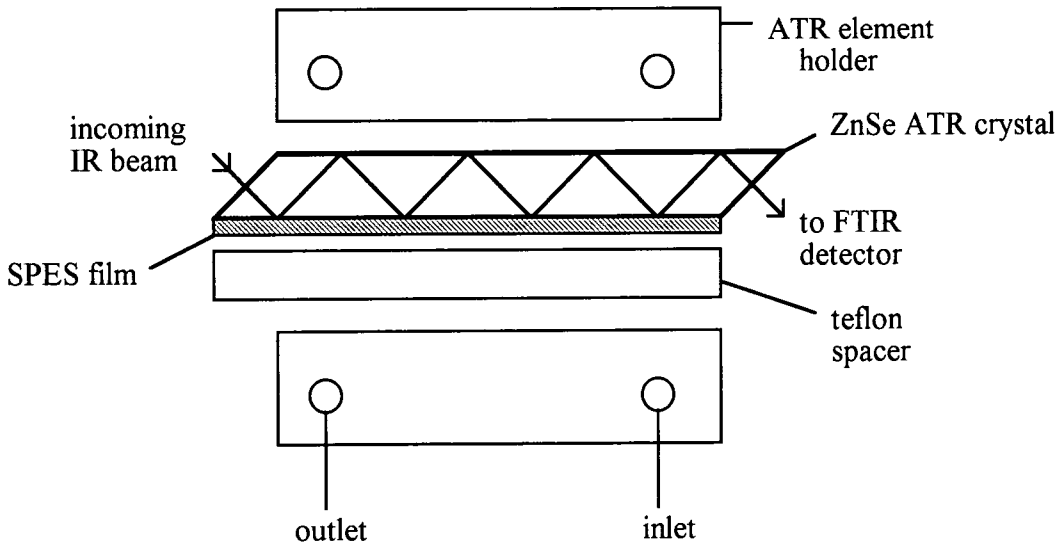

Fig. 3.4 - Schematic representation of the liquid cell.

3.3 - *RESULTS AND DISCUSSION*

Fourier transform infrared spectroscopy is a powerful technique for detecting small changes in the vibrational spectrum of a molecule[77,105-111]. Frequently, changes in the local electronic environment of a specific functional group will cause a measurable change in the infrared spectrum of the molecule. In these cases, FT-IR can provide a sensitive probe for evaluating the effects of variations in the local environment on particular functional groups in a complex molecule.

Because the sulphonate group is actively involved in the swelling, the electrolyte uptake, ion exchange capacity and ion transport characteristics of sulphonated membranes, a careful study of the effect of hydration on the membrane structure seems to be required. Therefore, in this work, FT-IR has been utilised to monitor the symmetric $\nu_s(SO_3^-)$ and antisymmetric $\nu_a(SO_3^-)$ vibrational modes as the degree of hydration was varied. The particular behaviour of H_2O bands will also be included on the present discussion.

There are a number of factors that frustrate molecular spectroscopists and make the characterisation of ionomers difficult. First, ionomers are hydrophilic and normally contain polar sites that are vulnerable to hydrogen bonding by proton donors. Consequently it is not surprising that the presence of water can detrimentally affect the physical, mechanical and electrical properties of ionomeric materials. From an infrared spectroscopist's point of view, water tends to complicate the spectra of ionomers by broadening the normal vibrations of interest. In addition, in the presence of water, salt structures established in fully neutralised ionomers can transform into other species, such as acid salts and acid dimers, depending upon the particular cation studied. Accordingly, we believe that a meticulous elimination of water is a necessary prerequisite for initial ('baseline') experiments if we are to correctly interpret the infrared spectra of ionomers.

3.3.1 - Effects of the Drying Conditions

Fig. 3.5 shows two dry samples of SPES(S5) films obtained by dipping and with thicknesses in the same range. Such spectra were obtained using the dry cell. Basically, the only difference between the samples was related to the solvent evaporation conditions. Sample A was heated at 80°C for 42h while sample B was heated at 60°C for 24h. As we can see from fig. 3.5 the absorption in the 3800-3400 cm^{-1} region is present in both cases indicating that even for sample A the temperature used was not high enough to produce completely dry membranes. However the sample dried at a lower temperature (sample B) shows a more intense band in that region. From these results we can conclude that the drying conditions are extremely important since they are intimately related to the initial amount of water in the membrane and consequently the membrane structure. Naturally the more severe condition (80°C/42h) is the one that produces the membrane with lower water content and hence should be the best one to use. Unfortunately the ZnSe crystal used as the ATR element is very sensitive to temperature and is damaged when exposed at 80°C especially for long and repeated times. Therefore, although the 60°C/24h was not the "ideal" drying condition it was the one used on the following experiments.

Zundel[112] has discussed in great detail the infrared spectra of dry and hydrated sulphonated polystyrene membranes. It is believed[117] that most of his observations also apply to sulphonated polyethersulphones. Therefore his studies from the basis for the discussion given below.

According to the author[1112], the absorption at 2950 cm^{-1} is assigned to vibrations of OH in the hydrogen bridges crosslinking two acid molecules and such band is very sensitive to temperature variations. Corresponding bands have also been found by numerous authors in investigating many other types of acid[113-116].

Another band that according to Zundel[112] seems to be very sensitive to temperature variations (and consequently water content) is the one at 800 cm^{-1}. Usually this band is assigned to the stretching vibration of the S-O(OH) single bond of the

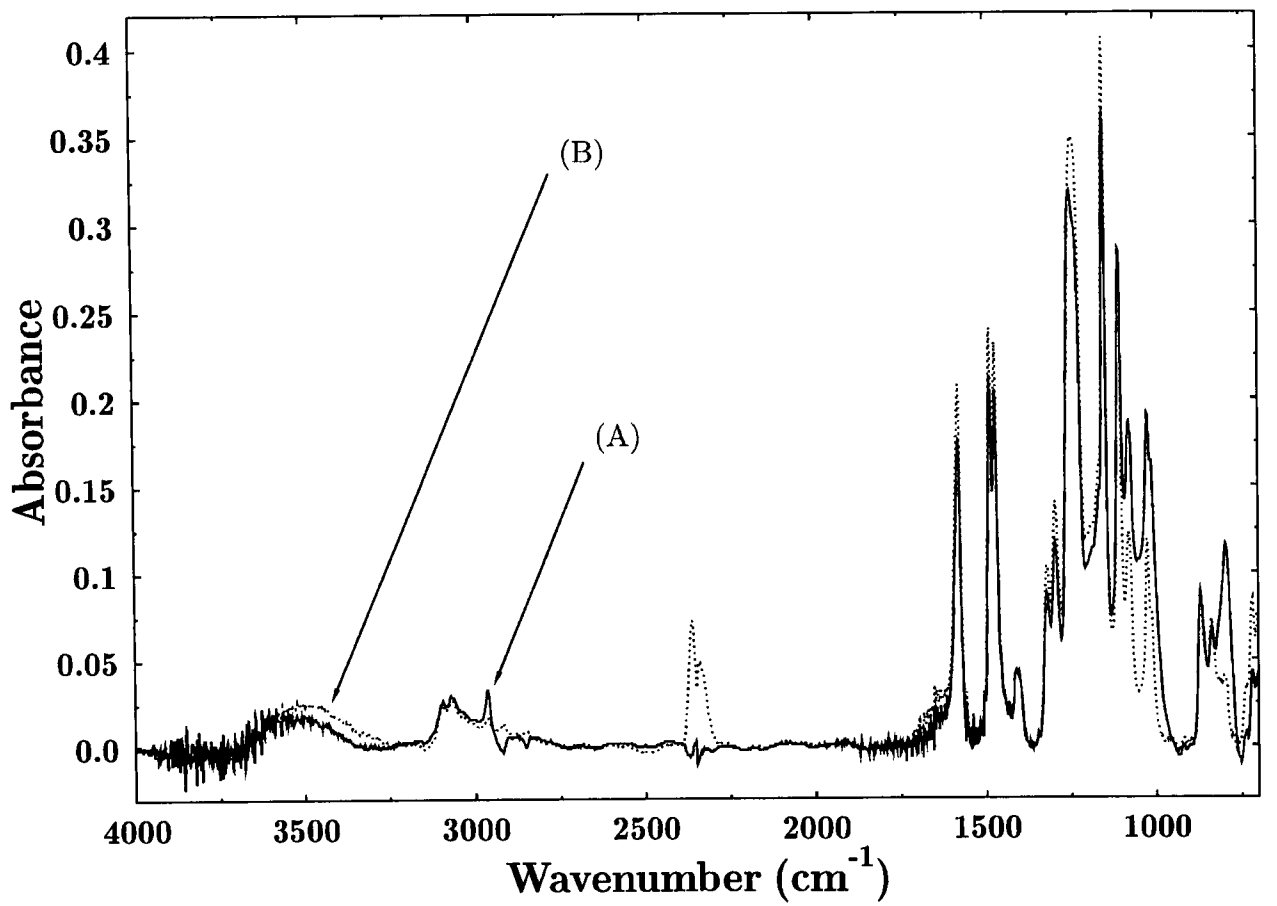

Fig. 3.5 - Dry samples of SPES(S=5)/Formic acid obtained by different heating conditions. (A) 80 °C/48h and (B) 60°C/24h.

sulphonic acid group[112]. In our case, the bands localised at 2950 cm^{-1} and 800 cm^{-1} are probably a result of contamination of the membrane by PDMS (polydimethylsiloxane). This possibility has been confirmed by subtracting sample A from sample B and comparing the result of subtraction with the PDMS spectra found on literature[118]. Fig. 3.6 shows the spectra of PDMS reproduced from literature[118] and fig. 3.7 shows the result of subtraction. As we can see, the subtracted spectrum contains most of the bands characteristic of PDMS. According to these results we can conclude that the 2950 cm^{-1} and 800 cm^{-1} bands belong to PDMS and therefore should not be considered when analysing the hydration effects on the structure of the membrane.

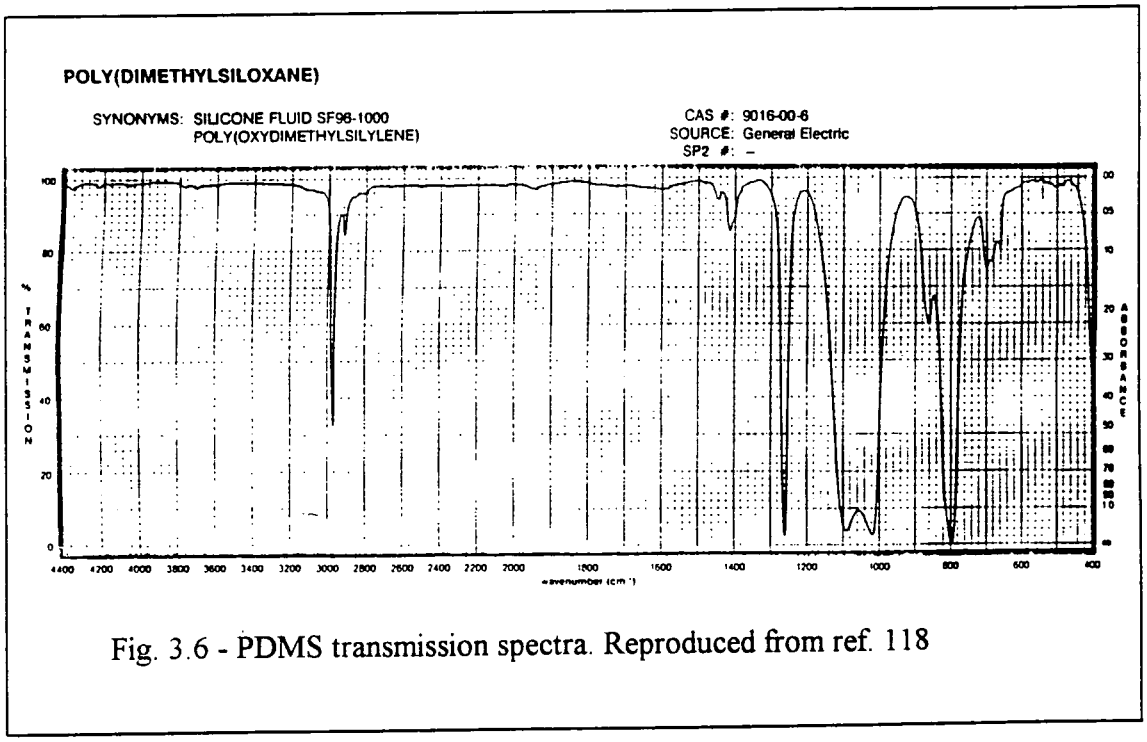

Fig. 3.6 - PDMS transmission spectra. Reproduced from ref. 118

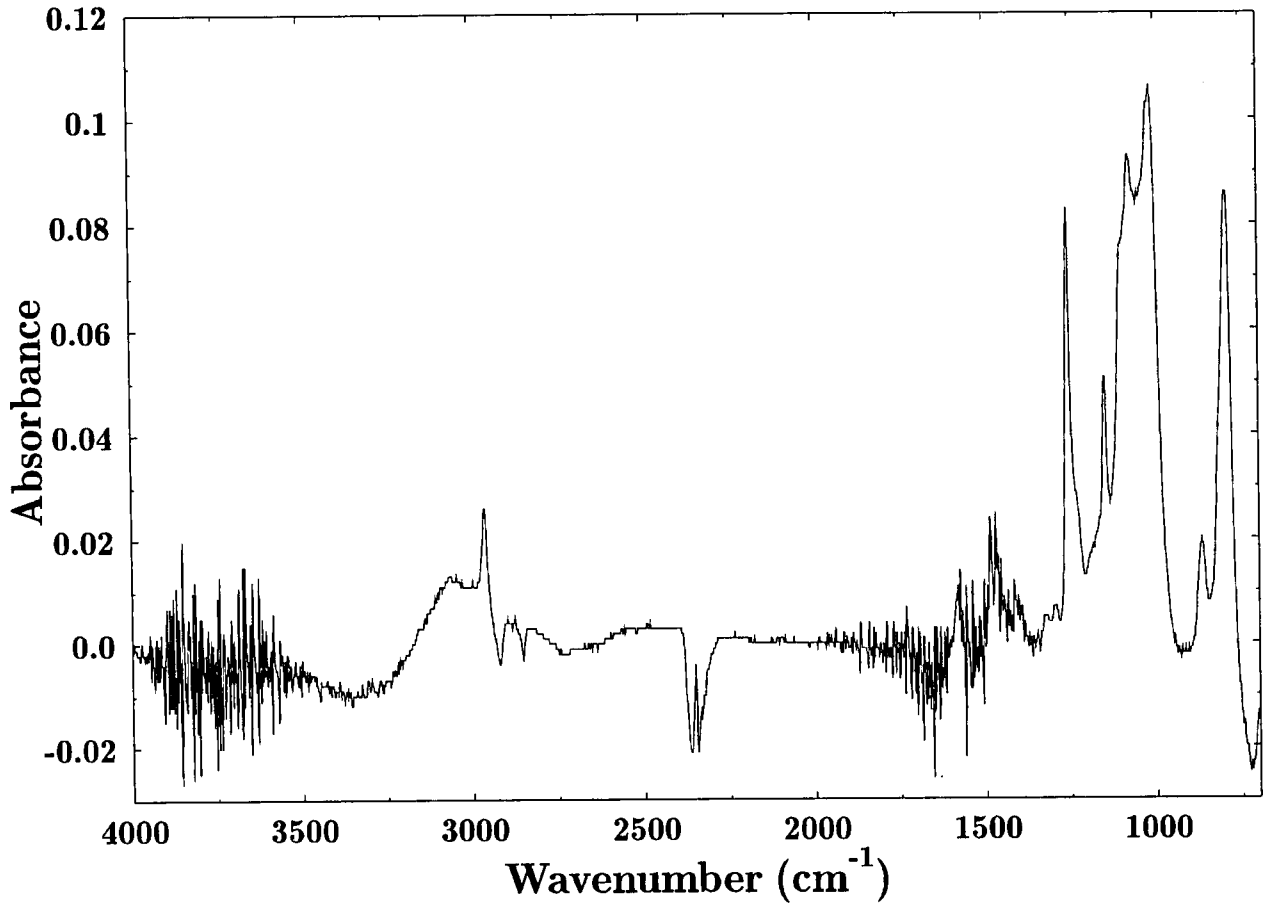

Fig. 3.7 - Result of subtraction: sample A - sample B.

3.3.2 - Spectral Changes Caused by Hydration

The results discussed so far were obtained using the dry cell. Although such a device worked very well for obtaining information about the dry and hydrated samples, it does not allow *in situ* measurements of the water uptake specially in this case where this process seems to be very fast. Therefore, at this point in order to analyse the spectral changes caused by the hydration of the membrane, the liquid cell started to be used. As it will be demonstrated, the liquid cell can produce much more information about the hydration process.

Some spectral variations brought about by interaction between water and the membranes will now be described and discussed. Parameters such as sulphonation level, and film thickness will be analysed. The first step was try to assign the main bands found in the spectra. Table 3.2 shows the result. The bands were assigned by comparing them with the assignments given by other authors in their investigations of similar compounds[111-112,117].

Fig. 3.8 shows the hydration effects on a small region of the SPES(S5) spectra. As shown on fig. 3.5, the membrane spectra are very rich so, we decide to divide them in small regions where the observed differences could become clear.

According to fig. 3.8, in dry SPES(S5), bands were found at 1108, 1080, 1073, 1025 and 1010 cm^{-1}. The bands at 1108 and 1080 cm^{-1} are in-plane skeleton vibrations of the benzene ring, with strong participation of the substituents. That at 1010 cm^{-1} is a ring vibration of p-substituted aryl ether.

The $\nu_s(SO_3^-)$ is generally localised in the spectral region around 1040 cm^{-1}. There is agreement that, the counterion (Li, Ca, Rb, Cs) imposes a strong electrostatic field on the SO_3^- ion that polarises the S-O dipole and shifts the symmetric vibration to higher frequencies in the dry form[117]. In our case, because we are working with the acid form, this band should appear at lower frequency and, in fact, as can be observed in fig.3.8 it lies at 1025 cm^{-1}.

Table 3.2 - Assignments for SPES

Wavenumber(cm^{-1})	Assignments
3095, 3068	Aromatic C-H stretching
1579, 1487, 1471, 1408	Aromatic C=C stretching
1321, 1296	Doublet resulting from antisymmetric O=S=O stretching of the sulphone groups.
1240	Antisymmetric C-O-C stretching of the aryl ether group
1167	Antisymmetric O=S=O stretching of the sulphonate group
1151	Symmetric O=S=O stretching of sulphone group
1107, 1080	Aromatic ring vibrations
1024	Symmetric O=S=O stretching of the sulphonate group
1010	Ring vibration of p-substituted aryl ether
869, 850	Out of plane C-H deformation of isolated H in 1,2,4 substituted benzene ring

The $\nu_{as}(SO_3^-)$ mode is expected at around 1200 cm^{-1} but very frequently (as seem to be case here) is not readily observable due to overlapping bands in that region.

Concerning these bands, if the dry and hydrated spectra are compared, we can see that the 1080 cm^{-1} band of the benzene ring increased with hydration. Accordingly, we suppose that this band is the in-plane skeleton vibration of benzene when the substituent has the ionic form instead of the acid one. The change observed was probably caused by displacement of the electrons in the benzene ring. The figure also shows that the increase on the 1080 cm^{-1} band goes hand in hand with the increase of the $\nu_s(SO_3^-)$ that lies at 1025 cm^{-1}. These results show that on hydration, the acid groups are dissociated into SO_3^- ions. Hence, we can conclude that the structural transformation of the ions under the influence of the proton can lead to a considerable change of intensity of the band which arises from modes of the benzene ring. In other words, changes do occur in the benzene ring mode that are dependent on the degree of hydration.

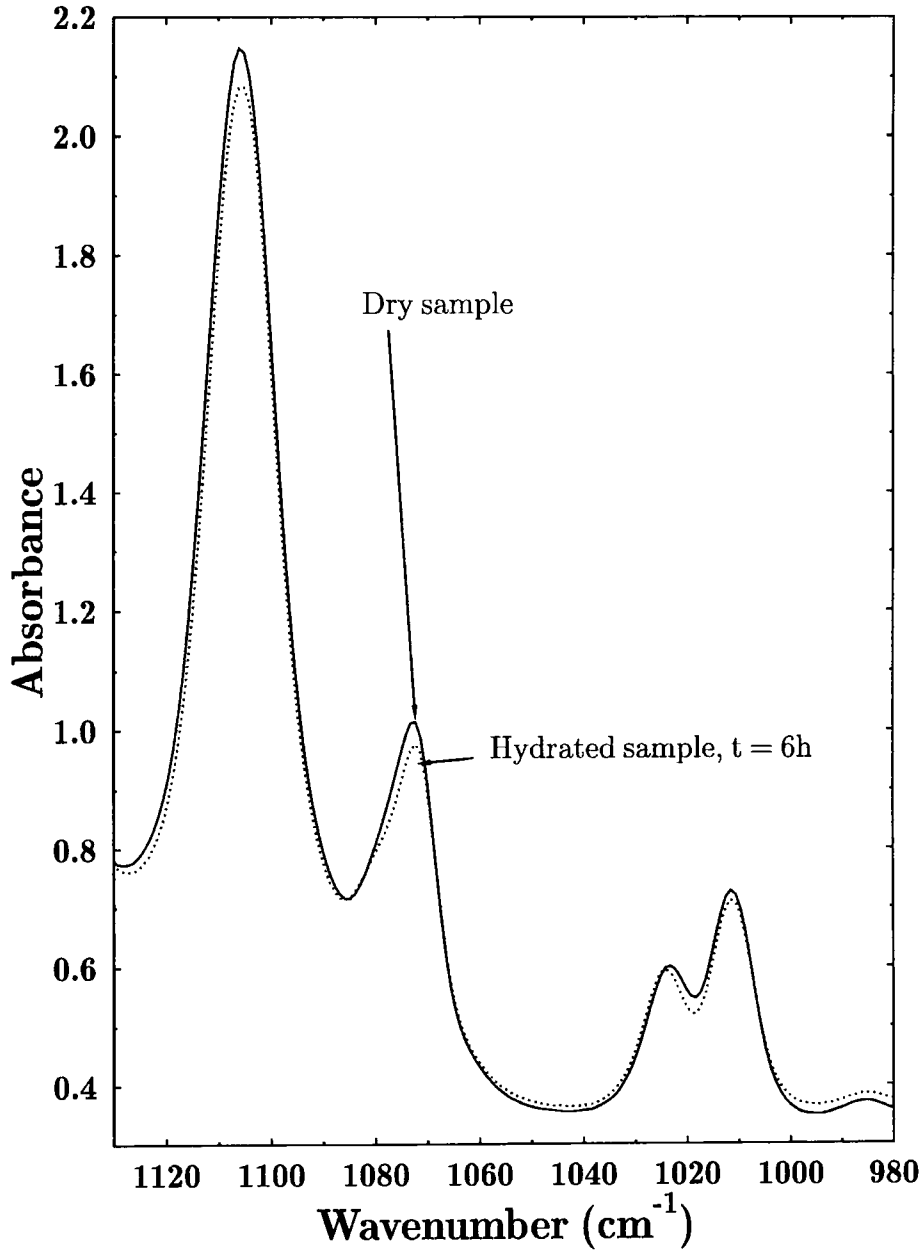

Fig. 3.10 - Hydration effects on SPES(S=20)/NMP.

Fig. 3.8 also shows that as the water content increased the $\nu_s(SO_3^-)$ (at 1021 cm^{-1} initially), is shifted to higher wavenumber. Shifts on frequency can be caused by hydrogen bonding since it alters the force constant of both groups, the proton donor and the proton acceptor. By definition, a stronger hydrogen bonding acceptor property leads to stronger bridges and hence to a stronger shift of the band toward smaller wavenumber. According to fig.3.8 the dry membrane could contain structures like:

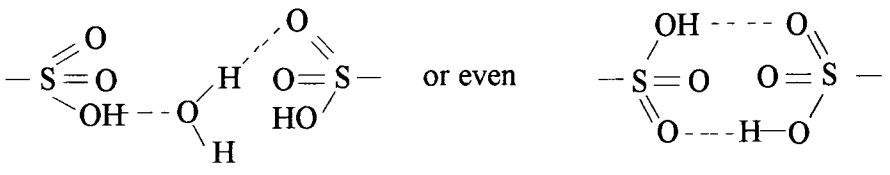

that have atoms considerably more effective as acceptors for hydrogen bridges than the oxygen atoms of the SO_3^- ions. Hence, as the as the hydration process occurs, the number of SO_3^- present increases and consequently the $\nu_s(SO_3^-)$ is shifted to higher frequencies (weaker hydrogen bridges).

According to theses results, the hydration process can be described as shown in fig. 3.9.

Fig.3.10 shows the effect of hydration, on the same spectral region for the less sulphonated membrane (SPES(S20)) and, as we can see such effects can hardly be observed. These results must certainly be connected to the lower concentration of sulphonate groups on this membrane.

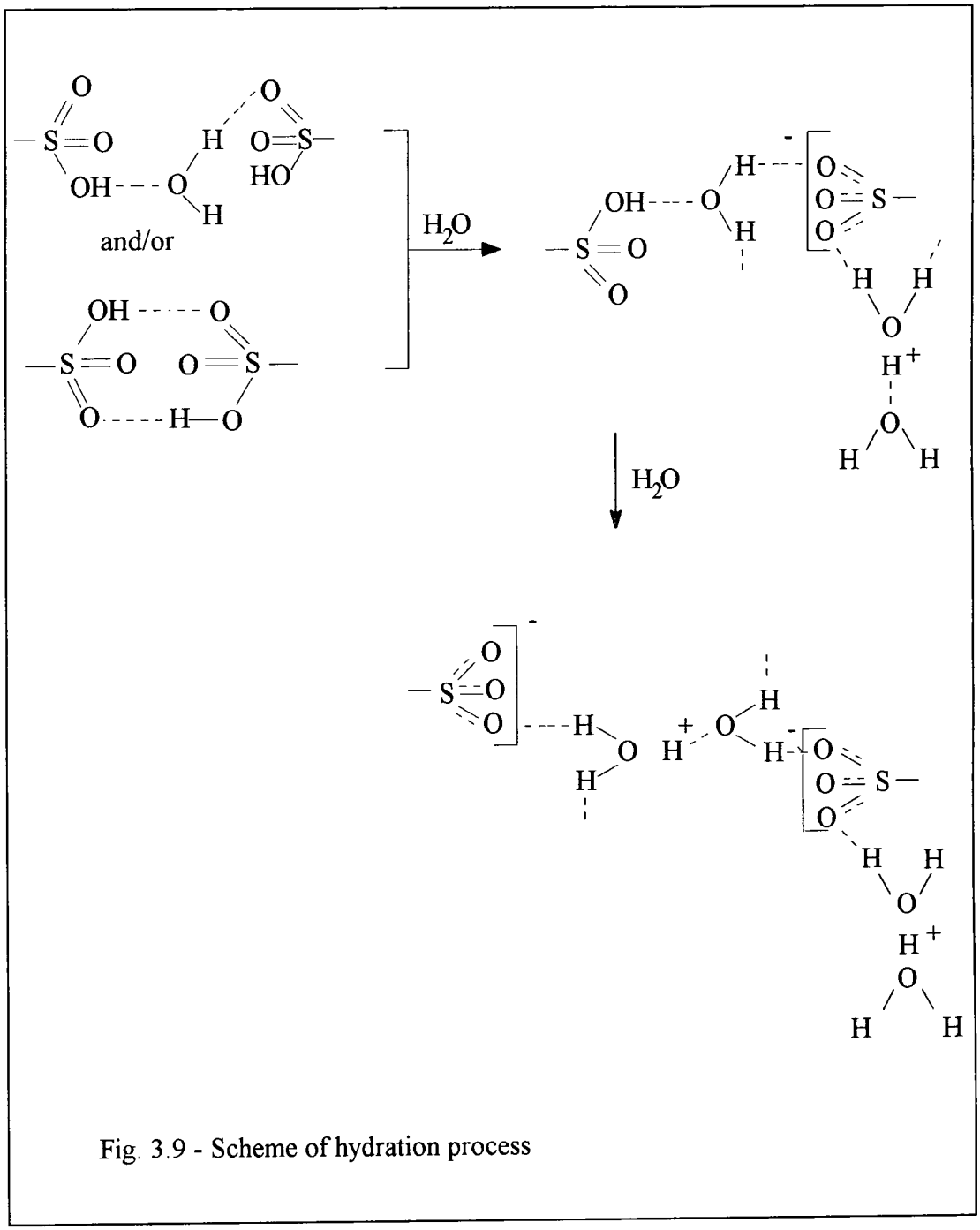

Fig. 3.9 - Scheme of hydration process

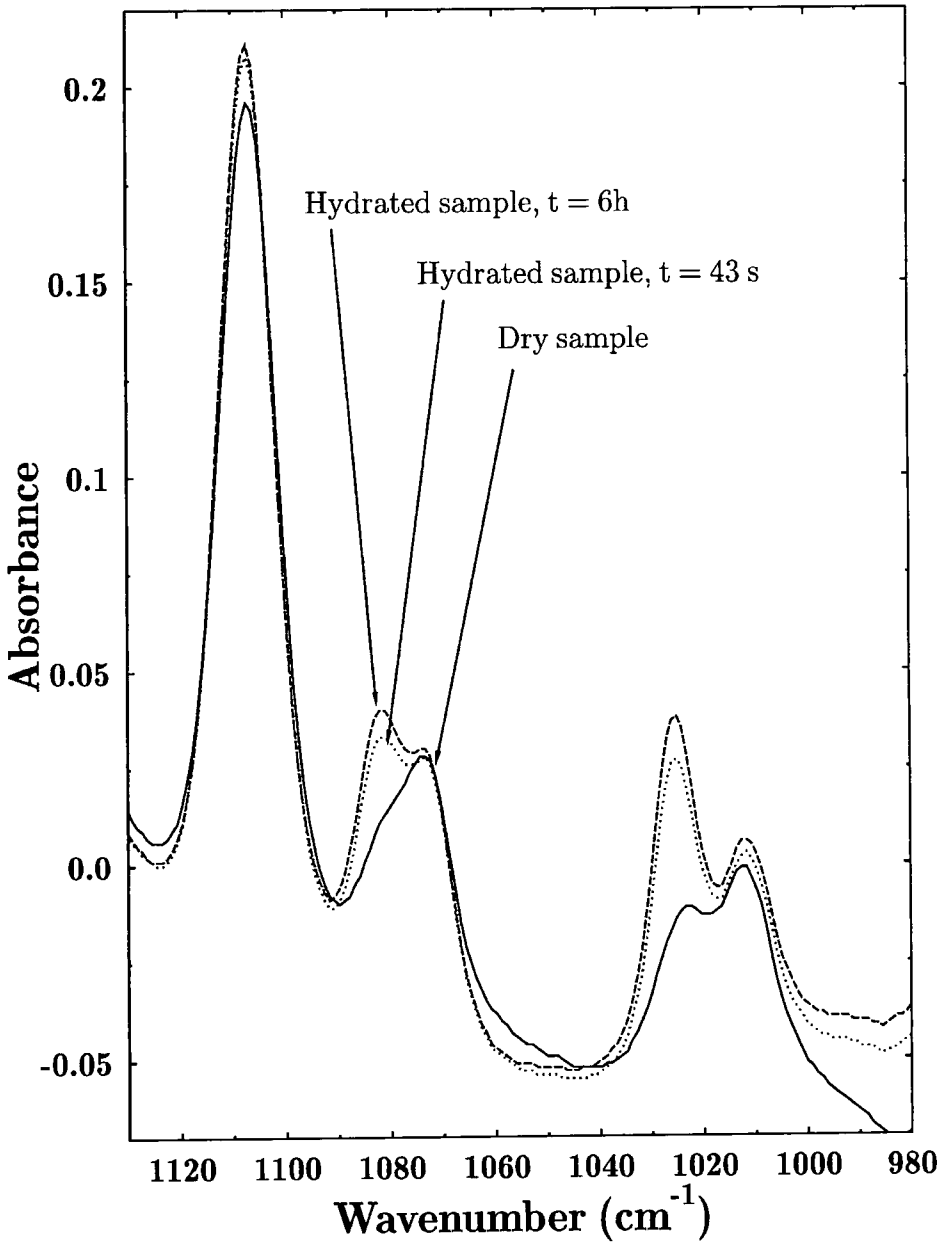

Fig. 3.8 - Hydration effects on SPES(S=5)/Formic acid.

3.3.2.1 - **Influence of the Electric Field Decay**

This section contains a discussion of the variations on the water ν(OH) band as a function of time for films with different thicknesses.

Fig.3.11a shows the OH band intensity variations as a function of time for a 0.1 μm thick film. Fig.3.11b compares the hydroxyl stretching region for pure liquid water and the hydrated membrane. Fig.3.12a and b show the same region but now using a 15 μm thick film. As we can see, in both cases, the water uptake was very fast. After approximately 2 hours an equilibrium is achieved. Regarding the band shapes and equilibrium absorbances sensible differences could be observed and will be discussed below:

Considering the level of absorbance we can see that on thin films the equilibrium absorbance was much more intense than on the thick one. In fact, on the thin film the equilibrium absorbance was almost as intense as the pure liquid water as shown on fig.3.11b. This apparently surprising result can be easily understood considering the basic principles of the ATR theory already discussed on chapters 1 and 2. According to the theory, a thin film is defined as a film where the electric field amplitude remains essentially constant over the thickness, t, that is, $t<<d_p$ while a thick film is a film where the electric field amplitude falls to a very low value within the thickness, t, that is $t>>d_p$.

In fig.3.11 we are working with a thin film where, by definition, medium 2 (sample) is too thin to have a controlling effect on the evanescent field. In this case, medium 3 (air for the dry and water for the hydrated sample), behind medium 2 would control the decay of the field and therefore must be considered on d_p calculation. Thus, for the thin film case, n_{21} must be replaced by $n_{31} = n_3/n_1$. The calculated values of d_p are shown in table 3.3.

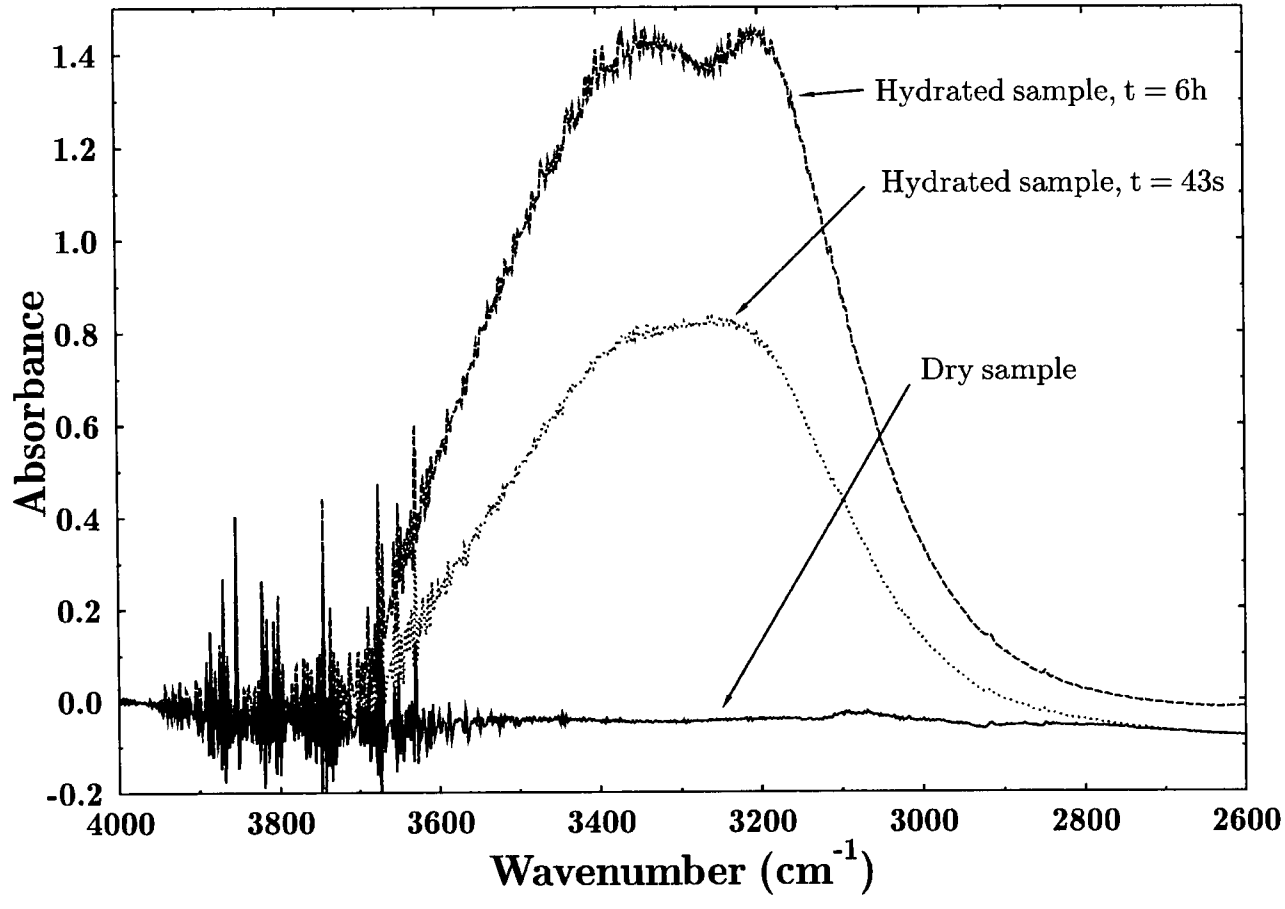

Fig. 3.11a - Hydration process observed using 0.1 μm film and a liquid cell.
System: SPES(S=5)/Formic acid.

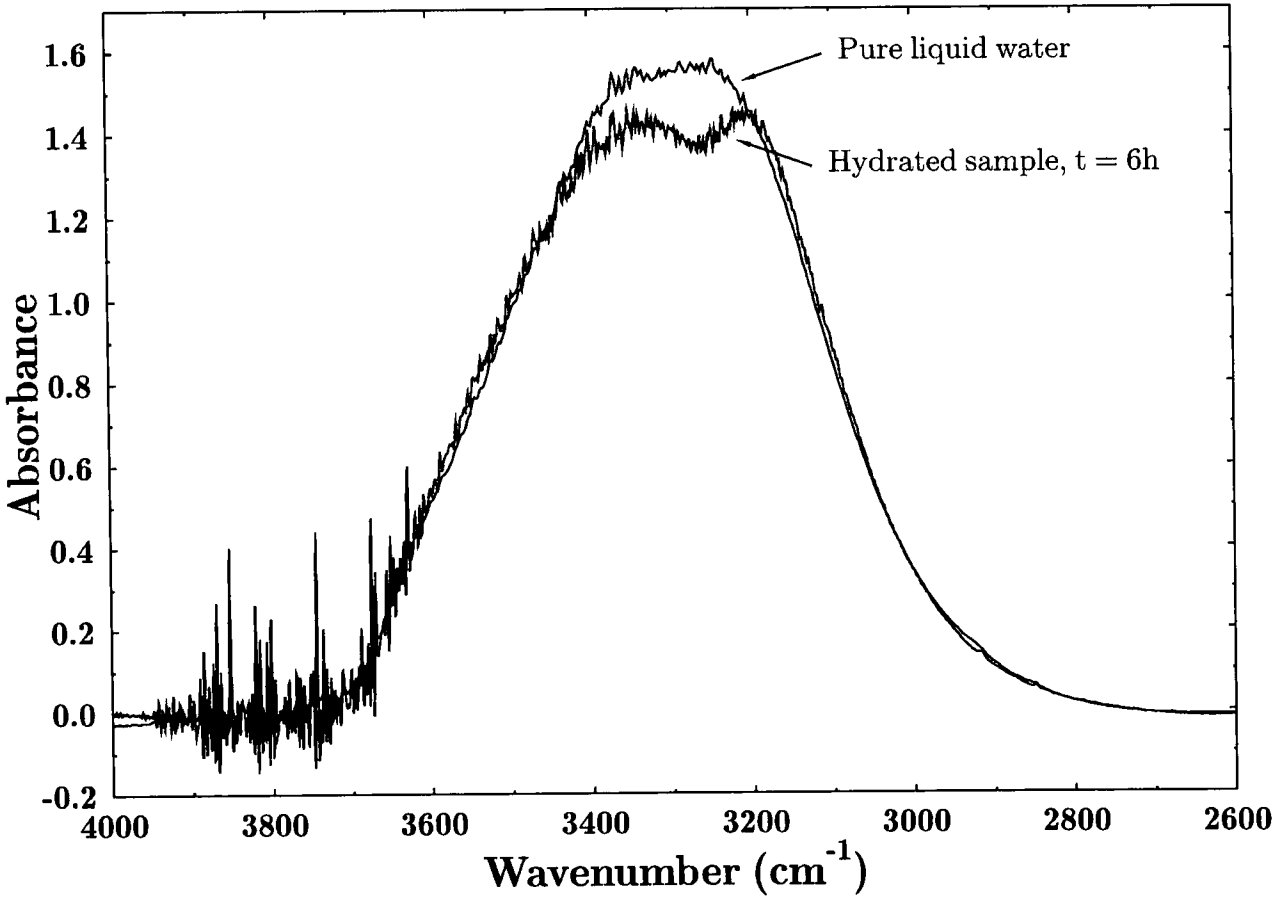

Fig. 3.11b - Comparison of OH stretching region for a thin hydrated film and pure liquid water. System: SPES(S=5)/Formic acid.

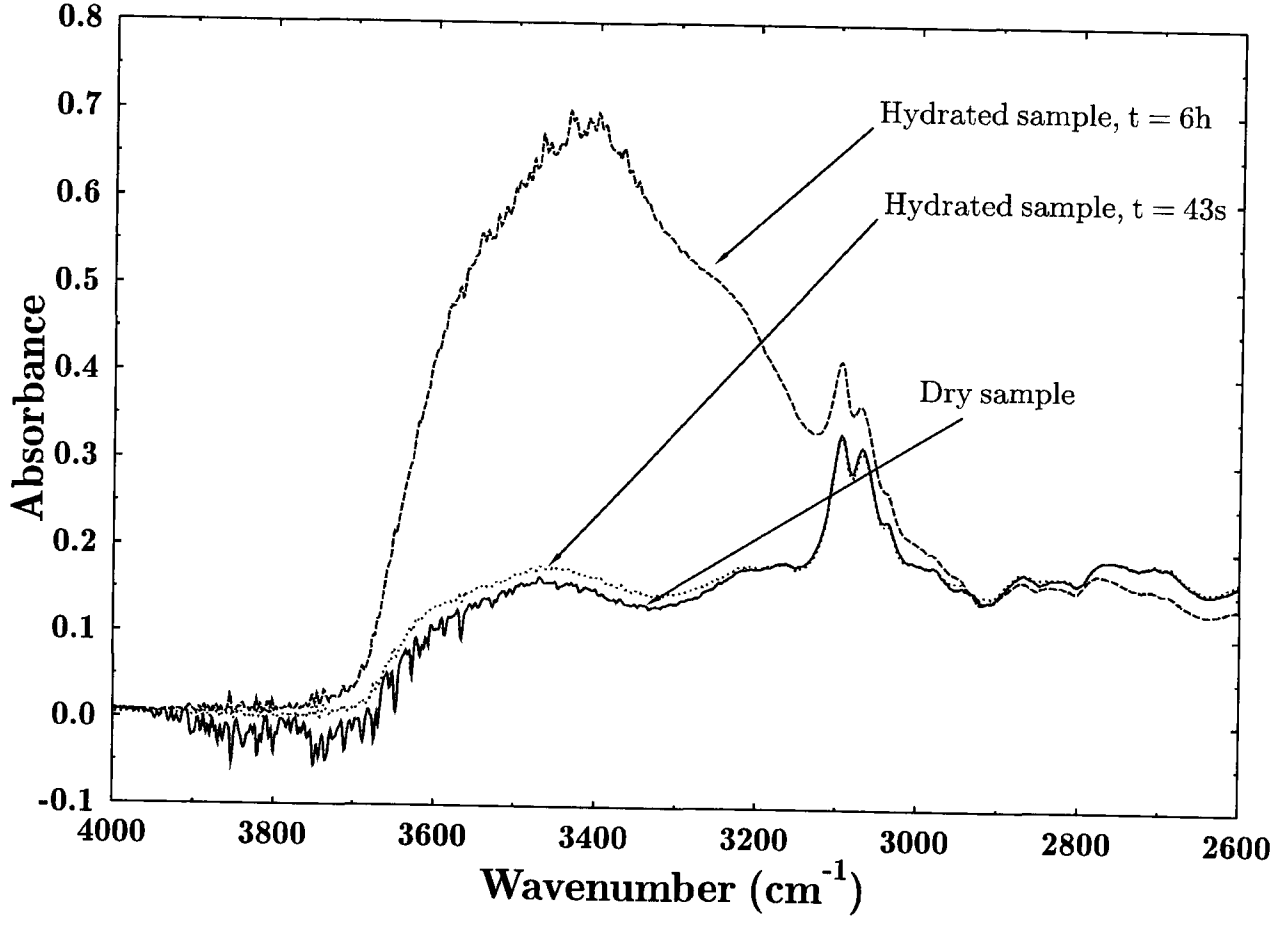

Fig. 3.12a - Hydration process observed using 0.1 μm film and a liquid cell.
System: SPES(S=5)/Formic acid.

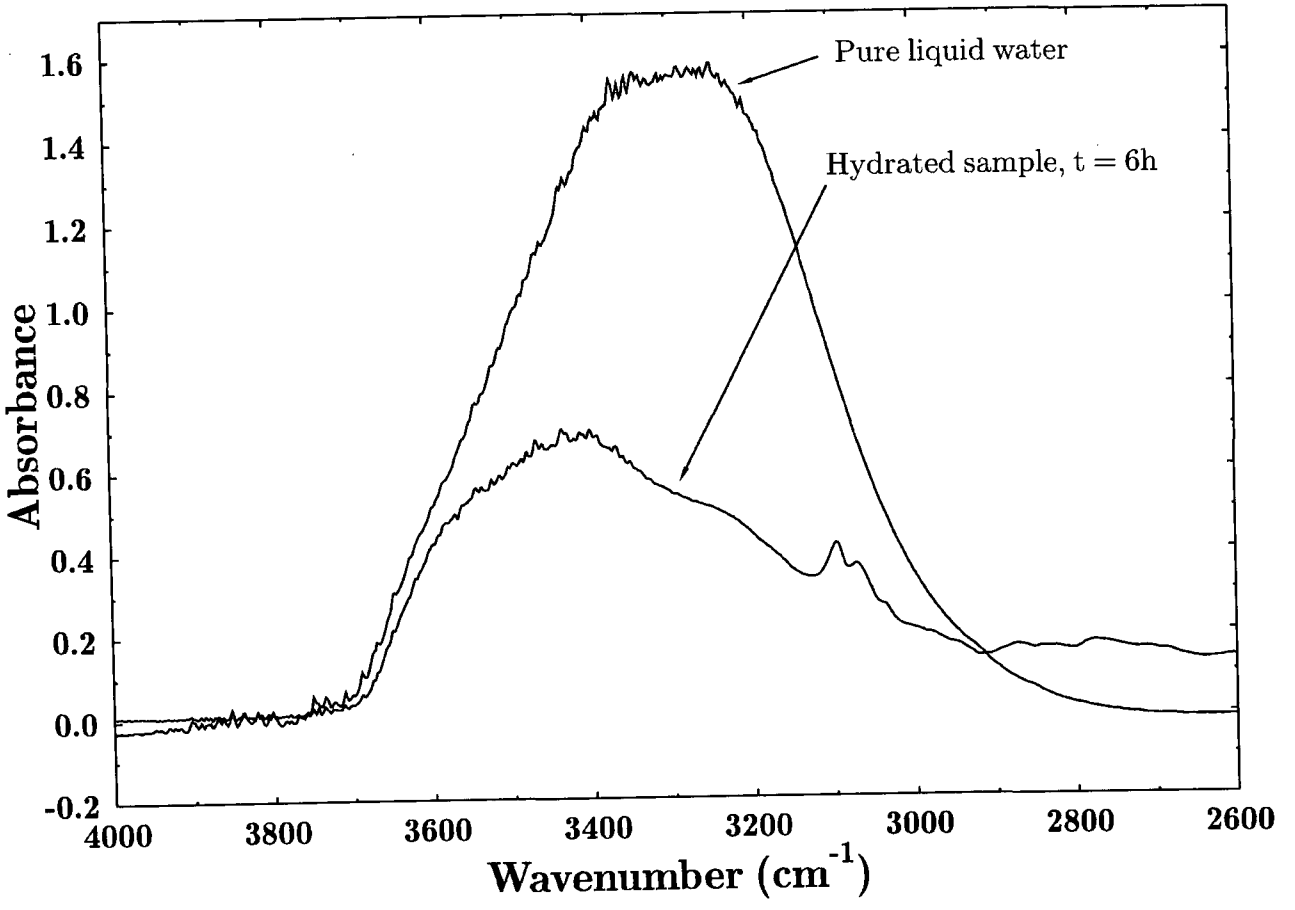

Fig. 3.12b - Comparison of OH stretching region for a thin hydrated film and pure liquid water. System: SPES(S=5)/Formic acid.

Table 3.3 - d_p Calculation for Thin and Thick Films

		d_p (μm)		
λ (cm^{-1})	$\lambda_1 = \frac{\lambda}{n_1}$ (μm)	n_{21}	n_{31} (H_2O)	n_{31} (air)
4000	1.04	1.00	0.38	0.29
3500	1.19	1.14	0.43	0.33
3000	1.39	1.34	0.50	0.39

Where n_1 is the refractive index of the IRE, n_2 is the refractive index of the sample and n_3 is the refractive index of water (for hydrated samples) or air (for the dry ones). With that values of d_p it is possible to calculate the electric field decay as a function of the depth from the interface. The results are shown in fig. 3.13.

Considering fig. 3.13 we can see that if we are working with a 0.1μm thick film the electric field will not decay completely inside the film but on medium 3 as well. So the spectra of fig. 3.11 contains information not only about water absorbed by the membrane but also about liquid water surrounding the sample. This fact explains the bigger intensity observed for the thin film. In fig. 3.12 where the film thickness is much bigger than dp, the spectra contain only information about water absorbed by the film since the electric field decays completely inside it.

The results discussed above and many others obtained using films with different thicknesses showed that, although the liquid cell has the great advantage of allowing *in situ* measurements of water absorption, the results must be very carefully analysed

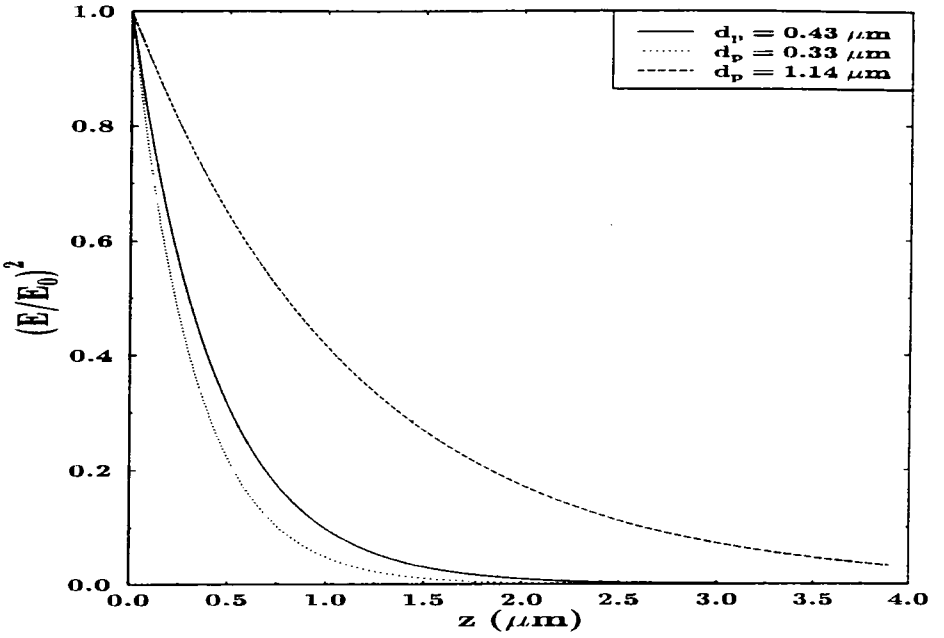

Fig. 3.13 - Electric field decay as a function of the depth from the interface for $\lambda = 3400\ cm^{-1}$.

especially when using thin films, in order to determine exactly the amount of water absorbed by the membrane.

3.3.3 - Results of Subtraction

3.3.3.1 - ν(OH) Band Variations

Because in the thin film case we are also sampling liquid water, to obtain only the spectra of water absorbed by the membrane it is necessary to subtract the pure liquid

water spectra from the membrane-water spectra. However, as we can see from fig.3.12b the hydroxyl bands for pure liquid water are more intense than the hydroxyl band intensities for the membrane-water system (as is expected since the membrane is an absorbing material and in this case is working as a barrier layer) and therefore the subtraction would produce negative bands. In order to avoid this problem, instead of subtracting the pure liquid water spectrum we subtracted the membrane-water spectra in the first hydration time from the membrane-water spectra at different times. The subtraction can be represented as follow:

$(\text{membrane-water}_{in} + \text{water}_{out})_t$ - $(\text{membrane-water}_{in} + \text{water}_{out})_{t=43sec}$ = *amount of water absorbed by the membrane as a function of time*

Where water_{in} means water inside the membrane and water_{out} means liquid water outside the membrane. In that way we can eliminate the influence of liquid water. The subtracted spectra will be basically the difference in water absorbed by the membrane as a function of time after t = 43 seconds. If the membrane spectrum was not modified by the presence of water the subtracted spectra should present just hydroxyl band variations. If, however the membrane spectrum was modified by hydration, these changes must be present on the subtracted spectra.

Fig. 3.14 shows the results of subtraction for the ν(OH) band in the thin film case. As we can see, once the pure liquid water was removed, the remaining spectral band, which represents only the water absorbed by the membrane is very small. This result is now in agreement with the fact that the absorption capacity is directly proportional to the film thickness and therefore the thin film should absorb less than the thick one.

Once the differences in absorbances are understood, we will try now to elucidate the state of water on the membrane by analysing the shape of the pure liquid and sorbed water.

Luck[99,121] has provided an extensive review of the structure of water in solution and in desalination membranes using near infrared spectroscopy. According to this author, the ν(OH) band can be divided into three component bands. Component peak I is attributed to OH groups of water molecules that are not hydrogen bonded, peak II to very weakly bonded OH groups, perhaps water dimers, and peak III to linear hydrogen bonds that are characteristic of extended water structures such as are found in ice[121]. The frequency of this band in various desalination membranes is higher than that of pure water, due to the overall weaker hydrogen bonding in such environment. This would favour an efficient flux of water through the membranes.

The character of sorbed water in ionomers has also been studied by several other authors using near and mid infrared absorbance bands[89,99,120]. This research has been reviewed by Falks[100,105], The main conclusions in this case were that the average hydrogen bond strength of the sorbed water is considerably lower than that in pure water and that two (instead of three as in Luck's work) spectroscopically distinct forms of OH environments can be detected. The first form consist of OH groups that do not participate in hydrogen bonding and the second and predominant type represents those which have relatively weak hydrogen bonds. Hydrogen bonding of water to itself and to sulphonate groups are likely, although more than one type cannot be seen. The conclusion is that these may have similar hydrogen bonding strengths.

The water molecule has three normal modes of vibration, a symmetrical stretching mode ν_1, a bending mode (scissor mode) ν_2, and an antisymmetric stretching mode ν_3. The positions of the bands of these normal modes are given in table 3.4 for the free water molecule.

Table 3.4 - The Bands of the Free Water Molecule[112]

Molecule	$\nu_1(cm^{-1})$	$\nu_2(cm^{-1})$	$\nu_3(cm^{-1})$
H_2O	3650	1590	3750

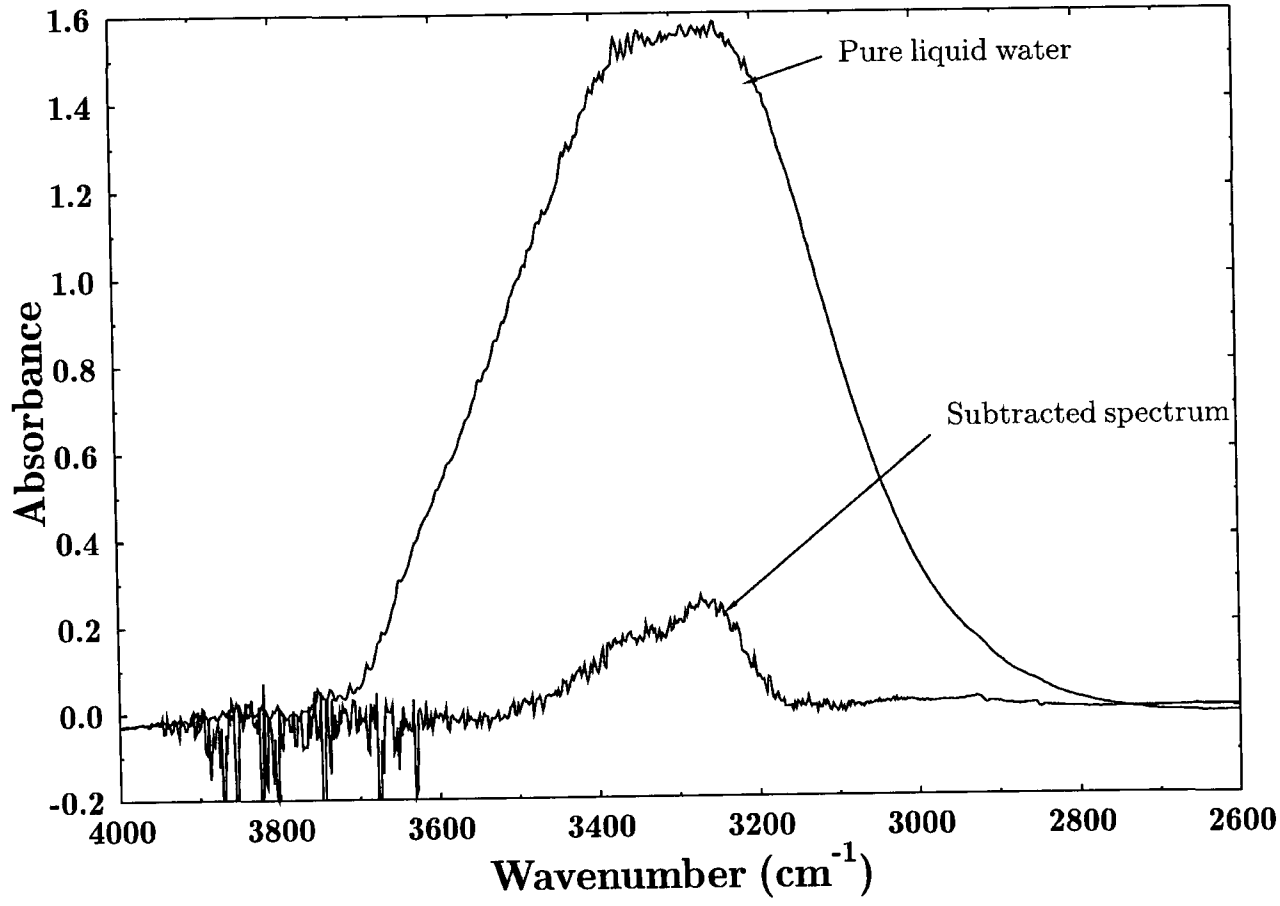

Fig. 3.14 - Result of subtraction on a thin film. System: SPES(S=5)/Formic acid.

If the water molecule is bound to its surroundings by hydrogen bridges, the bands ν_1 and ν_3 of the stretching vibrations of water molecules are shifted to lower wavenumbers, and the ν_2 band is shifted toward higher wavenumbers compared with that of the free water.

The positions of the bands of liquid water are summarised in table 3.5.

Table 3.5 - The bands of Liquid Water(20°C)[112]

Molecule	Free OH Groups (cm^{-1})	OH in Hydrogen Bridges (cm^{-1})	Overtones of the Scissor Vibration, $2\nu_2$ (cm^{-1})	Scissor Vibration + Torsion Vibration (cm^{-1})	Scissor Vibration, ν_2 (cm^{-1})
H_2O	3615	3400	3225	2110	1640

In liquid water, the band of the OH stretching vibration of the hydrogen bridges is found at about 3400 cm^{-1}. Under the present conditions, the band of the antisymmetric ν_3 and the symmetric ν_1 stretching vibrations almost coincide. This is a consequence of interaction of the water molecules one with another[112].

From fig. 3.12a we can see that the dry sample presents a prominent feature in the OH stretching region at about 3500 cm^{-1}, that is greater than the main OH stretching absorption band for liquid water, centred at about 3400 cm^{-1}(according to table 3.5) Possibly we are dealing here with some free OH of the sulphonic acid present on the dry membrane or some water molecules whose hydrogen bonding is weaker than in liquid water.

As the water content increases two features appears, one at about 3400 cm^{-1} and a second at 3250 cm^{-1}. In both cases the intensities increased rapidly with hydration time. Comparing the hydrated spectra with the pure liquid water spectra we can see that, especially in the thick film case, the main ν(OH) stretching band localised at 3400 cm^{-1} is considerably above the value found for liquid water (3330 cm^{-1} in our case). These observations indicate that the average hydrogen bonding strength of the sorbed water is

lower than in liquid water This fact will favour the efficient flux of water through the membranes, as already stated by Luck[121] and Falk[100].

3.3.3.2 - Other Changes Brought About by Subtraction

In this section we will discuss other significant results produced by the subtraction. As stated on previous chapters, subtraction is one of the powerful tools when using FTIR and can be used for different purposes like confirmation of the identity of a sample using a standard and quality control. A valuable use of scaled absorbance subtraction is the identification of molecular changes. In our case, the difference spectrum will indicate any molecular changes caused by hydration since any constant features will be removed by the subtraction procedure. It should be noted that scaled absorbance subtraction, or difference spectrometry, is not a solution to all the problems. Scaled subtraction is not possible, for example, if the absorbances are too high. In other words, we need to ensure that Beer's law is obeyed. A good rule to follow for scaled subtraction is to be certain that the spectra under study have absorbances less than 0.5 absorbance units.

Fig. 3.15 shows the subtracted spectra for a hydration time of 7 hours. As we can see, the most intense bands are the stretching and bending vibrations of water. However, the figure also shows that there are some bands that were not completely removed indicating some molecular change caused by hydration. These bands are the symmetric stretching of the SO_3^- groups at 1025 cm^{-1}, and the 1080 cm^{-1} benzene ring vibration already discussed. The band at 1150 cm^{-1} and the doublet at 1300 cm^{-1} are related to the stretching vibrations of the sulphone groups. Fig. 3.16 compares the subtracted with the non-subtracted spectra of the hydrated sample to give an idea about the magnitude of the residual bands.

Fig. 3.17 shows the same spectra used on fig. 3.16 but now on the superimposed form, where both spectra, subtracted and non-subtracted are displayed on the same scale (in this case the scale of the subtracted spectra). This format was chosen in order to clarify the differences observed.

According to the figure, the most significant result is the appearance of a band at 1200 cm^{-1} that could not be observed in the non-subtracted spectra. Returning to table 3.2 we can see that this spectral region is usually assigned for the antisymmetric O=S=O stretching of the sulphonate groups. As stated before, this band, very frequently, is not readily observable due to overlapping bands in the region. With the subtraction this band is now clearly defined. According to the literature[112,117] the SO_3^- ion has a C_{3v} symmetry and all SO bonds are identical. The antisymmetric vibration of a group with C_{3v} symmetry is doubly degenerate. This means that there are two modes of vibration with the same energy and hence, in the degenerate case, only one band. As seen in fig.3.17 this band seems to be split indicating possibly that the degeneracy has been removed. The following paragraph describes some possible explanations for the removal of degeneracy. However, because the band intensities are very small in the subtracted spectra, we should not rely too much on these results and in order to confirm the possibility of removal of degeneracy more experimental work would be necessary.

There are two possibilities to explain the removal of degeneracy. The first one is that the removal of degeneracy arises from linkage of the SO_3^- ion to another group. In our case, the spliting of the band could arise from that disturbance of symmetry produced by linkage of the anion to the benzene ring. Another possibility is that the counterion removes the degeneracy. This can be caused, by motion of the mass of the counterion in the vibration of the SO_3^- ion. On the other hand, the interaction between the counterion and the SO_3^- ion, and, in particular, the effect of the electrostatic field of the counterion on the anion, may disturb the C_{3v} "local" symmetry. Considering that the counterion is unsymmetricaly bound to the anion, the counterion field that polarises the anion unsymmetrically disturbs the mesomeris bond resonance in these anions and the

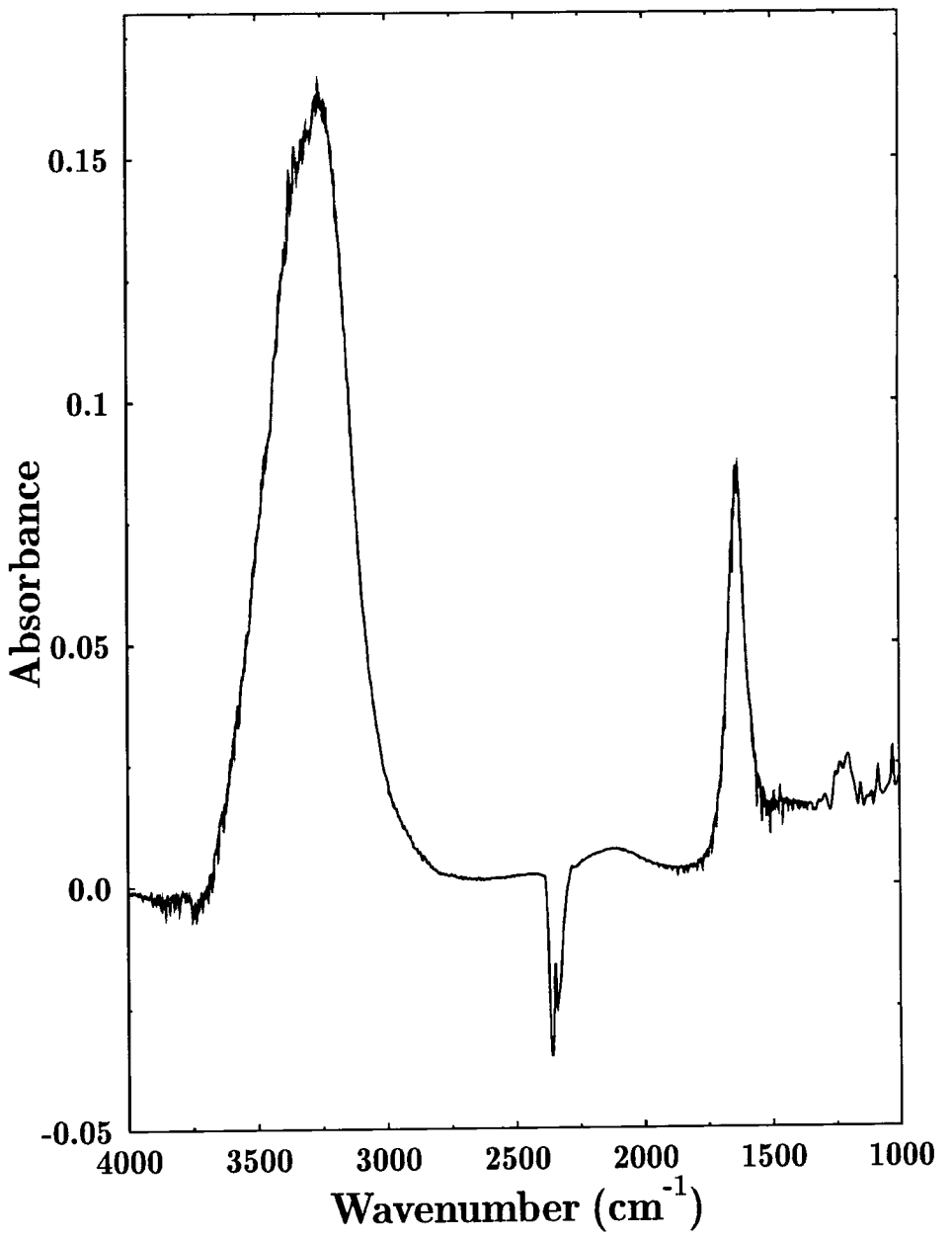

Fig. 3.15 - Result of subtraction. System SPES(S=5)/ Formic acid.

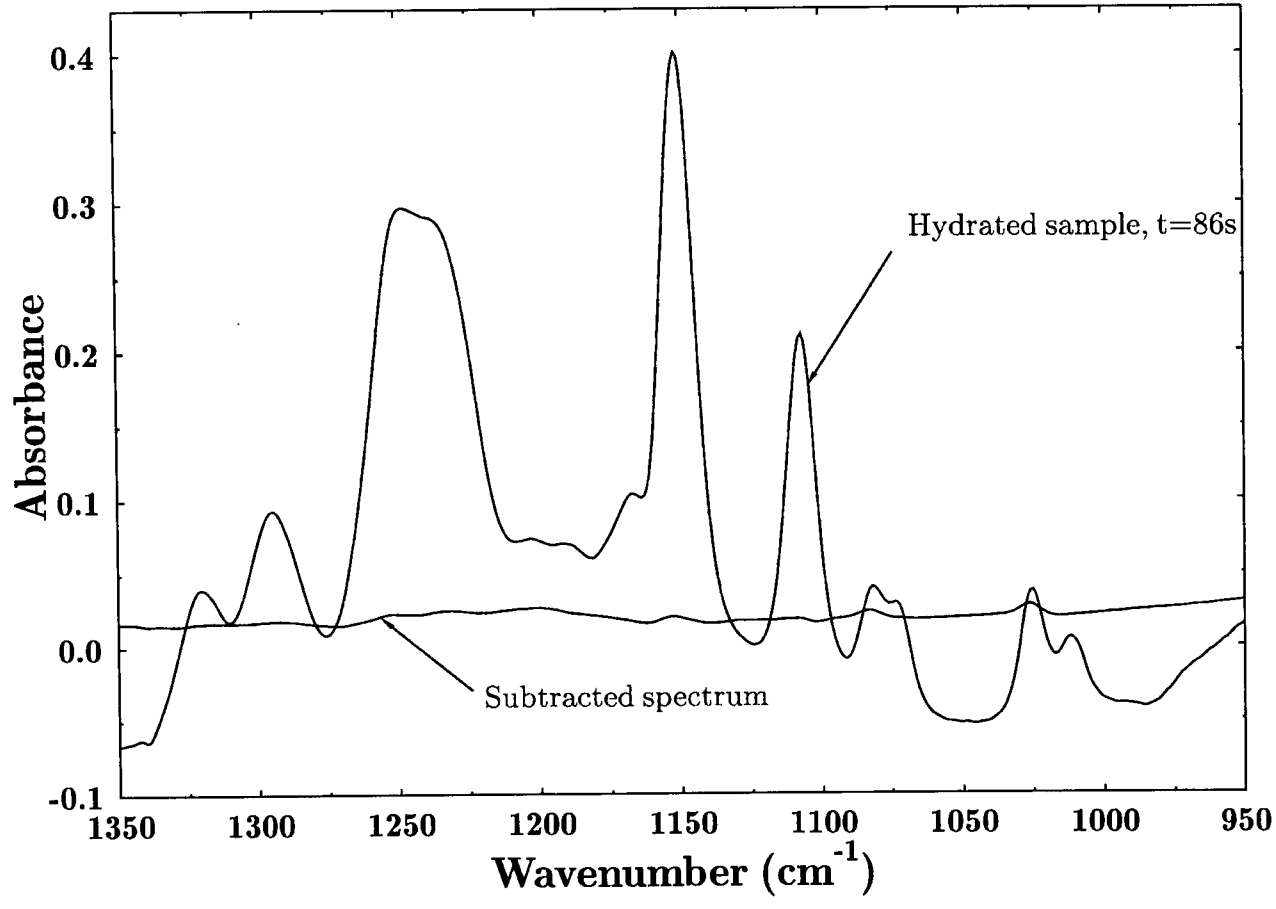

Fig. 3.16 - Comparison between subtracted and non-subtracted spectra on a thin hydrated filme. System: SPES(S=5)/Formic acid.

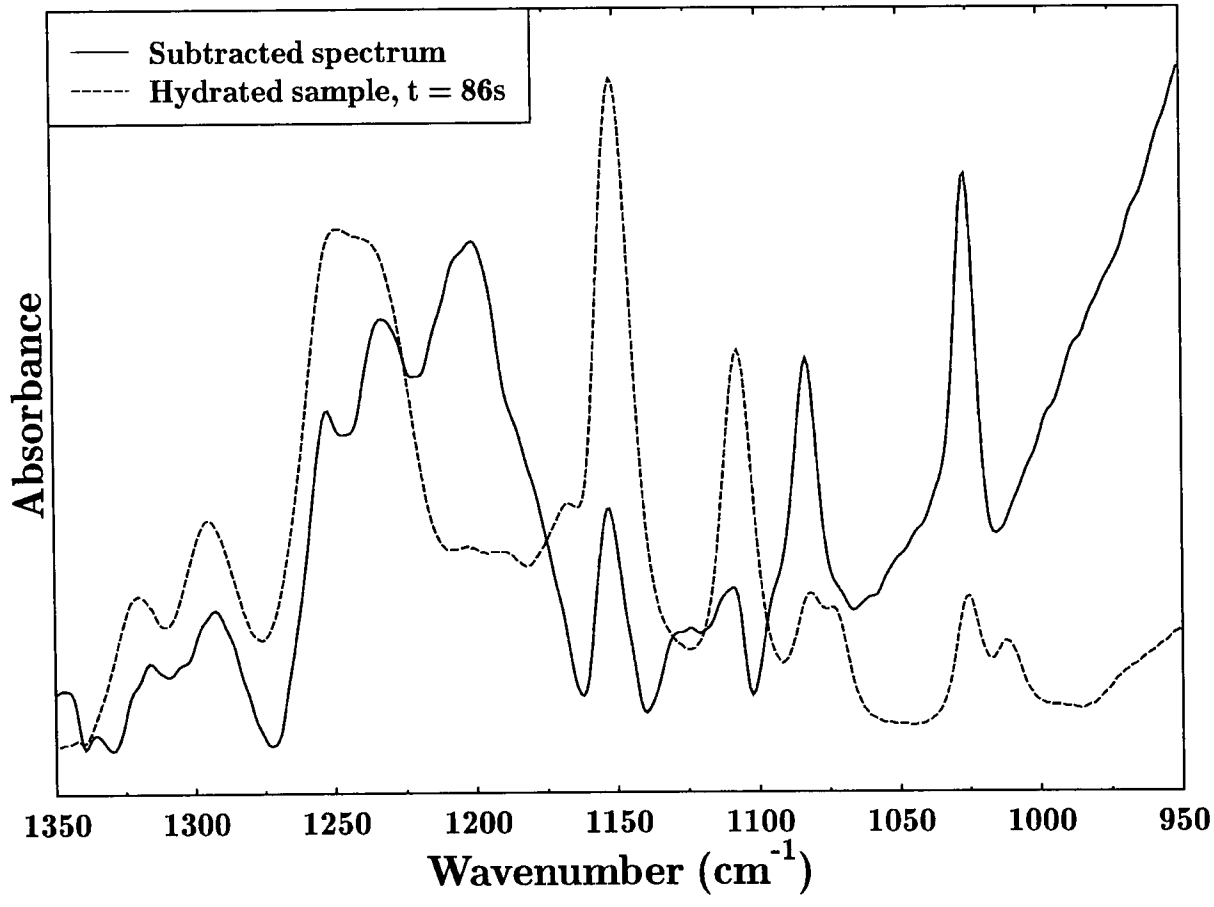

Fig. 3.17 - Comparison between subtracted and non-subtracted spectra on a thin hydrated filme. Superimposed spectra. System: SPES(S=5)/Formic acid.

C_{3v} "local" symmetry changes to C_s symmetry. This, in turn, removes the degeneracy of the antisymmetric stretching vibration. In this case the splitting will be dependent on the strength of the counterion field, since the stronger the field, the more strongly is the anion polarised.

In summary, we demonstrate in this chapter that FTIR-ATR may provide a useful, non-destructive technique for detecting changes on particular functional groups in a complex molecule during exposure to water. The proposed method also provides information about the state of water at the membrane/water interface. In following chapters we will describe how the same method can also be used to get information about the kinetic of water absorption on the membranes. A set of calculations will be presented to demonstrate that FTIR-ATR can be used as a convenient approach to measuring the diffusion of water in polymeric membranes.

Chapter 4

FTIR- ATR Spectroscopic Determination of Diffusion Coefficient of Water in Polymeric Membranes. Part I

CONTENTS

4.1 - *INTRODUCTION*

This chapter decribes some of the basic principles of the process of permeation through polymeric membranes and demonstrates how FTIR-ATR spectroscopy can be used to calculate the diffusion coefficient of polymeric membranes.

As discussed in the previous chapters, the film thickness is a parameter that must be carefully analysed in connection with the electric field decay. Because of that, two different approaches were developed, one for thin films and another for thicker ones.

Another point investigated relates to the sorption kinetics. Two models were proposed to describe the diffusion of water in sulphonated polyethersulphones as a) Fickian and b) case II. The experimental results were used to identify each process as appropriate. In summary, four approaches were developed, as shown below:

- Fickian diffusion
  - Thin film
  - Thick film
- Case II diffusion
  - Thin film
  - Thick film

4.2 - *THEORETICAL BACKGROUND*

Membrane filtration processes are now being used industrially as an alternative to conventional separation methods such as distillation, centrifugation and extraction. In all these cases, diffusion processes play an important role in the transport mechanism of the solutes. The various processes that can occur during processes in which membranes are involved are summarised in table 4.1[122].

Table 4.1 - Summary of the various areas where diffusion occurs[122].

1 - In membranes	(a) in dense membranes (gas separation, pervaporation)
	(b) in porous membranes
	- gases
	- liquids
	- facilitated transport (liquid membranes)
	- solutes (controlled release)
	- electrodialysis
2 - In the boundary layer near the membrane	
3 - During membrane formation	

Diffusion is defined as a process by which matter is transported from one part of the system to another as a result of random molecular motion[66]. The motion of a single molecule can be described in terms of the "random walk" picture. It is possible, statistically, to calculate the mean-square distance it has travelled in a given time interval, but is impossible to predict in what direction a given molecule will have moved in that time[2,67]. Transport, or diffusion, is a function of structure of both the polymer and the penetrant. This includes both local chemical structure and longer range order described as morphology. In glassy polymers a time dependent deformation induced by the solvation process, can give rise to a dramatic change in the diffusion rate. This question has not been fully explored[80,123-126].

The process of permeation through polymeric membranes is generally explained in terms of the solution diffusion model[127]. This model postulates that the permeation of a molecule through a polymer film occurs in three stages (1) sorption on to the polymer, (2) diffusion through the polymer and (3) desorption from the opposite face. Temperature, solubility, reactivity, orientation and composition modify the transport process. N.E.Schlotter[126] has published a comprehensive review about how such parameters can affect the transport properties on polyolefins. The general conclusions

can be summarised. Increasing the crystallinity without introducing defects will tend to reduce the diffusion rates. Orientation of semicrystalline polyolefins and thermal processing can lead to contradictory results due to a lack of understanding of the morphologies being formed. Increasing molecular size, or rigidity of the diffusant will decrease the diffusion rates. Increasing the surface-to-volume ratio increases the loss of diffusants if they can volatilize or transfer to a liquid at the surface. Temperature tends to increase diffusion rates, but there is a delicate thermodynamic balance related to phase transformations available to the diffussants. Other factors like film thickness, crosslinking shape and chemical nature of the diffusant have also been reported but an understanding of diffusion still needs significant improvement to be useful for quantitative prediction.

4.2.1 - Sorption

The term "sorption" is used here to describe the initial penetration and dispersal of permeant molecules into the polymeric matrix. The term includes adsorption, absorption, incorporation into microvoids and cluster formation[67]. The permeant may undergo several modes of sorption simultaneously in the same polymer. In addition, the distribution of permeant between the different sorption modes may change with concentration, temperature and swelling of the matrix as well as with time.

The extent to which permeant molecules are sorbed and their mode of sorption in a polymer depends upon the enthalpy and entropy of permeant/polymer mixing, *i.e.* upon the activity of the permeant within the polymer at equilibrium. Here, a brief description is given of the most common types of sorption isotherms which have been used to describe permeation in polymers.

Sorption behaviour has been classified on the basis of the relative strengths of the interactions between the permeant molecules and the polymer or between the permeant molecules themselves within the polymer.

4.2.1.1 - Henry's Law Sorption

The simplest type of sorption arises when both polymer/permeant and permeant/permeant interactions are weak relative to polymer/polymer interactions, *i.e.* when ideally dilute solution behaviour occurs and Henry's law is obeyed. The solubility coefficient S is a constant, independent of sorbed concentration at a given temperature. Consequently, the sorption isotherm shows a linear dependence of concentration *vs.* pressure(p)[127].

$$C = Sp \qquad \text{(eq. 4.1)}$$

Typically, this type of behaviour is observed when permeant gases are sorbed by rubbery polymers at low ($<10^5$Pa) pressure and arises from the very low solubility (<0.2%) of the permeant gases in the polymer[127].

4.2.1.2 - Langmuir-type Sorption

Langmuir Sorption indicates a tendency for significant levels of sorption to occur at relatively low pressures. Physically, this represents initial sorption in some kind of specific site or immobilisation of permeant molecules, in microvoids in the polymer. When nearly all the sites are occupied, a very small amount of permeant randomly dissolves in the polymer. The concentration, C_H of the permeant sorbed by these holes or sites is represented by the Langmuir equation[127]:

$$C_H = \frac{C_H' bp}{1 + bp} \qquad \text{(eq. 4.2)}$$

Where C_H is a hole or site saturation constant and b is a hole or site "affinity" constant, representing the ratio of rate constants for adsorption and desorption. Typically, this type

of behaviour occurs when gases or vapours are absorbed by polymers containing dispersed porous particles of high surface area, *e.g.* inorganic fillers such as carbon black or silica gel[128].

4.2.1.3 - Dual-mode Sorption

A combination of Henry's law sorption with that of the Langmuir type has been used to explain the sorption isotherm commonly observed in microheterogeneous media. Its applications include such diverse topics as the transport of gases in glassy polymers and dyes in textiles fibres[129]; drug transport in skin[75] and water clustering in reverse osmosis membranes[130]. The dual-mode theory views sorption occurring in two distinct modes. Originally, it was thought that some of the sorbed molecules are present as a mobile population dissolved in the bulk of the polymer according to Henry's law, and are free to diffuse down a concentration gradient, whilst the remaining gas molecules are bound at a fixed number of adsorption site or holes occuring within the polymer. It was assumed that the bound and mobile molecules are in equilibrium. The total concentration C_{eq} of sorbed molecules at sufficiently low concentrations (where Henry's law is obeyed) is then obtained from eq. (4.1) and (4.2).

$$C_{eq} = Sp + \frac{C_H' bp}{1 + bp} \qquad \text{(eq. 4.3)}$$

Therefore, as the pressure increases, the total sorbed concentration tends towards the limit of Henry's law.

4.2.1.4 - Sorption Kinetics

The transport of small penetrants into glassy polymers has been classified according to the relative rates of mobility of the penetrant and of the polymer segments. Such classification produces three basic categories of behaviour as follows[126-128].

4.2.1.4.1 - Case I Sorption

This arises in polymer/penetrant systems which obey Fick's law (described later in section 4.2.2). The rate of diffusion is much less than the relaxation rate of the polymer. Sorption equilibrium is rapidly established, leading to time-independent boundary conditions which exhibit no dependence on swelling kinetics.

Some of the characteristic features of case I sorption are as follow[128]:

i) Both sorption and desorption curves as function of the square root of time are linear in the initial stage.

ii) Above the linear portion both absorption and desorption curve are concave to the abscissa.

iii) The sorption behaviour obeys the film thickness scaling law, i.e. reduced sorption curves for films of different thickness are all superimposable.

iv) The temperature dependence of D can be expressed by the Arrhenius relationship:

$$D = D_0 \exp (-E_a / RT) \qquad \text{(eq. 4.4)}$$

Where D_0 is the permeability index, E_a is the activation energy of the diffusion process and R is the gas constant.

The diffusion coefficient is calculated by:

$$D = \pi (K\, b / 4M_\infty)^2 \qquad \text{(eq. 4.5)}$$

Where M_∞ is the equilibrium mass sorption and K is the slope of the linear portion of the plot of M_t versus $t^{1/2}$.

For diffusion into a semi-infinite medium from an infinite solvent source, mass sorption is proportional to $t^{1/2}$. However, for a semi-infinite planar sheet in an infinite solvent source, the $t^{1/2}$ relation holds only at short times, at best.

Deviations from Fickian diffusion usually accompany diffusion of organic vapours into glassy polymers. According to the literature[127-128], the non-Fickian, anomalous diffusion and case II behaviour are interrelated and are direct consequences of the glass transition in these systems. The nature of that glass transition is as yet far from being fully understood and there exists no general theory for anomalous diffusion in polymers. Extensive literature has been published of experimentally observed diffusion anomalies in various polymer systems[131-135].

4.2.1.4.2 - Case II Sorption

Case II sorption, is the other extreme case in which diffusion and penetrant mobility are much faster compared to the polymer relaxation process. It is characterised by the development of a sharp boundary between the outer swollen shell surrounding the inner glassy core of the polymer. The polymer glass on the swollen side of the boundary attains equilibrium immediately, while at the boundary there is a discontinuity in the solvent penetrant concentration. The boundary advances at a constant velocity - being the basic parameter of case II diffusion - and the core diminishes in size until all the polymer attains equilibrium penetrant content.

Since the advent of synthetic high polymers there have been many observations of their ability to absorb substantial quantities of penetrating liquids. In some cases, the equilibrium swelling is sufficient to double the original volume or more, and materials that are originally hard and perhaps glassy become rubbers or gels[127].

A growing recognition of the reality and significance of moving boundaries in swelling polymer systems and linear, as opposed to Fickian, sorption kinetics was marked by Alfrey[136] who named such behaviour "case II". Once named, the process has appeared to attract increasing interest[134-135]. The essential attributes, namely sharp step-like penetrant profiles moving inwards from the surfaces with constant velocity which give, for sheet specimens, weight gain plots which are also linear with time, have now been frequently observed and widely recorded[137-138]. Also, further detailed features of the process, such as the induction period and front acceleration in the latter stages, have recently been noted for some conditions[139-140].

Although moving boundary phenomena are well know in cases of reaction fronts and phase changes, the concentration profiles predicted by Fick's equations with constant diffusion coefficients are in no sense sharp boundaries. It is important to note, however, that any assumption of constant diffusion coefficient is likely to be highly inappropriate for swelling polymer systems. In many cases swelling penetrants plasticise a polymer glass to the extent that it becomes a gel, and a consequent increase in diffusion coefficient (D) can be several orders of magnitude[137,138].

The dual mode sorption model, uses a modified form of Fick's first law to describe the diffusion process. The concentration of penetrant in this model is written as the sum of concentrations of the mobile and immobilised species. However, it is assumed that only the mobile species diffuses. The resulting partial equation can be written in terms of an effective diffusion coefficient which is less than the true diffusion coefficient, illustrating that the kinetics of the sorption process is slowed down because of the immobilisation of a proportion of the penetrant molecules. It is a non-linear differential equation for which numerical solutions have been found using finite difference techniques[141]. In later works, Paul[142-143] and Petropoulos[144] have modified or eliminated the restriction that the immobilised species cannot diffuse. Both authors assume that one species is totally mobile, the other only partially mobile. Petropoulos employs thermodynamics diffusion coefficients and the chemical potential of the penetrant in a differential equation to describe diffusion. Henry's law and a Langmuir

expression are used to describe the solubility of the penetrant in the polymer, but both species are allowed to diffuse. Paul[142-143] developed a diffusion equation in which all the mobile species and a fraction of the site-bound species are allowed to diffuse. A further extension of the dual mode theory was done by Vieth[145] where it was assumed that Langmuir isotherms are obeyed by each species and that all species are partially mobile.

4.2.1.4.3 - Case III, Anomalous or non-Fickian Sorption

Case III, anomalous or non-Fickian sorption occurs when the sorption and polymer relaxation rate are similar[127-128]. Basically all cases that cannot be modelled by cases I and II are collected as case III.

A number of models have been proposed to describe anomalous (case III) behaviour, but all of them are designed to only describe certain features of the behaviour. Following is a very brief outline of the principal assumptions of some of the models.

According to the time dependent boundary condition model the sorption process is still diffusion-controlled. The surface concentration attains an initial value instantaneously then rises exponentially to a new equilibrium value. The Berens-Hopfenberg first order relaxation model[146] considers absorption as a contribution of two independent processes, namely, Fickian diffusion and molecular relaxation. The combination of case I and case II models take into account the internal stresses that arise from the swelling of the polymer, and consider the velocity of solvent penetration as a direct consequence of the internal stress effect. Both the diffusion coefficient and the velocity are assumed to be constant.

4.2.2 - Diffusion

The mathematical theory of diffusion in isotropic substances is based on the hypothesis that the rate of transfer of a diffusing substance through the unit area of a section is proportional to the concentration gradient measured normal to the section. This hypothesis is expressed by the empirical relation known as Fick's first law[147-148]. The law states that (eq.4.6) the flux in the x-direction (F_x) is proportional to the concentration gradient ($\partial c/\partial x$):

$$F_x = -D\,(\partial c/\partial x) \qquad \text{(eq. 4.6)}$$

Flux is the amount of substance diffusing across unit area in unit time and D is the diffusion coefficient. The first law can only be directly applied to diffusion in the steady state, that is, where concentration is not varying with time. For the unsteady-state condition where the concentration gradient of permeant across the membrane varies with time, the rate of change of permeant concentration at any point (assuming that D is a constant independent of x, t and C) is given by Fick's second law :

$$\partial c/\partial t = D\,(\,\partial^2 c/\partial x^2 + \partial^2 c/\partial y^2 + \partial^2 c/\partial z^2\,) \qquad \text{(eq. 4.7)}$$

Under circumstances where diffusion is limited to the x-direction it simplifies to:

$$\partial c/\partial t = D\,(\,\partial^2 c/\partial x^2\,) \qquad \text{(eq. 4.8)}$$

This equation can be modified to incorporate diffusion constants that depend on concentration, inhomogeneous media, and a host of boundary condition which assume many forms. In many cases these modifications result in complicated solutions, even for relatively simple models. In any situation, the problem is to find a solution to the

appropriate form of the second equation. Some solutions can be found in Crank's book on the mathematics of diffusion[147].

4.3 - *TECHNIQUES USED TO STUDY DIFFUSION*

One of the most common experimental techniques for studying diffusion of small molecules in polymers is the method of sorption kinetics. For Fickian diffusion a calculation model has been developed by Crank[147], based on a symmetric structure for a free-standing film immersed at t=0 in an infinite solution. This model is also applicable to having only one face in contact with the liquid phase and an impermeable barrier at the centre of the film. This is equivalent to the free film because there is no net mass transport through the plane at the centre of the free film. If the initial concentration of penetrant is zero, then the concentration, C, at any position in the film, z, and any time, t, is given by[147]:

$$\frac{C_{(t)}-C_0}{C_\infty-C_0}=1-\frac{4}{\pi}\sum_{n=0}^{\infty}\frac{(-1)^n}{2n+1}\exp\left[-D(2n+1)^2\pi^2 t/4L^2\right]\cos\frac{(2n+1)\pi z}{2L} \qquad \text{(eq. 4.9)}$$

Where L is the film thickness.

In sorption kinetics experiments the mass sorbed penetrant is measured as a function of time. The sorbed mass is obtained by integrating eq. 4.9 over the thickness of the film. If M_t denotes the total amount of diffusing substance which has entered the film at time t and M_∞ the corresponding quantity after infinite time the result of integration is:

$$\frac{M_t}{M_\infty}=1-\sum_{n=0}^{\infty}\frac{8}{(2n+1)^2\pi^2}\exp\left[-D(2n+1)^2\pi^2 t/4L^2\right] \qquad \text{(eq. 4.10)}$$

Sorption kinetics experiments are commonly used to determine diffusion coefficients for penetrants in polymers. For non-condensable gases such as methane,

nitrogen and carbon dioxide, pressure decay techniques are often used[142-143]. For more condensable gases or vapours, gravimetric techniques that directly follow mass changes with time are used[146,149-150]. Polymer samples are mounted on a quartz spring microbalance and the change in mass is recorded as a function of time. The recorded weight is corrected for buoyancy to obtain the mass of the sample. This technique can be extremely accurate provided a sensitive microbalance is used.

Quartz spring microbalances are difficult to apply to liquid sorption kinetics. Since the density of the liquid medium is close to the density of polymer, correction for buoyancy results in considerably less accurate values of sorbed mass. Instead, so called "pat-and-weigh" techniques are used for liquid sorption. This involves immersing the polymer in the liquid penetrant and periodically removing the sample, blotting the surfaces to remove excess liquid and then weighing the sample on a conventional laboratory balance. If the sample is too thin or the diffusion coefficient is too high, a significant amount of penetrant may desorb during the time it is not immersed. This can be remedied by using thicker samples, but this can significantly increase the time required for a single experiment. The repeated handling of the sample can result in an erroneous rate of mass uptake.

Other techniques used to follow diffusion include the optical detection of chemical labels[151-152], mass label detection using Rutherford backscattering (RBS)[153], radioactive labels[151-152], Raman microprobe spectroscopy of sections[156], rotating-polariser ellipsometer[155], laser interferometry to follow thickness changes[156], capillary column inverse gas chromatography[157], mechanical measurement of thickness changes as a function of swelling[158-162], birefringence[161], NMR[161], UV adsorption[161] and optical density of thin layers[126]. An alternative approach has been to measure steady state transport across a polymer membrane, thereby extracting diffusion constants; one such method relies on the permeation of argon gas through thin films[126].

Most of these techniques for the determination of diffusion coefficients require sophisticated and often indirect methods for the detection of the analyte diffusing through the membrane that, generally do not allow monitoring of the diffusion process

continuously. In this work we are trying to establish experimentally simple and straightforward method employing FTIR-ATR spectroscopy to measure liquid sorption kinetics *in situ*. The transparency of the membrane in study, allied with its ability to absorb substantial amounts of penetrant liquids without dissolving, means that it is possible to observe and measure the sorption process optically. The method is based on monitoring the time-dependent change in absorption due to diffusion of water into the membrane. After reaching a steady state, the normalised absorbance plot versus time can be used to numerical evaluation. As showed in the previous chapter, along with the sorption kinetics, a spectroscopic technique has the advantage of providing information regarding the molecular state of the penetrant at various times in the diffusional process. If, for example, there are changes in the polymer matrix as the diffusion proceeds, they can be followed in the changing spectroscopic record. This would include conformational changes, crystallisation and the formation of new chemical bonds inter and intra-molecular.

Another advantage is that the method can be applied to systems of thin polymer films with penetrants that are spectroscopically active including multi-component systems, provided each penetrant absorbs in a unique region of the infra-red spectrum.

4.3 - *EXPERIMENTAL*

All the details of film preparation, ATR measurements and film thickness measurements have been already described in the experimental section of chapter 3.

4.4 - *METHOD*

Infrared spectroscopy is based on the relationship between the absorption of electromagnetic waves and the quantity of the absorbing material. In FTIR-transmission

spectroscopy, at low absorbances, this relationship is expressed by the Lambert-Beer law that in its differential form can be written as[3]:

$$\frac{dI}{I} = -\varepsilon.c.dz \qquad \text{(eq. 4.11)}$$

Where I is the light intensity at position z, ε is the extinction coefficient and c is the concentration of absorbing group. Integration of eq. 4.11 gives:

$$A = -\ln\frac{I}{I_0} = \int_0^L \varepsilon.c.dz \qquad \text{(eq. 4.12)}$$

Where A is the measured absorbance, I_0 is the intensity of the incident light I is the intensity of the transmitted light and L is the thickness of the sample.

The absorbance given in eq. 4.12 is analogous to the mass uptake in eq. 4.10 since it involves an integration of the concentration profile over the film thickness. Using transmission spectroscopy to measure sorption kinetics with eq. 4.12 suffers from many of the same limitations that are inherent in the "pat-and-weigh" technique. The polymer must be removed from the penetrant bath and blotted before spectroscopic analysis. Although it may provide molecular information about the state of the penetrant, transmission FTIR cannot be used to measure small molecule sorption *in situ*.

However, by the nature of the experimental arrangement, FTIR-ATR can be used to obtain sorption kinetics while in direct contact with the penetrant. ATR spectroscopy differs from normal transmission spectroscopy in the nature of the incident light path. The ATR theory has already been described on previous chapters. In order to combine the evanescent field strength equation with the Lambert-Beer law, it is necessary to assume that only weak absorption occurs. With that assumption:

$$\frac{I}{I_0} = e^{-A} \approx (1-A) \qquad \text{(eq. 4.13)}$$

and

$$dI = -I_0 dA \qquad \text{(eq. 4.14)}$$

We can substitute eq. 4.14 into the differential form of the Lambert Beer law (eq. 4.11) and get:

$$\frac{-I_0 dA}{I} = -\varepsilon.c.dz \qquad \text{(eq. 4.15)}$$

Integrating:

$$A = \int_0^L \varepsilon.c.\frac{I}{I_0}.dz \qquad \text{(eq. 4.16)}$$

In the ATR configuration, penetrant only enters the film from one side, hence the integration from 0 to L. Since the intensity at a given point in the film can be expressed as a function of the electric field, we can substitute the field strength of the evanescent wave ($E = E_0 \exp^{-z/d_p}$) and rewrite the expression as :

$$A = \int_0^L \frac{\varepsilon}{I_0}.c.E_0^2 \exp(-2z/d_p)dz \qquad \text{(eq. 4.17)}$$

4.4.1 - Fickian Diffusion/Thick Films

The equation that describes a Fickian kinetics of sorption was obtained by substituting eq. 4.9, the Fickian concentration profile, into eq. 4.17. The result of integration is given by:

$$\frac{A_{(t)}-A_0}{A_\infty-A_0}=1-\frac{8}{\pi d_p(1-e^{-2L/d_p})}\sum_{j=0}^{\infty}\frac{1}{2j+1}\left[\frac{e^{-2L/d_p}\left(\frac{2j+1}{2L}\pi\right)+(-1)^j\frac{2}{d_p}}{\left(\frac{2j+1}{2L}\pi\right)^2+\frac{4}{d_p^{\,2}}}\right]e^{-\left(\frac{2j+1}{2L}\pi\right)^2 Dt}$$

(eq.4.18)

Eq. 4.18 is analogous to the mass uptake equation used in gravimetric sorption experiment (eq. 4.10), the important difference being that the Fickian concentration profile is convoluted with the FTIR-ATR absorption equation before it is integrated. In eq. 4.18, A_∞ represents the absorbance at equilibrium (or saturation) and it is analogous to M_∞.

Eq. 4.18 represents the exact solution for FTIR-ATR absorption of a penetrant in a film considering a Fickian sorption kinetics and produces the diffusion coefficient values. The next paragraphs describe details of the eq. 4.18 resolution.

For sake of simplification, eq. 4.18 will be rewritten here in the following way:

$$\frac{A_{(t)}-A_0}{A_\infty-A_0}=1-\beta\sum_1 \qquad \text{(eq. 4.19a)}$$

where

$$\beta=\frac{8}{\pi d_p(1-\alpha)} \qquad \text{(eq. 4.19b)}$$

$$\sum_1=\sum_{j=0}^{\infty}\frac{1}{2j+1}\left[\frac{\alpha K_j+(-1)^j 2/d_p}{(K_j^2+4/d_p^2)}\right]\exp(-K_j^2 Dt) \qquad \text{(eq 4.19c)}$$

$$\alpha=\exp(-2L/d_p) \qquad \text{(eq. 4.19d)}$$

$$K_j=\frac{2j+1}{2L}\pi \qquad \text{(eq. 4.19e)}$$

The diffusion coefficient, D was determined through the minimisation of the chi-square merit function χ^2 [162]:

$$\chi^2 = \sum_{i=1}^{n} \left[\frac{1 - \beta\Sigma_1 - \frac{A_{(i)} - A_0}{A_\infty - A_0}}{\Delta Y_i} \right]^2 \qquad \text{(eq. 4.20)}$$

Where ΔY_i is the error propagation considering that each data point (A_∞, A_0 and A_i) has its own standard deviation.

Defining

$$1 - \frac{A_i - A_0}{A_\infty - A_0} = Y_i = \frac{A_\infty - A_i}{A_\infty - A_0}$$

We get:

$$\chi^2 = \sum_{i=1}^{n} \left[\frac{Y_i - \beta\Sigma_1}{\Delta Y_i} \right]^2 \qquad \text{(eq. 4.21)}$$

Where

$$\Delta Y_i \approx \frac{\Delta A_{(i)} + \Delta A_\infty + Y_i(\Delta A_0 - \Delta A_\infty)}{A_\infty - A_0} \qquad \text{(eq. 22)}$$

Appendix 1 describes in details how the error propagation was calculated.

Clearly, if the sample distribution and the assumed parent distribution agree exactly, then $\chi^2 = 0$. This is, of course, extremely unlikely. Consequently, the larger χ^2 is, the more disagreement there is between the two values. Accordingly:

$$\frac{\partial \chi^2}{\partial D} = 0 \Rightarrow f(D) = 0 \qquad \text{(eq. 4.23)}$$

The derivative of χ^2 as a function of D produces:

$$f(D) = 2\beta \sum_{i=1}^{n} \frac{(Y_i - \beta\Sigma_1)}{\Delta Y_i^2} \Sigma_2 = 0 \qquad \text{(eq. 4.24)}$$

Where Σ_2 that is the derivative of Σ_1 as a function of D is :

$$\Sigma_2 = -t_i \sum_{j=0}^{\infty} \frac{K_j^2}{(2j+1)} \left[\frac{\alpha K_j + (-1)^j 2/d_p}{(K_j^2 + 4/d_p)} \right] \exp(-K_j^2 Dt) \qquad \text{(eq. 4.25)}$$

Eq. 4.25 was solved using the Newton-Raphson method[162]. The method is probably one of the most celebrated of all one-dimensional root finding routines. The root finding routines proceeds by interaction. Starting from some guessed trial solution, a useful algorithm will improve the solution until some predetermined convergence criterion is satisfied. According to the Newton - Raphson formula[162],

$$x_{n+1} = x_n - \frac{f(x_n)}{f'(x_n)} \qquad \text{(eq. 4.27)}$$

By analogy,

$$D_{n+1} = D_n - \frac{f(D_n)}{f'(D_n)} \qquad \text{(eq. 4.28)}$$

Where $f'(D)$ will be the derivative eq. 4.24 as a function of D. The result of the derivative is:

$$f'(D) = 2\beta \sum_{i=1}^{n} \frac{1}{\Delta Y_i^2} \left[-\beta\Sigma_2^2 + (Y_i - \beta\Sigma_1) \times \Sigma_3 \right] \qquad \text{(eq. 4.29)}$$

Where Σ_3 is the derivative of Σ_2 as a function of D, given by:

$$\Sigma_3 = t_i^2 \sum_{j=0}^{\infty} \frac{K_j^4}{(2j+1)} \left[\frac{\alpha K_j + (-1)^j 2/d_p}{(K_j^2 + 4/d_p^2)} \right] \exp(-K_j^2 Dt) \qquad \text{(eq. 4.30)}$$

In our case the initial guess used was the value found on literature[163] for the diffusion coefficient of polysulphones and the convergence criterion was:

$$\frac{D_{n+1} - D_n}{D_n} \leq 10^{-10}$$

The results obtained by the above described resolution of eq. 4.18 will be discussed in the next chapter.

The method described above assumes that the value of A_∞ can be measured independently and accurately. However, experimental conditions may make accurate determinations of the equilibrium infrared absorption unreliable or impossible (this issue will be discussed in more details in next chapter). Therefore, another method was developed, where now the A_∞ value is calculated as a second adjustable value in addition to the diffusion coefficient. In order to do that, eq. 4.19a was rewritten as:

$$A_t = A_0 + (A_\infty - A_0)(1 - \beta\Sigma_1) \qquad \text{(eq. 4.31)}$$

and, accordingly, the chi-square merit function, χ^2 becames:

$$\chi^2 = \sum_{i=1}^{n} \left[\frac{[A_0 + (A_\infty - A_0)(1 - \beta\Sigma_1)] - A_t}{\Delta Y_i} \right]^2 \qquad \text{(eq. 4.32)}$$

The only difference in this case is that, now the derivative of eq. 4.32 can not be solved using the Newton-Raphson method anymore since we have now two adjustable parameters (A_∞ and D) instead of only one. Therefore, in this case, the values of the parameters were determined from data analysis using the Levenberg-Marquardt method. The also called Marquardt method has become the standard for non-linear least squares routines[162]. Details about the method are described in appendix II.

4.4.2 - Fickian Diffusion/Thin Films

This section describes an approach to calculate the diffusion coefficient when using thin film, i.e. films where the electric field does not decay completely inside the film. As already discussed in previous chapter, when using these films attention must be paid to distinguish between water absorbed by the membrane and pure liquid water outside it.

As showed in eq. 4.17, the intensity at a given in the film can be expressed as being proportional to the electric field decay. Integration of eq. 4.17 produces:

$$A = \frac{\varepsilon}{I_0}.c.E_0^2(-d_p/2)\left[\exp(-2z/d_p)\right]_0^L \qquad \text{(eq. 4.33)}$$

Calling k all the constant terms of eq. 4.33, it becomes:

$$A = k\left[1-\exp(-2L/d_p)\right] \qquad \text{(eq. 4.34a)}$$

Where

$$k = \frac{\varepsilon.c.E_0^2.d_p}{2I_0} \qquad \text{(eq. 4.34b)}$$

Eq. 4.34a can be used to predict the influence of thickness on the band intensity. For the thin film case, the absorbance at any time during the diffusional process($A_{t,total}$) will be given by:

$$A_{t,total} = A_{t,membrane} + A_{H_2O} \qquad \text{(eq. 4.35)}$$

Where $A_{t,membrane}$ means the absorbance of the water absorbed by the membrane at a time t and A_{H2O} means absorbance of pure liquid water.

Correspondingly, the absorbance at equilibrium will be:

$$A_{\infty,total} = A_{\infty,membrane} + A_{H_2O} \qquad \text{(eq. 4.36)}$$

Where $A_{\infty,total}$ is the equilibrium absorbance obtained experimentally and $A_{\infty,membrane}$ is the amount of water absorbed only by the membrane, at equilibrium. Rearranging eq. 4.36 above, we get:

$$A_{H_2O} = A_{\infty,total} - A_{\infty,membrane} \qquad \text{(eq.4.37)}$$

Now we can substitute A_{H2O} on eq. 4.35 by the expression obtained in eq. 4.37 and get:

$$A_{t,total} = A_{t,membrane} + A_{\infty,total} - A_{\infty,membrane} \qquad \text{(eq. 4.38)}$$

The value of $A_{\infty,membrane}$ can be calculated using eq. 4.34a. Substituting eq. 4.34a into eq. 4.38 above we get:

$$A_{t,total} = A_{t,membrane} + A_{\infty,total} - K\left[1-\exp(-2L/d_p)\right] \qquad \text{(eq. 4.39)}$$

The next step was simply use the same eq. 4.18 that describes the Fickian concentration profile using now eq 4.39 above in the place of A_t and eq. 4.34a in the place of A_∞. As a result, eq. 4.19a becomes:

$$\frac{A_{i,membrane} + A_{\infty,total} - K\left[1-\exp(-2L/d_p)\right] - A_0}{k\left[1-\exp(-2L/d_p)\right] - A_0} = 1-\beta\Sigma_1 \qquad \text{(eq.4.40)}$$

The value of K was calculated from experiments using very thick films, since K can be defined as the equilibrium absorbance for a film of infinite absorbance. This issue will be discussed in more detail in the next chapter.

Once the value of K was determined, eq. 4.40 was solved in exactly the same way as the previous equation used for thick films. The Newton-Raphson method was used because it was experimentally observed that thin films produced by dipping did not

present delamination after the end of the process and so, we can assume that the A_∞ values observed were reliable.

4.4 3 - Case II Diffusion/Thick Films

A second possibility is that the membranes will not present a Fickian behaviour but a dual sorption mode instead. To analyse the diffusion process for a dual mode sorption, a more complex model is necessary since we must use a modified form of Fick's first law to calculate the diffusion coefficients. The next section describes such modifications .

According to the dual sorption mode theory[141,145] a fraction of the penetrant molecules is immobilised at a fixed number of adsorption sites or holes (in our case the SO_3^- groups) and the remaining penetrant molecules are present as a mobile population dissolved in the bulk of the polymer and are free to diffuse through the network. As in the Petropoulos's work[144] we eliminate the restriction that the immobilised species cannot diffuse. We are assuming that one species is totally mobile and the other only partially mobile. Normal diffusion across a membrane is described by Fick's second law in one dimension (eq. 4.8). The model can be described as:

$$\frac{\partial C_1}{\partial t} = D_1 \frac{\partial^2 C_1}{\partial z^2} \qquad \text{(eq. 4.41a)}$$

where $C_1(0) = x_1 C_0$ and

$C_1(t=\infty) = x_1 C_\infty$ for the partially mobile molecules, and

$$\frac{\partial C_2}{\partial t} = D_2 \frac{\partial^2 C_2}{\partial z^2} \qquad \text{(eq. 4.41b)}$$

Where $C_2(0) = x_2 C_0$ and

$C_2(t=\infty) = x_2 C_\infty$ for the totally mobile molecules.

Values of x_1 and x_2 are related to the fraction of partially and totally mobile molecules respectively and, naturally $x_1 + x_2 = 1$.

If now we substitute these boundary conditions on (eq. 4.19a) and by analogy substitute C by A, we get:

$$\frac{A_1 - x_1 A_0}{x_1 A_\infty - x_1 A_0} = 1 - \beta \sum_1 \quad ...or... \frac{A_1 - x_1 A_0}{x_1 (A_\infty - A_0)} = 1 - \beta \sum_1 \qquad \text{(eq. 4.42a)}$$

for the first sorption mode, and

$$\frac{A_2 - x_2 A_0}{x_2 A_\infty - x_2 A_0} = 1 - \beta \sum_1^{'} \quad ...or... \frac{A_2 - x_2 A_0}{x_2 (A_\infty - A_0)} = 1 - \beta \sum_1^{'} \qquad \text{(eq 4.42b)}$$

for the second one. In this case $\Sigma_1^{'}$ will be similar to Σ_1 the only difference being that the diffusion coefficient, D will be denominated D_1 in Σ_1 and D_2 in Σ_2. We can now rearrange eq. (4.42a) and (4.42b) as:

$$A_1 = (1 - \beta \Sigma_1) x_1 (A_\infty - A_0) + x_1 A_0 \qquad \text{(eq. 4.43a)}$$

and

$$A_2 = (1 - \beta \Sigma_1^{'}) x_2 (A_\infty - A_0) + x_2 A_0 \qquad \text{(eq. 4.43b)}$$

In this way the above equations can be added to produce the total absorbance at a time t:

$$A_t = (1 - \beta \Sigma_1) x_1 (A_\infty - A_0) + x_1 A_0 + (1 - \beta \Sigma_1^{'}) x_2 (A_\infty - A_0) + A_0 \qquad \text{(eq. 4.44)}$$

Rearranging the above equation and substituting x_2 by $1\text{-}x_1$ we got:

$$\frac{A_t - A_0}{A_\infty - A_0} = (1 - \beta \Sigma_1) x_1 + (1 - \beta \Sigma_1^{'})(1 - x_1) \qquad \text{(eq. 4.45)}$$

The same approach for determination of A_∞ was used here. So in this case, the parameters determined were now A_∞, D_1 and D_2. Such parameters were calculated using the already mentioned Maquardt method.

4.4.4 - Case II Diffusion/Thin Films

In case of thin films, the approach used was exactly the same used for thin films with Fickian diffusion. However, in these case the Maquardt method was used (as for the thick film case) because not only one, but three parameters D_1, D_2 and $A_{t,m}$ were calculated. The four approaches described above were transformed in computer routines using PASCAL language. Such programs are listed in appendix three.

Chapter 5

Models, Simulation and the Monte Carlo Method

CONTENTS

5.1 - INTRODUCTION

In last chapter we described how the diffusion coefficients can be calculated using the FTIR-ATR technique. As pointed out in that chapter, the variables used in the calculation were film thickness, and integrated intensities as a function of time. However, it should be noted that such parameters are not precise values and are, of course, subjected to random errors instead. These variations can be measured in the case of film thickness and elapsed time. As in the case of integrated intensities, they can be accessed according to the literature[3]. This chapter describes how computer simulation can be used to analyse the influence of the random errors present in each parameter, on the values of diffusion coefficients. Basically, simulation was used to replicate the experiments, using a random number generator, considering all variations that could occur in the system. The results of this analysis are presented as the errors bar on the values of diffusion coefficient shown in tables 6.1 and 6.2 in next chapter.

5.1.1 - Models

The first step in studying a system is building a model. A scientific model can be defined as an abstraction of some real system, an abstraction that can be used for prediction and control. The purpose of a scientific model is to enable the analyst to determine how one or more changes in various aspects of the modelled system may affect other aspects of the system or the system as a whole.

There are many types of models as described below[164]:

1 - Iconic models - Those that pictorially or visually represent certain aspects of a system.

2 - Analog models - Those that employ one set of properties to represent some other set of properties that the system being studied possesses.

3 - Symbolic models - Those that require mathematical or logical operations and can be used to formulate a solution to the problem at hand.

In this work, however, we are concerned only with symbolic models (which are also called *abstract* models), that is, we deal with a model consisting of mathematical symbols.

There are many advantages by using mathematical models. According to Rubinstein[165] they do the following:

1 - Enable investigators to organise their theoretical beliefs and empirical observations about a system and to reduce the logical implications of this organisation.

2 - Lead to improved system understanding.

3 - Bring into perspective the need for detail and relevance.

4 - Expedite the analysis.

5 - Provide a framework for testing the desirability of system modifications.

6 - Allow for easier manipulation than the system itself permits.

7 - Permit control over more sources of variation than direct study of a system would allow.

8 - Are generally less costly than the real experiment.

An additional advantage is that a mathematical model describes a problem more concisely than, for instance, a verbal description does.

On the other hand, there are also at least three reservations, which we should always bear in mind while constructing a model[165].

First, there is no guarantee that the time and effort devoted to modelling will return a useful result and satisfactory benefits. Occasional failures occur because the level of resources is too low. More often, however, failures result when the investigator relies too much on method and not enough on ingenuity; the proper balance between the two leads to the greatest probability of success.

The second reservation concerns the tendency of an investigator to treat his or her particular depiction of a problem as the best representation of reality. This is often

the case after much time and effort have been spent and the investigator expects some useful results.

The third reservation concerns the use of the model to predict the range of its applicability without proper qualification.

Mathematical models can be classified in many ways. Some models are *static*, others are *dynamic*. Static models are those that do not explicitly take time-variation into account, whereas dynamic models deal explicitly with time-variable interaction.

Another distinction concerns *deterministic* versus *stochastic* models. In a deterministic model all mathematical and logical relationships between the elements are fixed. As a consequence these relationships completely determine the solutions. In a stochastic model at least one variable is random[166].

After constructing a mathematical model for the problem under consideration, the next step is to derive a solution from this model. There are *analytic* and *numerical* solution methods.

An analytical solution is usually obtained directly from its mathematical representation in the form of formula.

A numerical solution is generally an approximate solution obtained as a result of substitution of numerical values for the variables and parameters of the model. Many numerical methods are iterative, that is, each successive step in the solution uses the results from the previous step. Newton-Raphson's method for approximating the root of a non-linear equation, used in this work, can serve as an example.

Two special types of numerical methods are simulation and the Monte Carlo method. The following section discusses these.

5.1.2 - Simulation and the Monte Carlo Method

Although simulation is often viewed as a "method of last resort" to be employed when everything else has failed, recent advances in simulation methodologies, availability

of software, and technical developments have made simulation one of the most widely used and accepted tools in system analysis and operations research.

There are many situations where simulation can be successfully used. Below we list some of them[164].

First, it may be either impossible or extremely expensive to obtain data from certain processes in the real word. In this case we say that the simulated data are necessary to formulate hypotheses about the system.

Secondly, the observed system may be so complex that it cannot be described in terms of a set of mathematical equations for which analytical solutions are obtainable. Simulation has been found to be extremely effective tool for dealing with problems of this type.

Thirdly, even though a mathematical model can be formulated to describe some system of interest, it may not be possible to obtain a solution to the model by straightforward analytical techniques.

Fourth, it may be either impossible or very costly to perform validating experiments on the mathematical models describing the system. In this case we say that the simulation data can be used to test alternative hypotheses.

In all these cases simulation is the only practical tool for obtaining relevant answers.

Computer simulation also enables us to replicate an experiment[162]. Replication means re-running an experiment with selected changes in parameters or operating conditions being made by the investigator. Simulation is indeed an invaluable and very versatile tool in those problems where analytic techniques are inadequate. However, it is by no means ideal. Simulation is an imprecise technique. It provides only statistical estimates rather than exact results, and it only compares alternatives rather than generating the optimum one. Simulation is also a slow and costly way to study the problem. It usually requires a large amount of time and great expense for analysis and programming.

Ripley[166] has defined simulation as a technique of performing *sampling experiments* on the model of the system This general definition is often called simulation in a wide sense, whereas simulation in a narrow sense, or *stochastic simulation,* is defined as experimenting with the model over the time; it includes sampling stochastic varieties from probability distribution. Therefore stochastic simulation is actually a statistical sampling experiment with the model. This sampling involves all the problems of statistical design analysis.

Because sampling from a particular distribution involves the use of random numbers, stochastic simulation is sometimes called *Monte Carlo simulation*. Historically, the Monte Carlo method was considered to be a technique, using random or pseudo random numbers, for solution of a model. The term "Monte Carlo" was introduced by von Neumann and Ulam during World War II, as a code word for the secret work at Los Alamos; it was suggested by the gambling casinos at the city of Monte Carlo in Monaco[165].

The Monte Carlo method is now the most powerful and commonly used technique for analysing complex problems and applications can be found in many fields. In the last few years the range of applications has been broadening, and the complexity and computational effort required has been increasing, because realism is associated with more complex and extensive problem descriptions

Reference 167 explores a whole range of the Monte Carlo Method and its application. Reference 168 contains a selected bibliography of Monte Carlo applications in polymer science.

5.1.3 - Random Numbers

The first thing needed for a stochastic simulation is a source of random numbers. A random number is defined as one selected at random from a population in such a fashion that every number of the population has an equal chance of being selected[162].

There are statistical tests to verify if a sequence of random number possesses these characteristics[162].

Truly random generators are natural process. Such processes include: radiation from radioactive substances, the path of free travel for a particle in Brownian motion, annual stream flows and so on.

Random numbers are essentially independent random variables uniformly distributed over the unit interval [0,1]. It may seem to be a conceptual impossibility to use a computer to produce "random numbers". Any program, after all will produce output that is entirely predictable, not truly random. Nevertheless, practical computer "random number generators" are in common use. Actually, what are available at computer centres are arithmetic codes for generating sequences of pseudo random digits, where each digit (0 through 9) occurs with approximately equal probability (likelihood). Consequently the sequences can model successive flips of a fair ten-side die. Such codes are called random number generators. Grouped together, these generated digits yield pseudo random numbers with any required number of elements.

5.2 - METHOD

5.2.1 - Generating a Random Number

Most Pascal compilers contain a set of predefined procedures for initialising, and then generating "random numbers".

The typical synopsis for invoking the random number generator when using Turbo Pascal is:

```
Var x :real
BEGIN
    randomise
    x := Random
```

The random number generator is initialised by invoking **randomise**. Each such call will result in a different random sequence, or at least a different starting point in some of the enormously long sequence. Successive random numbers in the sequence can be obtained by successive calls of **random**.

According to the literature[164-167] it can be very dangerous to use the system supplied **random,**. since regrettably, many of the so-called random functions supplied with the most wide spread computers are far from random, and many simulations studies have been invalidated as a consequence.

A recommended way to at least minimising this problem is to do additional randomising shuffle on the numbers generated by **random**. The shuffling procedure used here is based on the algorithm of Bays and Durham, described by Knuth[169] and illustrated in Figure 5.1.

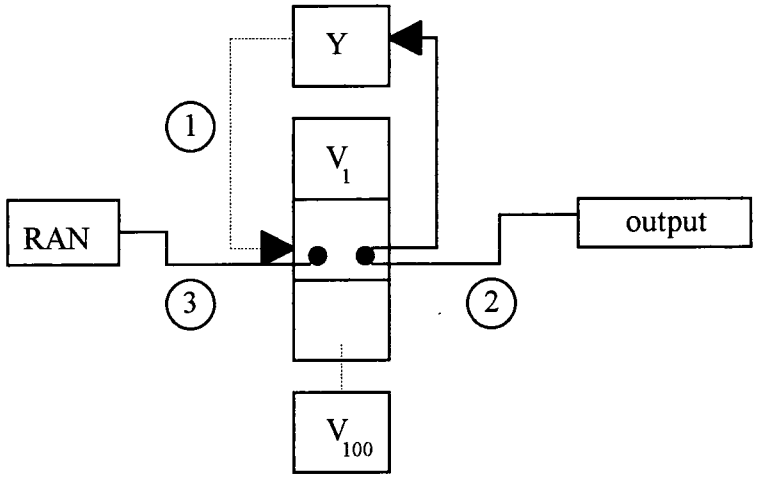

Fig. 5.1 - Shuffling procedure used to break up sequential correlations in a system-supplied random number generator. Circled numbers indicate the sequence of events. On each call the random number in RAN is used to choose a random element in the array RAN0V. That element becomes the output random number, and also is the next RAN0Y. Its position in RAN0V is refilled from the system-supplied routine. Reproduced from ref.162.

5.2.2 - Replication of the Experiments

As stated before each of the parameters used to calculate the diffusion coefficient has its own error. In the following paragraphs we describe how these errors were calculated.

a) Film Thickness - The film thickness, as already described, was measured mechanically and the values used were the average and standard deviation of 10 measurements made at different points of the film.

b) Integrated Absorbance - According to the literature[3], if a stable sample is left in a Fourier spectrometer and several spectra are measured consecutively, provided that the spectrometer is operating correctly, the spectra will usually be reproducible within 0.01 cm^{-1}. In our case, because we are working with the integrated intensities, in addition to the inherent instrument variation, errors can also occur if the integration limits are not exactly the same. Therefore we assumed that the integrated absorbance values have a maximum random error of 5%.

c) Time - Because the sample variations as a function of time are quite dramatic, especially at the beginning of the diffusion process, this parameter must be very well controlled. As stated before, the scan time was 30 seconds while the elapsed time (i.e. scan + processing + transmission) was 43 seconds. However, when using a stop clock to measure the elapsed time it was found that it varies between 41 and 45 seconds. Therefore, when generating time values we assumed a maximum random error of 3 seconds.

Considering the thickness as the example, it can be written that its variation will be:

$$(L - \Delta L) \leftarrow L \rightarrow (L + \Delta L)$$

Where (L-ΔL) is the minimum value and (L+ΔL) is the maximum for the thickness. Accordingly, the generated value (L_g) can be described as:

$$L_g = L_{\min} + 2\Delta L(RN) \qquad \text{(eq. 5.1)}$$

Where RN is the random number between 0 and 1. If now we substitute the L_{min} by (L-ΔL) we get:

$$L_g = L + \Delta L(2RN - 1) \qquad \text{(eq. 5.2)}$$

Eq. 5.2 clearly shows that:

$L_g = L - \Delta L = L_{\min}$ for RN = 0 and

$L_g = L + \Delta L = L_{\max}$ for RN = 1

Similar procedures were taken for the generation of values of absorbance and time. The respective equations can be described as:

$A_g = A + \Delta A(2RN - 1)$ for absorbance and,

$t_g = t + \Delta t(2RN - 1)$ for time

The procedure described above were incorporated to all the four PASCAL routines already mentioned in the previous chapter.

5.3 - RESULTS

The plots shown in this section represent the result of 1000 replications executed using the program developed for case II/thick films and can be used to exemplify the method. For the case of 1000 simulations the program generates 1000 values of L comprised between L_{min} and L_{max} ,1000 values of absorbance between A_{min} and A_{max} and 1000 values of t between t_{min} and t_{max}. For each set of parameters generated (one value of L, one of A and one of t) the value of the diffusion coefficients, x_a , and the absorbance at equilibrium were calculated using equation 4.18 shown in previous chapter. At the end of the 1000 simulations, the program calculates the average and standard deviation among the 1000 values of diffusion coefficient calculated, as well as x_a and absorbance of equilibrium. Figure 5.2c shows 1000 values of diffusion coefficient calculated using 1000 different values of L, A and t. Figure 5.2b shows the average and figure 5.2a, the standard deviation among the 1000 values. As shown in the figure at least 500 simulations are necessary for the values of D converge to an equilibrium value. Figure 5.3, 5.4 and 5.5 show the same results (i.e. 1000 simulations) for the values of K_d (defined by D_2/D_1), x_a , and the absorbance at equilibrium, respectively.

As stated before, the simulation procedure was incorporated to the Pascal routines already mentioned in the previous chapter. Consequently, the values of D and x_a that will be presented and analysed in the next chapter (tables 6.1 and 6.2) represent the average value obtained from 1000 simulations and the errors bar on these data represent the standard deviation.

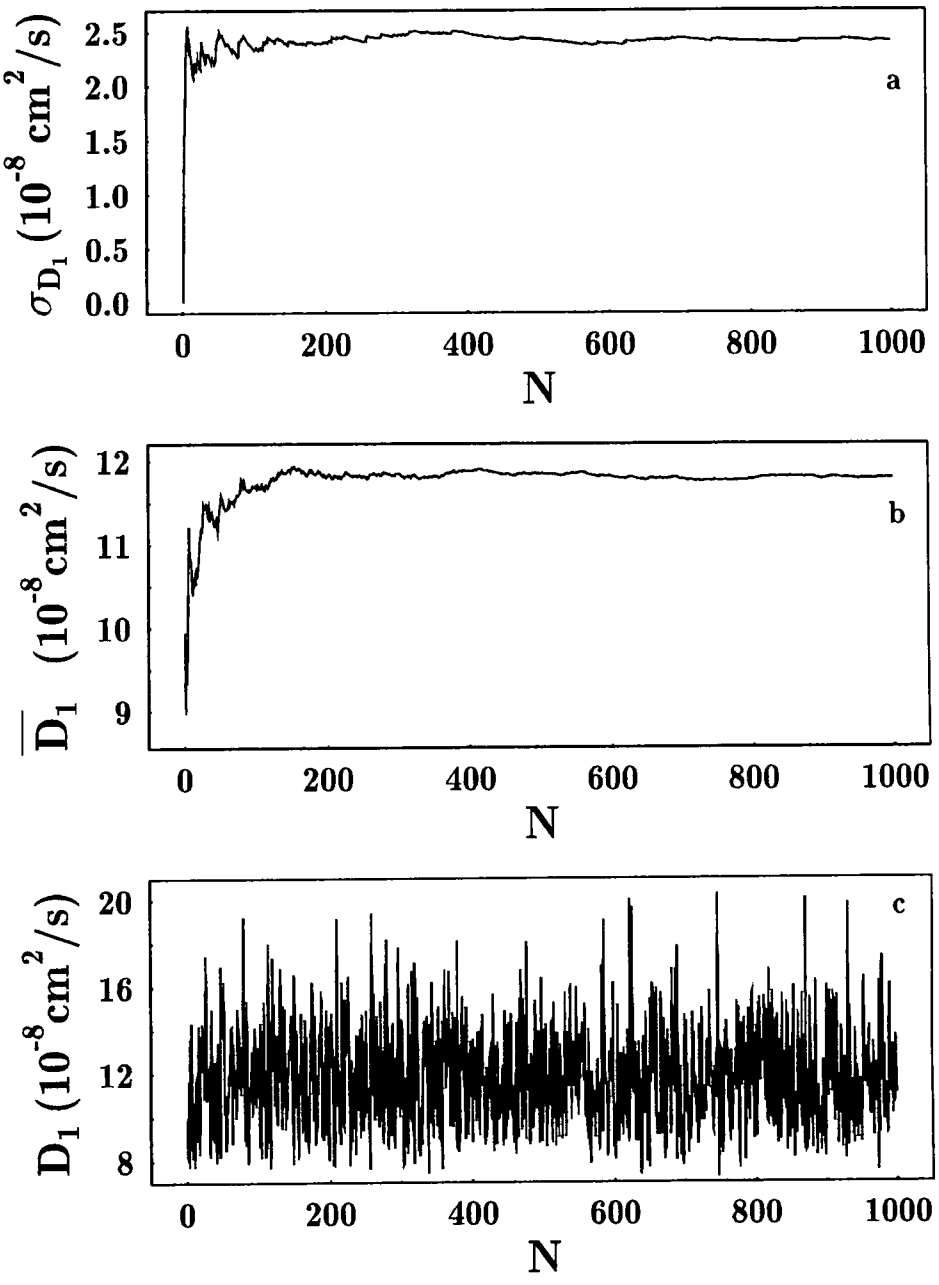

Fig. 5.2 - Values of D_1 obtained from 1000 replications (N): (a) standard deviation, (b) average, and (c) D_1 values.

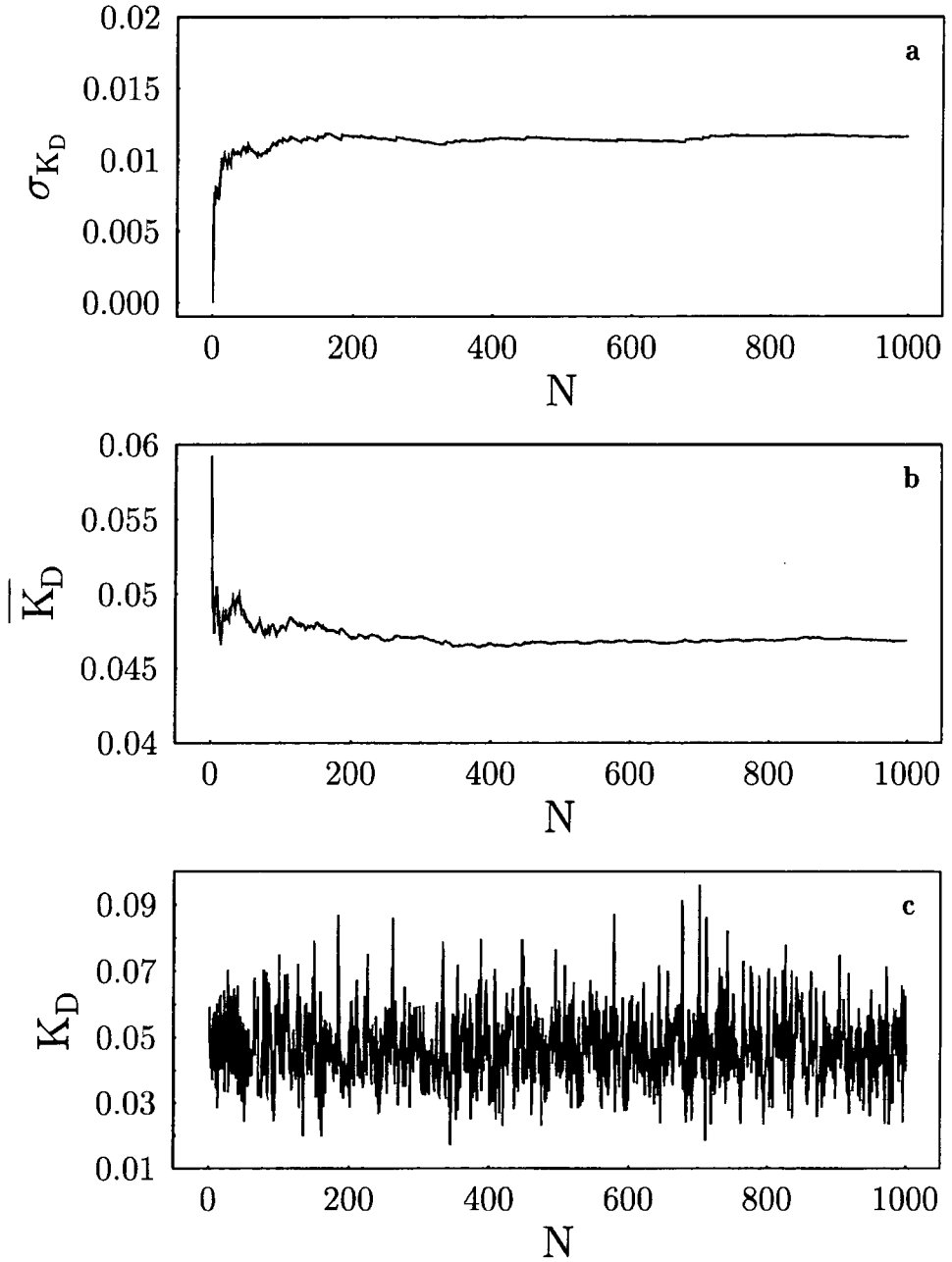

Fig. 5.3 - Values of K_D obtained from 1000 replications (N): (a) standard deviation, (b) average, and (c) K_D values.

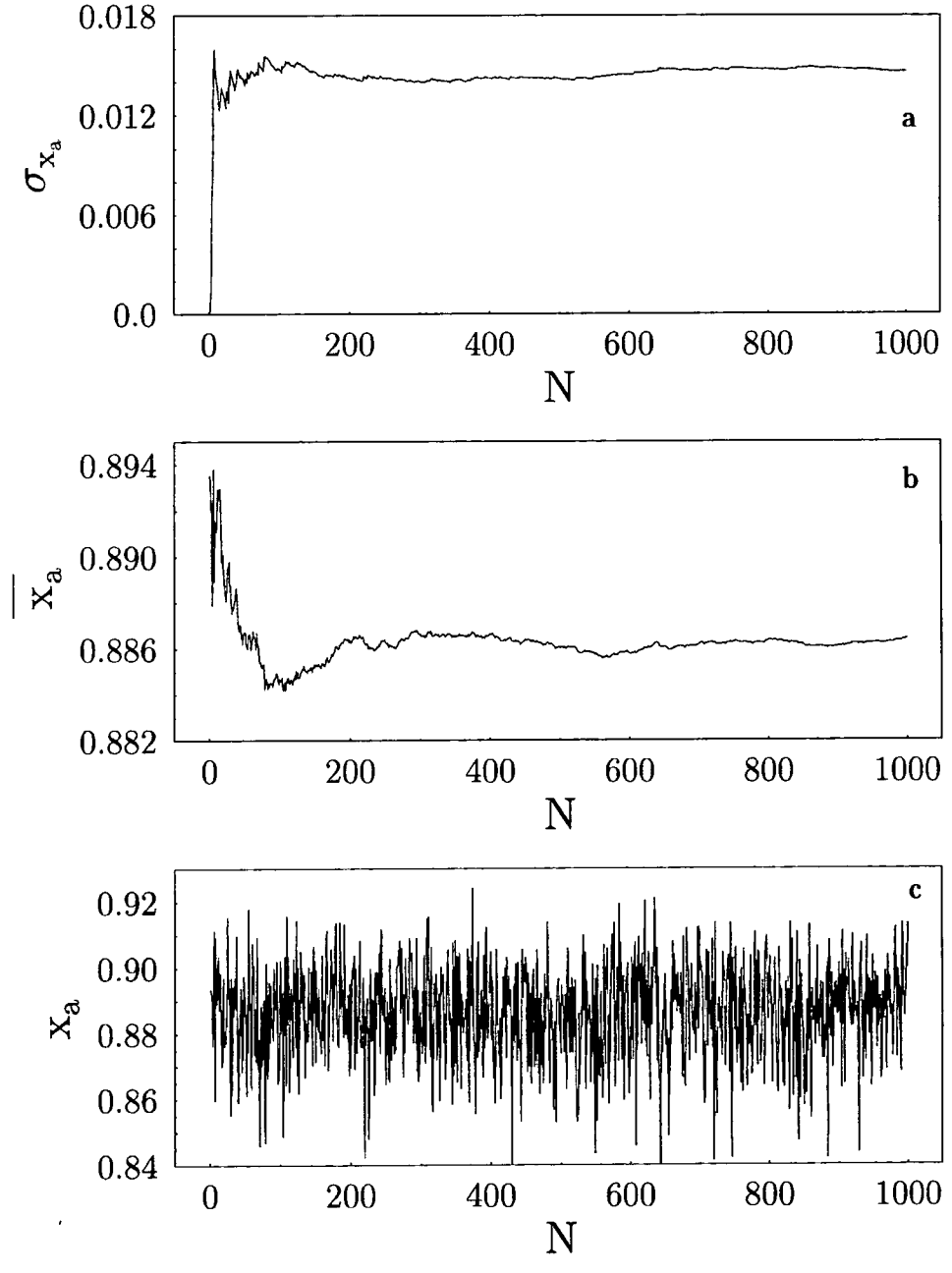

Fig. 5.4 - Values of X_a obtained from 1000 replications (N): (a) standard deviation, (b) average, and (c) X_a values.

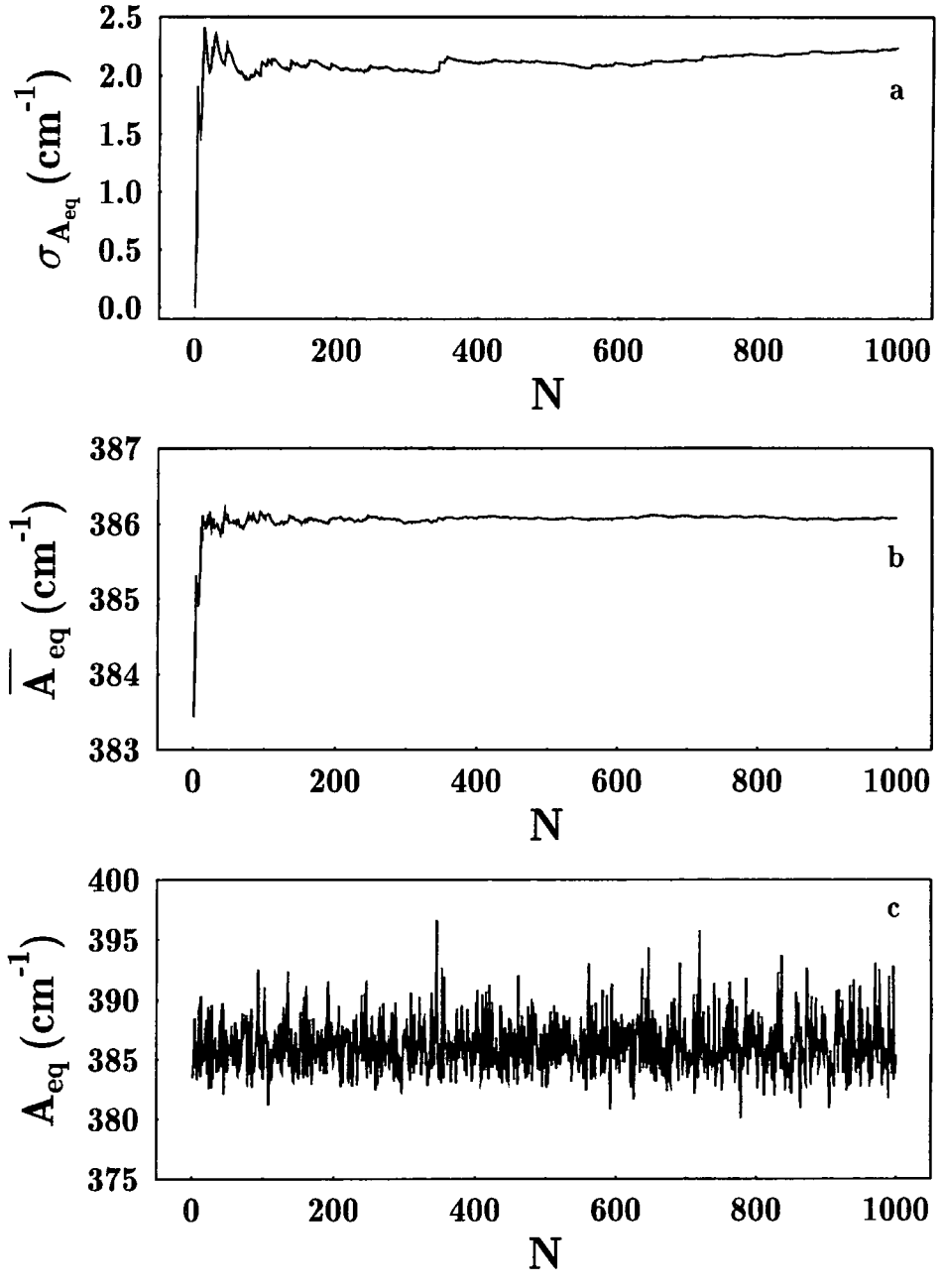

Fig. 5.5 - Values of A_{cq} obtained from 1000 replications (N): (a) standard deviation, (b) average, and (c) A_{cq} values.

Chapter 6

FTIR-ATR Spectroscopic Determination of Diffusion Coefficient of Water in Polymeric Membranes. Part II

CONTENTS

6.1 - RESULTS AND DISCUSSION

In this chapter, the experiments described and qualitatively discussed in chapter three will be analysed in a quantitative way. The approaches described in chapters four and five will be used to calculate the diffusion coefficients of the membranes and the results will be analysed as a function of different parameters such as solvent used, film thickness and sulphonation level.

6.1.1 - Evanescent Field Contribution to the Band Intensities

As already stated, the relationship between the infrared spectra obtained from the cell, during the experiment and, the mass sorption of water into the membrane involves the evanescent field intensity distribution starting at the ZnSe/polymer interface and extending into the polymer.

It was suggested in chapter 4 that eq. 4.34a might be used to predict the influence of thickness on the band intensity. Here, values obtained experimentally will be compared with the ones predicted by eq. 4.34a and the differences will be analysed. Fig 6.1 shows some examples of curves predicted by eq. 4.34 for a d_p = 1.20 μm and d_p = 0.43μm. As we can see, from the beginning, there is a strong relationship between sample thickness and band intensity but, after a certain value the intensity reaches a maximum and becomes independent of the sample thickness. This value of sample thickness is called the actual sampled depth (d_s) and is approximately three times the depth of penetration. According to the literature[16], for sampling depths that are three times d_p the field has decayed to about 5% of the original intensity. In our case the sampled depth (d_s) will be 3.60 μm and 1.29 μm for d_p = 1.20 μm and d_p = 0.43 μm, respectively.

Fig. 6.2 compares the curves produced by eq. 4.34 with the values of intensity at equilibrium obtained experimentally for films with different thicknesses using the system

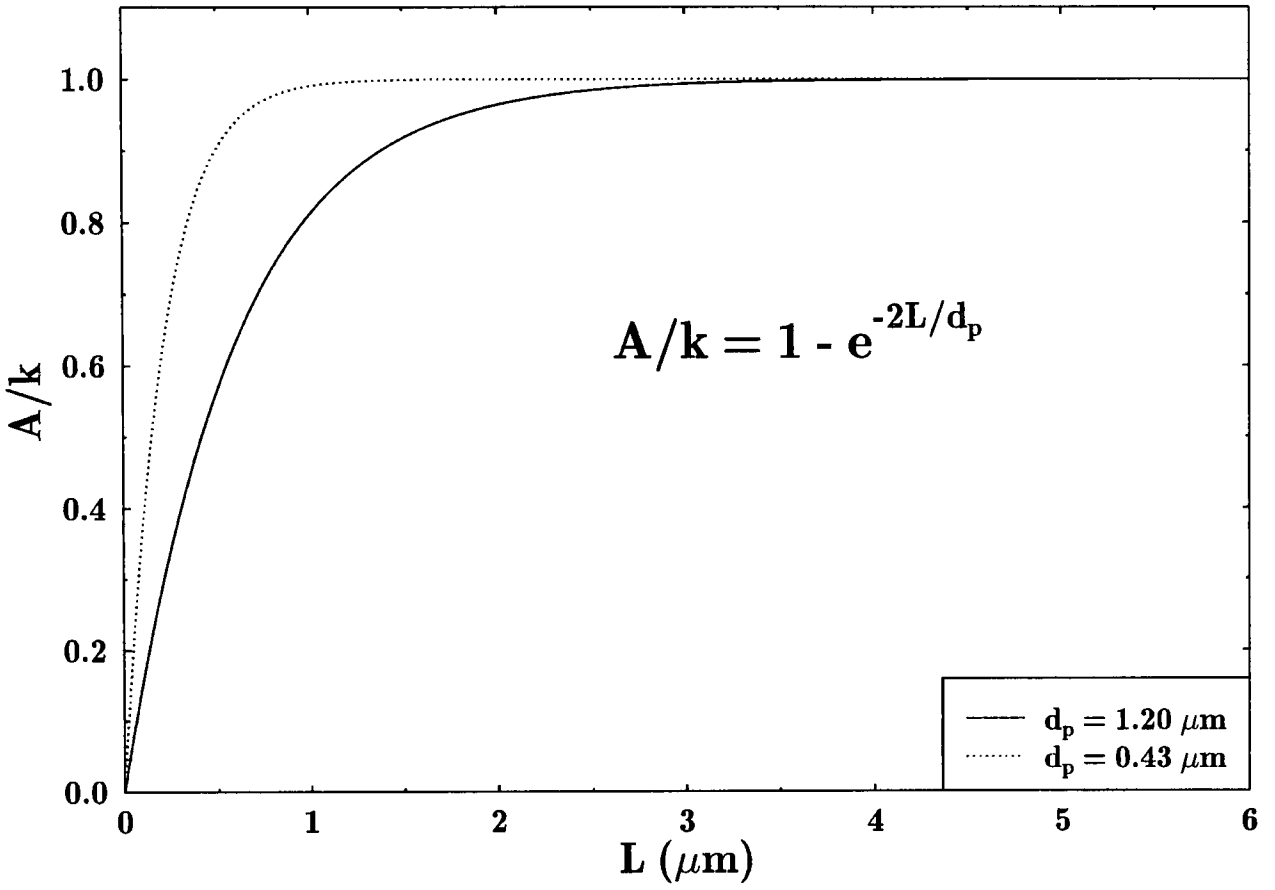

Fig. 6.1 - Theoretical curves generated by eq. 4.34. Solid line: thick films ($d_p = 1.20\ \mu m$) and dotted line: thin films ($d_p = 0.43\ \mu m$).

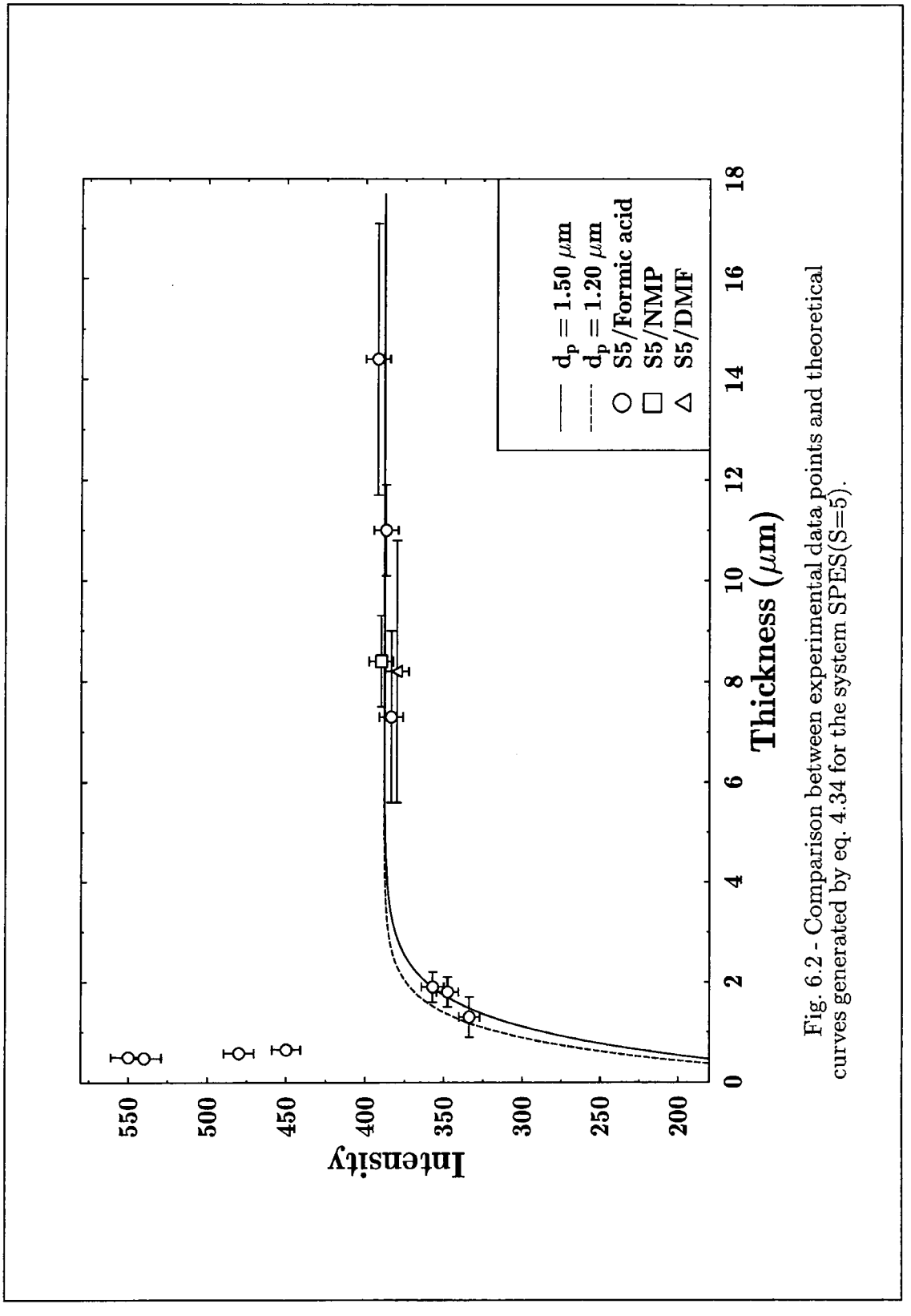

Fig. 6.2 - Comparison between experimental data points and theoretical curves generated by eq. 4.34 for the system SPES(S=5).

SPES(S5) in formic acid, NMP and DMF. The dotted line represents the curve generated using a calculated value of d_p of 1.20 μm. As we can see, such curve does not match the experimental data very well. Attempts to find the curve that best fits the data were performed and the result was the same curve generated by eq. 4.34 but in this case the value of d_p used was 1.50μm (solid line) rather than the calculated value of 1.20 μm (dotted line). Fig. 6.2 shows that, except for very thin films where the thickness is smaller than the depth of penetration (d_p) the value of d_p=1.50 fits the experimental values much better .

For the case of thick films (which are the ones where it was possible to predict the influence of the thickness on the equilibrium values of intensity), the values of d_p should remain constant even on hydration. In order to understand the observed variations we must return to the equation 1.24 used for d_p calculation. As we can see, in that equation the only parameter that could vary with hydration and consequently change the value of K on eq. 4.34 is n_2, i.e. the refractive index of the polymer. The refractive index (n) of a material is defined in terms of the speed of light in that material, compared with the speed of light in a vacuum[170] Therefore, it is not unreasonable to suppose that it will change from the dry to the fully hydrated membrane. In fact, Bohn and co-workers[171] have already measured changes in the refractive index of polystyrene with increased solvent inclusion in the polymer matrix using optical waveguide techniques. In our case, the variation in the refractive index of the membrane, (n_2) with hydration can be calculated using eq. 1.24. For that purpose is was only necessary to assume a value of 1.50 μm for d_p instead of 1.20 μm. The new value of n_2 found using such procedure was 1.67. If we compare this with the 1.65 given by the supplier we can see that there is a variation of about 1%. Because the variation on n_2 observed in this work is very small there is a possibility of such variation may be due to experimental error, especially since we do not know the precision of the value given for the dry membrane. However, the changes observed by Bohn[171] were also quite small (of the order of 2%) and hence it is very likely that the variation observed in this work is real and it was caused by the inclusion of water on the membrane. This would be another application of FTIR-ATR.

As well as determination of the diffusion coefficients, variations on the refractive index could also be monitored.

Fig 6.3 shows the plots of raw data (in the form of integrated intensity of the 3300 cm^{-1} band) versus time for several samples with different thicknesses. First we have two thin films with thickness (0.60 and 0.65μm) well below the d_s value for thin films. Then, we have four thicker films, two (1.3 and 1.8μm) with thickness below the d_s value for thick films and two with thickness (7.3 and 14.4μm) much bigger than d_s. The first feature to note is that the curve shapes, for any thickness, indicate a tendency for significant levels of sorption to occur at relatively short times. Physically, this represents initial sorption at some kind of specific site or immobilisation of water molecules in microvoids of the membrane. When all the sites are occupied, a very small amount of additional water randomly dissolves in the polymer on a much larger time scale. This is a typical behaviour of sorption by ionic polymers or polymers containing polar groups[137,141]. Water is a unique molecule because of its ability to form extensive hydrogen-bonded networks with itself and to hydrogen bond strongly to other polar materials. The interactions between water and membrane have already been discussed in more detail in chapter three.

The second feature to note is that the evanescent field contribution is clearly present on the values of intensity. If we start the analysis from the thick films we can see that as we increase the film thickness (from 1.3 to 7.0 μm for example) the band intensities tend to increase as well. These results show that for the thicker film, more water is being absorbed and because we still have not achieved the d_s value (3.60 μm) this increase in intensity could be detected. When we increase the film thickness from 7 to 14.4 μm however, the band intensities look very similar because, although the thicker film may absorb more water, the depth sampled is limited to 3.60 μm (3 x dp). Therefore for the 7, 14.4 μm films (and probably for even thicker films) we expect the same equilibrium values for band intensities when such measurement are made by the ATR technique.

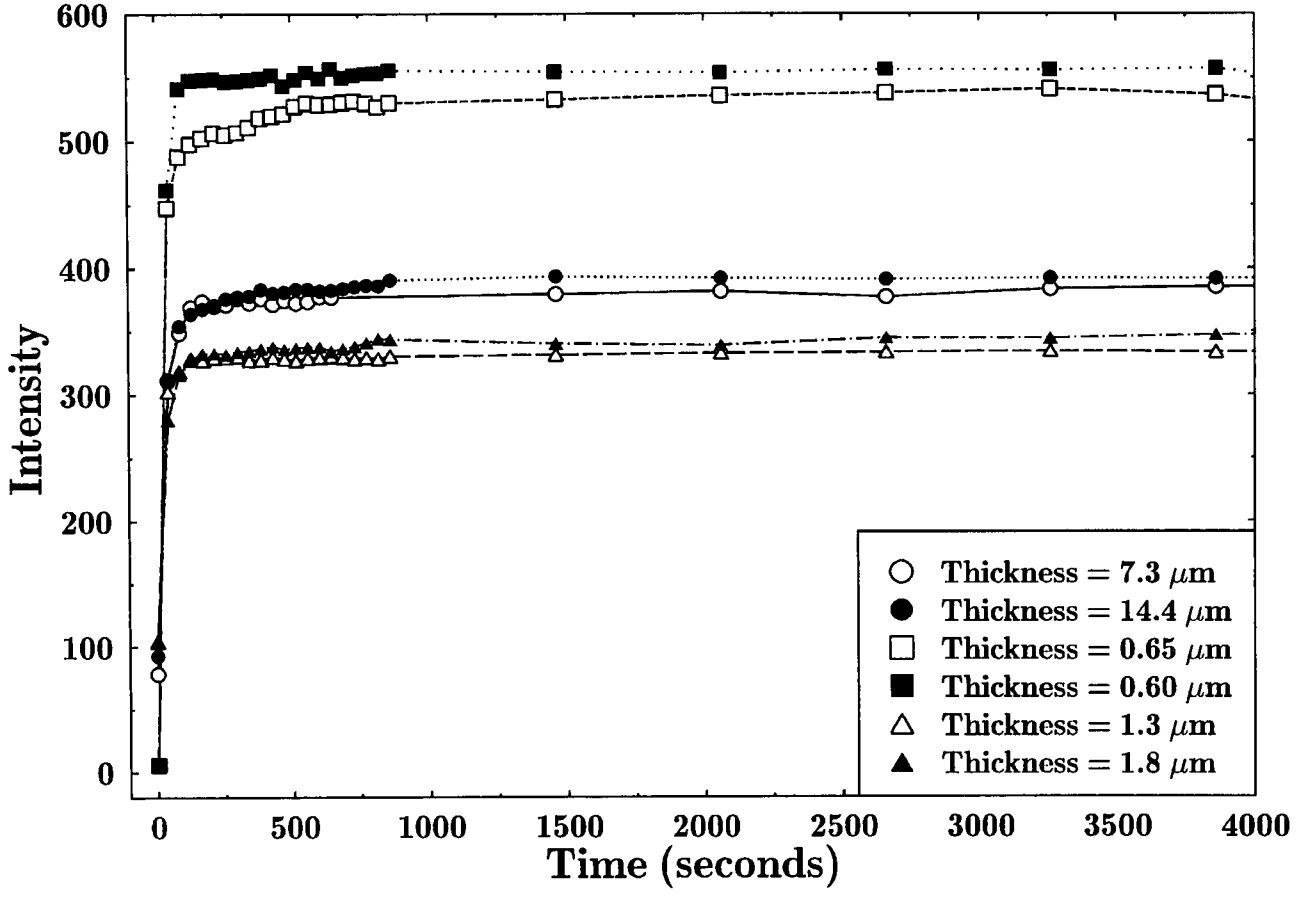

Fig. 6.3 - Changes on integrated intensity as a function of time for samples with different thicknesses. System used: SPES(S=5)/Formic acid.

Figure 6.3 also shows the results obtained with two thin films (0.60 and 0.65μm). As we can see the band intensities are bigger than for thick films. These apparently surprising results can be easily understood on the basis of the known electric field decay. As stated before, the sampled depth for thin films is 1.20 μm. So, if we are working with a 0.60 μm film the electric field will partially decay inside the film and partially inside medium 3 (water in this case). Therefore, in this case the OH band intensity represents not only water absorbed by the membrane but also pure liquid water in the reservoir, as already described qualitatively in chapter three. This explains the high intensities observed for thin films. Actually, if we subtract the pure liquid water band intensity at 3300 cm^{-1} (about 600 cm^{-1}) from the total values observed in thin films we can see that the amount of water absorbed is appropriated for a very small thickness.

Fig. 6.4 shows the same results except that the time scale is extended. As we can see, after approximately one hour, the thin film presents a completely different behaviour compared with the thick ones. After the first hour the thin film band intensities start to decrease progressively up to 8 hours (final experimental time). The most likely reason for this is that for the thin films we are *in situ* measuring the swelling of the film by water. Since the advent of synthetic polymers there have been many observations of their ability to absorb substantial quantity of penetrating liquid[127-129]. In same cases the liquid swelling is sufficient to double the original volume or more[135-136]. Considering that the swollen polymer will have increased in thickness but not in area (or very little) because it is attached to the rigid ZnSe crystal, we can expect that the electric field will decay more inside the swollen film compared with the non-swollen one and, consequently the band intensity will have a higher contribution from water inside the membrane than from pure liquid water in the reservoir. Since the film thickness is very small (even in the swollen form) the concentration of water in the film will also be very small. This could explain the decrease in the band intensities after one hour in water. The first hour is the necessary time for the swelling to occur and is usually called induction period[122].

For the other thicknesses studied, although the same process may occur, because the thickness is bigger than d_s the phenomenon could not be observed.

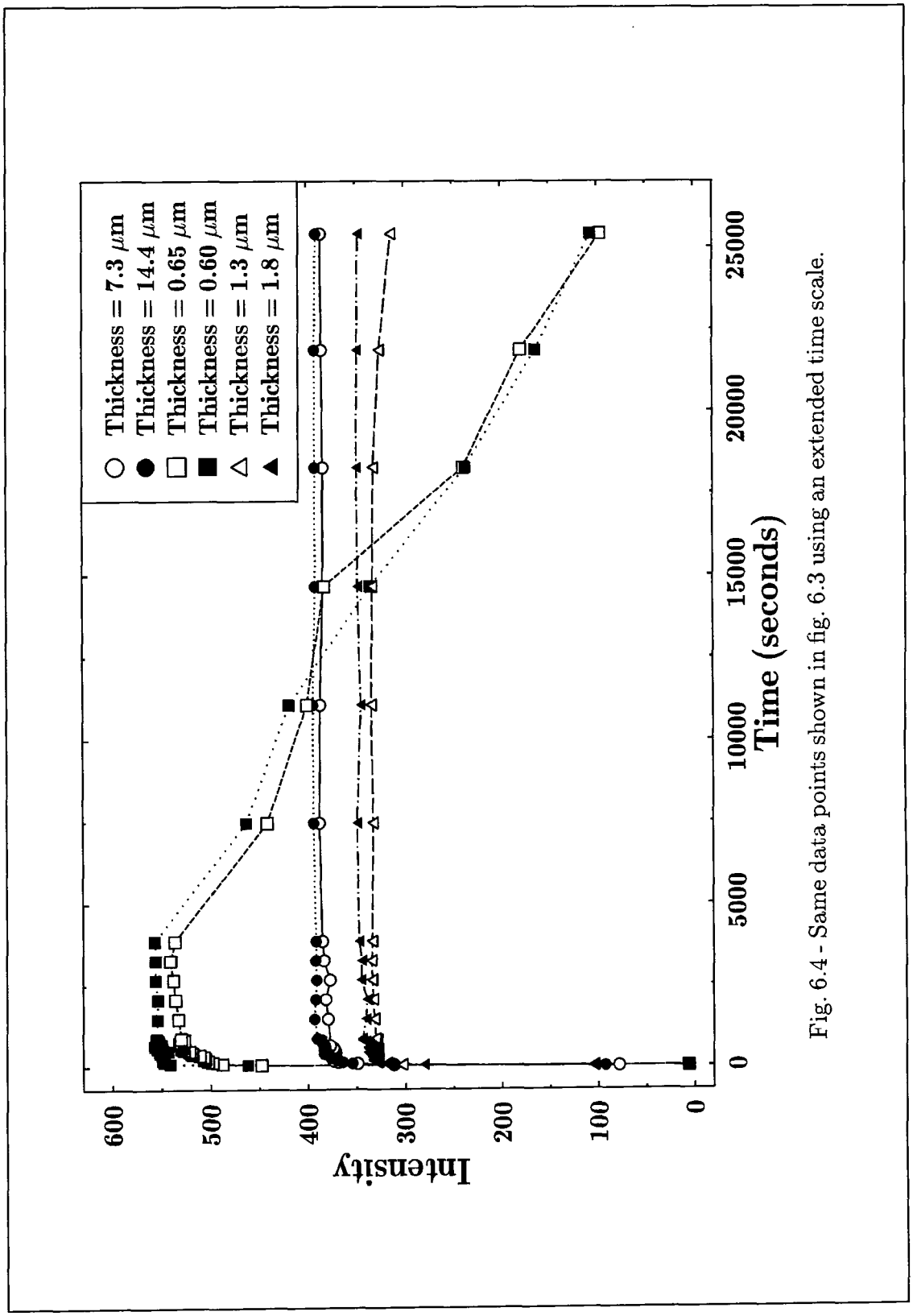

Fig. 6.4 - Same data points shown in fig. 6.3 using an extended time scale.

According to the literature some systems can present a change on the diffusion process (from non-Fickian to Fickian or vice-versa) as a function of thickness. For example, Berens[172] found that in the sorption of organic liquids and vapours by rigid poly(vinyl chloride)(PVC) at higher sorption levels, increasing film thickness produces a shift of the kinetics from case II to Fickian with apparent diffusivity values typical of rubbery polymers.

Using the same set of data, we can now produce a normalised curve, according to eq. 4.18 in order to check if the process of diffusion in our case is changing with film thickness. Fig. 6.5 shows the results and, as we can see the curve shapes are very similar and the absorbances of saturation tend to the same value. This similarity is indicative of the same mechanism of diffusion for all the samples, independent of thickness. The differences observed are possibly related to the kinetics of sorption and this subject will be discussed in more detail later in this chapter when calculating the diffusion coefficients for films with different thickness.

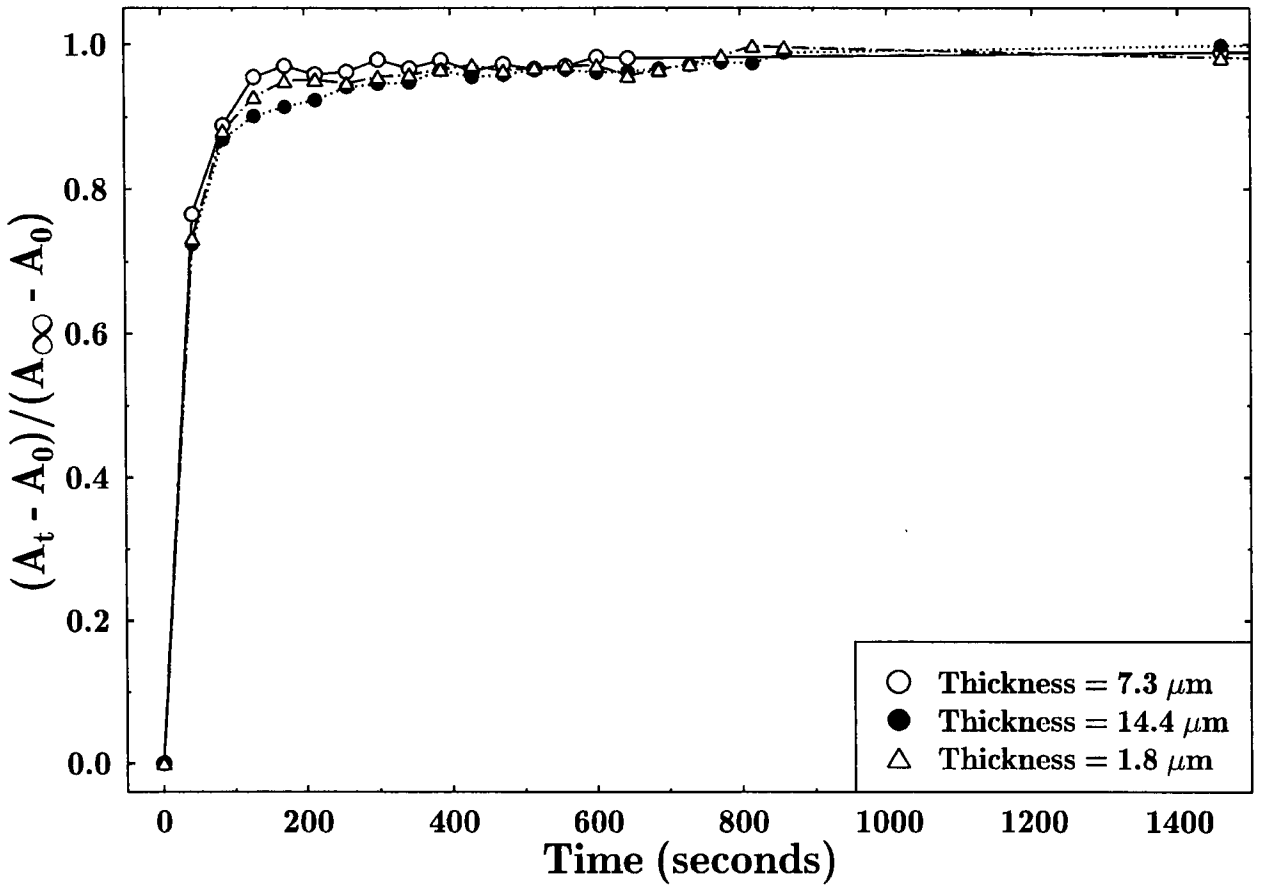

Fig. 6.5 - Experimental data normalised according to eq. 4.18.

6.1.2 - Diffusion Coefficient Calculations

In this section we will analyse the results obtained using the PASCAL routines already described in chapter four.

6.1.2.1 - Fickian Diffusion

The first step of data analysis was the quantification of spectral information for use in the proposed FTIR-ATR models. Fig. 6.6, 6.7 and 6.8 show some experimental results obtained for the system SPES(S5) in formic acid, NMP and DMF, respectively. The data points represent the integrated intensity measured as a function of time. The solid lines were obtained using eq. 4.18 used for Fickian diffusion, by fixing the values of D and back calculating the expected values of intensity. Comparison of the data points with the calculated curves in fig. 6.6, 6.7 and 6.8 show that the agreement between experimental data and theoretical curve was very poor. Since the equation used describes the Fickian concentration profile we can conclude that the system does not present a Fickian behaviour. These results were not very surprising and actually they were already expected since, as reported in the introduction, polymeric membranes are likely to present the dual sorption mode instead of a Fickian behaviour.

6.1.2.2 - The Dual Sorption Mode

In considering the transport of penetrant in and through a glassy polymer, it was originally assumed that the penetrant species dissolved in the polymer by mode (a) (ordinary dissolution) are mobile, whereas the species dissolved by mode (b) (filling of microcavities or absorption in specific sites) are completely immobilised[141]. Petropoulos[144] as well as Paul and Koros[142-143] have later suggested that the penetrant

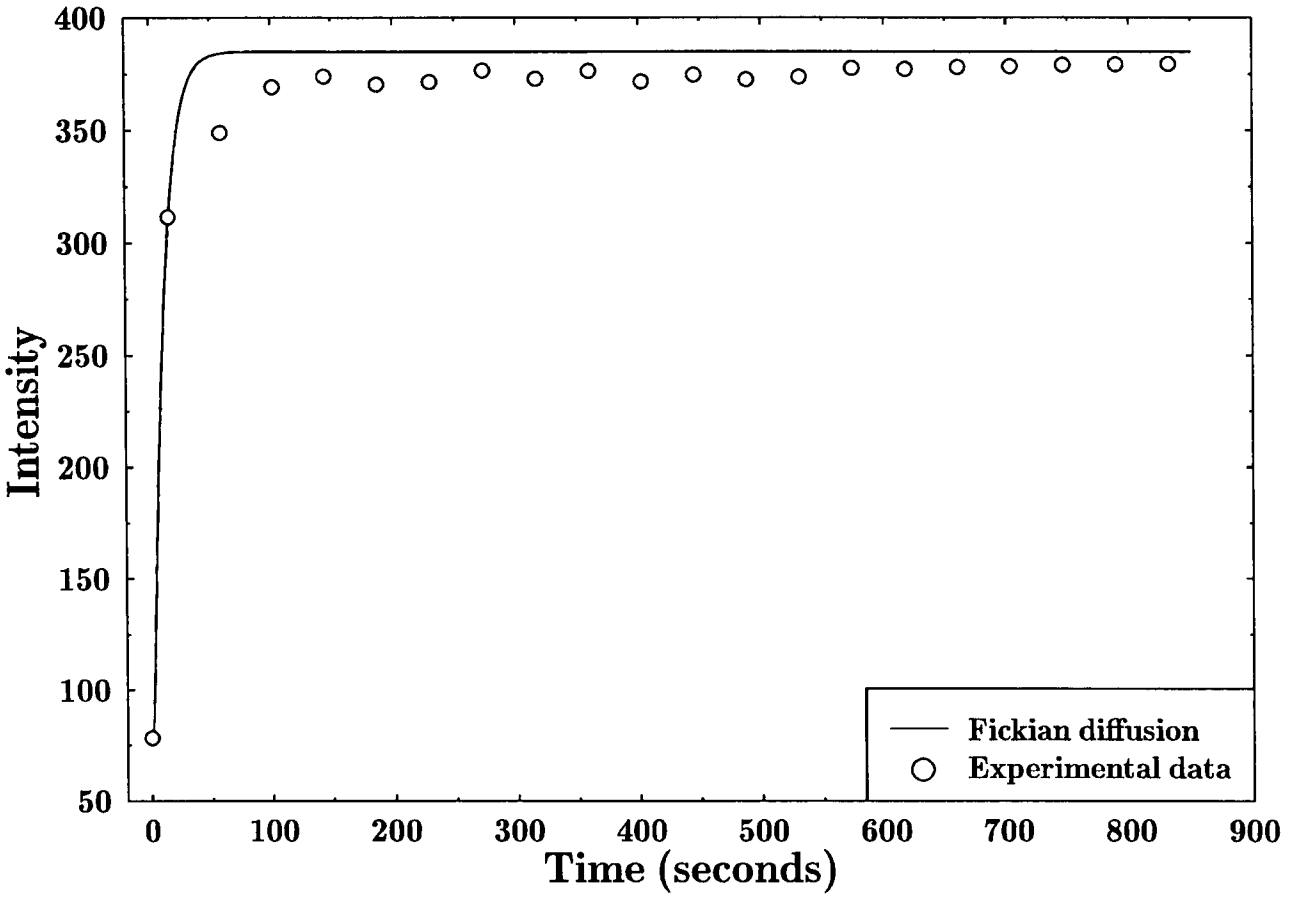

Fig. 6.6 - Comparison between experimental data points and curve generated by the equation that describes Fickian behaviour. System SPES(S=5)/Formic acid. Sample thickness (7.3 $\pm$1.7) μm.

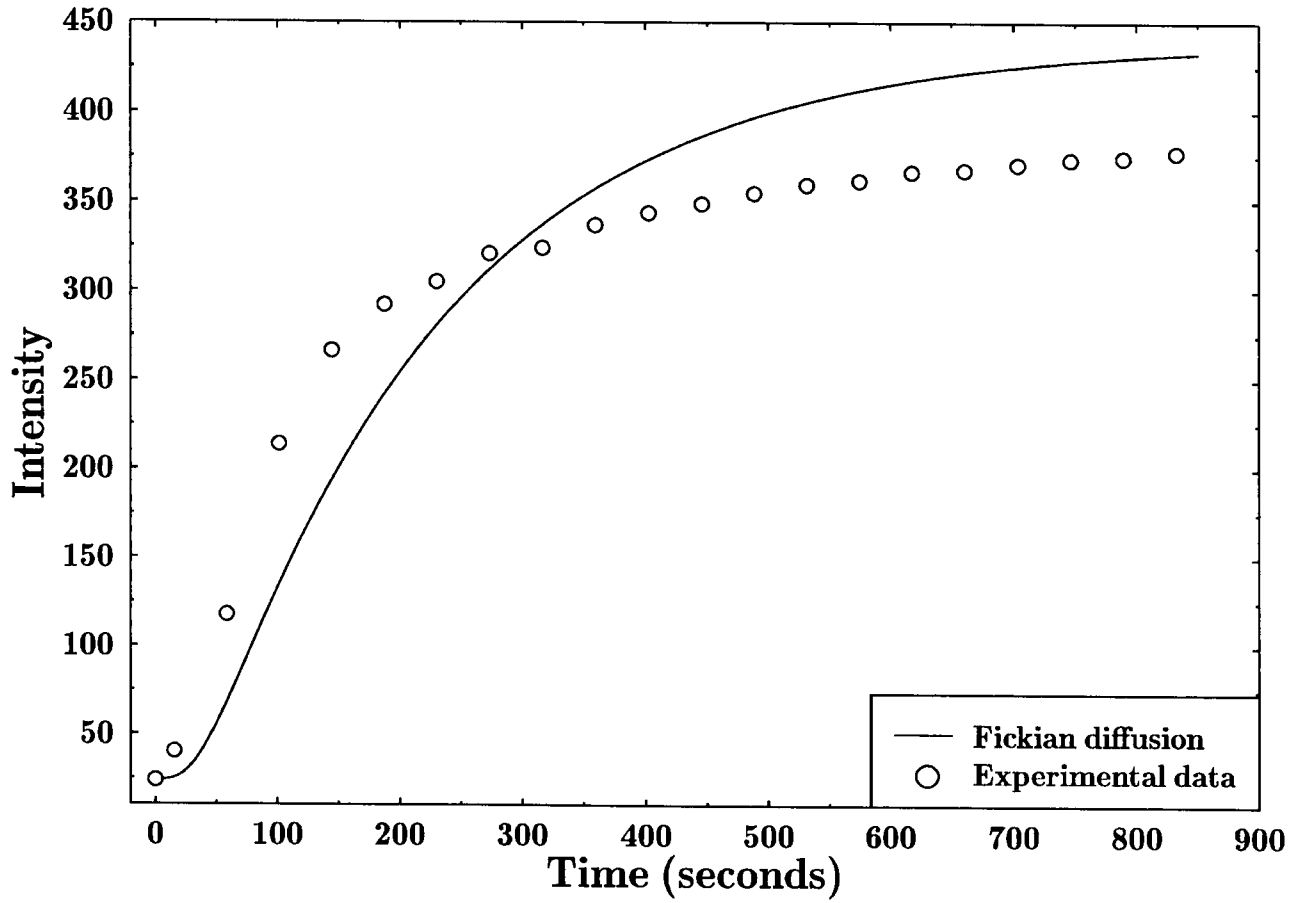

Fig. 6.7 - Comparison between experimental data points and curve generated by the equation that describes Fickian behaviour. System SPES(S=5)/NMP. Sample thickness (6.4 $\pm$1.0) μm.

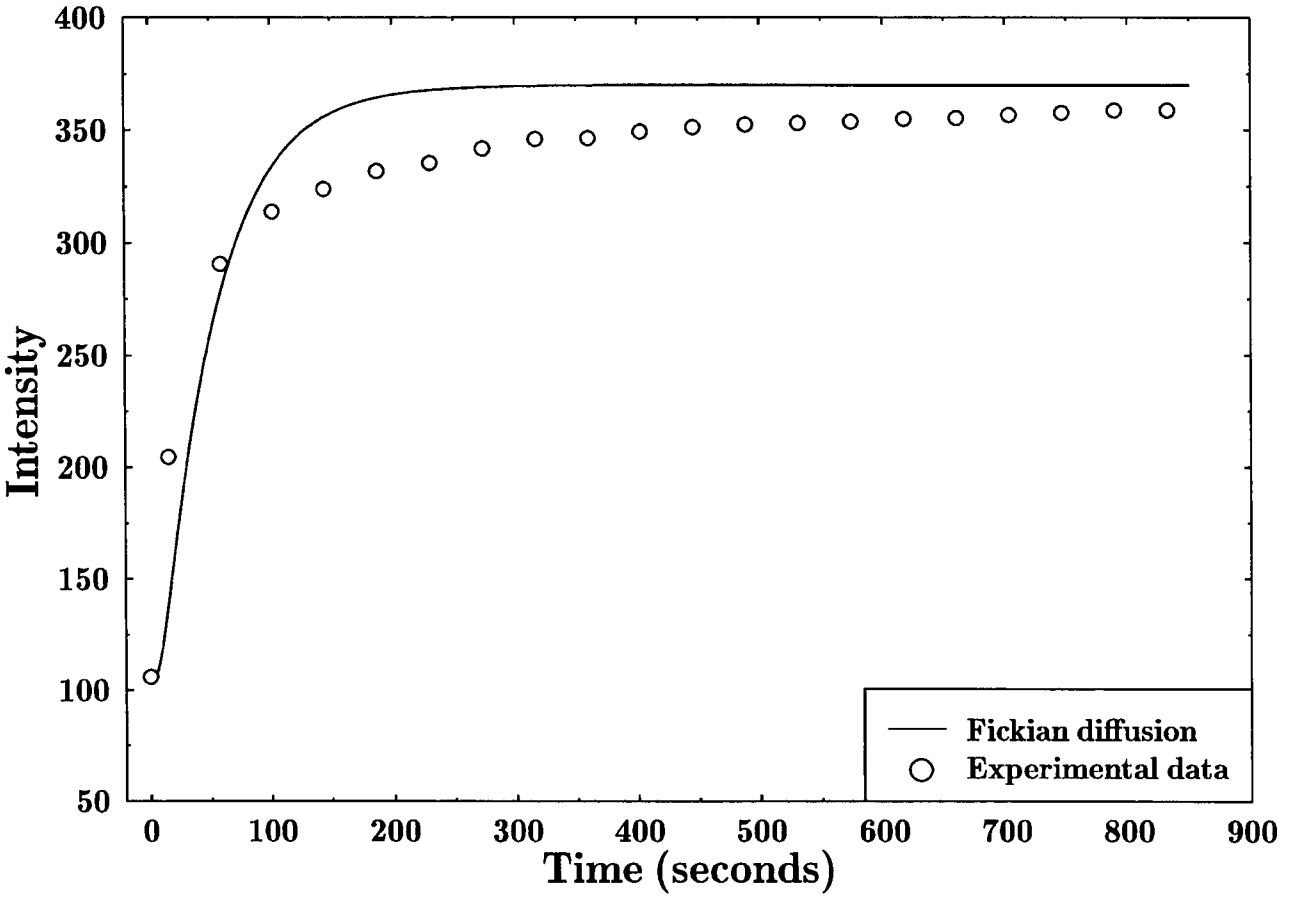

Fig. 6.8 - Comparison between experimental data points and curve generated by the equation that describes Fickian behaviour. System SPES(S=5)/DMF. Sample thickness (7.7 ±0.7) μm.

species dissolved by mode (b) may be only partially, rather than totally, immobilised. Two different diffusion coefficients, one for each penetrant species, are then necessary to describe the transport of penetrant in the polymer. The two diffusion coefficients were assumed by both Petropoulos[144] and Paul and Koros[142-143] to be constant at a given temperature.

In our work, to describe the diffusion process for the dual mode model we used a modified form of Fick's first law already described in chapter four. In the model used the concentration of penetrant is written as the sum of concentrations of the mobile and immobilised species. These concentrations were substituted on eq 4.19 and then added to produce a new equation (4.45) that describes the dual sorption model.

Eq. 4.45 describes a dual sorption model and produces two diffusion coefficients, one for the partially and the other for the totally mobile molecules.

Fig. 6.9, 6.10 and 6.11 show the same experimental data points showed on fig. 6.6, 6.7 and 6.8, now compared with the theoretical curve generated by the dual sorption model equation (eq. 4.45). The figures confirm that the dual mode model represents the membrane behaviour much better than the Fickian model. The same kind of agreement was found for the other system in study as well (SPES(S20)).

As already mentioned in chapter four, the experimental conditions may make accurate determinations of the equilibrium infrared absorption unreliable. In our case, for example, visual inspection of some of the films (especially those made by SPES(S20)) suggested that the polymer film had possibly become detached from the crystal after exposure to water for long periods of time. In order to solve this problem, it was proposed in chapter four that the A_{∞} value would be calculated as a second adjustable parameter (in addition to the diffusion coefficient, D). Fig. 6.12 shows one experiment where the delamination process was clearly detected (visually). The solid line represents the curve generated by the dual mode equation. According to the figure, the delamination process seems to start after about two hours of exposure to water. Because of the delamination, the experimental equilibrium value is higher than the calculated

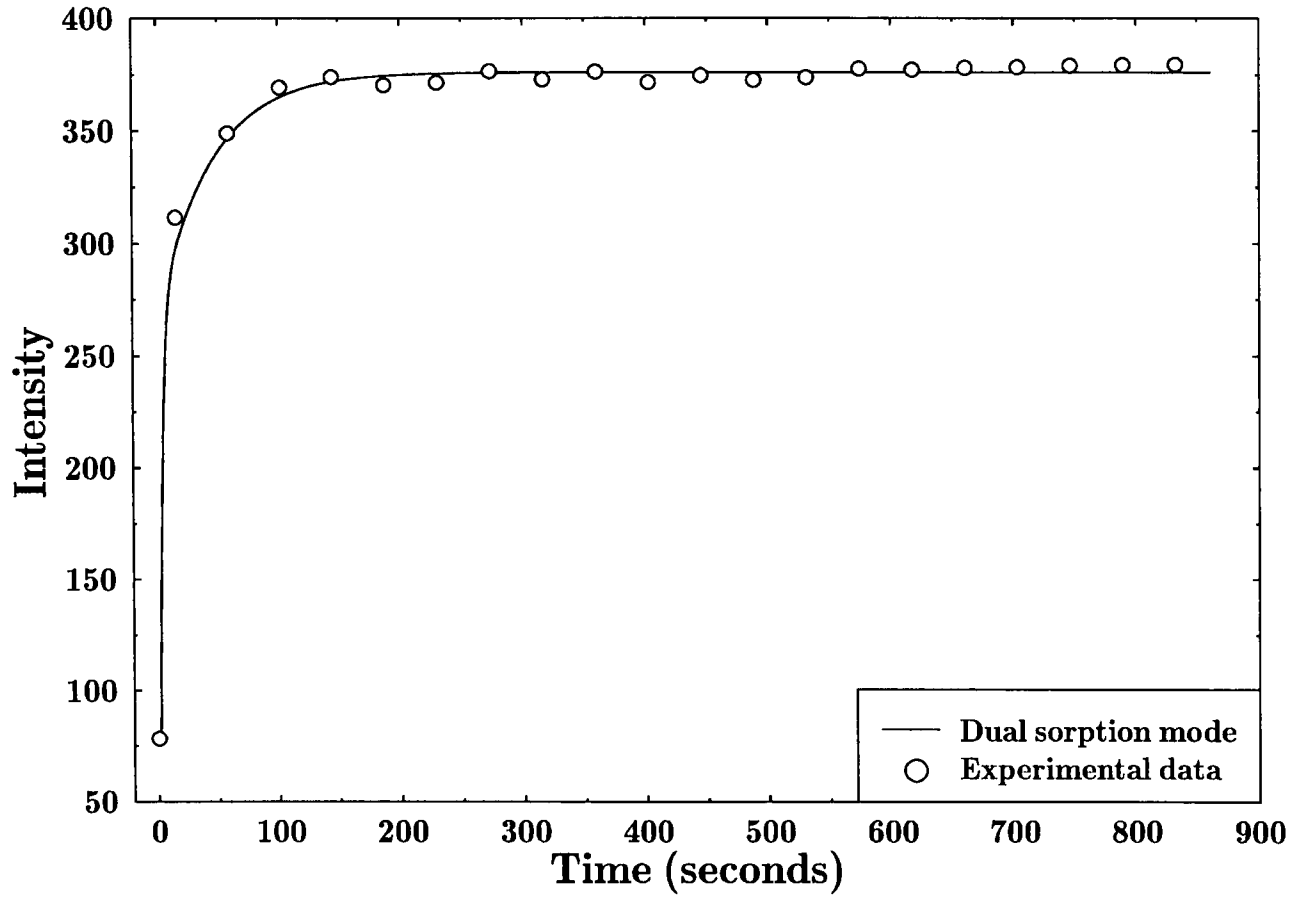

Fig. 6.9 - Comparison between experimental data points and curve generated by the equation that describes the dual sorption mode. System SPES(S=5)/Formic acid. Sample thickness (7.3 $\pm$1.7) μm.

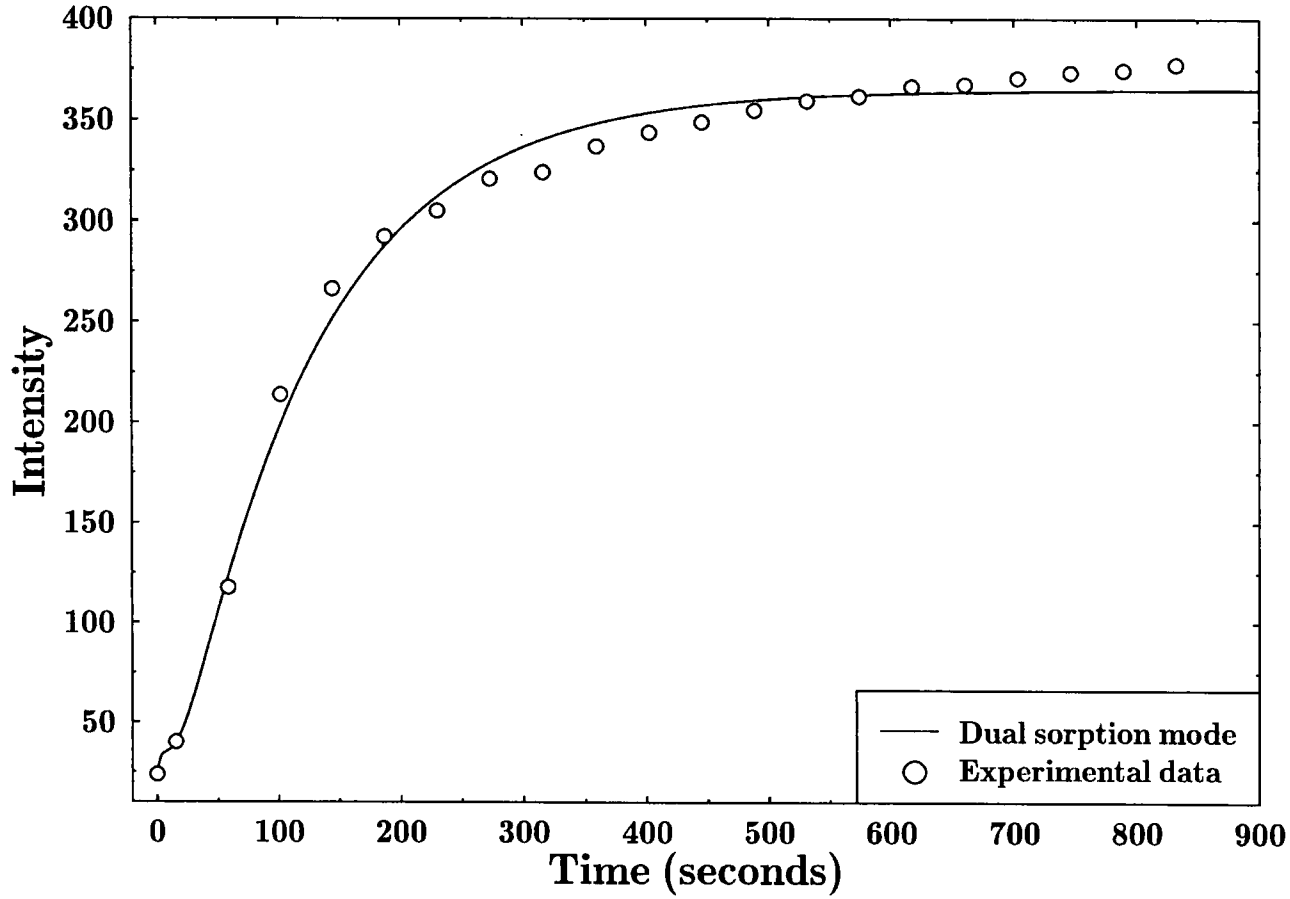

Fig. 6.10 - Comparison between experimental data points and curve generated by the equation that describes the dual sorption mode. System SPES(S=5)/NMP. Sample thickness (6.4 ±1.0) μm.

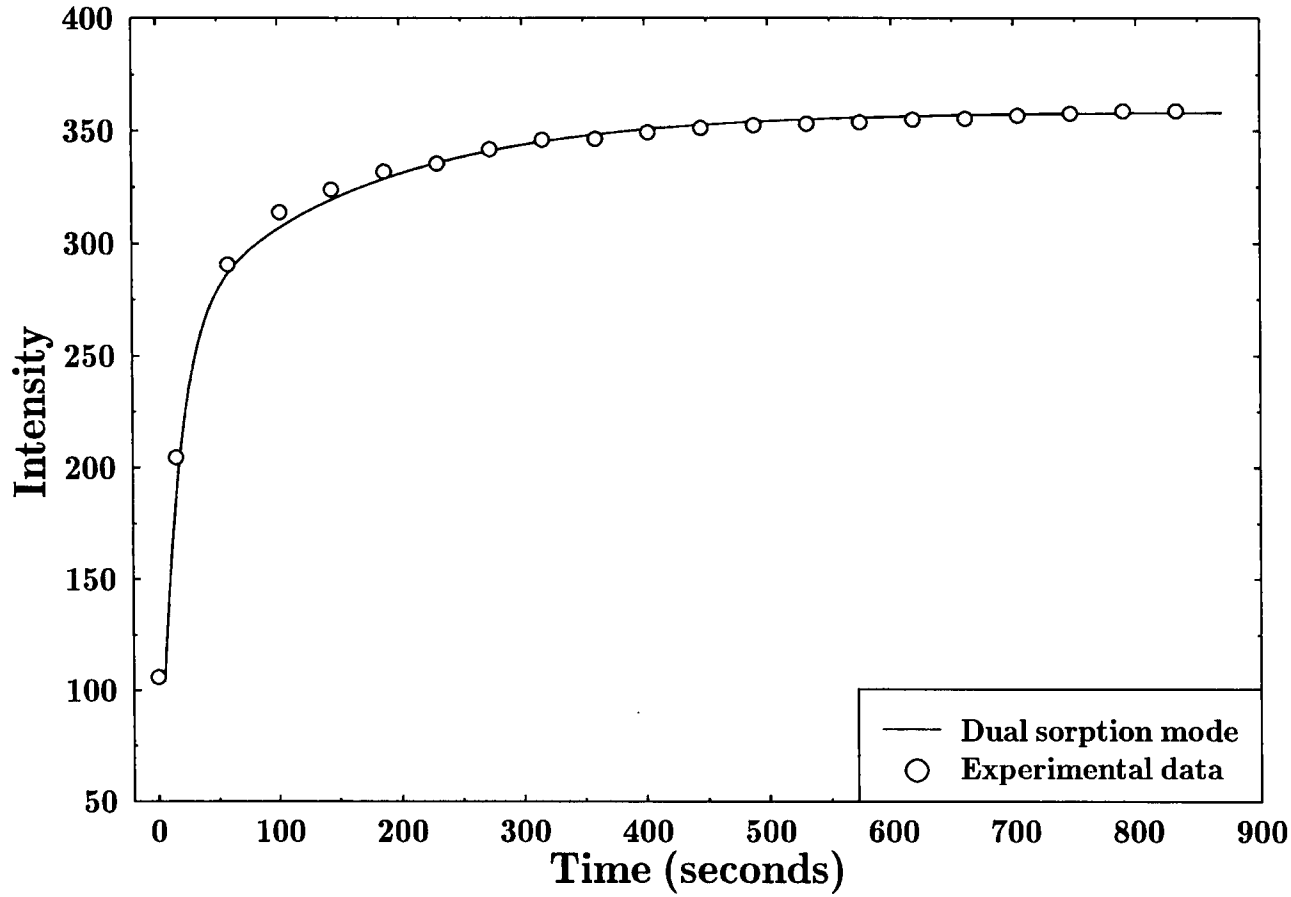

Fig. 6.11 - Comparison between experimental data points and curve generated by the equation that describes the dual sorption mode. System SPES(S=5)/DMF. Sample thickness (7.7 ±0.7) μm.

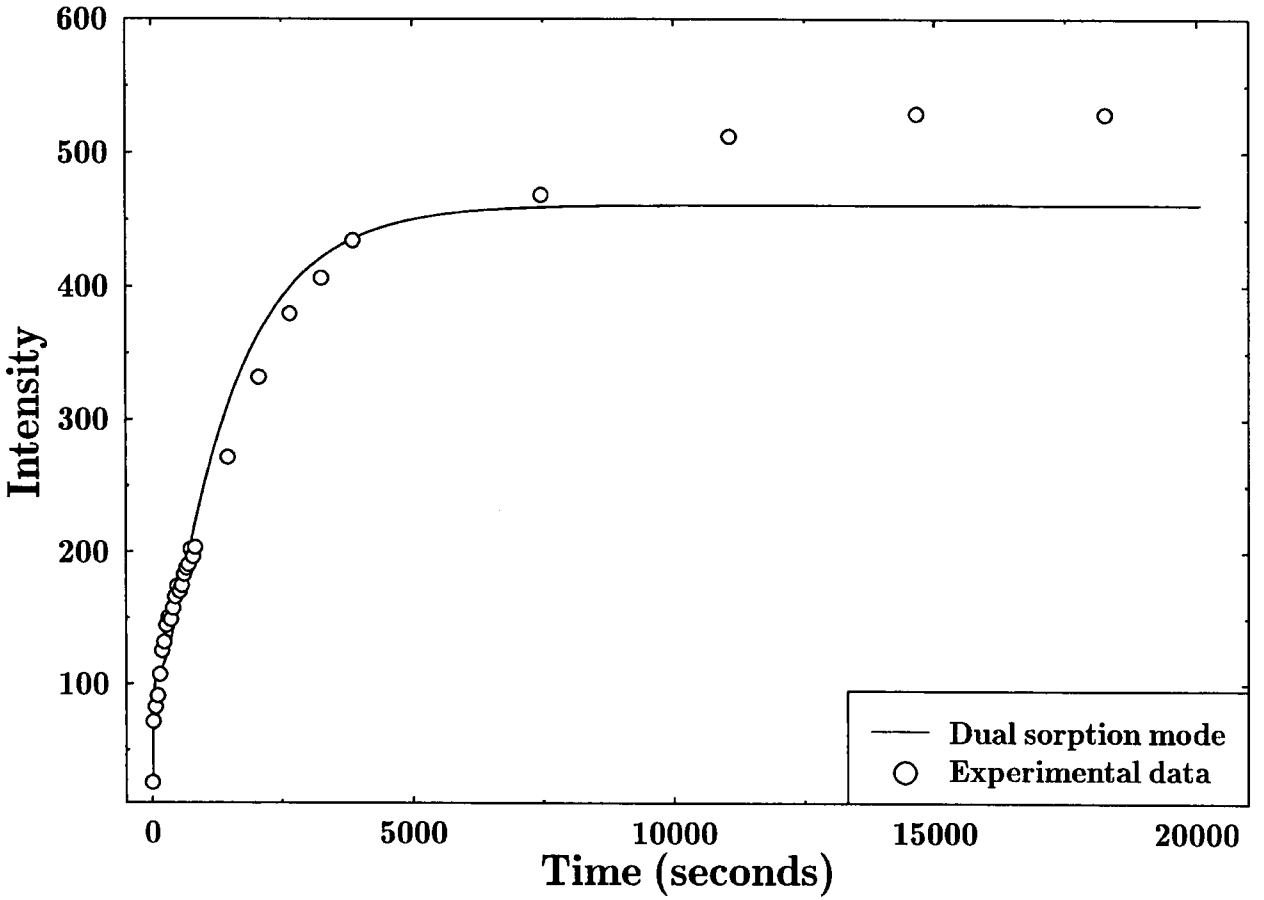

Fig. 6.12 - Comparison between experimental data points and curve generated by the equation that describes the dual sorption mode. System SPES(S=20)/DMF. Sample thickness (16.5 $\pm$1.5) μm.

ones. Assumption of the experimental value as the correct one in such cases could lead to serious errors on the diffusion coefficients.

The number of iterations necessary to determine the diffusion coefficient value was calculated for Fickian behaviour. The iteration process was already described in chapter four and will be only summarised here as:

1. Initialise the sum with $\Sigma = 0$
2. Add term n to the sum
3. Calculate next term ((n+1))
4. If error $\rangle$ 10^{-16} go to 2

Accordingly, to calculate the iteration number it was only necessary to add a subroutine in step 4 in order to count how many cycles were necessary until the relative error between the interactions reaches a value $\leq 10^{-16}$. Fig. 6.13 shows the results. As we can see the number of iterations will be higher for small values of Dt. The figure also shows that thicker films will require more iterations than the thinner ones. Both correlations (with Dt and L) are only mathematical and can be easily understood with basis on eq. 4.18.

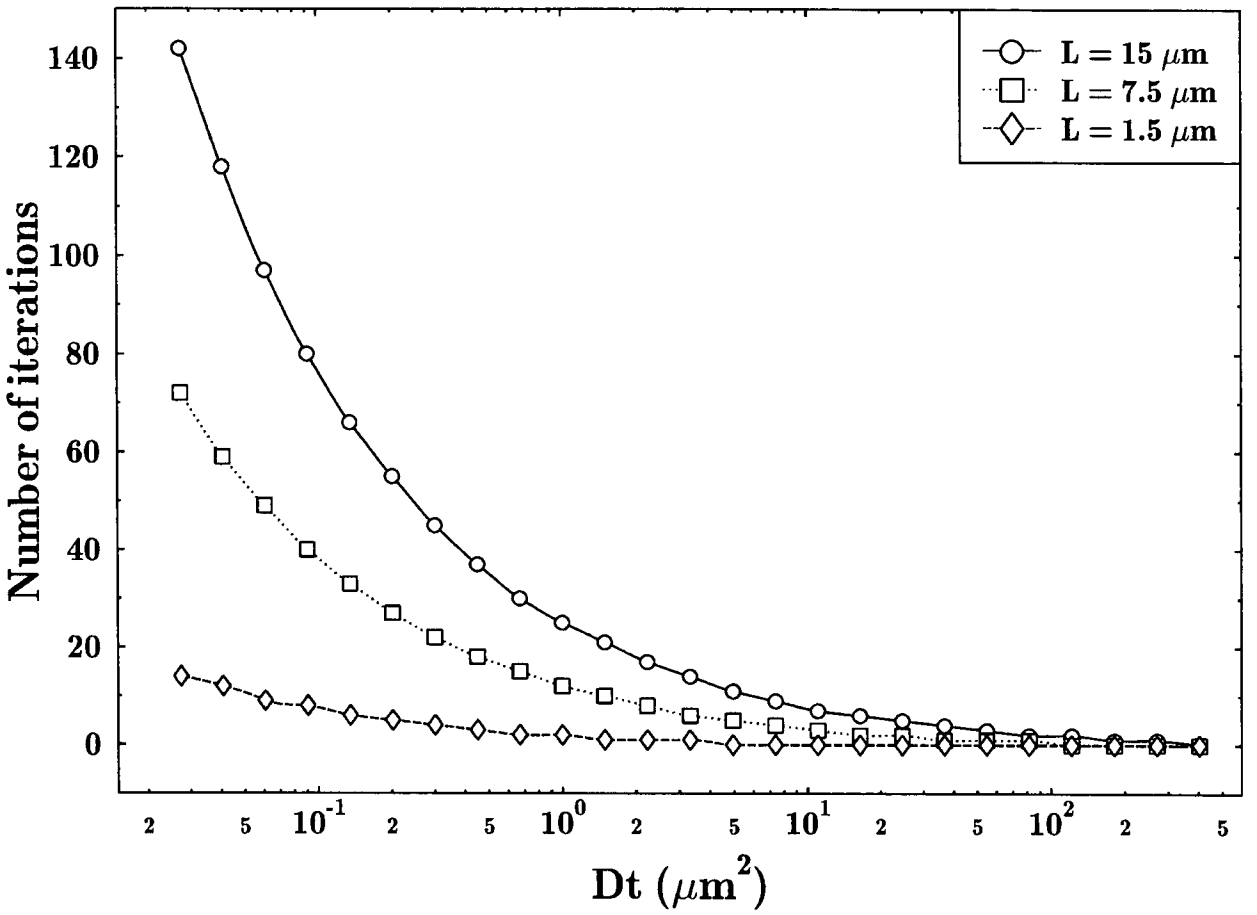

Fig. 6.13 - Number of iterations needed to obtain a value of A(t) as a function of Dt.

Table 6.1 presents the diffusion coefficient values calculated using Fick's law for the different systems used while table 6.2 shows the results obtained using the dual sorption mode for the same systems.

Table 6.1 - Diffusion Coefficient Values Calculated According to Fick's Law

System	thickness(μm)	D_1 (cm^2/sec)
S5/Formic Acid	1.3 ± 0.4	(1.34 ± 0.37) x 10^{-7}
S5/Formic Acid	1.8 ± 0.3	(2.59 ± 0.54) x 10^{-7}
S5/Formic Acid	1.9 ± 0.4	(2.84 ± 0.20) x 10^{-7}
S5/Formic Acid	7.3 ± 1.7	(2.43 ± 0.66) x 10^{-8}
S5/Formic acid	11.0 ± 0.9	(5.47 ± 1.20) x 10^{-8}
S5/Formic Acid	14.4 ± 3.7	(8.46 ± 2.70) x 10^{-8}
S5/NMP	9.4 ± 1.2	(1.36 ± 0.20) x 10^{-9}
S5/NMP	8.4 ± 0.9	(1.46 ± 0.18) x 10^{-9}
S5/DMF	8.2 ± 1.6	(8.34 ± 1.10) x 10^{-9}
S5/DMF	7.7 ± 0.7	(5.22 ± 0.64) x 10^{-9}
S20/NMP	12.5 ± 1.6	(7.38 ± 0.17) x 10^{-10}
S20/NMP	10.5 ± 1.9	(3.23 ± 0.65) x 10^{-10}
S20/DMF	16.5 ± 1.5	(2.34 ± 0.35) x 10^{-10}

Table 6.2 - Diffusion Coefficient Values Calculated According to the Dual Sorption Mode.

System	Thickness (μm)	D_1 (cm^2/sec)	D_2(cm^2/sec)	x_1
S5/Formic Acid	1.3 ± 0.4	(1.21±0.59) x 10^{-9}	(2.45±0.72) x 10^{-11}	0.944 ± 0.026
S5/Formic Acid	1.8 ± 0.3	(1.44±0.31) x 10^{-9}	(2.82±1.16) x 10^{-11}	0.895 ± 0.003
S5/Formic Acid	1.9 ± 0.4	(1.50±0.45) x 10^{-9}	(2.74±1.76) x 10^{-11}	0.895 ± 0.021
S5/Formic Acid	7.3 ± 1.7	(2.82±0.79) x 10^{-8}	(7.84±4.83) x 10^{-10}	0.918 ± 0.008
S5/Formic Acid	11.0 ± 0.9	(5.18±0.98) x 10^{-8}	(1.46±0.72) x 10^{-9}	0.900 ± 0.025
S5/Formic Acid	14.4 ± 3.7	(1.08±0.23) x 10^{-7}	(2.89±1.17) x 10^{-9}	0.889 ± 0.005
S5/NMP	9.4 ± 1.2	(2.17±0.29) x 10^{-9}	(3.30±1.85) x 10^{-10}	0.769 ± 0.019
S5/NMP	8.4 ± 0.9	(2.27±0.24) x 10^{-9}	(5.86±3.11) x 10^{-10}	0.730 ± 0.073
S5/DMF	8.2 ± 1.6	(2.11±0.83) x 10^{-8}	(9.03±1.48) x 10^{-10}	0.715 ± 0.026
S5/DMF	7.7 ± 0.7	(1.40±0.18) x 10^{-8}	(7.92±1.80) x 10^{-10}	0.756 ± 0.062
S20/NMP	12.5 ± 1.6	(1.62±0.43) x 10^{-9}	(3.55±1.01) x 10^{-10}	0.195 ± 0.052
S20/NMP	10.5 ± 1.9	(2.38±0.16) x 10^{-9}	(1.86±1.25) x 10^{-10}	0.206 ± 0.019
S20/DMF	16.5 ± 1.5	(5.77±1.08) x 10^{-8}	(8.13±1.67) x 10^{-10}	0.195 ± 0.028

6.1.3 - Parameters That Can Affect the Diffusion Coefficients

Using table 6.1 and 6.2 we will try now to analyse the influence of the following parameters on the diffusion coefficient.

- Sample thickness (for the system S5/formic acid)
- Solvent (formic acid, NMP and DMF)
- Sulphonation level (comparing S5 and S20 using NMP and DMF as solvent)

6.1.3.1 - Sample Thickness

Fig. 6.14 shows the variations on D_1 and D_2 values as a function of film thickness for the system SPES(S5)/formic acid. As we can see, the values of D_1 as well as D_2 tend to increase as we increase the sample thickness. The first information we can get from this behaviour is that the results confirm the hypothesis of a non-Fickian process occurring on the system since, as already pointed out on introduction, one of the main characteristics of Fickian diffusion is to be independent of thickness. In our system however, as stated before, although the same (non-Fickian) process is occurring, the diffusion coefficients apparently are greatly dependent on thickness.

According to the dual mode sorption the diffusion process occurs in two different ways. Firstly the penetrant is absorbed on specific sites. In our model we considered that these absorbed molecules are partially mobile. The second mode is related to the diffusion coefficient of the penetrant through the matrix. In this case the molecules are considered totally mobile.

It is important to remember that the first and second mode occur simultaneously and both contribute to the diffusion coefficient value. Naturally, because the kinetics are different the contribution of each one as a function of time will be different. The absorption on the specific sites is a very fast process and therefore it will occur at very short periods of time. On the other hand, the second mode is a slower one hence its

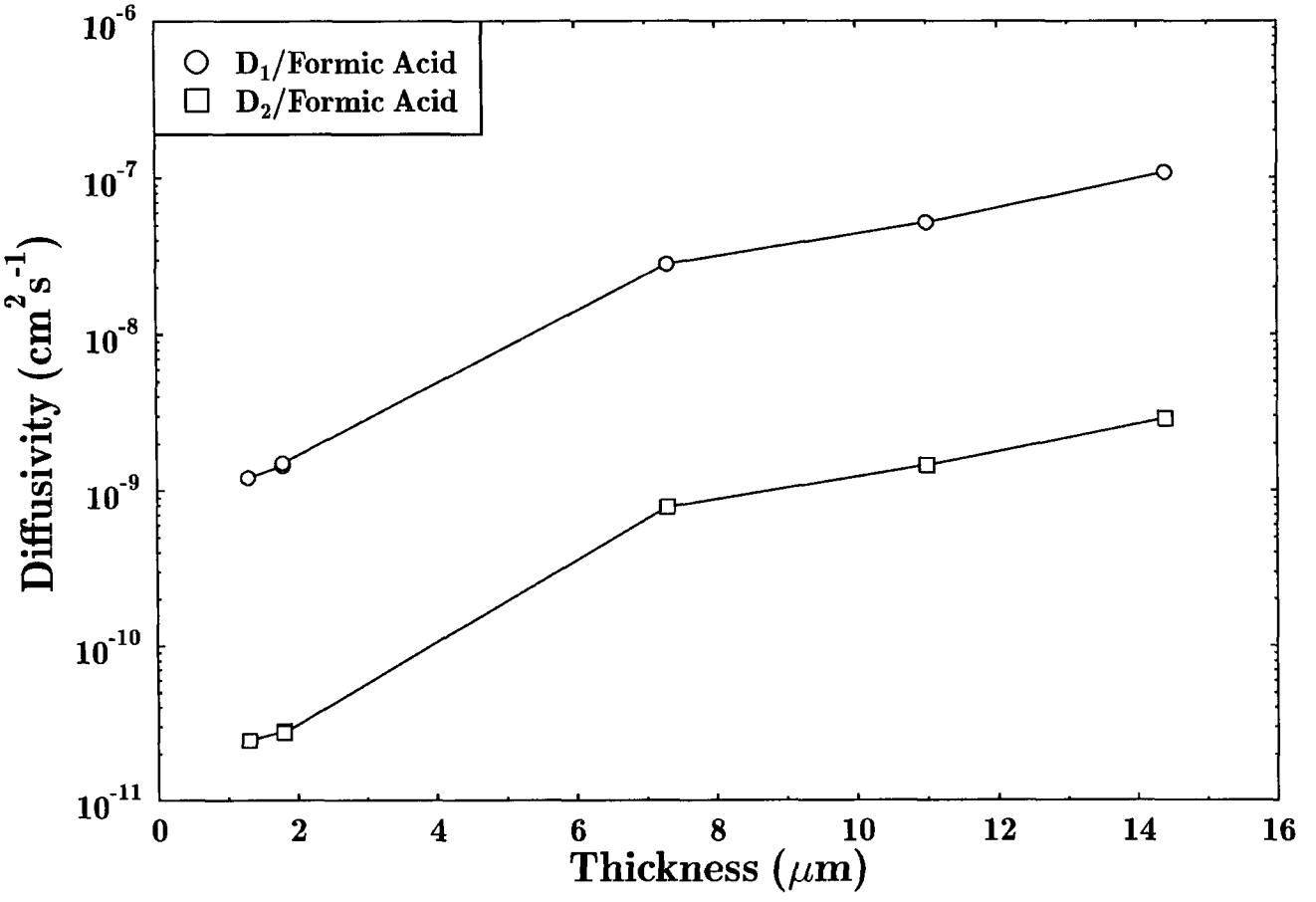

Fig. 6.14 - Variations on the diffusion coefficients as a function of sample thickness for the system SPES(S=5)/Formic acid.

contribution must be more important for long periods of time. The data in table 6.2 as well as fig 6.14 confirm that hypothesis. From table 6.2 we can see that for all systems investigated the D_1 values are always bigger than D_2.

This time dependence is observed especially in polymers below their glass transition since, at these temperatures the rate of diffusion is comparable with the rate of motion of the polymer segments[127]. As a result, the value of the diffusion coefficient attained at a given concentration in an element of the polymer will depend on the time for which this concentration has existed at the element. D has more time in which to approach its equilibrium value in thicker films. Therefore, sorption proceeds more rapidly the thicker the film[145].

In our case, we can say that if we are using a thin film to measure a very fast process probably we will lose information relative to very short times. As we increase the film thickness the contribution from D_1 can be more easily "detected" promoting an increase in values of D. On the other hand, for thin films the second process will be much more easily detected and in a way it will slow down the diffusion coefficient.

Table 6.2 also shows that the x_1 values are kept constant for the thickness range studied. The x_1 values represent the fraction of molecules partially immobilised on the absorption sites and give us an indication of how predominant one mode is in relation to the other. Since the number of sites is kept constant (because we are using the same polymer, i.e. with the same sulphonation level) it is reasonable to expect that uniformity of x_1 values as shown in the table.

6.1.3.2 - Solvent Used

In order to analyse the solvent influence three S5 film samples with similar thickness but different solvents were considered. The sample thicknesses were 7.3 ± 1.7 μm, 8.4 ± 0.9 μm and 7.7 ± 0.7 μm for formic acid, NMP and DMF, respectively.

Comparing firstly the results obtained using formic acid and DMF we can see that the D_1 and D_2 values are of the same order while the x_1 value is smaller for DMF than formic acid.

If now we compare the same parameters using NMP as solvent we can see that, in this case, both D_1 and x_1 values are sensibly smaller for this system.

These results confirm the influence of the solvent on the diffusion coefficient of the membranes. Relatively few studies have been reported on the influence of solvents on the structure and properties of ionic polymers[117]. Of these studies, most have been based on measurements of the viscosity of solutions. For example, Lundberg and Philips[173] studied the solution properties of sulphonated polystyrene ionomers in solvents of different dielectric constant, ε. They found that polar solvents tend to solvate the ions whereas non-polar solvents promote ion-pairs interactions between the ionic dipoles. Weiss and Fitzgerald[117] using different techniques demonstrated that for the same ionic polymer (i.e. sulphonated polystyrene) relatively non-polar solvents preferentially interact with the hydrocarbon matrix and leave the cluster morphology intact. Polar solvents, on the other hand, interact strongly with the ionic groups and tend to plasticise the cluster, weakening the intermolecular forces operating in these systems.

Table 6.3 presents the values of dielectric constant for most solvents in question and it will be used when trying to explain the observed results.

According to the table, water has the highest dielectric constant and, therefore in any of the systems in question it will expect to interact directly with the SO_3^- anion.

Comparing the values of dielectric constants for formic acid and DMF we can see that the former has a slightly higher value compared with the second but, both can be considered to have a relatively high polarity. Apparently the small difference on polarity is not enough to cause a considerable change in the diffusion coefficient values but is enough to decrease the value of x_1. Following Weiss and Lundberg theories we can say that DMF, being less polar than formic acid will preferentially interact with the polymer matrix promoting interactions between the ionic dipoles. These interactions could make the water interaction more difficult . This fact can be confirmed by the smaller value of

Table 6.3 - Dielectric Constants of Some Solvents

Solvent	Dielectric Constant, ε
Water	78.5
Formic acid	58.0
DMF	36.7
Pyridine	12.3
Pyrrolidone	7.48

x_1 that is related to the number of molecules immobilised on the adsorption sites.

The smaller value of D_1 for the NMP system can also be explained in terms of solvent polarity. Although it was not possible to find the dielectric constant of NMP, from the values for pyridine and pyrrolidone we expect it to be in the same range and hence well below the values for DMF and formic acid. Being the less polar solvent used, NMP is expected to promote the ion-pair interactions and leave the cluster morphology intact. In this case, the water absorption becomes much more difficult causing, not just a reduction on the x_1 value, but reducing even the D_1 value that is related to the speed at which the water molecules are absorbed by the absorption sites.

The D_2 values are, as stated before, related to the diffusion of totally mobile molecules though the polymeric matrix and consequently are not influenced by ion-pair interactions and/or cluster morphology. Since the polymer matrix is kept unchanged the D_2 values are the same for the three systems.

Fig. 6.15 shows the integrated intensity versus time plots for the 3 systems in question. As we can see their behaviour at very short times as well as the value of absorbance at equilibrium are quite different. The figure shows that the water uptake for the NMP system is slower compared with the two other solvents confirming the theory

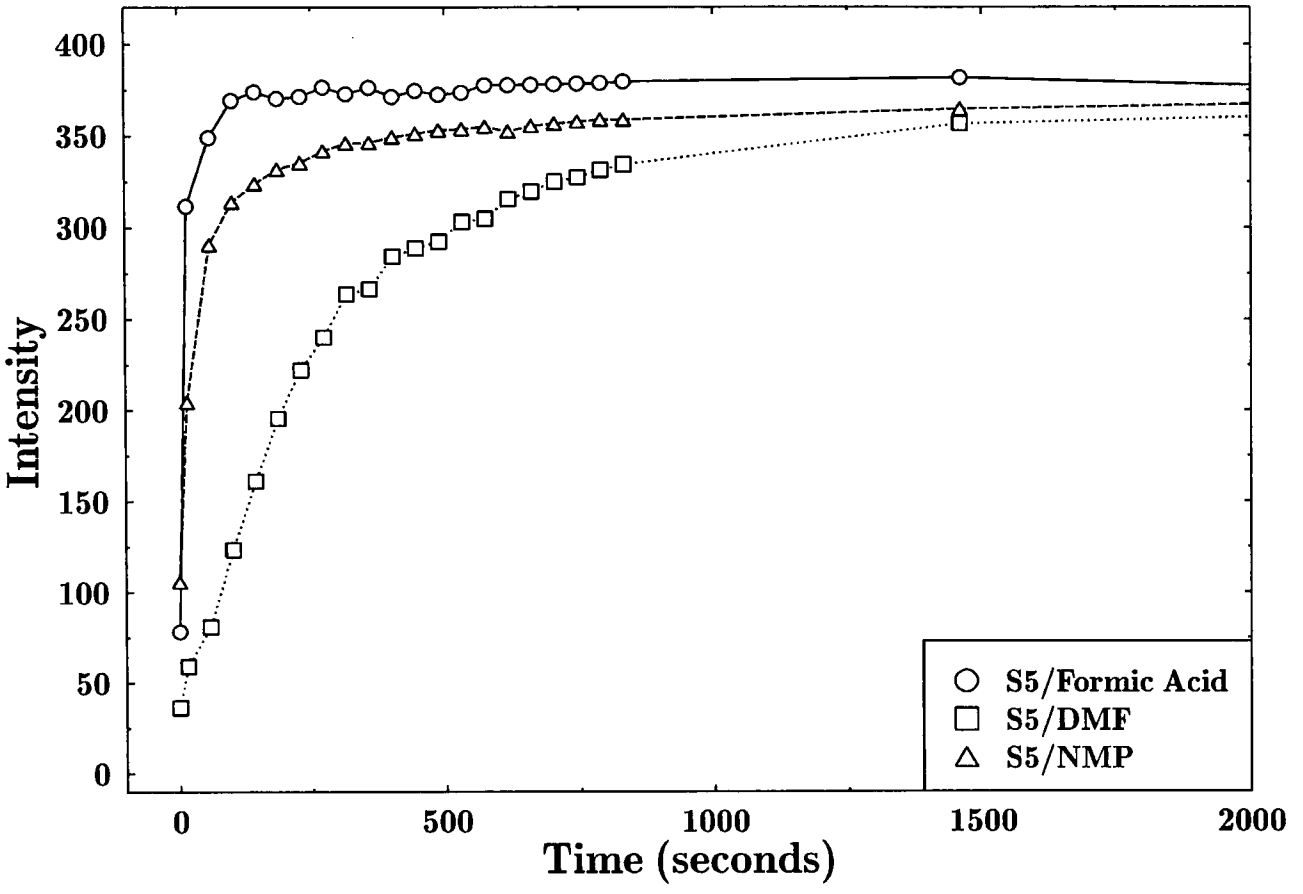

Fig. 6.15 - Results of water uptake as a function of time for SPES(S=5) in different solvents.

that the less polar solvent will make the water absorption onto the absorption sites much more difficult reducing the D_1 and x_1 values.

Although there are no results available for the system SPES(S20)/Formic acid, the ones obtained using DMF and NMP showed on table 6.2 confirm the same tendency observed for the most sulphonated polymer (SPES(S5)).

6.1.3.3 - Sulphonation Level

The sulphonation level influence was investigated using S5 and S20 film samples using NMP as solvent. Unfortunately it was not possible to do the same study using different solvents for practical reasons. The formic acid, for example, does not dissolve the less sulphonated polymer (S20) while DMF although dissolves both polymers seems to damage the ZnSe prism especially when films are heated for solvent evaporation purposes.

Table 6.2 shows that when we reduce the sulphonation level, the diffusion coefficients (D_1 and D_2) are kept constant while the x_1 value is reduced. The D_1 value is an indication of how much fast the water molecules are being absorbed by the specific sites. Since the absorption sites are the same for both polymers and since they are in both cases surrounded by the same environment (because we are using the same solvent) the absorption process is supposed to be the same and that explains the similarity found on values of D_1. Because the only difference between the S5 and S20 polymer is on the sulphonation level, the values of D_2 are also supposed to be kept constant. Fig 6.16 compares S5 with S20 for increase on band intensity as a function of time. The curve shows a slower increase on band intensity for the less sulphonated polymer. It is important to kept in mind that the D_1 value is just an indication of how fast the water molecules will be immobilised and that for the diffusion coefficient as a whole we need also to consider the x_1 factor. Hence, although the D_1 value is the same for both polymers, because the x_1 is much smaller for S20, the "global" diffusion coefficient will

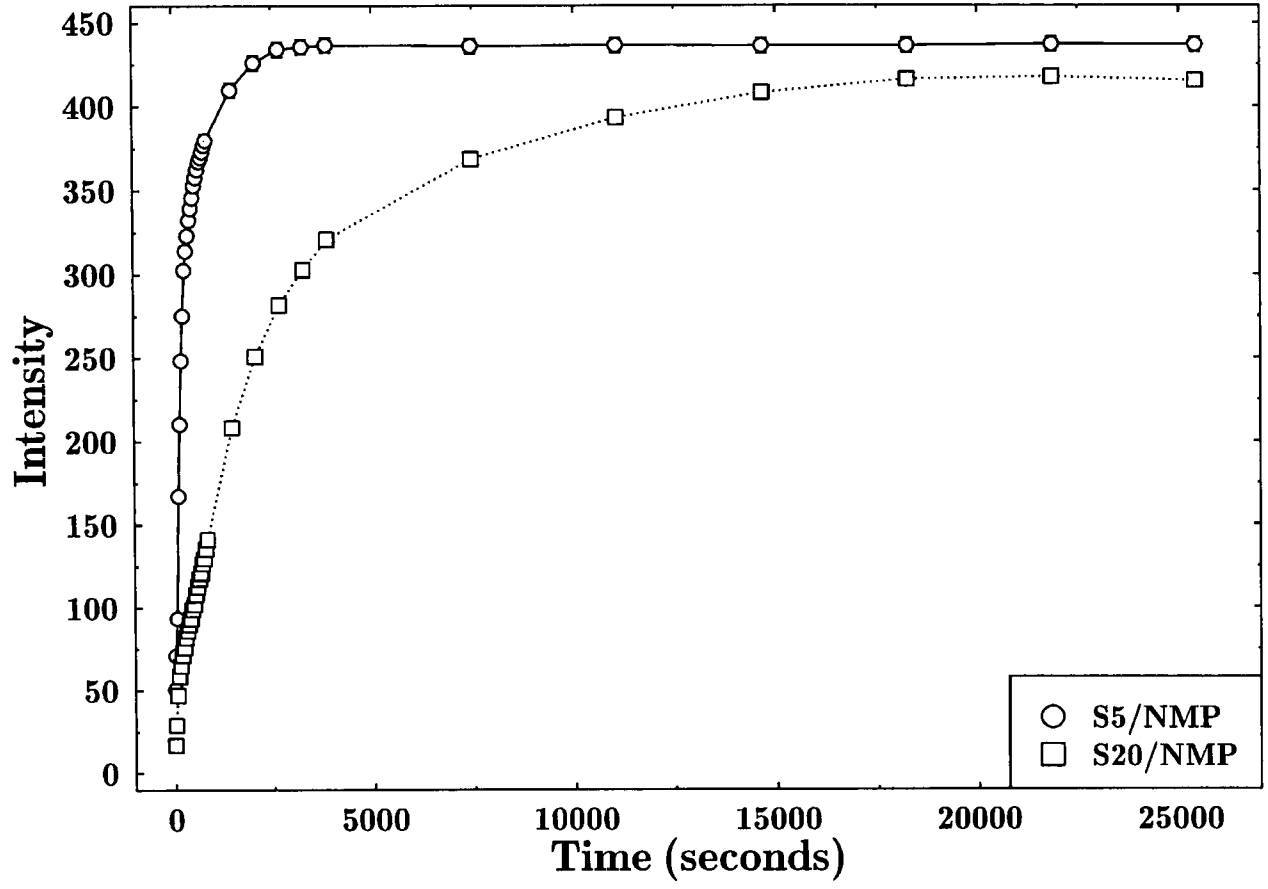

Fig. 6.16 - Results of water uptake for samples with different sulphonation levels.

be smaller for S20. This is confirmed when we calculate only one diffusion coefficient using Fick's law as showed on table 6.1. The value found using just one diffusion coefficient is, as expected, much close to the D_2 values than D_1 since the fraction of molecules partially immobilised for the S20 polymer is just 0.176. Finally, the reduction on x_1 value can be easily understood if we keep in mind that the number of absorption sites is reduced on S20 and therefore the fraction of molecules partially immobilised will also be reduced.

FINAL CONCLUSIONS AND FUTURE WORK

The main objective of this work was to use FTIR-ATR to study polymer/polymer and polymer/liquid interfaces.

Starting with the PMMA/PVOH laminate work we have demonstrated how different effective penetration depths can be achieved in very good agreement with the calculated electric field decay as a function of distance away from the substrate surface. The results show that the two-layered model system may be successfully employed to provide a semi-quantitative depth profile of the surface layer. This approach should be particularly interesting when working with laminate systems where the two layers are expected to have some interaction. In this case, some interfacial effects might be observed.

Following the polymer/polymer interfacial study, it was demonstrated how FTIR-ATR can also be used to study polymer/liquid interfaces. In this case polymeric membranes of sulphonated polyethersulphone were used and the main objective was to identify how the membrane structure can change, first as a function of the solvent used, but also as the hydration process occurs.

Because the sulphonate group is actively involved in the transport characteristics of the membranes, a detail monitoring of the symmetric and antisymmetric vibrational mode of the SO_3^- groups, as the degree of hydration was varied, were carried out by FTIR-ATR spectroscopy.

It was found that the symmetric mode of the SO_3^- group increases with hydration suggesting that, with hydration, the sulphonic acid groups of SPES are dissociated into SO_3^- ions. It was also found that the degree of hydration is also responsible for changes in the benzene ring vibrational band.

The antisymmetric stretching vibration of the SO_3^- group was not readily observable due to overlapping band in the same region. It was shown that, in this case, subtraction can be successfully employed to clearly define the band position.

The particular behaviour of ν(OH) of water was also analysed. The main conclusion in this case was that the average hydrogen bonding strength of the sorbed water is considerable lower than that in pure water. This fact may explains the efficient flux of water though the membrane.

The second part of the work with the sulphonated membranes was aimed at the analysis of the kinetics of sorption and the calculation of the diffusion coefficients of the membranes.

A method based on monitoring the time dependent changes in the ν(OH) vibrational mode of the water was developed. After reaching a steady state, the normalised absorbance plot versus time was used for numerical evaluation. Two models were proposed to describe the diffusion of water in the sulphonated membranes. The first describes the Fickian sorption and, the second the dual mode sorption (or case II). Both methods were transformed in Pascal programs and computer simulation was used to calculate the variability on the values of diffusion coefficient.

According to the experimental results, it was possible to conclude that the sulphonated membranes do not present a Fickian behaviour but a dual mode instead.

The values of diffusion coefficients were analysed as a function of three parameters: solvent used, film thickness and sulphonation level.

By using different solvents we confirmed the influence of the solvent on the structure of the polymer and hence on the diffusion coefficient. It was found that the most polar solvent interacts strongly with the ionic groups, weakening the intermolecular forces operating on the system and consequently, facilitating the water absorption. On the other hand, the less polar solvent promotes ion-pair interactions between the ionic dipoles. In this case, the water absorption becomes much more difficult.

The influence of the film thickness on the diffusion coefficient values was investigated for the system SPES(S5)/formic acid. It was found that thicker films present a higher diffusion coefficient. These results confirm the time dependent behaviour observed in polymers below their glass transition temperature[126].

The effects of sulphonation level were examined for the system SPES(S5) and SPES(20) using NMP and DMF as the solvent. It was found that although the values of D are kept constant, because the number of specific absorption sites is much smaller on the less sulphonated polymer, the water absorption will be slower in such polymer. This hypothesis was confirmed by comparing the values of x_a (portion of immobilised molecules) for both membranes. As it was showed that the value of x_a for SPES(S20) is much smaller than for SPES(S5).

There is an extensive literature demonstrating the effect of polymer structure on the diffusion process. In this work we have shown that the process can be reversed with information about the polymer structure being obtained by analysis of the diffusion process. With these results we demonstrate the potential use of transport phenomena in polymers to investigate polymer properties since these properties are sensitive to the molecular state and structure of the polymer and small morphological changes can cause large changes on the diffusion process.

Furthermore, because diffusion proceeds inwards from a polymer surface, the surface is the prime structural unit studied by the technique. Hence, diffusion analysis is expected to be an important tool for investigating the effect of processing on polymer surface structure.

In connection with future work on the same membranes it is suggested that the same kind of experiments could be performed using:

1) A sulphonated membrane with a sulphonation level in between 5 and 20.

2) The ionic form of the membrane (using Na^+, K^+, etc.) instead of the acid form.

3) Water at different pH and different temperatures.

Apart from this system, the approach described in this work can perfectly well used for an extensive number of other polymers, including ones which present Fickian behaviour.

BIBLIOGRAPHY

1. H.Ishida, Ed.; *Fourier Transform Infrared Characterisation of Polymers*, Vol. 36 Science and Technology - Plenum Press - N.Y. (1987).
2. L.D.Esposito, J.L.Koenig in *Fourier Transform Infrared Spectroscopy Applied to Chemical Systems*, J.R.Ferraro, L.J.Basile Eds., vol.1, Academic Press, N.Y. (1978).
3. P.R.Griffiths, J.A.de Haseth; *Fourier Transform Infrared Spectrometry*, John Wiley & Sons, N.Y. (1986).
4. J.L.Koenig; *8th International Conference on Fourier Transform Infrared Spectroscopy*, SPIE, vol 1575 (1991).
5. S.F.Johnston; *Fourier Transform Infrared - A constant evolving Technique*, Ellis Horwood , Sussex (1991).
6. J.M.Chalmers, M.W.Mackenzie in *Advances in Applied Fourier Transform Spectroscopy*, .W.Mackenzie Ed., John Wiley & Sons (1988).
7. B.Jasse in *Developments in Polymer Characterisation*-4, J.V.Dawkins Ed., Applied Science Publishers, London (1983).
8. S.C.Brown, A.B.Harrey in *Infrared and Raman Spectroscopy* -Part C, E.G.Brame, J.G.Grasselli Eds., Practical Spectroscopy Series, vol.1, Marcel Dekker, INC, N.Y., (1977).
9. D.I.Bower, W.F.Maddams Eds.; *The Vibrational Spectroscopy of Polymers*, Cambridge University Press, (1989).
10. G.Kortum; *Reflectance Spectroscopy*, Springer-Verlag, N.Y. (1964).
11. R.T.Graft, J.L.Koenig, H.Ishida; *J. Polym. Sci. and Techn.* 36, 1, (1987).
12. J.Fahrenfort; *Spectrochim. Acta.*, 698 (1968).
13. N.J.Harrick; *J. Phys. Chem.*, 69, 1110, (1960).
14. N.J.Harrick; *Internal Reflection Spectroscopy*, Harrick Scientific Corp., N.Y.(1967).
15. P.A.Wilkes Jr., T.Hirschfeld; *Appl. Spect. Review*, 1(1), 99, (1967).

16. F.M.Mirabella; *Appl. Spect. Reviews*, 21(1&2), 45, (1985).

17. F.M.Mirabella; *J.Pol.Sci., Polym Phys. Ed.*, 21, 2403, (1983).

18. F.Garbassi, E.Occhiello; *Anal. Chimica Acta*, 197, 1, (1987).

19. M.W.Urban; *Adv. Chem. Series*, 223, 295, (1989).

20. A.E.Tshel et all; *J. Macrom. Sci..Phys.* B(21), 243, (1982).

21. G.Gillberg; *J.Adhesion*, 21, 129, (1987).

22. J.L.Koenig; *Chemical Microstructure of Polymer Chains*, John Wiley & Sons, N.Y. (1980).

23. M.K.Antoon, L.D'Esposito, L.Koenig; *Appl. Spect.*, 33, 351, (1979).

24. R.G.Greener; *J. Chem. Phys.*, 44, 310, (1966).

25. B.G.M.Vandeginste, L.deGalan; *Anal. Chem.*, 47, 2124, (1975).

26. A.Goldman, P.Alon; *Appl. Spect.*, 27, 50, (1973).

27. W.F.Madams; *Appl. Spect.*, 34, 245, (1980).

28. M.M.Coleman, D.F.Varnell, J.P.Runt; *Pol. Sci. Techn.*, 20, 59, (1983).

29. D.A.Compton; J.R.Mooney, W.F.Madams; *Intern. Conf. On Fourier Transf. Infrared Spect.*, Paper 4.13, Durham, UK, (1983).

30. J.D.Andrade; *Surface and Interfacial Aspects of Biomedical Polymers*, vol. 1 Surface Chemistry and Physics, Plenum Press. N.Y. (1985).

31. H.L.Eager; *Structure and Properties of Ionomers*, Reidil, Dordrecht, (1987).

32. N.E.Schlotter, P.Y.Furlan; *Vibr. Spectr*, 3, 147, (1992).

33. G.Gill Bert; *Adhesion*, 21, 129, (1987).

34. E.Pluedamann, N.Collins; *Adh.Sci. and Tech.*, L.H.Ree Ed., Plenum, N.Y., (1975).

35. J.E.Fulghum, A.R.Chourasia; *Anal. Chem.*, 61,12, 243, (1989).

36. M.D.Porter; *Anal. Chem.*, 60(20), 1143, (1988).

37. F.Garbassi, E.Occhiello; *Anal. Chimia Acta*, 197, 1, (1987).

38. A.E.Tshmel, V.I.Vettegreen, V.M.Zolotarev; *J.Macrom. Sci.* B21(2), 243, (1982).

39. J.A.J.Jansen, J.H.van deer Maas, A.Posthuma de Boer; *Macromolecules*, 24, 4278, (1991).

40. I.M.Ward; *Adv. Pol. Sci*, 66, 81, (1985).

41. F.M.Mirabella Jr.; *J.Polym.Sci., Phys.Ed.*, 22, 1283 (1984).

42. J.W.Hong, J.B.Lando, J.L.Koenig; *Apll.Spectrosc.*, 45, 8, 1291 (1991).

43. C.S.Blackwell, P.J.Degen, F.D.Osterholtz; *Apll.Spectrosc.*, 32, 5, 480, (1978).

44. D.J.Carlsson, D.M.Wiles, *Macromol.*, 4, 173, (1971).

45. D.J.Carlsson, D.M.Wiles; *Macromol.*, 4, 179, (1971).

46. J.R.Webb, *J.Polym.Sci., Pol.Chem.Ed.;* 10, 2335, (1972).

47. D.J.Carlsson, D.M.Wiles; *Can.Chem.*, 48, 2397 (1970).

48. J.P.Hobbs, C.S.P.Sung, K.Krishnan, S.Hill; *Macromolecules.*,16, 193, (1983).

49. H.G.Tompkins; *Apll.Spectrosc.*, 28, 335, (1974).

50. F.M.Mirabella; *J.Pol.Sci., Pol.Phys.Ed.*, 21, 2403, (1983).

51. C.S.P.Sung, C.B.Hu, E.W.Merrill; *ACS Div.Pol.Chem., Pol.Prep.*, 19(1), 20, (1978).

52. C.S.P.Sung, C.B.Hu, E.W.Salzman; *J.Biomed.Mater.Res.*, 12, 791, (1978).

53. C.S.P.Sung, C.B.Hu; *Adv.Chem.Ser.*, 176, 69, (1979).

54. C.S.P.Sung, C.B.Hu; *ACS Div.Pol.Chem. Pol.Prepr,* 21,1, 156, (1980).

55. P.Groenveld; *J.Paint Technol.*, 43, 50.3, 561 (1971).

56. R.H.G.Brinkhius, A.J.Schouten; *Macromolecules., 24, 7,* 1487, (1991).

57. W. Klopffer; *Introduction to Polymer Spectroscopy,* Springer.Verlag, Germany, (1984).

58. L.J.Bellamy ; *The Infrared Spectra of Complex Molecules,* (1954)

59. J.Dybal, S.Krimm; *Macromolecules.*, 23, 1301, (1990).

60. S.Krimm, C.Y.Liang, G.B.B.Sutherland; *J.Pol.Sci.*, 22, 227, (1956).

61. H.Tadokoro et al.; *J.Pol.Sci.*,26, 1233 (1957).

62. P.Zschock, D.Quelemalz; *J.Membr.Sci.*, 22, 2.3, 325, (1985).

63. A.Warshawsky, O.Kedem; *J.Membr.Sci.*, 53, 37, (1990).

64. B.Kesler, G.Kovacs, A.Toth, I.Bertoti, M.Hegyi; *J.Membr.Sci.*,62, 2, 201, (1991).

65. B.Staude, L.Breitbach, *J.Appl.Polym.Sci.;* 43, 3, 559, (1991).

66. J.D.Andrade; Ed., *Polymer Surface Dynamics,* Plenum Press, N.Y. (1986).

67. R.E.Kesting; *Synthetic Polymeric Membranes. A Structural Perspective,* John Wiley & Sons, 2nd Edition (1985).

68. W.Pusch, A.Walch; *J.Membr.Sci.*, 10, 325, (1982).

69. A.Y.Tremblay, M.M.Dalcin; *Can.Jour.of Chem.Eng.*, 69, 6, 1348, (1991).

70. A.Jönsson, G.Trägårdh; *Chem.Eng.Proc.*, 27, 67, (1990).

71. S.Kimura; *Polym.J.*, 23, 5, 389, (1991).

72. S.Loeb, S.Sourirajan; *UCLA Eng.Report,* 60.60, (1960).

73. S.Sourirajan; *Eng.Chem.Fundam.*, 2(1), 51, (1963).

74. K.Lonsdale, U.Merten, R.Riley; *J.Appl.Polym.Sci.*, 6, 1341, (1965).

75. W.J.Koros, M.R.Coleman, D.R.B.Walker; *Ann.Rev.of Mater.Sci.*, 22, 47, (1992).

76. M.Lopez, B.Kipling, H.L.Yeager; *Anal.Chem.*, 48, 8, 1120, (1976).

77. R.A.Weiss, J.J.Fitzgerald; *J.Pol.Sci.Pol.Lett.*, 24, 6, 263, (1986).

78. M.Drzerwinski, W.J.Macknight; *J.Appl.Pol.Sci.*, 30, 12, 4753, (1985).

79. W.Koh, H.Silverman, K.Kem; *J.Electrochem.Soc.*, 130, 3, (1983).

80. G.Belfort; Ed. *Synthetic Membranes Process. Fundamental and Water Applications*, Academic Press, (1984).

81. A.Einsenberg, M.King; *Ions Containing Polymers. Physical Properties and Structure,* vol.2, Academic Press, (1977).

82. A.Einsenberg; Ed., *Ions in Polymers,* ACS Adv.Chem.Ser. 187, Washington DC (1980).

83. A.Einsenberg, M.Pineri; *Structure and Properties of Ionomers*, NATO ASI Series, vol.198, D.Reidel Publishing Company, Holland, (1986).

84. A.Einsenberg, F.E.Bailey; Eds. *Coulombic Interactions in Macromolecular Systems*, ACS Series, 302, (1986).

85. A.Einsenberg, B.Hird,R.B.Moore; *Macromolecules*, 23, 4098, (1990).

86. K.A.Mauritz,C.J.Hora, A.J.Hopfinger; *Pol.Prepr. ACS div.Pol.Chem.*, 19(2), 324, (1978).

87. W.J.Macknight, T.R.Earnest Jr.; *J.Pol.Sci.Macromol.Rev.*, 16, 41, (1981).

88. R.S.Yeo; *J.Electrochem.Soc.*, 130, 3, 533, (1983).

89. N.Sivashisky, G.B.Tanny; *J.Appl.Pol.Sci.*, 28, 10, 3235, (1983).

90. J.A.Lefelar, R.A.Weiss; *Macromolecules*, 17, 6, 1145, (1984).

91. A.F.Galambos, J.Koberstein, T.P.Russel; *Abs.Pap.ACS*, 195, 223, (1988).

92. C.Li, R.A.Register, S.L.Cooper; *Polymer*, 30, 7, 1227, (1989).

93. M.Coleman, J.Y.Lee, P.Painter; *Macromolecules*, 23, 2339, (1990).

94. M.Hara, P.Jar, J.A.Sarier; *Polymer*, 32, 8, 1380, (1991).

95. S.A.Visser, S.L.Cooper; *Polymer*, 35, 5, 920, (1992).

96. H.Keling, H.L.Williams; *J.Appl.Pol.Sci.*, 42, 1845, (1991).

97. H.Frank, W.Wen; *Dis.Far.Soc.*, 24, 133, (1957).

98. C.Toprak, J.N.Agar, M.Falk; *J.Chem.Soc.Far.Trans.I*, 14, 803, (1979).

99. W.A.P.Luck, D.Schioberg, U.Siemam; *J.Chem.Soc.Far.Trans.II*, 76, 136, (1980).

100. S.Quezado, J.C.T.KWak, M.Falk; *Can.J.of Chem.*, 62, 958, (1984).

101. M.Schlenkrich, K.Nicklas, J.Brickmann, P.Bopp; *Ber Bursenges Phy.Chem.*, 94, 133, (1990).

102. F.Frank; Ed., *Water Science Rev.3.Water Dynamics*, Cambridge Univ. Press, (1988).

103. H.Berendsen, C.Migchelsen; *Ann. N.Y. Acad. Sci.*, 25(2), 365, (1965).

104. A.Bunn, J.B.Rose; *Polymer*, 34, 5, 1114, (1993).

105. M.Falk, *Can.J.Chem.*; 58, 1495, (1980).

106. S.R.Lowry, K.A.Mauritz; *J.Amer.Chem.Soc.*, 102, 4665, (1980).

107. D.G.Peiffer, K.D.Ludeberg; *J.Pol.Sci..B*, 23, 9, 1869 (1985).

108. M.Fontyn, B.H.Bisjsterbosch; *J.Membr.Sci.*, 36, 141, (1987).

109. J.Ostrowbkaczubenko, B.Ostrowskagumkowska; *Eur.Pol.J.*, 24, 1, 65, (1985).

110. M.Oldani, G.Schock; *J.Membr.Sci.*, 43, 243, (1989).

111. W.Kujawski, J.Null; *J.Appl.Pol.Sci.*, 44, 951, (1992).

112. G.Zundel; *Hydration and Intermolecular Interaction*, Academic Press, N.Y., (1969).

113. L.J.Bellamy, L.Beecher; *J.Chem.Soc.*(London), 728 (1953).

114. M.Falk, P.A.Giguere; *Can.J.Chem.*, 36, 1680, (1958).

115. R.W.Lovejoy, E.L.Wagner, *J.Phys.Chem.*, 68, 544, (1964).

116. R.Blinc, D.Hadzi; *Mol.Phys.*, 1, 391, (1958).

117. page 360 on ref.83

118. D.L.Hansen, *Sprouse Collection of Infrared Spectra-Book I - Polymers*; Sprouse Scientific Systems, Inc, Pennsylvania, 1987.

119. B.C.Johnson, J.E.McGrath; *J.Pol.Sci.Pol.Chem.*, 22, 3, 721, (1984).

120. E.E.Boakye, H.L.Yeager; *J.Membr.Sci*, 69, 1.2, 155, (1992)

121. W.A.P.Luck; Chapter 2 in *Synthetic Membrane Process*, G.Belfort Ed., Academic Press, N.Y. (1984).

122. G.B.Van den Berg, C.A.Smolders; *J.Memb.Sci.* 73, 103, (1992).

123. J.S.Ventras, C.M.Ventras; *J.Pol.Sci.*, part B, 30, 9, 1005, (1992).

124. M.Best, J.W.Halley, B.Johnson, J.L.Valles; *J.Appl.Pol.Sci*, 48, 2, 319, (1993).

125. S.R.Lustig, J.G.VanAlslen, B.Hsiao; *Macromolecules.*, 26, 3885, (1993).

126. N.E.Shlotter, P.Y.Furlan; *Polymer*, 33, 16, 3323, (1992).

127. J.Comyn; "*Polymer Permeability*", Elsevier Applied Sci. Publishers Ltd, (1985).

128. Tim deV. Naylor in "*Comprehensive Polymer Science*", ed. G.Allen and J.C.Bevington; Pergamon Press, Oxford, (1980), vol. 2, chap. 20.

129. T.Shibusawa, Y,Chigira; *J. Polym. Sci.* Part.B, 30, 5, 563, (1992).

130. Y.Chen, T.Miyano, A.Found, T.Matsuura; *J.Memb.Sci.*, 48, 203, (1990).

131. H.Odani, T.Uyeda; *Polymer Journal*, 23, 5, 445, (1991).

132. I.Blume, E.Smith, M.Wessling, C.A.Smolders; *Makromoleculare Chemie . Macromolecular Symposia*, 45, May, 237, (1991).

133. C.K.Hayes, D.S.Cohen; *J. Polym. Sci.* Part B, 30, 2, 145, (1992).

134. R.W.Korsmeyer, S.R.Lustig, N.A.Peppas; *J. Pol. Sci.*, 24, 2, 395, (1986).

135. S.R.Lustig, N.A.Peppas; *J. Appl. Polym. Sci.*, 33, 2, 533, (1988).

136. T.Alfrey, E.F.Gurnee, W.G.Lloyd; *J. Polym. Sci.* Part C, 12, 249, (1966).

137. M.Senoume, J.Bouzon, J.M.Vergnaud; *J.Pol.Eng.*, 9, 3, 213, (1990).

138. S.B.Harogoppad, T.M.Aminabhavi; *J.Appl.Pol.Sci.*, 44, 10, 1687, (1992).

139. A.Bakhowya, A.Elbrouzi, J.Bouzon; *Eur.Pol.J.*, 28, 7, 809, (1992).

140. H.M.L.Huy, X.Huang, J.Rault; *Polymer*, 34, 2, 340, (1993).

141. W.Vieth, Mary Amini; *ACS.Div. Org. Coat. Plast. Chem. Pap.*, 34, 1, 442, 1974.

142. W.J.Koros, D.R.Paul; *J. Polym.Sci.* Part B, 14, 687, 1976.

143. W.J.Koros, D.R.Paul; *J. Polym. Sci.* Part B, 14, 1903, 1976.

144. J.H.Petropoulos; *J. Polym. Sci.*, A.2, 8, 1797, 1980.

145. W.R.Vieth, M.A.Amini; *Soc. Plast. Eng. Techn. Pap.* 22, 6, 1976.

146. H.B. Hopfenberg, V.Stannett, C.M.M.Jacques; *J. Appl. Polym. Sci.*, 19, 2439, 1975.

147. J.Crank; *Mathematics of Diffusion*, 2nd Ed., Oxford University Press, 1956.

148. J.Crank, G.S.Park Eds.; *Diffusion in Polymers*, Academic Press, (1968).

149. S.Kalachandra, D.T.Turner; *Polymer*, 28, 1749, (1987).

150. D.T.Turner, A.K.Abell; *Polymer*, 28, 297, (1987).

151. C.K.Rhee, J.D.Ferry; *J.Appl. Polym. Sci.*, 21, 773, (1977).

152. G.S.Park, T.V.Hoang; *Eur. Polym. J.*, 15, 817, (1979).

153. C.Y.Hui, K.C.Wu, R.C.Lasky, J.Kramer; *Appl. Physics*, 61, 5137, (1987).

154. J.Klier, N.A.Peppas; *Polymer Bull.*, 16, 359, (1986).

155. J.Manjkow, J.S.Papanu, D.S.Soong, D.W.Hess, A.T.Bell; *J. Appl.Phys.*, 62, 682, (1987).

156. H.M.Tong, K.L.Saenger, C.J.Durning; *J. Polym. Sci.* Part B, 27, 689, (1989).

157. C.A.Pawlisch, A.Macris, R.L.Laurence; *Macromolecules.*,20, 1564, (1987).

158. N.L.Thomas, A.H.Windle; *Polymer*, 18, 1195, (1977).

159. N.L.Thomas, A.H.Windle; *Polymer*, 19, 255, (1978).

160. N.L.Thomas, A.H.Windle; *Polymer*, 22, 627, (1981).

161. R.W.Korsmeyer, Von E.Mierwall, N.A.Peppas; *J. Polym. Sci.* Part B, 24, 409, (1986).

162. W.H.Press, B.P.Flannery, S.A.Teukosky, W.T.Vetterling; *Numerical Recipes in Pascal,* Cambridge University Press, (1990).

163. B.T.Swinyard, P.S.Sagoo, J.A.Barrie; *J.Appl.Pol.Sci.*, 1, 9, 2479, (1990).

164. S.J.Yakowitz; *Computational Probability and Simulation*, Addison.Wesley Publishing Company, Massachusetts, (1977).

165. R.Y.Rubstein; *Simulation and the Monte Carlo Method*, John Wiley & Sons, NY (1981).

166. D.B.Ripley; *Stochastic Simulation*, John Wiley & Sons, NY, (1987).

167. J.M.Hammersley, D.C.Handscomb; *Monte Carlo Methods*, Methuen & Co Ltd., NY, (1964).

168. W.Bruns, I.Motoc, O'Driscoll; *Monte Carlo Applications in Polymer Science*, Springer.Verlag.Berlin Heidelberg, (1981).

169. D.E.Khuth; *Seminumerical Algorithms*, 2nd Ed., Vol.2 in *The Art of Computer Programming*, Addison.Wesley Publishing Company . Reading, Massachusetts, (1981).

170. J.L.Kroschwitz Ed., *Concise Encyclopedia of Polymer Science and Engineering*, page 684, John Wiley &Sons, N.Y. (1990).

171. N.F.Fell, P.W.Bohn; *Appl. Spectroscopy*, 45,7,1085, (1991).

172. A.R.Berens; *J.Appl.Pol.Sci.*, 37, 901, (1989).

173. R.D.Lundberg, R.R.Phillips; *J.Pol.Sci., Part-B*, 20, 1143, (1982).

APPENDIX ONE

Calculation of the Standard Deviation Distribution

Let us suppose that y is a property calculated from the properties x_1, x_2, x_3,.....x_n. In other words:

$$y = f(x_1, x_2, x_3, ... x_n) \qquad \text{(eq. A1.1)}$$

This would imply that:

$$dy = \sum_{i=1}^{n} \frac{\partial y}{\partial x_i} dx_i \qquad \text{(eq. A1.2)}$$

Assuming that variations in $\left(\frac{\partial y}{\partial x_i}\right)$ are small for small variations in x_i (the partial derivatives can be considered constant) and the integration of eq. A1.2 yields:

$$\Delta y \approx \sum_{i=1}^{n} \frac{\partial y}{\partial x_i} (\Delta x_i) \qquad \text{(eq. A1.3)}$$

Expression A1.3 can be used as a form of calculation of the error propagation. Since the Δx_i errors (that can be negative or positive) do not have any relation of dependence between themselves, one can write:

$$\Delta y \approx \sum_{i=1}^{n} \left| \frac{\partial y}{\partial x_i} \right| (\Delta x_i) \qquad \text{(eq. A1.4)}$$

Where Δy is the propagated experimental error and Δx_i are the experimental errors related to the quantities used to calculate y.

For the specific case $Y_{(i)} = \frac{A_\infty - A_{(i)}}{A_\infty - A_0}$ we have:

$$\frac{\partial Y_{(i)}}{\partial A_{(i)}} = \frac{-1}{A_\infty - A_0} \qquad \text{(eq. A1.5)}$$

$$\frac{\partial Y_{(i)}}{\partial A_\infty} = \frac{(A_\infty - A_0) - (A_\infty - A_{(i)})}{(A_\infty - A_0)^2} = \frac{A_{(i)} - A_0}{(A_\infty - A_0)^2} = \frac{1 - Y_{(i)}}{A_\infty - A_0} \qquad \text{(eq. A1.6)}$$

$$\frac{\partial Y_{(i)}}{\partial A_0} = \frac{A_\infty - A_{(i)}}{(A_\infty - A_0)^2} = \frac{Y_{(i)}}{A_\infty - A_0} \qquad \text{(eq. A1.7)}$$

Finally, substitution of eq. A1.5, A1.6 and A1.7 in eq. A1.4 yields:

$$\Delta Y_i \approx \frac{\Delta A_{(i)} + \Delta A_\infty + Y_i(\Delta A_0 - \Delta A_\infty)}{A_\infty - A_0} \qquad \text{(eq. A1.8)}$$

APPENDIX TWO

Levenberg-Marquardt Method

Suppose χ^2 is the merit function of a given linearisation, dependent on the value of a given parameter a. If sufficiently close to the minimum, one expects the χ^2 function to be well approximated by a quadratic form, which can be written as

$$\chi^2(a) = w_0 - w_1 a + \frac{1}{2} w_2 a^2 \qquad \text{(eq. A2.1)}$$

If one considers when the model depends nonlinearly on the set of M unknown parameters a_k, $k = 1,2,3, \ldots, M$ (defined as the vector **a**), the same approach can be used:

$$\chi^2(\mathbf{a}) = \gamma - \mathbf{d} \cdot \mathbf{a} + \frac{1}{2} \mathbf{a} \cdot \mathbf{R} \cdot \mathbf{a} \qquad \text{(eq. A2.2)}$$

where **d** is an M-vector and **R** is a $M \times M$ matrix. If the approximation is a good one, one can jump from the current trial parameters $\mathbf{a}_{cur}$ to the minimising ones $\mathbf{a}_{min}$ in a single step, namely

$$\mathbf{a}_{min} = \mathbf{a}_{cur} + R^{-1} \cdot \left[-\nabla \chi^2(\mathbf{a}_{cur}) \right] \qquad \text{(eq. A2.3)}$$

On the other hand, (eq. A2.3) might be a poor local approximation to the shape of the function at $\mathbf{a}_{cur}$. In that case:

$$\mathbf{a}_{next} = \mathbf{a}_{cur} - \text{constant} \times \nabla \chi^2(\mathbf{a}_{cur}) \qquad \text{(eq. A2.4)}$$

where the constant is small enough not to exhaust the downhill direction.

Recalling that the model to be fitted is

$$Y = y(t; \mathbf{a}) \qquad \text{(eq. A2.5)}$$

and the χ^2 merit function is

$$\chi^2 = \sum_{i=1}^{n} \left[\frac{Y_i - Y_i(t_i; \mathbf{a})}{\Delta Y_i} \right]^2 \qquad \text{(eq. A2.6)}$$

The gradient of χ^2 with respect to the parameters **a**, which will be zero at the χ^2 minimum, has components

$$\frac{\partial \chi^2}{\partial a_k} = -2 \sum_{i=1}^{n} \frac{[Y_i - Y(t_i; \mathbf{a})]}{\Delta Y_i^2} \frac{\partial Y(t_i; \mathbf{a})}{\partial a_k} \qquad k = 1, 2, 3, \ldots, M \qquad \text{(eq. A2.7)}$$

Taking an additional partial derivative gives:

$$\frac{\partial^2 \chi^2}{\partial a_k \partial a_l} = 2 \sum_{i=1}^{n} \frac{1}{\Delta Y_i^2} \left[\frac{\partial Y(t_i; \mathbf{a})}{\partial a_k} \frac{\partial Y(t_i; \mathbf{a})}{\partial a_l} - [Y_i - Y(t_i; \mathbf{a})] \frac{\partial^2 Y(t_i; \mathbf{a})}{\partial a_l \partial a_k} \right] \qquad \text{(eq. A2.8)}$$

It is conventional to remove the factors of 2 by defining

$$\eta_k \equiv -\frac{1}{2} \frac{\partial \chi^2}{\partial a_k} \qquad \text{and} \qquad \mu_{kl} \equiv \frac{1}{2} \frac{\partial^2 \chi^2}{\partial a_k \partial a_l} \qquad \text{(eq. A2.9)}$$

Equation (eq. A2.3) can be rewritten as the set of linear equations

$$\sum_{l=1}^{M} \mu_{kl} \delta a_l = \eta_k \qquad \text{(eq. A2.10)}$$

This set is solved for the increments δa_l that, added to the current approximation, give the next approximation.

Equation (eq. A2.4) translates to

$$\delta a_l = Q_l \times \eta_l \qquad \text{(eq. A2.11)}$$

where Q_l is a constant.

Inclusion of the second-derivative term can in fact be destabilising if the model fits badly or is contaminated by outlier points that are unlikely to be offset by compensating points of opposite sign. This problem is overcome by re-defining μ_{kl} as

$$\mu_{kl} = \sum_{i=1}^{n} \frac{1}{\Delta Y_i^2} \left[\frac{\partial Y(t_i;\mathbf{a})}{\partial a_k} \frac{\partial Y(t_i;\mathbf{a})}{\partial a_l} \right] \qquad \text{(eq. A2.12)}$$

The quantity χ^2 is nondimensional. On the other hand, η_k has the dimensions of $1/a_k$, which may well be dimensional. The constant Q_l in (eq. A2.11) must therefore have the dimensions of a_k^2. There is only one obvious quantity with these dimensions, and that is $Q_l = 1/\mu_{kk}$. So that must set the scale of the constant. But that scale might itself be too big. That can be overcome if one divides the constant by a (nondimensional) factor λ, with the possibility of setting $\lambda >> 1$ to cut down the step. In other words, replace equation (eq. A2.11) by

$$\delta a_l = \frac{1}{\lambda \mu_{ll}} \eta_l \qquad \text{or} \qquad \lambda \mu_{ll} \delta a_l = \eta_l \qquad \text{(eq. A2.13)}$$

If one defines a new matrix μ' by the following prescription

$$\mu'_{jj} \equiv \mu_{jj}(1 + \lambda) \qquad \text{(eq. A2.14a)}$$

$$\mu'_{jk} \equiv \mu_{jk} \qquad (j \neq k) \qquad \text{(eq. A2.14b)}$$

and then replaces both (eq.A2.13) and (eq.A2.10) by:

$$\sum_{l=1}^{M} \mu'_{kl}\, \delta a_l = \eta_k \qquad \text{(eq. A2.15)}$$

When λ is very large, the matrix μ' is forced into being diagonally dominant, so equation (eq. A2.15) goes over to be identical to (eq.A2.13). On the other hand, as λ approaches zero, equation (eq. A2.15) goes over to (eq.A2.10).

Given an initial guess for the set of fitted parameters a, the recommended Marquardt recipe is as it follows:

Table A2.I (Marquardt Algorithm)

1	Compute $\chi^2(a)$;
2	Pick a modest value for λ, say $\lambda = 0.001$;
3	Solve the linear equations (LM.15) for $\delta\mathbf{a}$ and evaluate $\chi^2(\mathbf{a} + \delta\mathbf{a})$;
4	If $\chi^2(\mathbf{a} + \delta\mathbf{a}) \geq \chi^2(\mathbf{a})$, increase λ by a factor of 10 (or any other substantial factor), and go back to 3;
5	If $\chi^2(\mathbf{a} + \delta\mathbf{a}) < \chi^2(\mathbf{a})$, decrease λ by a factor of 10, update the trial solution $\mathbf{a} \leftarrow \mathbf{a} + \delta\mathbf{a}$, and go back to 3.

In the specific case of the minimisation of the function related to the diffusion process, we have:

$$Y_i = \beta(x\Sigma_{1_i} + (1-x)\Sigma_{1b_i}) \qquad \text{(eq. A2.15)}$$

where

$$\Sigma_{1_i} = \sum_{j=0}^{\infty} \frac{\alpha k_j + (-1)^j 2/d_p}{(2j+1)\left(k_j^{\,2} + 4/d_p^{\,2}\right)} e^{-k_j^{\,2} D t_i} \qquad \text{(eq. A2.16)}$$

$$\Sigma_{1b_i} = \sum_{j=0}^{\infty} \frac{\alpha k_j + (-1)^j 2/d_p}{(2j+1)\left(k_j^{\,2} + 4/d_p^{\,2}\right)} e^{-k_j^{\,2} k_d D t_i} \qquad \text{(eq.A2.17)}$$

So that for this particular case we have:

$$M = 3,\ a_1 \equiv \mathrm{D},\ a_2 \equiv k_d, \text{ and } a_3 \equiv x \qquad \text{(eq. A2.18)}$$

Step 1 of table (eq. A2.1) would then be executed by substituting (eq. A2.15-eq. A2.17) in (eq. A2.6).

Eq. (eq. A2.9-eq.A2.15) are calculated through

$$\mu_{11} = \frac{1}{2}\sum_{i=1}^{n}\frac{p_i^2}{\Delta Y_i^2} \qquad \mu_{12} = \mu_{21} = \sum_{i=1}^{n}\frac{p_i \times q_i}{\Delta Y_i^2} \qquad \mu_{13} = \mu_{31} = \sum_{i=1}^{n}\frac{p_i \times s_i}{\Delta Y_i^2}$$

$$\mu_{22} = \sum_{i=1}^{n}\frac{q_i^2}{\Delta Y_i^2} \qquad \mu_{23} = \mu_{32} = \sum_{i=1}^{n}\frac{q_i \times s_i}{\Delta Y_i^2} \qquad \text{(eq. A2.19)}$$

$$\mu_{33} = \sum_{i=1}^{n}\frac{s_i^2}{\Delta Y_i^2}$$

$$\eta_1 = \sum_{i=1}^{n}\Pi_i \times p_i \qquad \eta_2 = \sum_{i=1}^{n}\Pi_i \times q_i \qquad \eta_3 = \sum_{i=1}^{n}\Pi_i \times s_i \qquad \text{(eq. A2.20)}$$

where

$$p_i \equiv \frac{\partial Y(t_i;\mathbf{a})}{\partial a_1} = \beta(x\Sigma_{2_i} + k_d(1-x)\Sigma_{2b_i})$$

$$q_i \equiv \frac{\partial Y(t_i;\mathbf{a})}{\partial a_2} = \beta D(1-x_a)\Sigma_{2b_i} \qquad \text{(eq. A2.21)}$$

$$s_i \equiv \frac{\partial Y(t_i;\mathbf{a})}{\partial a_3} = \beta(\Sigma_{1_i} - \Sigma_{1b_i})$$

$$\Sigma_{2_i} = -t_i\sum_{j=0}^{\infty}k_j{}^2\frac{(-1)^j}{2j+1}\frac{(-1)^j\alpha k_j + 2/d_p}{k_j{}^2 + 4/d_p{}^2}e^{-k_j{}^2 Dt_i}$$

$$\Sigma_{2b_i} = -t_i\sum_{j=0}^{\infty}k_j{}^2\frac{(-1)^j}{2j+1}\frac{(-1)^j\alpha k_j + 2/d_p}{k_j{}^2 + 4/d_p{}^2}e^{-k_j{}^2 k_d Dt_i} \qquad \text{(eq. A2.22)}$$

$$\Pi_i \equiv \frac{Y_i - Y(t_i)}{\Delta Y_i^2} \qquad \text{(eq. A2.23)}$$

Step 3 is carried out through the evaluation of the increments δD, δK and δX from (eq.A2.24):

$$\begin{bmatrix} \lambda \times \mu_{11} & \mu_{12} & \mu_{13} \\ \mu_{21} & \lambda \times \mu_{22} & \mu_{23} \\ \mu_{31} & \mu_{32} & \lambda \times \mu_{33} \end{bmatrix} \bullet \begin{bmatrix} \delta D \\ \delta k_d \\ \delta x_a \end{bmatrix} = \begin{bmatrix} \eta_1 \\ \eta_2 \\ \eta_3 \end{bmatrix} \qquad \text{(eq. A2.24)}$$

Steps 4 or 5 are executed.

The algorithm is repeated until the relative variation of $\chi 2$ is smaller than 0.001 % or the relative variations on the parameters are smaller than 1×10^{-8} %.

APPENDIX THREE

Pascal Programs

Program one - Fickian Diffusion/Thick Films

```
program Diffusion {Version 1.0: Thick Films};
const
  Maximum_Error = 1e-10;
  Pi = 3.14159265358979323846;
  Ln_10 = ln(10);
var
  As, Abs_Err, Alpha, Beta, L, Dp, D, Derivative: double;
  Sum_1, Sum_2, Sum_3, Best_D: double;
  Residue, Old_L,Old_Dp, Old_As, Maximum_D, Minimum_D: double;
  DfDl, L_Error, Dp_Error, T_Error, Error: double;
  N, I, J: integer;
  Random_Array: array[1..100] of double;
  T, Y, Y_Error, Estimated_Y, Absorbance: array[0..200] of double;
  Old_Absorbance, Old_T, Absorbance_Error: array[0..200] of double;
  Data_File, Output_File, Results, Answer, Last_Answer: string;
  Data: text;
  First_Random_Number, Absorbance_Varies, Initialised: boolean;

procedure Read_and_Calculate_Parameters;
begin
  N := -1;
  writeln;
  write('Data in file: ');
  readln(Data_File);
  reset(Data, Data_File);
  repeat
    N := N + 1;
    readln(Data, T[N], Absorbance[N]);
  until eof(Data) or (T[N] < 0);
  close(Data);
  if (T[N] <= 0) then N := N -1;
  writeln;
  write('Absorbance at equilibrium: ');
  readln(As);
  writeln;
  write('Error in absorbance (%): ');
  readln(Abs_Err);
  for I := 0 to N do Absorbance_Error[I] := Abs_Err * Absorbance[I] / 100;
  writeln;
  write('Film thickness (L, in microns): ');
  readln(L);
  writeln;
  write('Depth of penetration (Dp, in microns): ');
  readln(Dp);
  writeln;
  write('Initial guess for the diffusion coefficient (D, in cm^2/sec): ');
  readln(D);
  D := D * 1e8;
end;

procedure Calculate_Sums(X: double);
```

```
const
  Sum_Maximum_Error = exp(- 300);
var
  J: integer;
  Sign: integer;
  Kj, Term_1, Term_2, Term_3, Error_1, Error_2, Factor: double;
  Old_Sum_1, Old_Sum_2, Old_Sum_3, Sign_1: double;
  Power_1, Power_2, Power_3, Error_3: double;
begin
  J := -1;
  Sum_1 := 0;
  Sum_2 := 0;
  Sum_3 := 0;
  repeat
    Old_Sum_1 := Sum_1;
    Old_Sum_2 := Sum_2;
    Old_Sum_3 := Sum_3;
    J := J + 1;
    Factor := trunc(J / 2) - J / 2;
    if (Factor = 0) then Sign := 1 else Sign := -1;
    Kj := Pi * (2 * J + 1) / (2 * L);
    Sign_1 := Alpha * Kj + Sign * 2 / Dp;
    Power_1 := - sqr(Kj) * D * X + ln(abs(Sign_1)) - ln(sqr(Kj) +
      4 / sqr(Dp)) - ln(2 * J + 1);
    Sign_1 := Sign_1 / abs(Sign_1);
    Power_2 := Power_1 + 2 * ln(Kj) + ln(X);
    Power_3 := Power_2 + 2 * ln(Kj) + ln(X);
    if (Power_1 >= - 300) then Term_1 := Sign_1 * exp(Power_1)
    else Term_1 := 0;
    if (Power_2 >= - 300) then Term_2 := - Sign_1 * exp(Power_2)
    else Term_2 := 0;
    if (Power_3 >= - 300) then Term_3 := Sign_1 * exp(Power_3)
    else Term_3 := 0;
    Sum_1 := Sum_1 + Term_1;
    Sum_2 := Sum_2 + Term_2;
    Sum_3 := Sum_3 + Term_3;
    Error_1 := abs(Sum_1 - Old_Sum_1) * Beta;
    Error_2 := abs(Sum_2 - Old_Sum_2) * Beta;
    Error_3 := abs(Sum_3 - Old_Sum_3) * Beta;
  until (Error_1 <= Sum_Maximum_Error)
    and (Error_2 <= Sum_Maximum_Error) and (Error_3 <= Sum_Maximum_Error);
  Sum_1 := Beta * Sum_1;
  Sum_2 := Beta * Sum_2;
  Sum_3 := Beta * Sum_3
end;

function Random_Number: double;
var
  Temp: double;
  Cell, x: integer;
begin
  if First_Random_Number then begin
    First_Random_Number := FALSE;
    x := seed(wallclock);
    for Cell := 1 to 100 do Random_Array[Cell] := random(x)
  end;
  repeat Cell :=  trunc(101 * random(x)) until (Cell >= 1) or (Cell <= 100);
  Temp := Random_Array[Cell];
  Random_Array[Cell] := random(x);
  Random_Number := Temp
end;
```

```
procedure Calculate_D;
const
  D_Maximum_Error = 1.0e-10;
var
  DfDd, Delta_Y, Delta_1, Delta_2, Next_D: double;
  Error_1, Error_2, Old_D: double;
  Inc_Max, Inc_Min, Q: integer;
  Newton_Raphson_Iterated: boolean;
  No_Maximum_D: boolean;
begin
  Inc_Max := 0;
  Inc_Min := 0;
  Residue := 0;
  Old_D := D;
  No_Maximum_D := TRUE;
  Minimum_D := 0;
  if not Initialised then begin
    Alpha := exp(- 2 * L / Dp);
    Beta := 8 / (Pi * Dp * (1 - Alpha));
    for Q := 1 to N do begin
      Y[Q] := (As - Absorbance[Q]) / (As - Absorbance[0]);
      Delta_1 := Absorbance_Error[0] + Absorbance_Error[Q];
      Delta_2 := Absorbance_Error[0] + As * Abs_Err / 100;
      Y_Error[Q] := (Delta_1 + Delta_2 * Y[Q]) / (As - Absorbance[0])
    end;
    Initialised := TRUE
  end;
  repeat
    Newton_Raphson_Iterated := TRUE;
    Derivative := 0;
    DfDd := 0;
    Residue := 0;
    if (D <= Minimum_D) or (not No_Maximum_D and
      (D >= Maximum_D)) then DfDd := 0
    else for I := 1 to N do begin
        Calculate_Sums(T[I]);
        Estimated_Y[I] := Sum_1;
        Delta_Y := Y[I] - Estimated_Y[I];
        Derivative := Derivative + Delta_Y * Sum_2 / sqr(Y_Error[I]);
        DfDd := DfDd + (Delta_Y * Sum_3 - sqr(Sum_2)) / sqr(Y_Error[I]);
        Residue := Residue + sqr(Delta_Y / Y_Error[I])
    end;
    if (DfDd = 0) then begin
      Newton_Raphson_Iterated := FALSE;
      if (D <= Minimum_D) then begin
        Minimum_D := Old_D;
        Next_D := 1.1 * Old_D * exp(Inc_Min * Ln_10);
        Inc_Min := Inc_Min + 1;
        Inc_Max := 0
      end
      else begin
        Maximum_D := Old_D;
        No_Maximum_D := FALSE;
        Next_D := 0.9 * Old_D * exp(- Inc_Max * Ln_10);
        Inc_Max := Inc_Max + 1;
        Inc_Min := 0
      end;
      Old_D := Next_D
    end
    else begin
      Next_D := D - Derivative / DfDd;
      Error_1 := abs((D - Next_D) / D);
```

```
    Error_2 := abs((D - Next_D) / Next_D)
   end;
   D := Next_D;
  until Newton_Raphson_Iterated and (Error_1 <= D_Maximum_Error)
   and (Error_2 <= D_Maximum_Error)
end;

procedure Randomize_Data;
var
  Q: integer;
begin
  if L_Error <> 0 then begin
   Old_L := L;
   L := L * (1 + L_Error * (2 * Random_Number - 1) / 100)
  end;
  if Dp_Error <> 0 then begin
   Old_Dp := Dp;
   Dp := Dp * (1 + Dp_Error * (2 * Random_Number - 1) / 100)
  end;
  if T_Error <> 0 then for Q := 1 to N do begin
   Old_T[Q] := T[Q];
   T[Q] := T[Q] + T_Error * (2 * Random_Number - 1)
  end;
  if Absorbance_Varies then begin
   Old_As := As;
   As := As * (1 + Abs_Err * (2 * Random_Number - 1) / 100);
   for Q := 0 to N do begin
    Old_Absorbance[Q] := Absorbance[Q];
    Absorbance[Q] := Absorbance[Q] +
     Absorbance_Error[Q] * (2 * Random_Number - 1)
   end
  end
end;

procedure Monte_Carlo_Simulate;
var
  Real_D: double;
  Experiments, Row, Sub_Row: integer;
  Answer_2: string;
  Calculated_D, Average_D, Deviation_D: array[1..1000] of double;
begin
  writeln;
  write('Results in file: ');
  readln(Results);
  rewrite(Data, Results);
  writeln;
  write('Number of "experiments" (maximum number: 1000): ');
  readln(Experiments);
  writeln;
  repeat
   write('Do you want variations in absorbance to be considered (y/n)? ');
   readln(Answer_2)
  until (Answer_2 = 'y') or (Answer_2 = 'Y') or (Answer_2 = 'n') or
   (Answer_2 = 'N');
  if (Answer_2 = 'Y') or (Answer_2 = 'y') then Absorbance_Varies := TRUE
  else Absorbance_Varies := FALSE;
  writeln;
  write('Error in L (%): ');
  readln(L_Error);
  writeln;
  write('Error in Dp (%): ');
  readln(Dp_Error);
```

```
  writeln;
  write('Error in time (t, in seconds): ');
  readln(T_Error);
  writeln;
  for Row := 1 to Experiments do begin
    Randomize_Data;
    Initialised := FALSE;
    D := D / 10;
    Calculate_D;
    Real_D := D * 1e-8;
    writeln(Row, ' ', Real_D, ' ', Residue);
    Calculated_D[Row] := Real_D;
    if Dp_Error <> 0 then Dp := Old_Dp;
    if L_Error <> 0 then L := Old_L;
    if T_Error <> 0 then for J := 1 to N do T[J] := Old_T[J];
    if Absorbance_Varies then begin
      As := Old_As;
      for J := 0 to N do Absorbance[J] := Old_Absorbance[J]
    end
  end;
  for Row := 1 to Experiments do begin
    Average_D[Row] := 0;
    for Sub_Row := 1 to Row do
      Average_D[Row] := Average_D[Row] + Calculated_D[Sub_Row];
    Average_D[Row] := Average_D[Row] / Row
  end;
  for Row := 1 to Experiments do begin
    Deviation_D[Row] := 0;
    for Sub_Row := 1 to Row do
      Deviation_D[Row] := Deviation_D[Row]
        + sqr(Calculated_D[Sub_Row] - Average_D[Row]);
    Deviation_D[Row] := Deviation_D[Row] / Row
  end;
  writeln;
  writeln('Average D := ', Average_D[Experiments]);
  writeln('Error := ', sqrt(Deviation_D[Experiments]));
  rewrite(Data, Results);
  writeln(Data, '! Best D (cm^2/sec) = ', Best_D);
  writeln(Data, '! Saturation Absorbance (As) = ', As:4:2);
  writeln(Data, '! Initial Absorbance (A0) = ', Absorbance[0]:4:2);
  writeln(Data, '! Average D (cm^2/sec) = ', Average_D[Experiments]);
  writeln(Data, '! Error in D (cm^2/sec) = ', sqrt(Deviation_D[Experiments]));
  writeln(Data);
  writeln(Data, '!Number    D      Average D     Standard Deviation');
  for Row := 1 to Experiments do
    writeln(Data, Row, Calculated_D[Row], Average_D[Row],
      sqrt(Deviation_D[Row]));
  close(Data)
end;

procedure Save_Diffusion_Curve;
var
  Increment, Time, Y_Curve, One_Y_Curve: double;
  NP: integer;
begin
  writeln;
  D := Best_D * 1e8;
  Initialised := FALSE;
  write('Save curve in file: ');
  readln(Output_File);
  rewrite(Data, Output_File);
  writeln(Data, '! As = ', As:4:2);
```

```
  writeln(Data, '! A0 = ', Absorbance[0]:4:2);
  writeln(Data, '! D (cm^2/sec) = ', Best_D);
  writeln(Data);
  writeln(Data, '!Time     (At-A0)/(As-A0)       1-(At-A0)/(As-A0)');
  writeln(Data, '  0                  0                    -');
  writeln;
  write('Number of points: ');
  readln(NP);
  Increment := (1.2 * ln(T[N]) - ln(1e-2)) / NP;
  for I := 0 to NP do begin
    Time := exp(I * Increment + ln(1e-2)) / 1.2;
    Calculate_Sums(Time);
    Y_Curve := 1 - Sum_1;
    if Y_Curve < 0 then begin
      Y_Curve := 0;
      One_Y_Curve := 1
    end
    else One_Y_Curve := Sum_1;
    writeln(Data, Time, ' ', Y_Curve, ' ', One_Y_Curve);
  end;
  close(Data)
end;

procedure Main_Program;
begin
  Initialised := FALSE;
  Read_and_Calculate_Parameters;
  Calculate_D;
  Best_D := D * 1e-8;
  writeln;
  writeln('D = ', Best_D, ' (cm^2/sec)');
  writeln('Residue = ', Residue);
  writeln('Average Residue = ', Residue / N);
  repeat
    writeln;
    repeat
      write('Monte Carlo simulation (y/n)? ');
      readln(Answer)
    until (Answer = 'Y') or (Answer = 'y') or (Answer = 'N')
      or (Answer = 'n');
    if (Answer = 'y') or (Answer = 'Y') then Monte_Carlo_Simulate
  until (Answer = 'N') or (Answer= 'n');
  writeln;
  repeat
    write('Save diffusion curve (y/n)? ');
    readln(Answer)
  until (Answer = 'y') or (Answer = 'Y') or (Answer = 'n')
    or (Answer = 'N');
  if (Answer = 'Y') or (Answer = 'y') then Save_Diffusion_Curve
end;

begin
  First_Random_Number := TRUE;
  repeat
    writeln;
    Main_Program;
    writeln;
    repeat
      write('Would you like to use the program again (y/n)? ');
      readln(Last_Answer);
    until (Last_Answer = 'y') or (Last_Answer = 'Y')
      or (Last_Answer = 'n') or (Last_Answer = 'N')
```

```
  until (Last_Answer = 'n') or (Last_Answer = 'N');
  for I := 1 to 5 do writeln
end.
```

Program Two - Fickian Diffusion/Thin Films

```
program Diffusion {Version 1.1: Thin Films};
const
  Maximum_Error = 1.0e-10;
  Pi = 3.14159265358979323846;
  Ln_10 = ln(10);
var
  As, Ast, Abs_Err, Alpha, Beta, L, Dp, D, Derivative: double;
  Sum_1, Sum_2, Sum_3, Best_D: double;
  Residue, Old_L,Old_Dp, Old_As, Old_Ast, Maximum_D, Minimum_D: double;
  L_Error, Dp_Error, T_Error, Error: double;
  N, I, J: integer;
  Random_Array: array[1..100] of double;
  T, Y, Y_Error, Estimated_Y, Absorbance: array[0..200] of double;
  Old_Absorbance, Old_T, Absorbance_Error: array[0..200] of double;
  Data_File, Output_File, Results, Answer, Last_Answer: string;
  Data: text;
  First_Random_Number, Absorbance_Varies, Initialised: boolean;

procedure Read_and_Calculate_Parameters;
begin
  N := -1;
  writeln;
  write('Data in file: ');
  readln(Data_File);
  reset(Data, Data_File);
  repeat
    N := N + 1;
    readln(Data, T[N], Absorbance[N]);
  until eof(Data) or (T[N] < 0);
  close(Data);
  if (T[N] <= 0) then N := N -1;
  writeln;
  write('Absorbance at equilibrium: ');
  readln(Ast);
  writeln;
  write('Saturation absorbance for a film of infinite thickness: ');
  readln(As);
  writeln;
  write('Error in absorbance (%): ');
  readln(Abs_Err);
  for I := 0 to N do Absorbance_Error[I] := Abs_Err * Absorbance[I] / 100;
  writeln;
  write('Film thickness (L, in microns): ');
  readln(L);
  writeln;
  write('Depth of penetration (Dp, in microns): ');
  readln(Dp);
  writeln;
  write('Initial guess for the diffusion coefficient (D, in cm^2/sec): ');
  readln(D);
  D := D * 1e8;
end;
```

```
procedure Calculate_Sums(X: double);
const
  Sum_Maximum_Error = exp(- 300);
var
  J: integer;
  Sign: integer;
  Kj, Term_1, Term_2, Term_3, Error_1, Error_2, Factor: double;
  Old_Sum_1, Old_Sum_2, Old_Sum_3, Sign_1: double;
  Power_1, Power_2, Power_3, Error_3: double;
begin
  J := -1;
  Sum_1 := 0;
  Sum_2 := 0;
  Sum_3 := 0;
  repeat
    Old_Sum_1 := Sum_1;
    Old_Sum_2 := Sum_2;
    Old_Sum_3 := Sum_3;
    J := J + 1;
    Factor := trunc(J / 2) - J / 2;
    if (Factor = 0) then Sign := 1 else Sign := -1;
    Kj := Pi * (2 * J + 1) / (2 * L);
    Sign_1 := Alpha * Kj + Sign * 2 / Dp;
    Power_1 := - sqr(Kj) * D * X + ln(abs(Sign_1)) - ln(sqr(Kj) +
      4 / sqr(Dp)) - ln(2 * J + 1);
    Sign_1 := Sign_1 / abs(Sign_1);
    Power_2 := Power_1 + 2 * ln(Kj) + ln(X);
    Power_3 := Power_2 + 2 * ln(Kj) + ln(X);
    if (Power_1 >= - 300) then Term_1 := Sign_1 * exp(Power_1)
    else Term_1 := 0;
    if (Power_2 >= - 300) then Term_2 := - Sign_1 * exp(Power_2)
    else Term_2 := 0;
    if (Power_3 >= - 300) then Term_3 := Sign_1 * exp(Power_3)
    else Term_3 := 0;
    Sum_1 := Sum_1 + Term_1;
    Sum_2 := Sum_2 + Term_2;
    Sum_3 := Sum_3 + Term_3;
    Error_1 := abs(Sum_1 - Old_Sum_1) * Beta;
    Error_2 := abs(Sum_2 - Old_Sum_2) * Beta;
    Error_3 := abs(Sum_3 - Old_Sum_3) * Beta;
  until (Error_1 <= Sum_Maximum_Error)
    and (Error_2 <= Sum_Maximum_Error) and (Error_3 <= Sum_Maximum_Error);
  Sum_1 := Beta * Sum_1;
  Sum_2 := Beta * Sum_2;
  Sum_3 := Beta * Sum_3
end;

function Random_Number: double;
var
  Temp: double;
  Cell, x: integer;
begin
  if First_Random_Number then begin
    First_Random_Number := FALSE;
    x := seed(wallclock);
    for Cell := 1 to 100 do Random_Array[Cell] := random(x)
  end;
  repeat Cell :=  trunc(101 * random(x)) until (Cell >= 1) or (Cell <= 100);
  Temp := Random_Array[Cell];
  Random_Array[Cell] := random(x);
  Random_Number := Temp
end;
```

```
procedure Calculate_D;
const
  D_Maximum_Error = 1.0e-10;
var
  DfDd, Delta_Y, Delta_1, Delta_2, Next_D: double;
  Error_1, Error_2, Old_D: double;
  Inc_Max, Inc_Min, Q: integer;
  Newton_Raphson_Iterated: boolean;
  No_Maximum_D: boolean;
begin
  Inc_Max := 0;
  Inc_Min := 0;
  Residue := 0;
  Old_D := D;
  No_Maximum_D := TRUE;
  Minimum_D := 0;
  if not Initialised then begin
    Alpha := exp(- 2 * L / Dp);
    Beta := 8 / (Pi * Dp * (1 - Alpha));
    for Q := 1 to N do begin
      Y[Q] := (Ast - Absorbance[Q]) / (As * Beta - Absorbance[Q]);
      Delta_1 := (Ast + Absorbance[0]) * Abs_Err / 100;
      Delta_2 := (As * Beta + Absorbance[0]) * Abs_Err / 100;
      Y_Error[Q] := (Delta_1 + Delta_2 * Y[Q]) / (As * Beta - Absorbance[0])
    end;
    Initialised := TRUE
  end;
  repeat
    Newton_Raphson_Iterated := TRUE;
    Derivative := 0;
    DfDd := 0;
    Residue := 0;
    if (D <= Minimum_D) or (not No_Maximum_D and
      (D >= Maximum_D)) then DfDd := 0
    else for I := 1 to N do begin
        Calculate_Sums(T[I]);
        Estimated_Y[I] := Sum_1;
        Delta_Y := Y[I] - Estimated_Y[I];
        Derivative := Derivative + Delta_Y * Sum_2 / sqr(Y_Error[I]);
        DfDd := DfDd + (Delta_Y * Sum_3 - sqr(Sum_2)) / sqr(Y_Error[I]);
        Residue := Residue + sqr(Delta_Y)
    end;
    if (DfDd = 0) then begin
      Newton_Raphson_Iterated := FALSE;
      if (D <= Minimum_D) then begin
        Minimum_D := Old_D;
        Next_D := 1.1 * Old_D * exp(Inc_Min * Ln_10);
        Inc_Min := Inc_Min + 1;
        Inc_Max := 0
      end
      else begin
        Maximum_D := Old_D;
        No_Maximum_D := FALSE;
        Next_D := 0.9 * Old_D * exp(- Inc_Max * Ln_10);
        Inc_Max := Inc_Max + 1;
        Inc_Min := 0
      end;
      Old_D := Next_D
    end
    else begin
      Next_D := D - Derivative / DfDd;
```

```
      Error_1 := abs((D - Next_D) / D);
      Error_2 := abs((D - Next_D) / Next_D)
    end;
    D := Next_D
  until Newton_Raphson_Iterated and (Error_1 <= D_Maximum_Error)
    and (Error_2 <= D_Maximum_Error)
end;

procedure Randomize_Data;
var
  Q: integer;
begin
  if L_Error <> 0 then begin
    Old_L := L;
    L := L * (1 + L_Error * (2 * Random_Number - 1) / 100)
  end;
  if Dp_Error <> 0 then begin
    Old_Dp := Dp;
    Dp := Dp * (1 + Dp_Error * (2 * Random_Number - 1) / 100)
  end;
  if T_Error <> 0 then for Q := 1 to N do begin
    Old_T[Q] := T[Q];
    T[Q] := T[Q] + T_Error * (2 * Random_Number - 1)
  end;
  if Absorbance_Varies then begin
    Old_As := As;
    Old_Ast := Ast;
    As := As * (1 + Abs_Err * (2 * Random_Number - 1) / 100);
    Ast := Ast * (1 + Abs_Err * (2 * Random_Number - 1) / 100);
    for Q := 0 to N do begin
      Old_Absorbance[Q] := Absorbance[Q];
      Absorbance[Q] := Absorbance[Q] +
        Absorbance_Error[Q] * (2 * Random_Number - 1)
    end
  end
end;

procedure Monte_Carlo_Simulate;
var
  Real_D: double;
  Experiments, Row, Sub_Row: integer;
  Answer_2: string;
  Calculated_D, Average_D, Deviation_D: array[1..1000] of double;
begin
  writeln;
  write('Results in file: ');
  readln(Results);
  rewrite(Data, Results);
  writeln;
  write('Number of "experiments" (maximum number: 1000): ');
  readln(Experiments);
  writeln;
  repeat
    write('Do you want variations in absorbance to be considered (y/n)? ');
    readln(Answer_2)
  until (Answer_2 = 'y') or (Answer_2 = 'Y') or (Answer_2 = 'n') or
    (Answer_2 = 'N');
  if (Answer_2 = 'Y') or (Answer_2 = 'y') then Absorbance_Varies := TRUE
  else Absorbance_Varies := FALSE;
  writeln;
  write('Error in L (%): ');
  readln(L_Error);
```

```
  writeln;
  write('Error in Dp (%): ');
  readln(Dp_Error);
  writeln;
  write('Error in time (t, in seconds): ');
  readln(T_Error);
  writeln;
  for Row := 1 to Experiments do begin
    Randomize_Data;
    Initialised := FALSE;
    D := D / 10;
    Calculate_D;
    Real_D := D * 1e-8;
    writeln(Row, ' ', Real_D, ' ', Residue);
    Calculated_D[Row] := Real_D;
    if Dp_Error <> 0 then Dp := Old_Dp;
    if L_Error <> 0 then L := Old_L;
    if T_Error <> 0 then for J := 1 to N do T[J] := Old_T[J];
    if Absorbance_Varies then begin
      As := Old_As;
      Ast := Old_Ast;
      for J := 0 to N do Absorbance[J] := Old_Absorbance[J]
    end
  end;
  for Row := 1 to Experiments do begin
    Average_D[Row] := 0;
    for Sub_Row := 1 to Row do
      Average_D[Row] := Average_D[Row] + Calculated_D[Sub_Row];
    Average_D[Row] := Average_D[Row] / Row
  end;
  for Row := 1 to Experiments do begin
    Deviation_D[Row] := 0;
    for Sub_Row := 1 to Row do
      Deviation_D[Row] := Deviation_D[Row]
        + sqr(Calculated_D[Sub_Row] - Average_D[Row]);
    Deviation_D[Row] := Deviation_D[Row] / Row
  end;
  writeln;
  writeln('Average D = ', Average_D[Experiments]);
  writeln('Error = ', sqrt(Deviation_D[Experiments]));
  rewrite(Data, Results);
  writeln(Data, '! Best D (cm^2/sec) = ', Best_D);
  writeln(Data, '! Total Saturation Absorbance = ', Ast:4:2);
  writeln(Data, '! Saturation Absorbance (As) = ',
    As * (1 - exp(2 * L / Dp)):4:2);
  writeln(Data, '! Initial Absorbance (A0) = ', Absorbance[0]:4:2);
  writeln(Data, '! Average D (cm^2/sec) = ', Average_D[Experiments]);
  writeln(Data, '! Error in D (cm^2/sec) = ', sqrt(Deviation_D[Experiments]));
  writeln(Data);
  writeln(Data, '!Number    D      Average D     Standard Deviation');
  for Row := 1 to Experiments do
    writeln(Data, Row, Calculated_D[Row], Average_D[Row],
      sqrt(Deviation_D[Row]));
  close(Data)
end;

procedure Save_Diffusion_Curve;
var
  Increment, Time, Y_Curve, One_Y_Curve: double;
  NP: integer;
begin
  writeln;
```

```
  D := Best_D * 1e8;
  Initialised := FALSE;
  write('Save curve in file: ');
  readln(Output_File);
  rewrite(Data, Output_File);
  writeln(Data, '! Ast = ', Ast:4:2);
  writeln(Data, '! As = ', As * (1 - exp(- 2 * L / Dp)):4:2);
  writeln(Data, '! A0 = ', Absorbance[0]:4:2);
  writeln(Data, '! D (cm^2/sec) = ', Best_D);
  writeln(Data);
  writeln(Data, '!Time     (At-A0)/(As-A0)     Ln(1-(At-A0)/(As-A0))');
  writeln(Data, '  0                    0                    -');
  writeln;
  write('Number of points: ');
  readln(NP);
  Increment := (1.2 * ln(T[N]) - ln(1e-2)) / NP;
  for I := 0 to NP do begin
    Time := exp(I * Increment + ln(1e-2)) / 1.2;
    Calculate_Sums(Time);
    Y_Curve := 1 - Sum_1;
    if Y_Curve < 0 then begin
      Y_Curve := 0;
      One_Y_Curve := 1
    end
    else One_Y_Curve := Sum_1;
    writeln(Data, Time, ' ', Y_Curve, ' ', One_Y_Curve)
  end;
  close(Data)
end;

procedure Main_Program;
begin
  Initialised := FALSE;
  Read_and_Calculate_Parameters;
  Calculate_D;
  Best_D := D * 1e-8;
  writeln;
  writeln('D = ', Best_D, ' (cm^2/sec)');
  writeln('Total saturation absorbance = ', Ast:4:2);
  writeln('Film saturation absorbance = ', As * (1 - exp(- 2 * L / Dp)):4:2);
  writeln('Residue = ', Residue);
  writeln('Derivative = ', Derivative);
  repeat
    writeln;
    repeat
      write('Monte Carlo simulation (y/n)? ');
      readln(Answer)
    until (Answer = 'Y') or (Answer = 'y') or (Answer = 'N')
      or (Answer = 'n');
    if (Answer = 'y') or (Answer = 'Y') then Monte_Carlo_Simulate
  until (Answer = 'N') or (Answer= 'n');
  writeln;
  repeat
    write('Save diffusion curve (y/n)? ');
    readln(Answer)
  until (Answer = 'y') or (Answer = 'Y') or (Answer = 'n')
    or (Answer = 'N');
  if (Answer = 'Y') or (Answer = 'y') then Save_Diffusion_Curve
end;

begin
  First_Random_Number := TRUE;
```

```
  repeat
    writeln;
    Main_Program;
    writeln;
    repeat
      write('Would you like to use the program again (y/n)? ');
      readln(Last_Answer);
    until (Last_Answer = 'y') or (Last_Answer = 'Y')
      or (Last_Answer = 'n') or (Last_Answer = 'N')
  until (Last_Answer = 'n') or (Last_Answer = 'N');
  for I := 1 to 5 do writeln
end.
```

Program Three - Dual Mode/Thick Films

```
{$N+,E+}
program Diffusion;
{Version 2.04: two diffusion coefficients; Marquardt Method}
const
  Pi = 3.14159265358979323846;
var
  Data_Point, N, Row, Column: integer;
  D, Kd, Xa, Db, L, Dp, Saturation_Absorbance: double;
  Alpha, Beta, Ln_Beta, Percentage_Absorbance_Error: double;
  T, Absorbance, Absorbance_Error, Y, Y_Error: array[0..200] of double;
  Old_T, Old_Absorbance: array[0..200] of double;
  Sum_1, Sum_2, Delta_Y, S1, S2, S1b, S2b, New_Residue, Fraction, Ln_15: double;
  Best_D, Best_Kd, Best_Xa, Best_Residue, Old_Saturation_Absorbance: double;
  Residue_I, L_Error, Dp_Error, T_Error, Old_L, Old_Dp, Old_Residue: double;
  A: array[1..3, 1..4] of double;
  DA: array[1..3] of double;
  Random_Array: array[1..100] of double;
  Initialised, First_Random_Number, Absorbance_Varies: boolean;
  Data_File, Last_Answer: string;
  Data: text;

function Random_Number: double;
var
  Temp: double;
  Cell, X: integer;
begin
  if First_Random_Number then begin
    First_Random_Number := FALSE;
    for Cell := 1 to 100 do Random_Array[Cell] := random
  end;
  repeat Cell :=  trunc(101 * random) until (Cell >= 1) or (Cell <= 100);
  Temp := Random_Array[Cell];
  Random_Array[Cell] := random;
  Random_Number := Temp
end;

procedure Read_Data;
begin
  N := -1;
  writeln;
  write('Data in file: ');
  readln(Data_File);
  assign(Data, Data_File);
  reset(Data);
```

```
  repeat
    N := N + 1;
    readln(Data, T[N], Absorbance[N]);
  until eof(Data) or (T[N] < 0);
  close(Data);
  if (T[N] <= 0) then N := N -1;
  writeln;
  write('Absorbance at equilibrium: ');
  readln(Saturation_Absorbance);
  writeln;
  write('Error in absorbance (%): ');
  readln(Percentage_Absorbance_Error);
  for Data_Point := 0 to N do Absorbance_Error[Data_Point] :=
    Percentage_Absorbance_Error * Absorbance[Data_Point] / 100;
  writeln;
  write('Film thickness (L, in microns): ');
  readln(L);
  writeln;
  write('Depth of penetration (Dp, in microns): ');
  readln(Dp);
  writeln;
  write('Estimated value of the diffusion coefficient (D, in cm^2/sec): ');
  readln(D);
  D := D * 1e8;
  writeln;
  write('Estimated value of Kd: ');
  readln(Kd);
  writeln;
  write('Estimated value of Xa: ');
  readln(Xa)
end;

procedure Calculate_Sums(T, D: double);
const
  Sum_Maximum_Error = 1e-15;
var
  J: integer;
  Sign: integer;
  Kj, Power_1, Power_2, Factor, Term_1, Term_2: double;
  Old_Sum_1, Old_Sum_2, Error_1, Error_2: double;
begin
  J := -1;
  Sum_1 := 0;
  Sum_2 := 0;
  repeat
    Old_Sum_1 := Sum_1;
    Old_Sum_2 := Sum_2;
    J := J + 1;
    Factor := trunc(J / 2) - J / 2;
    if (Factor = 0) then Sign := 1 else Sign := -1;
    Kj := Pi * (2 * J + 1) / (2 * L);
    Factor := Alpha * Kj + Sign * 2 / Dp;
    Power_1 := - sqr(Kj) * D * T + ln(abs(Factor)) - ln(sqr(Kj) +
      4 / sqr(Dp)) - ln(2 * J + 1);
    Factor := Factor / abs(Factor);
    if Factor < 0 then Sign := - 1 else Sign := 1;
    Power_2 := Power_1 + 2 * ln(Kj) + ln(T);
    if (Power_1 >= Ln_15) then Term_1 := Sign * exp(Power_1)
    else Term_1 := 0;
    if (Power_2 >= Ln_15) then Term_2 := - Sign * exp(Power_2)
    else Term_2 := 0;
    Sum_1 := Sum_1 + Term_1;
```

```
    Sum_2 := Sum_2 + Term_2;
    Error_1 := abs(Sum_1 - Old_Sum_1) * Beta;
    Error_2 := abs(Sum_2 - Old_Sum_2) * Beta
  until (Error_1 <= Sum_Maximum_Error) and (Error_2 <= Sum_Maximum_Error);
  Sum_1 := Sum_1 * Beta;
  Sum_2 := Sum_2 * Beta
end;

function Residue_II(D, Kd, Xa: double): double;
var
  Res: double;
begin
  Res := 0;
  for Data_Point := 1 to N do begin
    Calculate_Sums(T[Data_Point], D);
    S1 := Sum_1;
    Db := Kd * D;
    Calculate_Sums(T[Data_Point], Db);
    S1b := Sum_1;
    Delta_Y := Y[Data_Point] - Xa * S1 - (1 - Xa) * S1b;
    Res := Res + sqr(Delta_Y / Y_Error[Data_Point])
  end;
  Residue_II := Res
end;

procedure Calculate_Derivatives(D, Kd, Xa: double);
var
  Derivative: array[1..3] of double;
begin
  Residue_I := 0;
  for Row := 1 to 3 do
    for Column := 1 to 4 do A[Row, Column] := 0;
  for Data_Point := 1 to N do begin
    Calculate_Sums(T[Data_Point], D);
    S1 := Sum_1;
    S2 := Sum_2;
    Db := Kd * D;
    Calculate_Sums(T[Data_Point], Db);
    S1b := Sum_1;
    S2b := Sum_2;
    Delta_Y := Y[Data_Point] - Xa * S1 - (1 - Xa) * S1b;
    Residue_I := Residue_I + sqr(Delta_Y / Y_Error[Data_Point]);
    Derivative[1] := Xa * S2 + (1 - Xa) * Kd * S2b;
    Derivative[2] := (1 - Xa) * D * S2b;
    Derivative[3] := S1 - S1b;
    for Row := 1 to 3 do begin
      for Column := 1 to 3 do A[Row, Column] := A[Row, Column] +
        Derivative[Row] * Derivative[Column] / sqr(Y_Error[Data_Point]);
      A[Row, 4] :=
        A[Row, 4] + Derivative[Row] * Delta_Y / sqr(Y_Error[Data_Point])
    end
  end
end;

procedure Calculate_Increments(Lambda: double);
var
  Sub_Row: integer;
begin
  for Row := 1 to 3 do A[Row, Row] := A[Row, Row] * (1 + Lambda);
  for Row := 1 to 2 do
    for Sub_Row := (Row + 1) to 3 do
      for Column := Row to 4 do
```

```
      A[Sub_Row, Column] := A[Sub_Row, Column] -
        A[Row, Column] * A[Sub_Row, Row] / A[Row, Row];
  DA[3] := A[3, 4] / A[3, 3];
  DA[2] := (A[2, 4] - A[2, 3] * DA[3]) / A[2, 2];
  DA[1] := (A[1, 4] - A[1, 3] * DA[3] - A[1, 2] * DA[2]) / A[1, 1]
end;

procedure Initialise;
var
  Delta_As, Delta_At, Delta_A0: double;
begin
  Alpha := exp(- 2 * L / Dp);
  Beta := 8 / (Pi * Dp * (1 - Alpha));
  Ln_Beta := ln(Beta);
  Delta_As := Percentage_Absorbance_Error * Saturation_Absorbance / 100;
  Delta_A0 := Percentage_Absorbance_Error * Absorbance[0] / 100;
  for Data_Point := 1 to N do begin
    Delta_At := Percentage_Absorbance_Error * Absorbance[Data_Point] / 100;
    Y[Data_Point] :=
      (Saturation_Absorbance - Absorbance[Data_Point]) /
        (Saturation_Absorbance - Absorbance[0]);
    Y_Error[Data_Point] := (Y[Data_Point] * (Delta_A0 - Delta_As) +
      Delta_At + Delta_A0) / (Saturation_Absorbance - Absorbance[0])
  end;
  Initialised := TRUE
end;

procedure Calculate_Parameters;
const
  Maximum_Residue_Error = 1e-4;
var
  Lambda_is_Small: boolean;
  Lambda: double;
  Next_D, Next_Kd, Next_Xa, Residue_Difference: double;
begin
  Lambda := 1e-10;
  Old_Residue := Residue_II(D, Kd, Xa);
  repeat
    if not Initialised then Initialise;
    Calculate_Derivatives(D, Kd, Xa);
    Calculate_Increments(Lambda);
    Next_D := D + DA[1];
    Next_Kd := Kd + DA[2];
    Next_Xa := Xa + DA[3];
    if (Next_D > 0) and (Next_Kd > 0) and
      (Next_Kd <= 1) and (Next_Xa >= 0) and (Next_Xa <= 1) then begin
        New_Residue := Residue_II(Next_D, Next_Kd, Next_Xa);
        if (New_Residue >= Old_Residue) then begin
          if ((DA[1] / D) <= 1e-10) and
            ((DA[2] / Kd) <= 1e-10) and
              ((DA[3] / Xa) <= 1e-10) then begin
            Residue_Difference := 0;
            Lambda_is_Small := FALSE;
            New_Residue := Old_Residue
          end
          else begin
            Lambda_is_Small := TRUE;
            Lambda := Lambda * 10
          end
        end
        else begin
          Lambda_is_Small := FALSE;
```

```
        Lambda := Lambda / 10;
        D := Next_D;
        Kd := Next_Kd;
        Xa := Next_Xa;
        Residue_Difference := abs(Old_Residue - New_Residue) / Old_Residue;
        Old_Residue := New_Residue
      end
    end
    else begin
     if (Next_D > 0) then D := Next_D;
     Xa := Random_Number;
     Kd := Random_Number;
     Lambda := 1e-4;
     Lambda_is_Small := TRUE;
     Old_Residue := Residue_II(D, Kd, Xa)
    end
  until (not Lambda_is_Small) and
    (Residue_Difference <= Maximum_Residue_Error)
end;

procedure Save_Diffusion_Curve;
var
  Increment, Time, Lower_Time, Ya, Yb, Abs: double;
  Number_of_Points, Point: integer;
  Output_File: string;
begin
  writeln;
  D := Best_D * 1e8;
  Initialised := FALSE;
  write('Save curve in file: ');
  readln(Output_File);
  assign(Data, Output_File);
  rewrite(Data);
  writeln;
  write('Number of points: ');
  readln(Number_of_Points);
  writeln;
  write('Curve begining at time (seconds) = ');
  readln(Lower_Time);
  writeln;
  Increment := (1.2 * ln(T[N]) - ln(Lower_Time)) / Number_of_Points;
  for Point := 0 to Number_of_Points do begin
    Db := Best_Kd * D;
    Fraction := Xa;
    Time := exp(Point * Increment + ln(Lower_Time)) / 1.2;
    Calculate_Sums(Time, D);
    S1 := Sum_1;
    Calculate_Sums(Time, Db);
    S1b := Sum_1;
    Ya := Best_Xa * S1;
    Yb := (1 - Best_Xa) * S1b;
    Abs := Saturation_Absorbance
      - (Ya + Yb) * (Saturation_Absorbance - Absorbance[0]);
      writeln(Data, Time, Abs)
  end;
  close(Data)
end;

procedure Main_Program;
var
  Answer: string;
begin
```

```
    Read_Data;
    Initialised := FALSE;
    Calculate_Parameters;
    Best_D := D * 1e-8;
    Best_Kd := Kd;
    Best_Xa := Xa;
    Best_Residue := New_Residue;
    writeln;
    writeln('D =', Best_D);
    writeln('Kd =', Best_Kd);
    writeln('Xa =', Best_Xa);
    writeln('Residue = ', Best_Residue);
    writeln('Average Residue = ', Best_Residue / N);
    repeat
      writeln;
      repeat
        write('Monte Carlo simulation (y/n)? ');
        readln(Answer)
      until (Answer = 'Y') or (Answer = 'y') or (Answer = 'N')
        or (Answer = 'n');
      if (Answer = 'y') or (Answer = 'Y') then Monte_Carlo_Simulate
    until (Answer = 'N') or (Answer= 'n');
    writeln;
    repeat
      write('Save diffusion curve (y/n)? ');
      readln(Answer)
    until (Answer = 'y') or (Answer = 'Y') or (Answer = 'n')
      or (Answer = 'N');
    if (Answer = 'Y') or (Answer = 'y') then Save_Diffusion_Curve
  end;

  begin
    First_Random_Number := TRUE;
    Ln_15 := ln(1e-15);
    repeat
      writeln;
      Main_Program;
      writeln;
      repeat
        write('Would you like to use the program again (y/n)? ');
        readln(Last_Answer);
      until (Last_Answer = 'y') or (Last_Answer = 'Y')
        or (Last_Answer = 'n') or (Last_Answer = 'N')
    until (Last_Answer = 'n') or (Last_Answer = 'N');
    for Data_Point := 1 to 5 do writeln
  end.
```

Program Four - Dual mode/Thin Films

```
{$N+}
program Diffusion;
{Version 2.051: two diffusion coefficients
  and unknown equilibrium absorbance - thin film; Marquardt Method}
const
  Pi = 3.14159265358979323846;
var
  N, Data_Point, Row, Column: integer;
  Sat_Abs, D, Kd, Xa, Percentage_Absorbance_Error: double;
  L, Dp, Sum_1, Sum_2, Alpha, Beta, Ln_15: double;
  L_Error, Dp_Error, T_Error, Old_L, Old_Dp, Old_Residue, New_Residue: double;
```

```
  Best_Sat_Abs, Best_D, Best_Kd, Best_Xa, Best_Residue, Q: double;
  Sat_Inf, Old_Sat_Inf, Sat_Inf_Error: double;
  Time, Absorbance, Absorbance_Error, Old_T, Old_Abs: array[0..100] of double;
  Random_Array: array[1..100] of double;
  A: array[1..4] of array[1..5] of double;
  DA: array[1..4] of double;
  First_Random_Number, Initialised, Absorbance_Varies: boolean;
  Last_Answer: string;

function Gamma(P: double): double;
const
  Stp = 2.50662827465;
var
  X, TMP, Ser: double;
begin
  X := P - 1;
  TMP := X + 5.5;
  TMP := (X + 0.5) * ln(TMP) - TMP;
  Ser := 1 + 76.18009173 / (X + 1) - 86.50532033 / (X + 2) +
    24.01409822 / (X + 3) - 1.231739516 / (X + 4) + 0.120858003e-02 / (X + 5)
      - 0.536382e-5 / (X + 6);
  Gamma := Stp * Ser * TMP
end;

function Goodness(N, Residue: double): double;
var
  I: integer;
  A, X, Sum, Term, Denom: double;
begin
  A := (N - 2) / 2;
  X := Residue / 2;
  Sum := 0;
  I := -1;
  Denom := Gamma(A);
  repeat
    I := I + 1;
    Denom := Denom * A;
    A := A + 1;
    Term := exp(I * ln(X))/ Denom;
    Sum := Sum + Term
  until Term <= 1e-16;
  Goodness := 1 - Sum * exp(- X + A * ln(X))
end;

function Random_Number: double;
var
  Temp: double;
  Cell, X: integer;
begin
  if First_Random_Number then begin
    X := seed(wallclock);
    First_Random_Number := FALSE;
    for Cell := 1 to 100 do Random_Array[Cell] := random(X)
  end;
  repeat Cell :=  trunc(101 * random(X)) until (Cell >= 1) or (Cell <= 100);
  Temp := Random_Array[Cell];
  Random_Array[Cell] := random(X);
  Random_Number := Temp
end;

procedure Read_Data;
var
```

```
    Data_File: string;
    Data: text;
  begin
   N := -1;
   writeln;
   write('Data in file: ');
   readln(Data_File);
   reset(Data, Data_File);
   repeat
    N := N + 1;
    readln(Data, Time[N], Absorbance[N]);
   until eof(Data) or (Time[N] < 0);
   close(Data);
   if (Time[N] <  0) then N := N -1;
   writeln;
   write('Error in absorbance (%): ');
   readln(Percentage_Absorbance_Error);
   writeln;
   write('Film thickness (L, in microns): ');
   readln(L);
   writeln;
   write('Depth of penetration (Dp, in microns): ');
   readln(Dp);
   writeln;
   write('Value of Eq.Abs. for a  film of infinite thickness (Eq.Abs.Inf., in 1/cm): ');
   read(Sat_Inf);
   Sat_Inf_Error := Sat_Inf * Percentage_Absorbance_Error / 100;
   writeln;
   write('Estimated value of the equilibrium absorbance for  this film (Eq.Abs., in 1/cm): ');
   read(Sat_Abs);
   writeln;
   write('Estimated value of the diffusion coefficient (D, in cm^2/sec): ');
   readln(D);
   D := D * 1e8;
   writeln;
   write('Estimated value of Kd: ');
   readln(Kd);
   writeln;
   write('Estimated value of Xa: ');
   readln(Xa)
  end;

  procedure Initialise;
  begin
   Alpha := exp(- 2 * L / Dp);
   Beta := 8 / (Pi * Dp * (1 - Alpha));
   for Data_Point := 0 to N do Absorbance_Error[Data_Point] :=
    Percentage_Absorbance_Error * Absorbance[Data_Point] / 100;
   Initialised := TRUE
  end;

  procedure Calculate_Sums(T, D: double);
  const
   Sum_Maximum_Error = 1e-15;
  var
   J: integer;
   Sign: integer;
   Kj, Power_1, Power_2, Factor, Term_1, Term_2: double;
   Old_Sum_1, Old_Sum_2, Error_1, Error_2: double;
  begin
   J := -1;
   Sum_1 := 0;
```

```
    Sum_2 := 0;
    repeat
      Old_Sum_1 := Sum_1;
      Old_Sum_2 := Sum_2;
      J := J + 1;
      Factor := trunc(J / 2) - J / 2;
      if (Factor = 0) then Sign := 1 else Sign := -1;
      Kj := Pi * (2 * J + 1) / (2 * L);
      Factor := Alpha * Kj + Sign * 2 / Dp;
      Power_1 := - sqr(Kj) * D * T + ln(abs(Factor)) - ln(sqr(Kj) +
        4 / sqr(Dp)) - ln(2 * J + 1);
      Factor := Factor / abs(Factor);
      if Factor < 0 then Sign := - 1 else Sign := 1;
      Power_2 := Power_1 + 2 * ln(Kj) + ln(T);
      if (Power_1 >= Ln_15) then Term_1 := Sign * exp(Power_1)
      else Term_1 := 0;
      if (Power_2 >= Ln_15) then Term_2 := - Sign * exp(Power_2)
      else Term_2 := 0;
      Sum_1 := Sum_1 + Term_1;
      Sum_2 := Sum_2 + Term_2;
      Error_1 := abs(Sum_1 - Old_Sum_1) * Beta;
      Error_2 := abs(Sum_2 - Old_Sum_2) * Beta
    until (Error_1 <= Sum_Maximum_Error) and (Error_2 <= Sum_Maximum_Error);
    Sum_1 := Sum_1 * Beta;
    Sum_2 := Sum_2 * Beta
  end;

  function Residue(Sat_Abs, D, Kd, Xa: double): double;
  var
    Res, S1, S1b, Db: double;
  begin
    Res := 0;
    for Data_Point := 1 to N do begin
      Calculate_Sums(Time[Data_Point], D);
      S1 := Sum_1;
      Db := Kd * D;
      Calculate_Sums(Time[Data_Point], Db);
      S1b := Sum_1;
      Res := Res + sqr((Absorbance[Data_Point] - Sat_Abs  +
        (Sat_Inf * exp(-2 * L / Dp)  - Absorbance[0]) * (Xa * S1 +
          (1 - Xa) * S1b)) / Absorbance_Error[Data_Point])
    end;
    Residue := Res
  end;

  procedure Calculate_Derivatives(Sat_Abs, D, Kd, Xa: double);
  var
    Derivative: array[1..4] of double;
    S1, S2, Db, S1b, S2b, Delta_Abs: double;
  begin
    for Row := 1 to 4 do
      for Column := 1 to 5 do A[Row, Column] := 0;
    for Data_Point := 1 to N do begin
      Calculate_Sums(Time[Data_Point], D);
      S1 := Sum_1;
      S2 := Sum_2;
      Db := Kd * D;
      Calculate_Sums(Time[Data_Point], Db);
      S1b := Sum_1;
      S2b := Sum_2;
      Delta_Abs := Sat_Inf * exp(- 2 * L / Dp) - Absorbance[0];
      Derivative[1] := 1;
```

```
    Derivative[2] := - Delta_Abs * (Xa * S2 + (1 - Xa) * Kd * S2b);
    Derivative[3] := - Delta_Abs * (1 - Xa) * D * S2b;;
    Derivative[4] := - Delta_Abs * (S1 - S1b);
    for Row := 1 to 4 do begin
     for Column := 1 to 4 do A[Row, Column] := A[Row, Column] +
      Derivative[Row] * Derivative[Column] /
       sqr(Absorbance_Error[Data_Point]);
     A[Row, 5] :=
      A[Row, 5] + Derivative[Row] * (Absorbance[Data_Point] - Sat_Abs +
       Delta_Abs * (Xa * S1 + (1 - Xa) * S1b)) /
        sqr(Absorbance_Error[Data_Point])
   end
  end
end;

procedure Calculate_Increments(Lambda: double);
var
 Sub_Row: integer;
begin
 for Row := 1 to 4 do A[Row, Row] := A[Row, Row] * (1 + Lambda);
 for Row := 1 to 3 do
  for Sub_Row := (Row + 1) to 4 do
   for Column := Row to 5 do
    A[Sub_Row, Column] := A[Sub_Row, Column] -
     A[Row, Column] * A[Sub_Row, Row] / A[Row, Row];
 DA[4] := A[4, 5] / A[4, 4];
 DA[3] := (A[3, 5] - A[3, 4] * DA[4]) / A[3, 3];
 DA[2] := (A[2, 5] - A[2, 4] * DA[4] - A[2, 3] * DA[3]) / A[2, 2];
 DA[1] := (A[1, 5] - A[1, 4] * DA[4] - A[1, 3] * DA[3] -
  A[1, 2] * DA[2]) / A[1, 1]
end;

procedure Calculate_Parameters;
const
 Maximum_Residue_Error = 1e-4;
var
 Lambda_is_Small: boolean;
 Lambda, Next_Sat_Abs, Next_D, Next_Kd, Next_Xa: double;
 Residue_Difference: double;
begin
 Lambda := 1e-10;
 if not Initialised then Initialise;
 Old_Residue := Residue(Sat_Abs, D, Kd, Xa);
 repeat
  Calculate_Derivatives(Sat_Abs, D, Kd, Xa);
  Calculate_Increments(Lambda);
  Next_Sat_Abs := Sat_Abs + DA[1];
  Next_D := D + DA[2];
  Next_Kd := Kd + DA[3];
  Next_Xa := Xa + DA[4];
  if (Next_D > 0) and (Next_Kd > 0) and
   (Next_Kd <= 1) and (Next_Xa >= 0) and (Next_Xa <= 1) then begin
    New_Residue := Residue(Next_Sat_Abs, Next_D, Next_Kd, Next_Xa);
    if (New_Residue >= Old_Residue) then begin
     if ((DA[1] / Sat_Abs) <= 1e-10) and ((DA[1] / D) <= 1e-10) and
      ((DA[2] / Kd) <= 1e-10) and ((DA[3] / Xa) <= 1e-10) then begin
       Residue_Difference := 0;
       Lambda_is_Small := FALSE;
       New_Residue := Old_Residue
     end
     else begin
      Lambda_is_Small := TRUE;
```

```
          Lambda := Lambda * 10
         end
        end
        else begin
         Lambda_is_Small := FALSE;
         Lambda := Lambda / 10;
         Sat_Abs := Next_Sat_Abs;
         D := Next_D;
         Kd := Next_Kd;
         Xa := Next_Xa;
         Residue_Difference := abs(Old_Residue - New_Residue) / Old_Residue;
         Old_Residue := New_Residue
        end
      end
      else begin
       if (Next_D > 0) then D := Next_D;
       Xa := Random_Number;
       Kd := Random_Number;
       Lambda := 1e-4;
       Lambda_is_Small := TRUE;
       Old_Residue := Residue(Sat_Abs, D, Kd, Xa)
      end
    until (not Lambda_is_Small) and
     (Residue_Difference <= Maximum_Residue_Error)
  end;

  procedure Randomize_Data;
  begin
   if L_Error <> 0 then begin
    Old_L := L;
    L := L + L_Error * (2 * Random_Number - 1)
   end;
   if Dp_Error <> 0 then begin
    Old_Dp := Dp;
    Dp := Dp + Dp_Error * (2 * Random_Number - 1)
   end;
   if T_Error <> 0 then for Data_Point := 1 to N do begin
    Old_T[Data_Point] := Time[Data_Point];
    Time[Data_Point] := Time[Data_Point] + T_Error * (2 * Random_Number - 1)
   end;
   if Absorbance_Varies then begin
    Old_Sat_Inf := Sat_Inf;
    Sat_Inf := Sat_Inf + Sat_Inf_Error * (2 * Random_Number - 1);
    for Data_Point := 0 to N do begin
     Old_Abs[Data_Point] := Absorbance[Data_Point];
     Absorbance[Data_Point] := Absorbance[Data_Point] +
     Absorbance_Error[Data_Point] * (2 * Random_Number - 1)
    end
   end
  end;

  procedure Monte_Carlo_Simulate;
  type
    Simu_Res =
     record
      A: double;
      Dif: double;
      X: double;
      K: double
     end;
  var
   Input_: Simu_Res;
```

```
  Results, Average, Deviation: file of Simu_Res;
  Real_D: double;
  Total_Experiments, Experiment, Sub_Experiment: integer;
  Answer_2: string;
  Calculated_Sat_Abs, Average_Sat_Abs, Deviation_Sat_Abs: double;
  Calculated_D, Average_D, Deviation_D: double;
  Calculated_Xa, Average_Xa, Deviation_Xa: double;
  Calculated_Kd, Average_Kd, Deviation_Kd: double;
  Results_Sat_Abs, Results_D, Results_Kd, Results_Xa: string;
  Data_Sat_Abs, Data_D, Data_Kd, Data_Xa: text;
begin
  writeln;
  write('Results for "D" in file: ');
  readln(Results_D);
  writeln;
  write('Results for "Kd" in file: ');
  readln(Results_Kd);
  writeln;
  write('Results for "Xa" in file: ');
  readln(Results_Xa);
  writeln;
  write('Results for Eq.Abs. in file: ');
  readln(Results_Sat_Abs);
  writeln;
  write('Number of "experiments": ');
  readln(Total_Experiments);
  writeln;
  repeat
    write('Do you want variations in absorbance to be considered (y/n)? ');
    readln(Answer_2)
  until (Answer_2 = 'y') or (Answer_2 = 'Y') or (Answer_2 = 'n') or
    (Answer_2 = 'N');
  if (Answer_2 = 'Y') or (Answer_2 = 'y') then Absorbance_Varies := TRUE
  else Absorbance_Varies := FALSE;
  writeln;
  write('Error in L (microns): ');
  readln(L_Error);
  writeln;
  write('Error in Dp (microns): ');
  readln(Dp_Error);
  writeln;
  write('Error in time (seconds): ');
  readln(T_Error);
  writeln;
  rewrite(Results);
  rewrite(Average);
  rewrite(Deviation);
  for Experiment := 1 to Total_Experiments do begin
    Randomize_Data;
    Initialised := FALSE;
    Sat_Abs := Best_Sat_Abs;
    D := Best_D * 1e8;
    Kd := Best_Kd;
    Xa := Best_Xa;
    Calculate_Parameters;
    Real_D := D * 1e-8;
    writeln('Experiment # ', Experiment);
    writeln('D = ', Real_D);
    writeln('Kd = ', Kd);
    writeln('Xa = ', Xa);
    writeln('Eq.Abs. =', Sat_Abs);
    writeln('Residue = ', Old_Residue);
```

```
  writeln('Average Residue = ', Old_Residue / N);
  writeln;
  with Input_ do begin
    A := Sat_Abs;
    Dif := Real_D;
    K := Kd;
    X := Xa
  end;
  write(Results, Input_);
  if Dp_Error <> 0 then Dp := Old_Dp;
  if L_Error <> 0 then L := Old_L;
  if T_Error <> 0 then
    for Data_Point := 1 to N do Time[Data_Point] := Old_T[Data_Point];
  if Absorbance_Varies then begin
    for Data_Point := 0 to N do
      Absorbance[Data_Point] := Old_Abs[Data_Point];
    Sat_Inf := Old_Sat_Inf
  end
 end;
 for Experiment := 1 to Total_Experiments do begin
  reset(Results);
  Average_Sat_Abs := 0;
  Average_D := 0;
  Average_Kd := 0;
  Average_Xa := 0;
  for Sub_Experiment := 1 to Experiment do begin;
    read(Results, Input_);
    with Input_ do begin
      Average_Sat_Abs := Average_Sat_Abs + A;
      Average_D := Average_D + Dif;
      Average_Xa := Average_Xa + X;
      Average_Kd := Average_Kd + K
    end
  end;
  Average_Sat_Abs := Average_Sat_Abs / Experiment;
  Average_D := Average_D / Experiment;
  Average_Kd := Average_Kd / Experiment;
  Average_Xa := Average_Xa / Experiment;
  with Input_ do begin
    A := Average_Sat_Abs;
    Dif := Average_D;
    K := Average_Kd;
    X := Average_Xa
  end;
  write(Average, Input_)
 end;
 reset(Average);
 for Experiment := 1 to Total_Experiments do begin
  reset(Results);
  read(Average, Input_);
  with Input_ do begin
    Average_Sat_Abs := A;
    Average_D := Dif;
    Average_Kd := K;
    Average_Xa := X
  end;
  Deviation_D := 0;
  Deviation_Kd := 0;
  Deviation_Xa := 0;
  Deviation_Sat_Abs := 0;
  for Sub_Experiment := 1 to Experiment do begin
    read(Results, Input_);
```

```
      with Input_ do begin
        Deviation_Sat_Abs := Deviation_Sat_Abs + sqr(A - Average_Sat_Abs);
        Deviation_D := Deviation_D + sqr(Dif - Average_D);
        Deviation_Kd := Deviation_Kd + sqr(K - Average_Kd);
        Deviation_Xa := Deviation_Xa + sqr(X - Average_Xa)
      end
    end;
    Deviation_D := sqrt(Deviation_D / Experiment);
    Deviation_Sat_Abs := sqrt(Deviation_Sat_Abs / Experiment);
    Deviation_Kd := sqrt(Deviation_Kd / Experiment);
    Deviation_Xa := sqrt(Deviation_Xa / Experiment);
    with Input_ do begin
      A := Deviation_Sat_Abs;
      Dif := Deviation_D;
      K := Deviation_Kd;
      X := Deviation_Xa
    end;
    write(Deviation, Input_)
  end;
  writeln('D (cm^2/sec) =', Average_D, ' +/- ', Deviation_D);
  writeln('Kd =', Average_Kd, ' +/- ', Deviation_Kd);
  writeln('Xa =', Average_Xa, ' +/- ', Deviation_Xa);
  writeln(
    'Eq.Abs. (1/cm) =', Average_Sat_Abs, ' +/- ', Deviation_Sat_Abs);
  rewrite(Data_D, Results_D);
  rewrite(Data_Sat_Abs, Results_Sat_Abs);
  rewrite(Data_Kd, Results_Kd);
  rewrite(Data_Xa, Results_Xa);
  writeln(Data_D, '! Best D (cm^2/sec) =', Best_D);
  writeln(Data_D, '! Best Kd =', Best_Kd);
  writeln(Data_D, '! Best Xa =', Best_Xa);
  writeln(Data_D, '! Best Eq.Abs. = ', Best_Sat_Abs:4:2);
  writeln(Data_D, '! Initial Absorbance = ', Absorbance[0]:4:2);
  writeln(Data_D, '! D (cm^2/sec) =', Average_D, ' +/- ', Deviation_D);
  writeln(Data_D, '! Kd =', Average_Kd, ' +/-', Deviation_Kd);
  writeln(Data_D, '! Xa =', Average_Xa, ' +/-', Deviation_Xa);
  writeln(Data_D,'! Eq.Abs. (1/cm) ='
    , Average_Sat_Abs, ' +/- ', Deviation_Sat_Abs);
  writeln(Data_D, '! Column 1: Number of Experiment');
  writeln(Data_D, '! Column 2: D/Kd/Xa/Sat_Abs | Column 3: Average D/Kd/Xa/Sat_Abs');
  writeln(Data_D, '! Column 3: Deviation D/Kd/Xa/Sat_Abs | Column 4: Average Deviation
D/Kd/Xa/Sat_Abs');
  writeln(Data_D);
  reset(Results);
  reset(Average);
  reset(Deviation);
  for Experiment := 1 to Total_Experiments do begin
    read(Results, Input_);
    with Input_ do begin
      Calculated_D := Dif;
      Calculated_Kd := K;
      Calculated_Xa := X;
      Calculated_Sat_Abs := A
    end;
    read(Average, Input_);
    with Input_ do begin
      Average_D := Dif;
      Average_Kd := K;
      Average_Xa := X;
      Average_Sat_Abs := A
    end;
    read(Deviation, Input_);
```

```
    with Input_ do begin
      Deviation_D := Dif;
      Deviation_Kd := K;
      Deviation_Xa := X;
      Deviation_Sat_Abs := A
    end;
    writeln(Data_D, Experiment, Calculated_D, Average_D, Deviation_D);
    writeln(Data_Kd, Experiment, Calculated_Kd, Average_Kd, Deviation_Kd);
    writeln(Data_Xa, Experiment, Calculated_Xa, Average_Xa, Deviation_Xa);
    writeln(Data_Sat_Abs,
      Experiment, Calculated_Sat_Abs, Average_Sat_Abs, Deviation_Sat_Abs)
  end;
  close(Data_D);
  close(Data_Kd);
  close(Data_Xa);
  close(Data_Sat_Abs);
  close(Results);
  close(Average);
  close(Deviation)
end;

procedure Save_Diffusion_Curve;
var
  Increment, T, Lower_Time, Ya, Yb, Abs: double;
  S1, S1b, Db, Fraction: double;
  Number_of_Points, Point: integer;
  Output_File: string;
  Data: text;
begin
  writeln;
  D := Best_D * 1e8;
  Initialised := FALSE;
  write('Save curve in file: ');
  readln(Output_File);
  rewrite(Data, Output_File);
  writeln(Data, '! Eq.Abs. = ', Sat_Abs:4:2);
  writeln(Data, '! Initial_Absorbance = ', Absorbance[0]:4:2);
  writeln(Data, '! D (cm^2/sec) = ', Best_D);
  writeln(Data, '! Kd = ', Best_Kd);
  writeln(Data, '! Xa = ', Best_Xa);
  writeln(Data);
  writeln(Data, '! First Column: Time');
  writeln(Data, '! Second Column: Absorbance');
  writeln;
  write('Number of points: ');
  readln(Number_of_Points);
  writeln;
  write('Curve begining at time (seconds) = ');
  readln(Lower_Time);
  writeln;
  Increment := (ln(Time[N]) - ln(Lower_Time) + 0.1) / Number_of_Points;
  for Point := 0 to Number_of_Points do begin
    Db := Best_Kd * D;
    Fraction := Xa;
    T := exp(Point * Increment + ln(Lower_Time)) / 1.1;
    Calculate_Sums(T, D);
    S1 := Sum_1;
    Calculate_Sums(T, Db);
    S1b := Sum_1;
    Ya := Best_Xa * S1;
    Yb := (1 - Best_Xa) * S1b;
    Abs := Best_Sat_Abs - (Best_Sat_Abs - Absorbance[0]) * (Ya + Yb);
```

```
      writeln(Data, T, Abs)
    end;
    close(Data)
  end;

  procedure Main_Program;
  var
    Answer: string;
  begin
    Read_Data;
    Initialised := FALSE;
    Calculate_Parameters;
    Best_Sat_Abs := Sat_Abs;
    Best_D := D * 1e-8;
    Best_Kd := Kd;
    Best_Xa := Xa;
    Best_Residue := New_Residue;
  {  Q := Goodness(N, Best_Residue);}
    writeln;
    writeln('D (cm^2/sec) =', Best_D);
    writeln('Kd =', Best_Kd);
    writeln('Xa =', Best_Xa);
    writeln('Equ.Abs. (1/cm) =', Best_Sat_Abs);
    writeln('Residue =', Best_Residue);
    writeln('Average Residue =', Best_Residue / N);
    writeln('Q =', Q);
    repeat
      writeln;
      repeat
        write('Monte Carlo simulation (y/n)? ');
        readln(Answer)
      until (Answer = 'Y') or (Answer = 'y') or (Answer = 'N')
        or (Answer = 'n');
      if (Answer = 'y') or (Answer = 'Y') then Monte_Carlo_Simulate
    until (Answer = 'N') or (Answer= 'n');
    writeln;
    repeat
      write('Save diffusion curve (y/n)? ');
      readln(Answer)
    until (Answer = 'y') or (Answer = 'Y') or (Answer = 'n')
      or (Answer = 'N');
    if (Answer = 'Y') or (Answer = 'y') then Save_Diffusion_Curve
  end;

  begin
    First_Random_Number := TRUE;
    Ln_15 := ln(1e-15);
    repeat
      writeln;
      Main_Program;
      writeln;
      repeat
        write('Would you like to use the program again (y/n)? ');
        readln(Last_Answer);
      until (Last_Answer = 'y') or (Last_Answer = 'Y')
        or (Last_Answer = 'n') or (Last_Answer = 'N')
     until (Last_Answer = 'n') or (Last_Answer = 'N');
     for Data_Point := 1 to 5 do writeln
  end.
```

APPENDIX FOUR

The board of studies in chemistry requires that each posgraduate research thesis contain an appendix listing:

(a) all research conferences attended during the period when the research for the thesis was carried out;

- Mattson Third Annual Users Group Meeting, York - April/1991.
- International Symposium in Polymer Surfaces and Interfaces, Durham University - July/1991.
- Aspects of Contemporary Polymer Chemistry - Durham University - April/1992.
- International Symposium in "Surface Properties of Biomedical Materials", Manchester - May/1992.
- Interdisciplinar Research Center (IRC) in Polymer Science and Technology - Industrial Club Seminar, Durham University - September/1993. A poster was presented.
- Infrared and Raman Discussion Group (142nd) meeting, University of Nottingham - April/1994. A poster was presented.

(b) all research colloquia, seminars and lectures arranged by the department of chemistry during the period of the author's residence as a posgraduate student. This list is appended bellow, those events attended by the author are marked (•).

Publication

"Depth Profile of Polymer Laminates Using FT infrared (ATR) Spectroscopy. The Barrier Film Technique".

M.R.Pereira, J.Yarwood , Journal of Polymer Science, Part-B (in press)

REVISED VERSION

UNIVERSITY OF DURHAM

Board of Studies in Chemistry

COLLOQUIA, LECTURES AND SEMINARS GIVEN BY INVITED SPEAKERS 1ST AUGUST 1990 TO 31ST JULY 1991

ALDER, Dr. B.J. (Lawrence Livermore Labs., California) — 15th January, 1991
Hydrogen in all its Glory

BELL†, Prof. T. (SUNY, Stoney Brook, U.S.A.) — 14th November, 1990
Functional Molecular Architecture and Molecular Recognition

BOCHMANN†, Dr. M. (University of East Anglia) — 24th October, 1990
Synthesis, Reactions and Catalytic Activity of Cationic Titanium Alkyls

BRIMBLE, Dr. M.A. (Massey University, New Zealand) — 29th July, 1991
Synthetic Studies Towards the Antibiotic Griseusin-A

BROOKHART, Prof. M.S. (University of N. Carolina) — 20th June, 1991
Olefin Polymerizations, Oligomerizations and Dimerizations Using Electrophilic Late Transition Metal Catalysts

BROWN, Dr. J. (Oxford University) — 28th February, 1991
Can Chemistry Provide Catalysts Superior to Enzymes?

BUSHBY†, Dr. R. (Leeds University) — 6th February, 1991
Biradicals and Organic Magnets

COWLEY, Prof. A.H. (University of Texas) — 13th December, 1990
New Organometallic Routes to Electronic Materials

CROUT, Prof. D. (Warwick University) — 29th November, 1990
Enzymes in Organic Synthesis

DOBSON†, Dr. C.M. (Oxford University) — 6th March, 1991
NMR Studies of Dynamics in Molecular Crystals

GERRARD†, Dr. D. (British Petroleum) — 7th November, 1990
Raman Spectroscopy for Industrial Analysis

HUDLICKY, Prof. T. (Virginia Polytechnic Institute) — 25th April, 1991
Biocatalysis and Symmetry Based Approaches to the Efficient Synthesis of Complex Natural Products

JACKSON†, Dr. R. (Newcastle University) — 31st October, 1990
New Synthetic Methods: α-Amino Acids and Small Rings

KOCOVSKY†, Dr. P. (Uppsala University) — 6th November, 1990
Stereo-Controlled Reactions Mediated by Transition and Non-Transition Metals

LACEY, Dr. D. (Hull University) Liquid Crystals	31st January, 1991
LOGAN, Dr. N. (Nottingham University) Rocket Propellants	1st November, 1990
MACDONALD, Dr. W.A. (ICI Wilton) Materials for the Space Age	11th October, 1990
MARKAM, Dr. J. (ICI Pharmaceuticals) DNA Fingerprinting	7th March, 1991
PETTY, Dr. M.C. (Durham University) Molecular Electronics	14th February, 1991
PRINGLE†, Dr. P.G. (Bristol University) Metal Complexes with Functionalised Phosphines	5th December, 1990
PRITCHARD, Prof. J. (Queen Mary & Westfield College, London University) Copper Surfaces and Catalysts	21st November, 1990
SADLER, Dr. P.J. (Birkbeck College London) Design of Inorganic Drugs: Precious Metals, Hypertension + HIV	24th January, 1991
SARRE, Dr. P. (Nottingham University) Comet Chemistry	17th January, 1991
SCHROCK, Prof. R.R. (Massachusetts Institute of Technology) Metal-ligand Multiple Bonds and Metathesis Initiators	24th April, 1991
SCOTT, Dr. S.K. (Leeds University) Clocks, Oscillations and Chaos	8th November, 1990
SHAW†, Prof. B.L. (Leeds University) Syntheses with Coordinated, Unsaturated Phosphine Ligands	20th February, 1991
SINN†, Prof. E. (Hull University) Coupling of Little Electrons in Big Molecules. Implications for the Active Sites of (Metalloproteins and other) Macromolecules	30th January, 1991
SOULEN†, Prof. R. (South Western University, Texas) Preparation and Reactions of Bicycloalkenes	26th October, 1990
WHITAKER†, Dr. B.J. (Leeds University) Two-Dimensional Velocity Imaging of State-Selected Reaction Products	28th November, 1990

† Invited specifically for the postgraduate training programme.

UNIVERSITY OF DURHAM

Board of Studies in Chemistry

COLLOQUIA, LECTURES AND SEMINARS FROM INVITED SPEAKERS

1991 – 1992 (August 1 – July 31)

1991

October	17	Dr. J.A. Salthouse, University of Manchester Son et Lumiere – a demonstration lecture
October	31	Dr. R. Keeley, Metropolitan Police Forensic Science Modern forensic science
November	6	Prof. B.F.G. Johnson†, Edinburgh University Cluster–surface analogies
November	7	Dr. A.R. Butler, St. Andrews University Traditional Chinese herbal drugs: a different way of treating disease
November	13	Prof. D. Gani†, St. Andrews University The chemistry of PLP–dependent enzymes
November	20	Dr. R. More O'Ferrall†, University College, Dublin Some acid–catalysed rearrangements in organic chemistry
November	28	Prof. I.M. Ward, IRC in Polymer Science, University of Leeds The SCI lecture: the science and technology of orientated polymers
December	4	Prof. R. Grigg†, Leeds University Palladium–catalysed cyclisation and ion–capture processes
December	5	Prof. A.L. Smith, ex Unilever Soap, detergents and black puddings
December	11	Dr. W.D. Cooper†, Shell Research Colloid science: theory and practice

1992

January	22	Dr. K.D.M. Harris†, St. Andrews University Understanding the properties of solid inclusion compounds
January	29	Dr. A. Holmes†, Cambridge University Cycloaddition reactions in the service of the synthesis of piperidine and indolizidine natural products

January	30	Dr. M. Anderson, Sittingbourne Research Centre, Shell Research Recent Advances in the Safe and Selective Chemical Control of Insect Pests
February	12	Prof. D.E. Fenton†, Sheffield University Polynuclear complexes of molecular clefts as models for copper biosites
February	13	Dr. J. Saunders, Glaxo Group Research Limited Molecular Modelling in Drug Discovery
February	19	Prof. E.J. Thomas†, Manchester University Applications of organostannanes to organic synthesis
February	20	Prof. E.Vogel, University of Cologne *The Musgrave Lecture* Porphyrins: Molecules of Interdisciplinary Interest
February	25	Prof. J.F. Nixon, University of Sussex *The Tilden Lecture* Phosphaalkynes: new building blocks in inorganic and organometallic chemistry
February	26	Prof. M.L. Hitchman†, Strathclyde University Chemical vapour deposition
March	5	Dr. N.C. Billingham, University of Sussex Degradable Plastics – Myth or Magic?
March	11	Dr. S.E. Thomas†, Imperial College Recent advances in organoiron chemistry
March	12	Dr. R.A. Hann, ICI Imagedata Electronic Photography – An Image of the Future
March	18	Dr. H. Maskill†, Newcastle University Concerted or stepwise fragmentation in a deamination–type reaction
April	7	Prof. D.M. Knight, Philosophy Department, University of Durham Interpreting experiments: the beginning of electrochemistry
May	13	Dr. J–C Gehret, Ciba Geigy, Basel Some aspects of industrial agrochemical research

† Invited specially for the postgraduate training programme.

UNIVERSITY OF DURHAM

Board of Studies in Chemistry

COLLOQUIA, LECTURES AND SEMINARS FROM INVITED SPEAKERS

1992 - 1993 (August 1 - July 31)

1992

October 15	Dr M. Glazer & Dr. S. Tarling, Oxford University & Birbeck College, London It Pays to be British! - The Chemist's Role as an Expert Witness in Patent Litigation
October 20	Dr. H. E. Bryndza, Du Pont Central Research Synthesis, Reactions and Thermochemistry of Metal (Alkyl) Cyanide Complexes and Their Impact on Olefin Hydrocyanation Catalysis
October 22	Prof. A. Davies, University College London *The Ingold-Albert Lecture* The Behaviour of Hydrogen as a Pseudometal
October 28	Dr. J. K . Cockcroft, University of Durham Recent Developments in Powder Diffraction
October 29	Dr. J. Emsley, Imperial College, London The Shocking History of Phosphorus
November 4	Dr. T. P. Kee, University of Leeds Synthesis and Co-ordination Chemistry of Silylated Phosphites
November 5	Dr. C. J. Ludman, University of Durham Explosions, A Demonstration Lecture
November 11	Prof. D. Robins, Glasgow University Pyrrolizidine Alkaloids : Biological Activity, Biosynthesis and Benefits
November 12	Prof. M. R. Truter, University College, London Luck and Logic in Host - Guest Chemistry
November 18	Dr. R. Nix, Queen Mary College, London Characterisation of Heterogeneous Catalysts
November 25	Prof. Y. Vallee. University of Caen Reactive Thiocarbonyl Compounds
November 25	Prof. L. D. Quin, University of Massachusetts, Amherst Fragmentation of Phosphorous Heterocycles as a Route to Phosphoryl Species with Uncommon Bonding
November 26	Dr. D. Humber, Glaxo, Greenford AIDS - The Development of a Novel Series of Inhibitors of HIV
December 2	Prof. A. F. Hegarty, University College, Dublin Highly Reactive Enols Stabilised by Steric Protection
December 2	Dr. R. A. Aitken, University of St. Andrews The Versatile Cycloaddition Chemistry of $Bu_3P.CS_2$
December 3	Prof. P. Edwards, Birmingham University The SCI Lecture - What is Metal?
December 9	Dr. A. N. Burgess, ICI Runcorn The Structure of Perfluorinated Ionomer Membranes

1993

January 20	Dr. D. C. Clary, University of Cambridge Energy Flow in Chemical Reactions
January 21	Prof. L. Hall, Cambridge NMR - Window to the Human Body
January 27	Dr. W. Kerr, University of Strathclyde Development of the Pauson-Khand Annulation Reaction : Organocobalt Mediated Synthesis of Natural and Unnatural Products
January 28	Prof. J. Mann, University of Reading Murder, Magic and Medicine
February 3	Prof. S. M. Roberts, University of Exeter Enzymes in Organic Synthesis
February 10	Dr. D. Gillies, University of Surrey NMR and Molecular Motion in Solution
February 11	Prof. S. Knox, Bristol University *The Tilden Lecture* Organic Chemistry at Polynuclear Metal Centres
February 17	Dr. R. W. Kemmitt, University of Leicester Oxatrimethylenemethane Metal Complexes
February 18	Dr. I. Fraser, ICI Wilton Reactive Processing of Composite Materials
February 22	Prof. D. M. Grant, University of Utah Single Crystals, Molecular Structure, and Chemical-Shift Anisotropy
February 24	Prof. C. J. M. Stirling, University of Sheffield Chemistry on the Flat-Reactivity of Ordered Systems
March 10	Dr. P. K. Baker, University College of North Wales, Bangor 'Chemistry of Highly Versatile 7-Coordinate Complexes'
March 11	Dr. R. A. Y. Jones, University of East Anglia The Chemistry of Wine Making
March 17	Dr. R. J. K. Taylor, University of East Anglia Adventures in Natural Product Synthesis
March 24	Prof. I. O. Sutherland, University of Liverpool Chromogenic Reagents for Cations
May 13	Prof. J. A. Pople, Carnegie-Mellon University, Pittsburgh, USA *The Boys-Rahman Lecture* Applications of Molecular Orbital Theory
May 21	Prof. L. Weber, University of Bielefeld Metallo-phospha Alkenes as Synthons in Organometallic Chemistry
June 1	Prof. J. P. Konopelski, University of California, Santa Cruz Synthetic Adventures with Enantiomerically Pure Acetals
June 2	Prof. F. Ciardelli, University of Pisa Chiral Discrimination in the Stereospecific Polymerisation of Alpha Olefins
June 7	Prof. R. S. Stein, University of Massachusetts Scattering Studies of Crystalline and Liquid Crystalline Polymers

June 16 Prof. A. K. Covington, University of Newcastle
Use of Ion Selective Electrodes as Detectors in Ion Chromatography

June 17 Prof. O. F. Nielsen. H. C. Ørsted Institute, University of Copenhagen
Low-Frequency IR - and Raman Studies of Hydrogen Bonded Liquids

File Ref. CG137/E(CH)